Riparian Ecosystem Management Model:
Simulator for Ecological Processes in Riparian Zones

Introduction to the Acrobat pdf version

This Acrobat pdf of the REMM documentation is identical to the print version. However--

- The equations may appear to be in different type than in the print version. This is an artifact of the pdf creation process, and in any case does not affect the content of the equations.

- Problems have shown up when printing certain of the illustrations using some computer-printer combinations; experimentation may be necessary to produce accurate printouts. Displayed with Acrobat, the illustrations should be correct.

United States
Department of
Agriculture

Agricultural
Research
Service

Conservation
Research
Report 46

February 2002

Riparian Ecosystem Management Model

Simulator for Ecological Processes in Riparian Zones

Riparian Ecosystem Management Model

Simulator for Ecological Processes in Riparian Zones

Lee S. Altier, Richard Lowrance, Randall G. Williams, Shreeram P. Inamdar, David D. Bosch, Joseph M. Sheridan, Robert K. Hubbard, and Daniel L. Thomas

---

Altier was a horticulturist, Lowrance is an ecologist, Williams is an agricultural engineer, Bosch is a hydrologist, Sheridan is a hydraulic engineer, and Hubbard is a soil scientist with the Southeast Watershed Research Laboratory, USDA-ARS, Tifton, Georgia. Inamdar was a postdoctoral associate and Thomas is an associate professor at the University of Georgia, Tifton. Altier is presently an assistant professor at California State University, Chico. Inamdar is presently with the Department of Geography, Buffalo State College, Buffalo, NY.

Abstract

Altier, L.S., R. Lowrance, R.G. Williams, et al. 2002. Riparian Ecosystem Management Model: Simulator for Ecological Processes in Riparian Zones. United States Department of Agriculture, Agricultural Research Service, Conservation Research Report 46.

Riparian buffer zones are effective in mitigating nonpoint source pollution and have been recommended as a best management practice (BMP). Their potential use as a BMP has been limited because of the lack of a design procedure that can quantify their effectiveness for a given set of site conditions. The Riparian Ecosystem Management Model (REMM) has been developed for researchers and natural resource agencies as a modeling tool that can help to quantify the water quality benefits of riparian buffers under varying site conditions. Processes simulated in REMM include surface and subsurface hydrology; sediment transport and deposition; carbon, nitrogen, and phosphorus transport, removal, and cycling; and vegetation growth. Simulations are performed on a daily basis and can be continued in excess of 100 years. Management options such as vegetation type, size of the buffer zone, and biomass harvesting can also be simulated. REMM can be used in conjunction with upland models, empirical data, or estimated loadings to examine scenarios of buffer zone design for a hillslope.

Keywords. BMP, buffer systems, ecosystem model, nonpoint source pollution, riparian zones, water quality.

While supplies last, single copies of this publication can be obtained at no cost from:

R. Lowrance, USDA-ARS
P.O. Box 946
Tifton, GA 31793

Copies of this publication may be purchased from the National Technical Information Service, 5285 Port Royal Road, Springfield, VA 22161; telephone (703) 605–6000.

Issued February 2002

Contents

Chapter 1
Water Quality Functions of Riparian Buffer Systems

Richard Lowrance

Riparian Buffer Systems (RBS) are streamside ecosystems that are managed for the enhancement of water quality through control of nonpoint source (NPS) pollution and protection of the stream environment. The use of riparian management zones is relatively well established as a best management practice (BMP) for water quality improvement in forestry (Comerford et al. 1992) but has been much less widely applied as a BMP in agricultural areas or in urban or suburban settings.

The Riparian Ecosystem Management Model (REMM) provides a tool for estimating the nonpoint source pollution control by field-scale riparian ecosystems. RBS are especially important on small streams, where there is intense interaction between terrestrial and aquatic ecosystems. First- and second-order streams make up nearly three-quarters of the total stream length in the United States (Leopold et al. 1964). Fluvial activities influence the composition of riparian plant communities along these small streams (Gregory et al. 1991). Likewise, terrestrial disturbances can have an immediate effect on aquatic populations (Webster et al. 1992, Sweeney 1993). Small streams can be completely covered by the canopies of streamside vegetation (Sweeney 1993). Riparian vegetation has well-known beneficial effects on the bank stability, biological diversity, and water temperatures of streams (Karr and Schlosser 1978). Riparian forests of mature trees (30 to 75 years old) are known to effectively reduce nonpoint source pollution from agricultural fields (Lowrance et al. 1985).

Compared to other NPS pollution control measures, RBScan lead to longer-term changes in the structure and function of agricultural landscapes. To produce long-term improvements in water quality, RBS must be designed with an understanding of the processes that remove or sequester pollutants entering the riparian buffer system; the effects of riparian management practices on pollutant retention; the effects of riparian forest buffers on aquatic ecosystems; the time to recovery after harvest of trees or re-establishment of riparian buffer systems; and the effects of underlying soil and geologic materials on chemical, hydrological, and biological processes.

This chapter consists of a brief overview of nonpoint source pollution problems, general information on the water quality functions of riparian ecosystems, a synthesis of the research and scientific judgments on which the RBS specification is based, and an evaluation of the applicability of RBS.

Nonpoint Source Pollution Control Relative to Nutrient Load Reduction Strategies

Nonpoint source pollution is the major cause of surface water impairment in the United States (Long 1991, Baker 1992) and has been addressed as a national priority since the 1978 passage of the Clean Water Act, Section 319, which requires "that programs for the control of nonpoint sources of pollution be developed and implemented." The effectiveness of the RBS is likely to be judged by their NPS pollution control effectiveness.

Although assessments are incomplete and do not include all states, it is estimated are that about 30 percent of U.S. waters are impaired—meaning they do not fully support their designated uses (U.S. EPA 1990a). Of impaired waters, about two-thirds of the problems are primarily from NPS pollution (U.S. EPA 1986). The nonpoint sources of pollution vary, but agriculture is the major contributor for rivers and lakes. Besides agriculture, the other major contributors of NPS pollution are urban areas, mining, atmospheric deposition, and natural origins. Nutrients and sediments are still the principal sources of surface water impairment (U.S. EPA 1986, 1990a,b). Sediments are the most important cause of impairment for rivers, and nutrients are the most important cause of impairment for estuaries. Although pesticides, metals, and priority pollutants are identified as problems in less than 20 percent of the assessed waters, the extent of this contamination, especially for pesticides, may be underestimated.

A systems approach for NPS pollution reduction will include structural BMPs and source load reductions, as well as approaches which seek to integrate the management and restoration of landscape features that retain pollutants through a combination of ecosystem processes. Examples of these pollutant sinks include natural wetlands, constructed wetlands, and riparian forest buffer systems (Fields 1992). As pollutant sinks increase in complexity from simple physical structures to diverse natural ecosystems, so increase both the importance and the difficulty of understanding processes that sequester or remove pollutants.

New Approaches to Nonpoint Source Pollution Estimation and Abatement

Risk assessment and source reduction are new approaches for NPS pollution control (Baker 1992). In some watersheds, a high percentage of total pollutant loadings comes from a relatively small portion of the watershed area because of improper management of sources, improper siting of facilities, problematic environmental and site conditions, or a combination of these factors. Watershed-scale risk assessment seeks to identify and reduce loadings from areas which contribute large amounts of NPS pollution.

Concurrent with identification of problem areas comes the opportunity for source reduction. Source reduction has been responsible for some of the more impressive successes of NPS pollution reduction, including the reduction of loadings of lead from automobile emissions and of organochlorine pesticides

(Baker 1992). Source reduction should be linked with watershed-scale risk assessments because the potential for source reduction may be greatest (and probably most economical) in areas generating the highest unit area loadings. The linkage of risk assessment and source reduction will depend on interacting factors such as type of pollutant (for example, purchased input vs. by-product), reason for high risk (such as poor management, siting of facilities, or inherent regional risks), and availability of alternative practices and sites.

Even when risk assessment and source reduction strategies lead to load reductions under average conditions, a third aspect of watershed management—maintenance and restoration of buffer systems between terrestrial and aquatic ecosystems—is necessary to reduce the contributions of extreme events to NPS pollutant loads. Under the best of conditions, source reduction will likely leave watersheds vulnerable to extreme events, including weather extremes as well as economically generated extremes (such as intensification of pollution-generating production practices). Watershed studies have demonstrated the importance of extreme events to water and pollutant transport. Extreme events within a year dominate annual totals, and wet years within multiyear cycles dominate long-term loadings (Lowrance and Leonard 1988, Jaworski et al. 1992, Magnien et al. 1992). Control of NPS pollution from extreme events will require integration of risk assessment and source reduction approaches with buffer systems as landscape-scale "insurance policies."

Buffer systems are also important in controlling watershed NPS pollutants because of the limitations of other BMPs for NPS pollution control. For example, Hall (1992) monitored changes in groundwater nitrate (NO_3^-–N) concentrations beneath heavily fertilized and manured fields in Lancaster County, Pennsylvania, following the implementation of "input management" techniques. Fertilizer/manure inputs decreased by 39 to 67 percent (222 to 423 kg ha^{-1}), but groundwater nitrate decreased by 12 to 50 percent. By the end of the study, nitrate concentrations in groundwater still exceeded federal drinking water standards. Shirmohammadi et al. (1991) used the CREAMS simulation model to evaluate the effects of seven different BMPs on groundwater nitrate concentrations beneath cropping systems on the Eastern Shore of Maryland. Although CREAMS does not provide absolute predictions, none of the BMPs were predicted to reduce groundwater nitrate concentrations to less than the federal drinking water standard. Under appropriate conditions, described in this report, RBS are likely to be an important component of NPS pollution control when in-field BMPs are inadequate.

Historical Overview of Scientific Interest in Riparian Ecosystems

Most of the knowledge of the effect of riparian ecosystems on water quality comes from research conducted since 1975. Two publications in 1978 galvanized scientific and management interest in riparian ecosystems. Karr and Schlosser (1978) concluded that stream environments are largely controlled by adjacent riparian ecosystems and provided an overview of relationships between water resources and riparian ecosystems (the land-water interface). Johnson and McCormick (1978) edited the proceedings of a symposium that included 55 reports on various aspects of riparian research, management, and policy. While the symposium proceedings contained excellent discussions of the late 1970s state of knowledge concerning riparian ecosystems and other types of wetlands (Brown et al. 1978, Wharton and Brinson 1978), only one paper (Mitsch 1978) dealt specifically and quantitatively with the water quality functions of a riparian ecosystem. The proceedings also included a review of the general water quality functions of wetlands (Kibby 1978) in which a number of publications on nutrient cycling in riparian and other wetlands were cited. Only a few of the citations dealt specifically with water quality effects of riparian ecosystems (Kitchens et al. 1975, Lee et al. 1975, Kuenzler et al. 1977, Richardson et al. 1978). Although the 1978 symposium contained numerous claims about the water quality functions of riparian ecosystems, few data were presented.

In the late 1970s a number of research projects began to develop a more quantitative understanding of the role played by riparian ecosystems in controlling NPS pollution by sediment and nutrients in agricultural watersheds (Lowrance et al. 1983, Peterjohn and Correll 1984, Jacobs and Gilliam 1985). These studies were primarily in the Coastal Plain physiographic province of the eastern United States, where the typical land-use pattern is intensive row-crop agriculture in upland areas, with riparian forests along low-order streams. These early studies shared at least two other important characteristics: (1) a relatively shallow aquiclude, which forced most infiltrated water to move laterally toward streams and pass through or near the riparian forest root zone and (2) naturally regenerated forests typical of the region rather than forests managed specifically for water quality functions. These studies focused on riparian processes related to nutrients and sediment with little or no attention to the fates of other pollutants or to the effects of riparian areas on the physical or trophic status of the stream.

As interest in the nonpoint source pollution control value of riparian ecosystems increased, recognition of their importance to the physical and trophic status of streams also developed. Karr and Schlosser (1978) quantified the effects of riparian vegetation on sunlight penetration and temperature of streams. Research in the 1980s confirmed the importance of large woody debris and leaf litter inputs to the habitat and trophic status of most small streams (Meyer and O'Hop 1983, Benke et al. 1985, Harmon et al. 1986). By 1987, it was well established that woody debris derived from riparian forests played an important role in

controlling channel morphology, the storage and routing of organic matter and sediment, and the amount and quality of fish habitat (Bisson et al. 1987).

Research Background for the Riparian Buffer System Specification

By the late 1980s, there was a clear need to synthesize the existing knowledge into management recommendations for the establishment, maintenance, and management of riparian ecosystems for a broad range of water quality functions (Lowrance 1991). In 1991 the U.S. Department of Agriculture (USDA) Forest Service with assistance from the Agricultural Research Service and Soil Conservation Service of USDA, the Stroud Water Research Center in Pennsylvania, the Pennsylvania Department of Environmental Resources, the Maryland Department of Natural Resources, and the U.S. Department of the Interior's Fish and Wildlife Service developed draft guidelines for riparian forest buffers. This effort resulted in a booklet titled "Riparian Forest Buffers—Function and Design for Protection and Enhancement of Water Resources" (Welsch 1991), which specified a riparian buffer system consisting of three zones:

- Zone 1 is permanent woody vegetation immediately adjacent to the stream bank.
- Zone 2 is managed forest occupying a strip upslope from zone 1.
- Zone 3 is an herbaceous filter strip upslope from zone 2.

The specification applies to areas where cropland, grasslands, or pasture are adjacent to riparian areas on permanent or intermittent streams, margins of lakes and ponds, margins of wetlands, or margins of groundwater recharge areas such as sinkholes.

The primary purposes of zone 3 of the RBS are to remove sediment from surface runoff and to convert channelized flow to sheet flow.

The primary function of zone 2 is to block transport of sediment and chemicals from upland areas into the adjacent wetland or aquatic ecosystem. Vegetation and litter in these zones form a mechanical barrier to sediment transport. Plant roots take up chemicals that become sequestered in growing biomass. Vegetation also produces organic matter that fosters chemical and biological processes that immobilize or transform pollutants.

Although most zone 2 functions also occur in zone 1, the primary purpose of zone 1 is to maintain the integrity of the stream bank and a favorable habitat for aquatic organisms. Shade and litter-fall provided by streamside vegetation have a direct influence on water temperature and dissolved chemicals.

The Forest Service report and specification were based on a synthesis of literature existing through 1989 and on in-depth discussions with scientists and managers working on various riparian ecosystems (Welsch 1991). Some of the generalizations which guided the design of RBS were based on studies of nutrient sequestering and nutrient transformations in agricultural watersheds (Correll 1983, Yates and Sheridan 1983, Lowrance et al. 1985). These watershed-scale studies indicated that riparian forests are important nutrient and sediment sinks in agricultural watersheds but provided little or no guidance on how to design an effective RBS. Process studies in these and other systems provided most of the original design guidance. Several studies on nitrate removal from shallow groundwater in riparian forest buffers found that most reduction in nitrate concentration takes place within the first 10 to 15 m of forest (Lowrance et al. 1984, Peterjohn and Correll 1984, Jacobs and Gilliam 1985) and that the width necessary for shallow groundwater nitrate removal could be relatively short. Although effective in reducing sediment and sediment-borne chemical concentrations in sheet flow (Peterjohn and Correll 1984), channelized flow can bypass riparian forests. To control channelized flow into a riparian forest, a herbaceous strip in zone 3 could be much more easily reshaped and revegetated than a forest. Herbaceous buffers, especially grass filters, are effective at removing coarse suspended sediments and some sediment-borne pollutants but may require frequent maintenance and are not very effective at nutrient removal from shallow groundwater (Magette et al. 1987, 1989, Dillaha et al. 1989).

Long-term sequestering and removal of nutrients and other contaminants in the RBS is the main purpose of zones 3 and 2. This can occur by accumulating sediment and adsorbed contaminants, microbial transformations (for nitrogen) and biochemical degradation (for pesticides), and incorporation of nutrients and other chemicals into woody biomass and soil organic matter. At least one study of coastal plain riparian forests showed substantial amounts of nutrient sequestering in woody biomass (Fail et al. 1986). The RBS specification encourages production and harvest of woody biomass from zone 2 to remove nutrients and other contaminants. Once vegetation has been removed from the stream channel, recovery through plant succession may take a long time and revegetation may be dominated by undesirable species (Sweeney 1993). Therefore, the need for permanent control of the stream physical and trophic environment requires that succession be directed toward desirable permanent vegetation in those portions of the RBS which directly influence the stream channel, in particular zone 1.

A number of practical matters were also considered in the RBS specification (Welsch 1991). Most RBS should be available for management to provide an economic return without sacrificing water quality functions. Characteristics of soils, hydrology, and potential vegetation should guide design and planning of

effective RBS. The RBS should be used in conjunction with sound upland management practices including nutrient management and erosion control. In-stream woody debris removal should be limited, but woody debris with the potential to form dams that cause inundation should be removed. The dimensions of the RBS should depend on the existing and potential NPS pollutant loads and the minimum size for sustained support of the aquatic environment.

References

Baker, L.A. 1992. Introduction to nonpoint source pollution in the United States and prospects for wetland use. Ecological Engineering 1:1–26.

Benke, A.C., R.L. Henry III, D.M. Gillespie, and R.H. Hunter. 1985. Importance of snag habitat for animal production in southeastern streams. Fisheries 10:8–13.

Bisson, P.A., R.E. Bilby, M.D. Bryant, et al. 1987. Large woody debris in forested streams in the Pacific Northwest: past, present, and future. *In* E.O. Salo and T.W. Cundy, eds., Streamside Management: Forestry and Fishery Interactions, pp. 143–190. Institute of Forest Resources, University of Washington, Seattle.

Brown, S., M.M. Brinson, and A.E. Lugo. 1978. Structure and function of riparian wetlands. *In* R.R. Johnson and J.F. McCormick, eds., Strategies for Protection and Management of Floodplain Wetlands and Other Riparian Ecosystems, pp. 17–31. U.S. Department of Agriculture, Forest Service, General Technical Report WO–12.

Comerford, N.B., D.G. Neary, and R.S. Mansell. 1992. The effectiveness of buffer strips for ameliorating offsite transport of sediment, nutrients, and pesticides from silvicultural operations. Natural Council of the Paper Industries for Air and Stream Improvement, New York, Technical Bulletin 631.

Correll, D.L. 1983. N and P in soils and runoff of three Coastal Plain land uses. *In* R. Lowrance et al., eds., Nutrient Cycling in Agricultural Ecosystems, pp. 207–224. University of Georgia, College of Agriculture, Athens, Special Publication No. 23.

Dillaha, T.A., R.B. Reneau, S. Mostaghimi, and D. Lee. 1989. Vegetative filter strips for agricultural nonpoint source pollution control. Transactions of the ASAE 32:513-519.

Fail, J.L., Jr., M.N. Hamzah, B.L. Haines, and R.L. Todd. 1986. Above and below ground biomass, production, and element accumulation in riparian forests

of an agricultural watershed. *In* D.L. Correll, ed., Watershed Research Perspectives, pp.193–224. Smithsonian Institution, Washington, DC.

Fields, S. 1992. Regulations and policies relating to the use of wetlands for nonpoint source pollution control. Ecological Engineering 1:135–142.

Gregory, S.V., F.J. Swanson, W.A. McKee, and K.W. Cummins. 1991. An ecosystem perspective of riparian zones. BioScience 41:540–551.

Hall, D.W. 1992. Effects of nutrient management on nitrate levels in ground water near Ephrata, Pennsylvania. Ground Water 30:720–730.

Harmon, M.E., J.F. Franklin, F.J. Swanson, et al. 1986. Ecology of coarse woody debris in temperate ecosystems. Advances in Ecological Research 15:133-302.

Jacobs, T.C., and J.W. Gilliam. 1985. Riparian losses of nitrate from agricultural drainage waters. Journal of Environmental Quality 14:472–478.

Jaworski, N.A., P.M. Groffman, A. Keller, and A.C. Prager. 1992. A watershed-scale analysis of nitrogen loading: the upper Potomac River. Estuaries 15:83–95.

Johnson, R.R., and J.F. McCormick, eds. 1978. Strategies for protection and management of floodplain wetlands and other riparian ecosystems. U.S. Department of Agriculture, Forest Service, General Technical Report WO–12.

Karr, J.R., and I.J. Schlosser. 1978. Water resources and the land-water interface. Science 201:229–234.

Kibby, H.V. 1978. Effects of wetlands on water quality. *In* R.R. Johnson and J.F. McCormick, eds., Strategies for Protection and Management of Floodplain Wetlands and Other Riparian Ecosystems, pp. 289–298. U.S. Department of Agriculture, Forest Service, General Technical Report WO–12.

Kitchens, W.H., J.M. Dean, L.H. Stevenson, and J.H. Cooper. 1975. The Santee Swamp as a nutrient sink in mineral cycling. *In* F. G. Howell, J. B. Gentry, and M. H. Smith, eds., Southeastern Ecosystems. U.S. Department of Agriculture, Forest Service, ERDA Symposium Series.

Kuenzler, E.J., P.J. Mulholland, L.A. Ruley, and R.P. Sniffen. 1977. Water quality in North Carolina coastal plain streams and effects of channelization. Water Resources Research Institute, University of North Carolina, Raleigh, Report No. 127.

Lee, G.F., E. Bentley, and R. Amundson. 1975. Effects of marshes on water quality. *In* A.D. Hasler, ed., Coupling of Land and Water Systems, pp. 105–127. Springer-Verlag, New York.

Leopold, L.B., M.G. Wolman, and J.P. Miller. 1964. Fluvial Processes in Geomorphology. W.H. Freeman and Company, San Francisco.

Long, C. 1991. National policy perspectives and issues regarding the prevention and control of nonpoint source pollution. USEPA–ORD Workshop on Nonpoint Source Pollution Control. U.S. Environmental Protection Agency, Washington, DC.

Lowrance, R. 1991. Effects of buffer systems on the movement of N and P from agriculture to streams p. 87-96. *In* V. Holter, ed., Proceedings of International Conference on Nitrogen, Phosphorus, Organic Matter. Danish Ministry of Environment, Copenhagen.

Lowrance, R., and R.A. Leonard. 1988. Streamflow nutrient dynamics in coastal plain watersheds. Journal of Environmental Quality 17:734–740.

Lowrance, R., R.A. Leonard, L.E. Asmussen, and R.L. Todd. 1985. Nutrient budgets for agricultural watersheds in the southeastern coastal plain. Ecology 66:287–296.

Lowrance, R.R., R.L. Todd, and L.E. Asmussen. 1983. Waterborne nutrient budgets for the riparian zone of an agricultural watershed. Agriculture, Ecosystems and Environment 10:371–384.

Lowrance, R., R.L. Todd, and L.E. Asmussen. 1984. Nutrient cycling in an agricultural watershed: I. Phreatic movement. Journal of Environmental Quality 13:22–27.

Magette, W.L., R.B. Brinsfield, R.E. Palmer, et al. 1987. Vegetative filter strips for agricultural runoff treatment. U.S. Environmental Protection Agency, Report No. CBP/TRS 2/87.

Magette, W.L., R.B. Brinsfield, R.E. Palmer, and J.D. Wood. 1989. Nutrient and sediment removal by vegetated filter strips. Transactions of the ASAE 32:663–667.

Magnien, R.E., R.M. Summers, and K.G Sellner. 1992. External nutrient sources, internal tools, and phytoplankton production in Chesapeake Bay. Estuaries 15:497–516.

Meyer, J.L., and J. O'Hop. 1983. The effects of watershed disturbance on dissolved organic dynamics of a stream. American Midland Naturalist 109:175–183.

Mitsch, W.J. 1978. Interactions between a riparian swamp and a river in southern Illinois. *In* R.R. Johnson and J.F. McCormick, eds., Strategies for Protection and Management of Floodplain Wetlands and Other Riparian Ecosystems, pp. 63–72. U.S. Department of Agriculture, Forest Service, General Technical Report No. WO–12.

Peterjohn, W.T., and D.L. Correll. 1984. Nutrient dynamics in an agricultural watershed: observations on the role of a riparian forest. Ecology 65:1466–1475.

Richardson, C.J., D.L. Tilton, J.A. Kuclee, et al. 1978. Nutrient dynamics of northern wetland ecosystems. *In* R.E. Good, D.F. Whigham, and R.L. Simpson, eds., Freshwater Wetlands Ecological Processes and Management Potential. Academic Press, New York.

Shirmohammadi, A., W.L. Magette, and L.L. Shoemaker. 1991. Reduction of nitrate loadings to ground water. Ground Water Monitoring Review, Winter 1991, pp. 91-97.

Sweeney, B.W. 1993. Streamside forests and the physical, chemical, and trophic characteristics of Piedmont streams in eastern North America. Water Science Technology 26:2653–2673.

U.S. Environmental Protection Agency. 1986. National Water Quality Inventory: 1984 Report to Congress. U.S. Government Printing Office, Washington, DC.

U.S. Environmental Protection Agency. 1990a. National Water Quality Inventory: 1988 Report to the Congress. U.S. Government Printing Office, Washington, DC.

U.S. Environmental Protection Agency. 1990b. Managing nonpoint source pollution: final report to Congress on section 319 of the Clean Water Act. U.S. Government Printing Office, Washington, DC.

Webster, J.R., S.W. Golladay, E.F. Benfield, et al. 1992. Catchment disturbance and stream response: an overview of stream research at Coweeta Hydrologic Laboratory. *In* P.J. Boon, P. Calow, and G.E. Petts, eds., River Conservation and Management, pp. 231–253. John Wiley & Sons, New York.

Welsch, D.J. 1991. Riparian Forest Buffers. U.S. Department of Agriculture, Forest Service, Radnor, PA, Publication No. NA–PR–07–91.

Wharton, C.H., and M.M. Brinson. 1978. Characteristics of southeastern river systems. *In* R.R. Johnson and J.F. McCormick, eds., Strategies for Protection and Management of Floodplain Wetlands and Other Riparian Ecosystems, pp. 32–40. U.S. Department of Agriculture, Forest Service, General Technical Report No. WO–12.

Yates, P., and J.M. Sheridan. 1983. Estimating the effectiveness of vegetated floodplains/wetlands as nitrate-nitrite and orthophosphorus filters. Agriculture, Ecosystems and Environment 9:303–314.

Chapter 2
Hydrology: Surface and Subsurface Water Movement

Randall G. Williams, Joseph M. Sheridan, Shreeram P. Inamdar, David D. Bosch, Richard Lowrance, Robert K. Hubbard, Daniel L. Thomas, and Lee S. Altier

Summary

Riparian buffer zones receive water from precipitation and from surface runoff and shallow groundwater. REMM simulates these movements of water into, through, and out of a riparian ecosystem. Although riparian buffers may also receive water from overbank flows (floods) and deeper groundwater, REMM does not consider these movements. In REMM, subsurface flows are allowed to move from adjacent uplands and between zones based on the hydraulic gradients and conductivities between the zones and on the available storage in the receiving zone. Water also moves among soil layers. Subsurface flow from a zone that is completely saturated and that cannot move into the adjacent zone can move through seepage or exfiltration. Eventually subsurface flow moves from zone 1 into the adjacent stream or aquatic system based on gradients between the water table in zone 1 and the bottom of the stream. Surface runoff is allowed to infiltrate based on available storage and a modified Green-Ampt equation except for a component of upland surface runoff which can be routed through based on depth and flow velocity. Surface runoff that does not infiltrate moves to the stream.

Movement and storage of water within riparian buffer systems is simulated by a process-based, two-dimensional water balance operating on a daily time step. The components of the water balance are shown in figure 2.1. The hydrologic compo-nent of the Riparian Ecosystem Management Model (REMM) is structured to facilitate subsequent computations of sediment and nutrient transport, as well as rates of biological and chemical transformations. A schematic detailing water budget components simulated in the REMM hydrology module is shown in figure 2.2. External inputs to the water balance include daily precipitation and daily surface and subsurface flow from upslope contributing areas.

On each day, subsurface vertical movement is calculated first, followed by horizontal movement, followed by precipitation. The calculations start with zone 3 and proceed down through zone 1. Outputs from the water balance simulation include daily evapotranspiration, deep seepage, and surface and subsurface losses to the water body. Conditions reported for a day constitute the status of the respective buffer system zone-layer at the end of the day, and hence represent the starting conditions for the next day. The water balance equation for each layer of each zone is—

$$\theta_t = \theta_{t-1} + P_t + DrainIn_t + Q_{SS,In,t} - Es_t - Ep_t + Up_t - Q_{S,t} - DrainOut_t - Q_{SS,Out,t} - DeepSeep_t \quad [2.1]$$

where, on day *t:* θ_t is soil moisture (mm);

P_t is incoming surface water—the sum of bulk precipitation or throughfall, upland surface runoff, and surface seeps (mm);

$DrainIn_t$ and $DrainOut_t$ are incoming and outgoing vertical drainage, respectively (mm);

$Q_{SS,In,t}$ and $Q_{SS,Out,t}$ are incoming and outgoing lateral subsurface flows, respectively (soil layers only) (mm);

Es_t is surface evaporation (from litter layer and upper soil layer only) (mm);

Ep_t is transpiration loss (mm);

Up_t is the movement of soil moisture from the water table to the soil layer (mm);

$Q_{S,t}$ is outgoing surface runoff (mm); and

$DeepSeep_t$ is seepage of saturated water from the lowest soil layer (mm).

Surface Runoff

Surface runoff is assumed to be generated when the sum of rainfall and upslope runoff depth exceeds the infiltration capacity. Excess runoff under these conditions is called "infiltration excess overland flow." Surface runoff is also assumed to be generated when the topmost soil layer is already saturated and cannot accept any additional water. Runoff generated under these circumstances is called "saturation overland flow." Both conditions are explicitly and independently simulated in the model.

Infiltration

Infiltration is estimated using the explicit form of the modified Green-Ampt equation (Stone et al. 1994). The total infiltration depth *F(t)* (in millimeters) for time *t* is given by—

$$F(t) = \psi\ (\eta - \theta)\ F_q^*(t_c^*) \quad [2.2]$$

where:

ψ is the average wetting front capillary potential (mm),

θ is the soil moisture content (mm),

η is the effective porosity (mm), and

$F^*_q(t_c^*)$ is the dimensionless infiltration depth, which is given by—

$$F_q^*(t_c^*) = t_c^* + \sqrt{2t_c^*} - 0.2987 t_c^{*0.7913} \quad [2.3]$$

where:

t_c^* is the dimensionless time computed using—

$$t_c^* = \frac{K_s(t+t_s-t_p)}{\psi(\eta-\theta)} \quad [2.4]$$

where:

K_s is the saturated vertical conductivity (mm s^{-1}),

t_p is the time to ponding (s), and

t_s is time shift parameter (s) given by—

$$t_s = \frac{F_{pp} - \left(\psi \ln\left[1+\frac{F_{pp}}{\eta-\theta}\right]\right)}{K_s} \quad [2.5]$$

where:

F_{pp} is the infiltration depth (mm) prior to ponding given by—

$$F_{pp} = R \times t_p \quad [2.6]$$

where:

R is the rainfall rate (mm s^{-1}).

The time to ponding t_p is given by—

$$t_p = \frac{K_s \psi (\eta-\theta)}{R(R-K_s)} \quad [2.7]$$

Surface Runoff Routing

Since REMM is essentially a mass balance model and since hydrologic computations are performed on a daily time step, a detailed surface runoff routing scheme is not included. Field investigations, though, show that surface runoff generated from fields during high-intensity rainfall events can have sufficient depth and velocity to traverse a significant distance down the riparian

slope before being lost to infiltration (Sheridan et al. 1996). This becomes especially significant when upland runoff enters the riparian zone as channelized or concentrated flow. To account for this phenomenon, a simple routing scheme, limited to upland runoff, is used in REMM. This scheme allows incoming upland runoff to be distributed down the riparian slope based on its depth and flow velocity. The distributed depth is then summed with throughfall for infiltration computations. The routing procedure is limited to incoming runoff. Runoff generated within the riparian area by infiltration excess overland flow or saturation overland flow is not subjected to routing. In future versions of REMM (when event simulations will be performed on a smaller time step) a more detailed runoff routing scheme will be used.

The upland runoff routing procedure assumes that runoff enters the riparian area as a rectangular slug with the length of the slug defined by the duration of flow and the volume of the slug defined by the total runoff excess. The duration of runoff is estimated as a function of the upslope drainage area/field and is based on the equation developed by Young et al. (1987):

$$t_{flowdur} = (1/6) \times RF \times \frac{A}{Q_p} \quad [2.8]$$

where:

$t_{flowdur}$ is flow duration (s),

RF is runoff depth (mm),

A is the upslope drainage area (ha), and

Q_p is the peak flow ($m^3\ s^{-1}$).

Equation 2.8 gives the duration of flow of the upland runoff at the upslope edge of the riparian buffer. To determine the movement of the slug down the slope, the time of concentration for each zone is computed by (Kerby 1959)—

$$T_c = 60.0 \times \left[\frac{2.2 \times n \times L}{\sqrt{S}}\right]^{0.467} \quad [2.9]$$

where:

T_c is the time of concentration (s),

n is the mannings roughness for the surface (unitless),

L is the length of the zone (m), and

S is the zone slope ($m\ m^{-1}$).

Comparison of the upland runoff duration and the time of concentration for each of the zones provides a measure of the distance of movement of upland surface runoff.

Vertical and Lateral Subsurface Movement

Subsurface drainage in both the vertical and lateral (downslope) directions is simulated by REMM. Vertical subsurface drainage is simulated as gravitational drainage between horizons and as deep groundwater seepage from the lower layer. Lateral subsurface processes include subsurface movement between zones as well as saturation excess seepage flows.

Vertical Drainage

Vertical unsaturated conductivity is simulated as a function of the soil moisture content given by Campbell's (1974) equation:

$$\frac{K(\theta)}{K_s} = \left(\frac{\theta}{\phi}\right)^{3 + 2/\lambda} \qquad [2.10]$$

where:

θ is the soil moisture (mm),

$K(\theta)$ is the unsaturated hydraulic conductivity corresponding to θ (mm hr^{-1}),

K_s is the saturated hydraulic conductivity (mm hr^{-1}),

ϕ is porosity (mm), and

λ is defined as the pore size distribution index for the soil (unitless).

The equation given above is based on the soil moisture characteristic curve. The shape of the moisture curve is included in the parameter λ. REMM requires that the user provide values of K_s, ϕ, and λ describing the soil moisture curves. Rawls and Brakensiek (1985) provide estimates for parameters describing moisture curves for different soil types.

Vertical Drainage in Presence of a Water Table

In the presence of a shallow water table, overlying soil layers are maintained at a higher (less negative) matric potential and consequently higher soil moisture contents (assuming that the soil layers are in equilibrium with the water table). This phenomenon is more significant where the water table is within 1–3 m of the soil layer. Assuming that the soil layer is in equilibrium with the water table, the matric potential (expressed in meters) at any point *p* within a soil layer can be approximated by the height *(z)* of the point above the water table (in meters). The moisture associated with *p* can then be determined using *z* and the moisture retention curve relating matric potential to the soil moisture content (based on

the assumption that *p* is in equilibrium with the water table). Using Campbell's equations, the relation between the matric potential and the soil moisture content is given by—

$$\frac{\theta}{\phi} = \left[\frac{H_b}{h}\right]^{\lambda} \qquad [2.11]$$

where:

H_b is the bubbling pressure head for the soil (mm), and

h is the matric potential (mm).

Upward Flux From a Shallow Water Table

In the absence of a shallow water table, evapotranspiration losses from a soil layer are limited to the soil moisture conditions within the soil layer (moisture loss occurs until wilting point moisture content for the layer is reached). However, in the presence of a shallow water table (1–3 m below the soil layer), a steady upward flux will occur from the water table to the soil layer to replenish evapotranspiration losses from the layer. This upward flux occurs in response to the gradient of matric potentials between the soil layer and the surface of the water table. The rate of upward water movement is determined by the matric potential gradient, unsaturated hydraulic conductivity, and depth of the water table below the soil layer. This evapotranspiration flux at point *p,* at distance *z* above the water table, can be described using the Darcy Buckingham equation given by Skaggs (1978):

$$\frac{\partial h}{\partial z} = \frac{E}{K(h)} + 1 \qquad [2.12]$$

where:

h is the matric potential or capillary suction (mm),

z is the distance (in meters) of the point from the water table (positive upward),

$\frac{\partial h}{\partial z}$ expresses the gradient of matric potential,

E is the upward flux of water from the water table (mm), and

$K(h)$ is the unsaturated hydraulic conductivity of the soil layer expressed as a function of the matric potential h (mm hr^{-1}).

The equation describing the relation between h and $K(h)$ can be expressed by—

$$\frac{K(h)}{K_s} = \left[\frac{H_b}{h}\right]^{3\lambda + 2} \qquad [2.13]$$

where:

K(h) is the vertical unsaturated conductivity corresponding to soil matric potential (mm hr^{-1}), and

the other terms are as defined earlier.

Equations 2.12 and 2.13 are solved using numerical procedures to yield values of upward flux corresponding to varying water table depths (Skaggs 1978).

Deep Seepage

Vertical drainage of shallow ground water from the lower horizon (alluvial storage) of REMM is considered deep groundwater seepage. The rate of downward movement from the lower layer is constrained by the maximum rate of transmission through deeper confining layers. The potential rate of deep seepage is indicated by saturated conductivities of confining horizons, and available estimates are input by the user for each zone.

Lateral Subsurface Movement

Subsurface movement of water downslope within the riparian buffer system $(Q_{SS,t})$ is computed using Darcy's equation:

$$Q_{SS,t} = -K \times a_t \frac{h_t}{L} \qquad [2.14]$$

where, on day *t:*

K is the soil hydraulic conductivity (m day^{-1}),

a_t is the saturated cross-sectional area of the soil horizon (m^2),

h_t is the difference in water surface elevations between two zones (m), and

L is the horizontal flow distance, calculated as the distance between centers of two adjacent zones (m).

Rates of lateral subsurface movement between zones are constrained by the lesser of the respective hydraulic conductivities for the donor and recipient soil horizon compartments. Testing of REMM has shown that saturated hydraulic conductivity determined from well pump tests is appropriate. If computed rates of soil water movement for the upslope compartment exceed transmission rates for the downslope recipient compartment, the soil water excess is accumulated in

the upslope compartment until it is saturated. Then a seep will occur to the surface of the downslope zone. Subsurface water that is moved downslope is removed from the appropriate upslope soil layer and moved to the lowest soil layer that is not saturated in the downslope zone.

In addition to lateral subsurface movement between zones, two special cases of lateral subsurface flow are also treated by REMM: (1) external subsurface inputs from upslope contributing areas and (2) subsurface losses from the buffer system to the drainage network or other downslope water body.

Subsurface hydrologic inputs to zone 3 from upslope contributing areas are provided by the user. The REMM hydrology module assumes that the potential gradient above zone 3 is equal to the zone 3 surface slope. The maximum allowable rate of subsurface movement into zone 3 is then calculated using Darcy's equation. If user-supplied subsurface inputs to REMM zone 3 exceed the potential rate of subsurface lateral movement into the zone 3 soil profile or if the volume of subsurface movement exceeds available storage within the zone 3 profile, the excess water is treated as surface seepage input to zone 3.

Lateral subsurface losses from the riparian system to the stream or water body are also computed using Darcy's equation. The potential gradient for subsurface losses to the stream is assumed to be equal to the smaller of the surface slope of zone 1 and the gradient from the water table elevation at the midpoint of zone 1 to the stream thalweg. At this time the thalweg elevation is a user input. A future version of the model will include dynamic simulation of the stream water surface elevation which will allow modeling stream recharge of zone 1.

References

Campbell, G.S. 1974. A simple method for determining unsaturated conductivity from moisture retention data. Soil Science 117:311–314.

Kerby, W.S. 1959. Time of concentration for overland flow. Civil Engineering (N.Y.) 29:174.

Rawls, W.J., and D.L. Brakensiek. 1985. Prediction of soil water properties for hydrologic modeling. *In* E.B. Jones, ed., Watershed Management in the Eighties, pp. 293–299. American Society of Civil Engineers.

Sheridan, J.M., R.R. Lowrance, and H.H. Henry. 1996. Surface flow sampler for riparian studies. Applied Engineering in Agriculture 12(2):183–188.

Skaggs, R.W. 1978. A water management model for shallow water table soils. Water Resources Research Institute, University of North Carolina Report No. 134.

Stone, J.J., R.H. Hawkins, and E.D. Shirley. 1994. Approximate form of the Green Ampt infiltration equation. Engineering Journal of Irrigation and Drainage 120(1):128–137.

Young, R.A., C.A. Onstad, D.D. Bosch, and W.P. Anderson. 1987. AGNPS: Agricultural Non-Point Source Pollution Model. U.S. Department of Agriculture, Conservation Research Report No. 35.

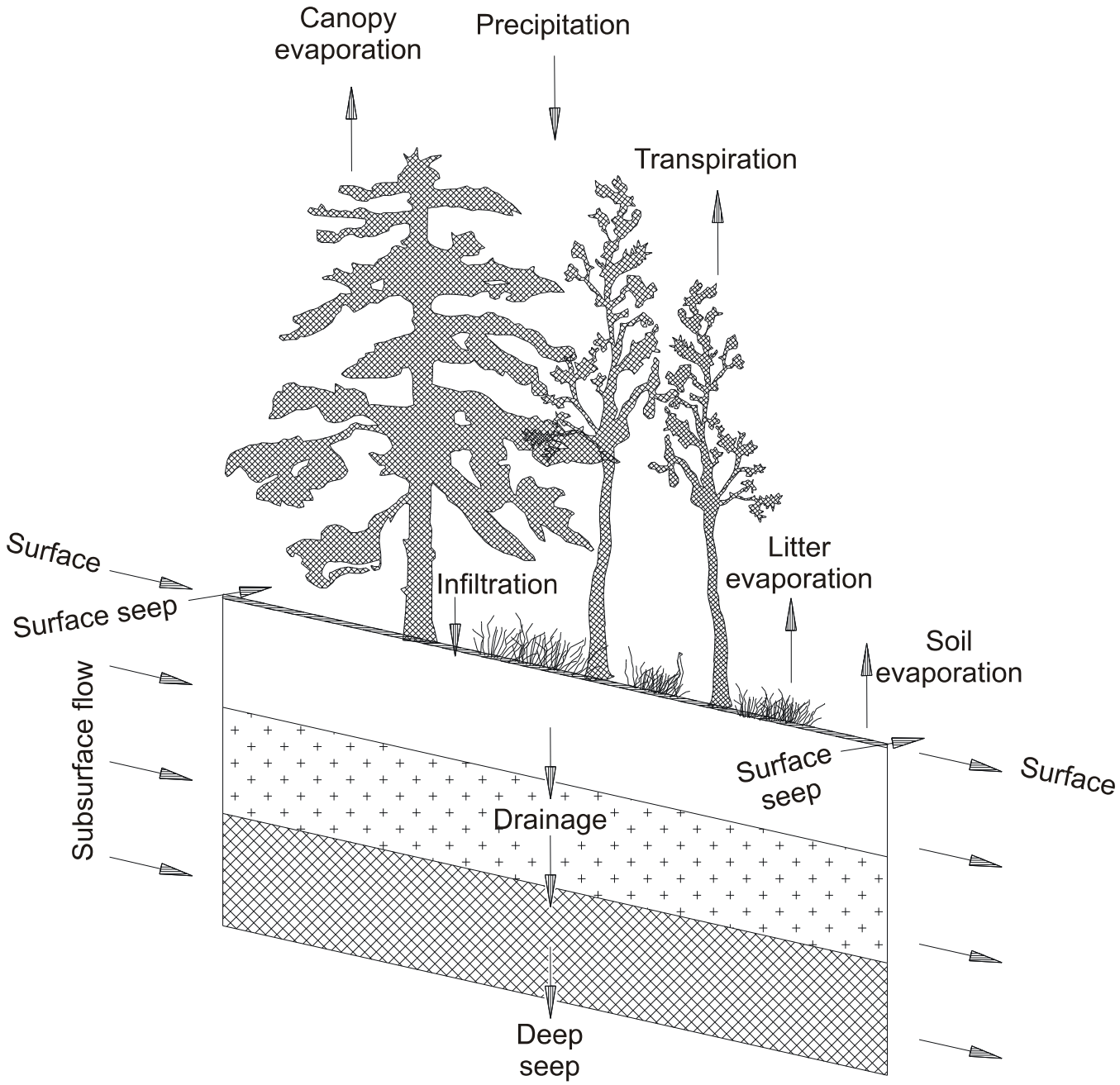

Figure 2.1. Water movements simulated in REMM

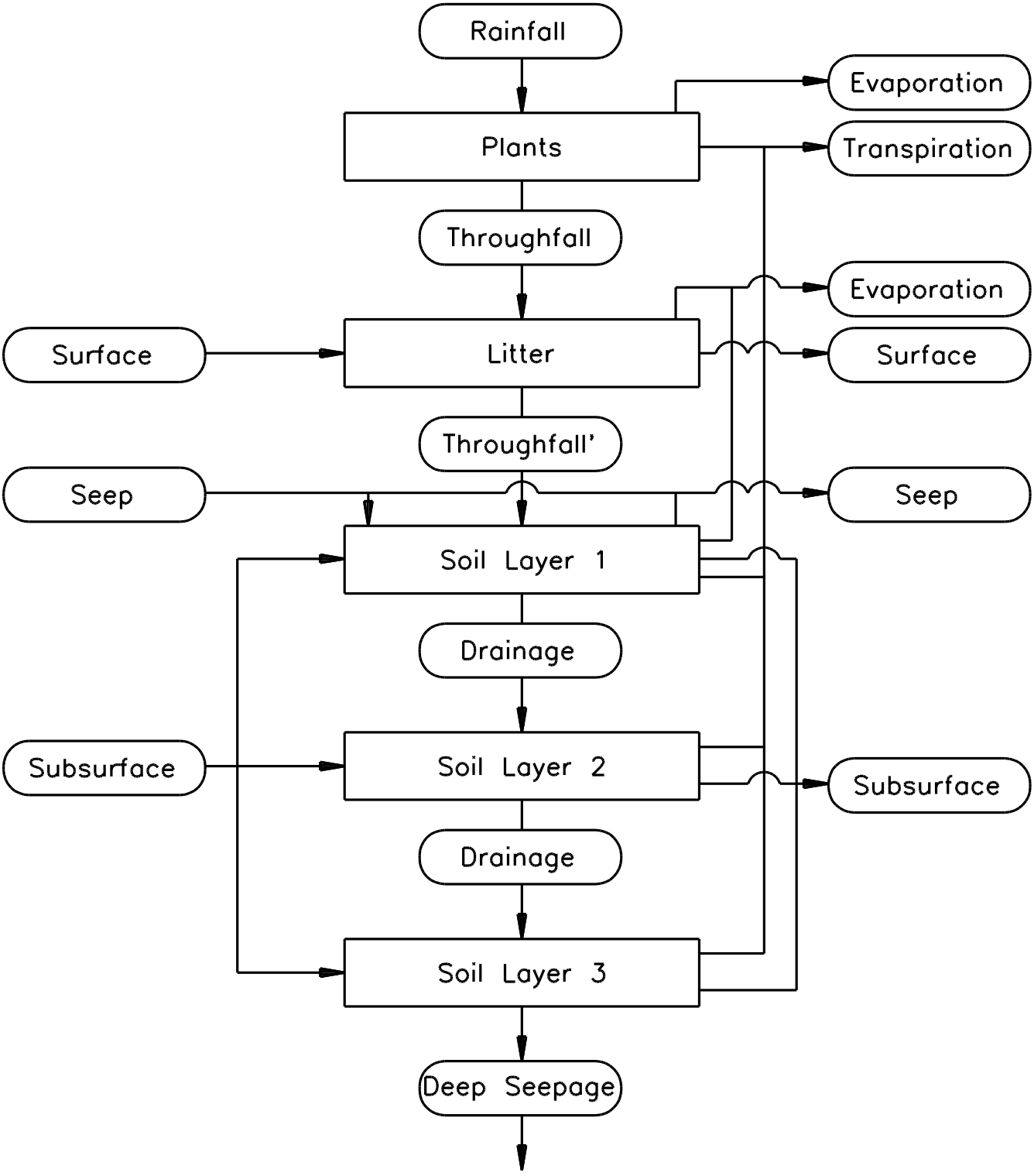

Figure 2.2. REMM water balance components for a single zone of the buffer system

Chapter 3
Hydrology: Interception and Evapotranspiration

Lee S. Altier and Randall G. Williams

Summary

Interception and evapotranspiration are the portions of the hydrologic cycle which are largely controlled by interactions among the plant community, precipitation amounts and patterns, and soil moisture availability. REMM simulates interception and evapotranspiration based on the leaf area index of the vegetation and the amount of water available for evapotranspiration in the soil and stored on leaf surfaces. Evapotranspiration, calculated from the Penman-Monteith equation, is constrained by the absence of roots in a soil layer and by appropriate soil factors such as hydraulic conductivity and wilting point. Evaporation from the soil is calculated in two stages depending on the soil moisture level.

Interception

Before precipitation reaches the soil surface, it is subject to interception by plant canopies and surface litter. Water balance computations would be significantly in error if evaporative losses of intercepted moisture were not included (Singh and Szeicz 1979). In forested areas, the Riparian Ecosystem Management Model (REMM) simulates two canopies at different heights above the ground surface, each comprising one or more species. The mass balance of water on leaf surfaces is computed as a function of interception and evaporation:

$$LeafWat_{v,c,t} = LeafWat_{v,c,t-1} - LfEvap_{v,c,t} + Int_{v,c,t} \quad [3.1]$$

where for vegetation type *v* in canopy *c* on day *t:*

$LeafWat_{v,c,t}$ is water on leaf surfaces (mm),

$LfEvap_{v.c.t}$ is evaporation of water on leaf surfaces (equation 10.35) (mm), and

$Int_{v,c,t}$ is intercepted moisture (mm).

Calculation of interception losses is based on a relationship by Thomas and Beasley (1986) that allows some of the water during a rainfall event to reach the soil surface, even if total precipitation is less than the interception capacity of the canopy. The equation of Thomas and Beasley was modified so that interception is not a linear function of canopy storage capacity (figure 3.1). Rather, for low amounts of rainfall, an immature canopy with a small leaf area index will intercept a relatively small proportion of rainfall compared to a full canopy:

$$Int_{v,c,t} = (CanFrac_{v,c,t} \times CSC_{v,c,t} - LeafWat_{v,c,t-1}) \times (1 - \exp(-Precip_{c,t} \times (CSC_{v,c,t} / PIT_v)^2)) \quad [3.2]$$

where for vegetation type *v* in canopy *c* on day *t:*

$Int_{v,c,t}$ is intercepted moisture (mm);

$CanFrac_{v,c,t}$ is the fraction of canopy occupied by the vegetation type (see section on light in chapter 10);

$CSC_{v,c,t}$ is interception storage, based on leaf area index, unadjusted for stand density (mm);

$Precip_{c,t}$ is precipitation (mm); and

PIT_v is the potential canopy storage capacity for the species at maximum leaf area index in a monocropped stand (mm).

Values for canopy storage capacities are calculated by—

$$CSC_{v,c,t} = LAI_{v,c,t} \times CSR_v \quad [3.3]$$

$$PIT_v = MaxLAI_v \times CSR_v \quad [3.4]$$

where for vegetation type *v:*

$LAI_{v,c,t}$ is leaf area index in canopy *c* on day *t* (m^2 m^{-2}),

MaxLAI is the maximum LAI attainable by a monocropped stand of a given species, and

CSR is the canopy storage capacity per leaf area index (mm).

The interception storage capacity is a function of leaf area index and species (herbaceous, conifer, or deciduous). Burgy and Pomeroy (1958) measured interception storage capacities of 1.0 to 1.2 mm for 25-cm-tall grass mixtures. The interception storage capacity for conifers is greater than that for deciduous trees in full leaf (Lull 1964). Lull suggests that vegetation can hold from 0.25 to 1.27 mm of water.

A more accurate estimate of interception loss would include a factor for evaporation during the rainfall event, since the evaporation occurring from the foliage during that time would have the effect of increasing the total intercepted moisture (Lull 1964). However, with a daily time step and a lack of data about duration of rainfall events in weather records, that approach is not feasible. It is assumed that when snow is intercepted in the canopy, only an amount of water equal to Int_t is held in the canopy.

Available precipitation for interception in equation 3.3 is reduced as it is intercepted by each succeeding canopy:

$$Precip_{c,t} = \begin{cases} Precip_t & \text{Upper canopy} \\ Precip_t - \sum_{c=1}^{c-1} \sum_{v=1}^{n} Int_{c,v,t} & \text{Lower canopies} \end{cases} \quad [3.5]$$

As with the plant canopies, interception of moisture in the litter layer occurs as incoming water fills the available moisture storage capacity of the litter. Letz (1958) found that a 5-cm layer of undecomposed pine needles (dry weight = 9.64 Mg ha^{-1}) could hold about 0.8 cm of moisture. The storage capacity of the litter is defined as the sum of the capacities of its component materials:

$$\theta_{cap,t} = 2.5\,(CRes_t \times WCap_{res} + CHum_t \times WCap_{hum}) + Mineral_t \times 10^6 \times FC_{Lyr1} / BD_{Mineral,t} \quad [3.6]$$

where

in the litter layer on day *t:*

$\theta_{cap,t}$ is the water content at full capacity (mm);

2.5 converts the weight of carbon to weight of biomass (assumed ratio of 0.4);

$WCap_{res}$ and $WCap_{hum}$ are water holding capacities for residue and humus, respectively (mm kg^{-1} biomass);

$CRes_t$ and $CHum_t$ are carbon in residue and humus material, respectively (kg ha^{-1});

$Mineral_t$ is mineral material (kg ha^{-1});

$BD_{Mineral,t}$ is bulk density of mineral material (kg m^{-3}); and

FC_{Lyr1} is field capacity of soil in layer 1 (mm).

All of the throughfall remaining after canopy interception, as well as incoming surface runoff, are assumed to be available for filling the moisture storage capacity of the litter layer. The incoming water is assumed to mix completely with the litter, so that there is no vertical drainage to the upper soil layer until the litter layer capacity is filled. All incoming water in excess of storage capacity is

assumed to move out of the litter immediately, either by infiltrating into the soil or as runoff into the next zone. Because of relatively large spaces within litter material, it is assumed that there is no subsequent gravitational drainage out of the litter.

Evapotranspiration

In REMM, potential evapotranspiration is computed using the Penman-Monteith equation. Evapotranspiration simulations are distinguished into two stages. If previously intercepted water is available on the vegetative canopy, evaporation of the intercepted water occurs first and transpiration losses do not occur. This represents the first stage of the simulation. During the first stage, all of the radiant energy is used to evaporate intercepted water. Transpiration is assumed to occur only after all moisture on the plant leaves has been evaporated. The leaf moisture balance is a function of interception and evaporation:

$$LeafWat_{v,c,t} = LeafWat_{v,c,t-1} + Int_{v,c,t} - E_{Lvs,v,c,t} \quad [3.7]$$

where for vegetation *v* of canopy *c* on day *t:*

$LeafWat_{v,c,t}$ is moisture on leaf surfaces (mm), and

$E_{Lvs,v,c,t}$ is evaporation of leaf surface moisture (mm).

Evaporation of moisture from leaves (E_{lvs}) is based on estimates of potential leaf transpiration:

$$E_{lvs,c,v,t} = \text{Maximum of} \begin{cases} 0 \\ LeafWat_{v,c,t-1} + Int_{v,c,t} - PLE_{v,c,t} \end{cases} \quad [3.8]$$

where:

$PLE_{v,c,t}$ is potential leaf surface evaporation from vegetation *v* in canopy *c* on day *t*.

Potential leaf evaporation $PLE_{v,c,t}$ (mm day^{-1}) is then given by (Running and Coughlan 1988)—

$$PLE_{v,c,t} = \frac{LAI_{v,c,t}}{LT_t} \left[\frac{Slope_t \times NRad_{cv,,t} \times 10^{-3} + \frac{PA_t \times CP \times VPD_t}{RA_{v,c,t}}}{Slope_t + \gamma_t} \right] \quad [3.9]$$

where:

$NRad_{v,c,t}$ is the net radiation (kJ m^{-2} day^{-1}),

$LAI_{v,c,t}$ is the canopy leaf area index on day *t,*

LT_t is the latent heat of vaporization (MJ kg^{-1}),

$Slope_t$ is the slope of the saturation vapor pressure curve (kPa ˚C^{-1}),

γ_t is the psychrometric constant (kPa),

$RA_{v,c,t}$ is the aerodynamic resistance (s m^{-1}),

PA_t is the air density (kg m^{-3}),

VPD_t is the vapor pressure deficit (kPa), and

CP is the specific heat of air at constant pressure, taken as 1.01 kJ kg^{-1} K^{-1}.

While computing potential evaporation the stomatal resistance term in the Penman-Monteith equation is neglected and assumed to be 0. Psychrometric constant γ_t (kPa) is given by—

$$\gamma_t = 0.1\ [0.646 + 0.0006 \times TAir_{Ave,t}] \qquad [3.10]$$

where:

$TAir_{Ave,t}$ is the daily average temperature (ºC).

Latent heat of vaporization LT_t (MJ kg^{-1}) is—

$$LT_t = 2.501 - 0.0024 \times TAir_{Ave,t} \qquad [3.11]$$

Aerodynamic resistance $RA_{v,c,t}$ (s m^{-1}) is computed using—

$$RA_{v,c,t} = \frac{\left[\ln\left(\frac{h_v + 2 - 0.67h_v}{0.123h_v}\right) \times \ln\left(\frac{h_v + 2 - 0.67h_v}{0.0123h_v}\right)\right]}{0.41^2\ U_r} \qquad [3.12]$$

where:

h_v is the vegetation height (m), and

U_r is the wind velocity for the day (m s^{-1}).

Air density PA_t (kg m^{-3}) is given by—

$$PA_t = 1.292 - 0.00428 \times TAir_{Ave,t} \quad [3.13]$$

Slope of the saturation vapor pressure curve $Slope_t$ (kPa $^oC^{-1}$) is given by—

$$Slope_t = \frac{4098\ ES_t}{237 + TAir_{Ave,t}} \quad [3.14]$$

where:

ES_t is the saturation vapor pressure (kPa) given by—

$$ES_t = 0.6108\ e^{\frac{17.27\ TAir_{Ave,t}}{237.3+TAir_{Ave,t}}} \quad [3.15]$$

The saturation vapor pressure *EStdew* at dew point temperature *Tdew* (°C) is computed by—

$$EStdew = 0.6108\ e^{\frac{17.27\ Tdew}{237.3+Tdew}} \quad [3.16]$$

The vapor pressure deficit VPD_t (kPa) is then given by—

$$VPD_t = ES_t - EStdew \quad [3.17]$$

Absolute humidity deficit *(ABSHD)* is computed using—

$$ABSHD_t = 0.000217\ VPD_t \times 10.0 \times (TAir_{Ave,t} + 273.16) \quad [3.18]$$

During the second stage, potential plant transpiration $PT_{v,c,t}$ (mm day^{-1}) is computed using—

$$PT_{v,c,t} = \frac{LAI_{v,c,t}}{LT_t}\left[\frac{Slope_t \times NRad_{v,c,t} \times 10^{-3} + \frac{PA_t \times CP \times VPD_t}{RA_{v,c,t}}}{Slope_t + \gamma_t \times \left[1 + \frac{RS_{v,c,t}}{RA_{v,c,t}}\right]}\right] \quad [3.19]$$

where:

$RS_{v,c,t}$ is the stomatal resistance (s m^{-1}).

The energy required for evaporation of intercepted moisture on the plant canopy decreases energy that would otherwise drive transpiration (Lull 1964). Net potential transpiration is determined after reducing potential transpiration by a

proportion of leaf surface evaporation. If moisture on the plant leaves is greater than $PLE_{v,c,t}$, there will be no transpiration on that day:

$$NetPT_{v,c,t} = \begin{cases} 0 & LeafWat_{v,c,t} \geq PLE_{v,c,t} \\ PT_{v,c,t} \times \left(1 - \frac{LeafWat_{v,c,t}}{PLE_{v,c,t}}\right) & PLE_{v,c,t} > LeafWat_{v,c,t} \end{cases} \quad [3.20]$$

where in canopy c for vegetation type v on day t:

$NetPT_{v,c,t}$ is net potential transpiration after evaporation of intercepted moisture on plant canopy (mm), and

$PT_{v,c,t}$ is estimate of potential transpiration before taking into account the evaporation of intercepted leaf moisture (mm).

Actual transpiration is limited by the availability of moisture in the soil and competition among the roots of the various plant types present. Transpiration losses from each soil layer are determined by proportions of root masses and the soil hydraulic conductivity as discussed in the following section.

Root Distribution and Water Uptake

Whitehead and Jarvis (1981) pointed out that when soil water content is high, plant uptake of water from different soil layers is a function of root distribution. As the soil dries, water extraction depends on both the root distribution and soil water content. Ritchie (1973) noted that when moisture has been depleted from an upper layer of soil, roots in deeper layers can maintain transpiration at potential rates if water is sufficient at deeper depths. Measurements of transpiration in *Pinus sylvestris* by Rutter (1967) indicated that even a small proportion of deep roots reaching water may be sufficient to prevent moisture stress.

Available moisture in soil layers is partitioned among the roots of each plant type according to equation 3.21. Water uptake is allocated among the soil layers from the surface downward. The maximum rate of water uptake from a layer is limited by its hydraulic conductivity, which corresponds to the soil moisture from the previous day. This allows any excess demand that is not realized by a layer to be transferred to the layer below. Water uptake by each plant type from a given soil layer is determined by multiplying available water by the proportion of total demand allocated for that plant type and soil layer combination:

$$WUptk_{v,c,j,t} = \text{Minimum of} \begin{cases} K(\theta)_{j,t} \\ \theta_{A,j,t} \times \dfrac{RPotTrans_{v,c,j,t} \times AdjMRF_{v,c,j,t}}{\sum_{v=1}^{m}\sum_{c=1}^{n}(RPotTrans_{v,c,j,t} \times AdjMRF_{v,c,j,t})} \end{cases} \quad [3.21]$$

where, for day *t:*

$WUptk_{v,c,j,t}$ is water uptake by vegetation *v* in canopy *c* from soil layer *j* (mm),

$K(\theta)_{j,t}$ is soil hydraulic conductivity defined by Campbell's equation for soil layer *j* (mm),

$RPotTrans_{v,c,j,t}$ is remaining potential transpiration demand by vegetation *v* in canopy *c* from soil layer *j* after water has been taken up from the upper soil layers (mm), and

$AdjMRF_{v,c,j,t}$ is a moisture factor adjusted for the fraction of the root mass of vegetation *v* from canopy *c* in soil layer *j* relative to its roots in the other layers and relative to all other roots in layer *j* (0–1 scalar).

$\theta_{A,j,t}$ is available water in soil layer *j* (mm):

$$\theta_{A,j,t} = \begin{cases} 0 & \theta_{j,t} < \theta_{WP} \\ \theta_{j,t} - \theta_{WP} & \theta_{WP} \le \theta_{j,t} \end{cases} \quad [3.22]$$

where:

$\theta_{j,t}$ is soil water in soil layer *j* on day *t*, (mm), and

θ_{WP} is soil water content at wilting point (mm).

So, for the first soil layer below the surface, the transpiration demand for a given plant type is equivalent to the total transpiration potential of that plant type. In succeeding layers, *RPotTrans* is reduced by the sum of uptake by all vegetation from upper layers:

$$RPotTrans_{v,c,j,t} = \begin{cases} NetPT_{v,c,t} & Layer\ 1 \\ NetPT_{v,c,t} - \sum_{j=1}^{j-1} WUptk_{j,t} & Layers\ 2,3 \end{cases} \quad [3.23]$$

The appropriate proportions of total water uptake demand are calculated as a function of a moisture factor adjusted for root mass fractions:

$$AdjMRF_{v,c,j,t} = MRF_{v,c,j,t} \times RFL_{v,c,j,t} / \sum_{v=1}^{m} \sum_{c=1}^{n} (MRF_{v,c,j,t} \times RFL_{v,c,j,t}) \quad [3.24]$$

$$MRF_{v,j,t} = MF_{j,t} \times RFV_{v,j,t} / \sum_{j}^{3} (MF_{j,t} \times RFV_{v,j,t}) \quad [3.25]$$

where, on day *t:*

$MRF_{v,c,j,t}$ is a moisture factor adjusted for the fraction of the root mass of vegetation *v* of canopy *c* in layer *j* relative to its roots in the other layers (0–1 scalar),

$RFV_{v,c,j,t}$ is the fraction of the root mass of vegetation *v* in canopy *c* that is in soil layer *j* relative to all other roots in layer *j*,

$MF_{j,t}$ is a moisture factor for layer *j* (0–1 scalar), and

$RFL_{v,c,j,t}$ is the fraction of the root mass of vegetation *v* in canopy *c* that is in soil layer *j* relative to its roots in the other layers.

The soil moisture factor *(MF)* represents the decreasing rate of transpiration that occurs as soil dries out (Hanks and Ashcroft 1980). It would be desirable to have this factor change during each day as evapotranspiration withdraws moisture from the soil layers, since it represents the influence of stomatal activity as well as rates of moisture diffusion to the roots. However, with a daily time step, it is calculated as a function of soil moisture status at the end of the previous day. The following relationship was used in the model as an approximation (Kanemasu et al. 1976):

$$MF_{j,t} = \text{Minimum of} \begin{cases} 1 \\ (\theta_{t-1} - \theta_{WP}) / (D\,(\theta_{FC} - \theta_{WP})) \end{cases} \quad [3.26]$$

where:

θ_{t-1} is soil moisture at the end of day *t*–1 (mm);

θ_{WP} is soil moisture at wilting point (mm),

θ_{FC} is soil moisture at field capacity (mm), and

D is a factor specific to the soil type that determines the influence of limiting soil water on evapotranspiration loss.

Litter and Soil Evaporation

Potential litter evaporation *PLitE* (mm day^{-1}) is—

$$\mathrm{PLitE}_t = \frac{1}{LT_t}\left[\frac{Slope_t \times NRad_{litter} \times 10^{-3} + \frac{PA_t \times CP \times VPD_t}{100.00}}{Slope_t + \gamma_t}\right] \quad [3.27]$$

where:

$NRad_{litter}$ is the radiation reaching the litter surface (kJ m^{-2} day^{-1}).

The actual litter evaporation $E_{ltr,t}$ though is limited by the moisture stored in the litter and is given by—

$$E_{Ltr,t} = \text{Minimum of}\begin{cases} PLitE_t \\ \theta_{Ltr,t-1} \end{cases} \quad [3.28]$$

Potential soil evaporation $PSE_{s,t}$ (mm day^{-1}) is—

$$\mathrm{PSE}_{s,t} = \frac{1}{LT_t}\left[\frac{Slope_t \times NRad_{soil} \times 10^{-3} + \frac{PA_t \times CP \times VPD_t}{100.00}}{Slope_t + \gamma_t}\right] \quad [3.29]$$

where:

$NRad_{soil}$ is the radiation reaching the soil surface (kJ m^{-2} day^{-1}).

The radiation reaching the soil surface is computed by multiplying the radiation reaching the litter surface by a litter blocking factor.

On each day, evaporative losses are removed only from the litter layer and upper soil layer. Based on studies by Gardner and Hillel (1962), evaporation from the soil is calculated in two stages. During conditions of high soil moisture content (stage 1), evaporation from the soil surface is limited only by the energy reaching the soil, and evaporation will equal potential evaporation (Bond and Willis 1970). This stage is represented by equation 3.30a:

$$E_{s,t} = \begin{cases} PSE_{s,t} & \left[\theta_{t-1} - PSE_{s,t}\right] > \theta_{S2} \quad [3.30a] \\ PSE_{s,t} - 0.4\,(\theta_{t-1} - \theta_{S2}) & \theta_{t-1} > \theta_{S2} > \left[\theta_{t-1} - PSE_{s,t}\right] \quad [3.30b] \\ \text{Minimum of} \begin{cases} PSE_{s,t} \\ \alpha_s i^{1/2} - \alpha_s (i-1)^{1/2} \end{cases} & \theta_{S2} \geq \theta_{t-1} \quad [3.30c] \end{cases}$$

where:

$E_{s,t}$ is evaporation from the upper soil layer on day t (mm),

θ_{S2} is soil moisture content at the beginning of stage 2 evaporation (mm),

α_s is a coefficient related to hydrologic properties of the soil, and

i is a coefficient related to the stage of evaporation.

As soil dries, the rate of moisture diffusion can reduce evaporation from the soil surface. The second stage of evaporation begins when the potential evaporation rate exceeds the rate of diffusion through the soil. For days when there is a transition from stage 1 to stage 2, evaporation is calculated as in equation 3.30b (Ritchie 1972). At this point, evaporation depends largely on properties of the soil rather than on potential evapotranspiration. However, the rate of evaporation is not allowed to exceed that of potential evaporation. Calculation of evaporation during stage 2 (equation 3.30c) is based on a time-dependent relationship determined from studies of evaporation from bare soil (Black et al. 1969, Ritchie 1972).

Using the approach from Smith and Williams (1980), the cutoff between stage 1 and stage 2 evaporation is defined by—

$$\theta_{S2} = \theta_{FC} - U \quad [3.31]$$

where:

U is the reduction in soil moisture below field capacity that can occur before the rate of diffusion inhibits evaporation from the soil surface (mm):

$$U = 9(\alpha_s - 3)^{0.42} \quad [3.32]$$

Ritchie (1972) pointed out that α_s values are approximately proportional to measured values of hydraulic conductivity of soil at –0.01 MPa soil matric potential (table 3.1).

The value of *i* in equation 3.30c represents a time factor corresponding to cumulative evaporation during stage 2 (Black et al. 1969). For the purposes of REMM, where the moisture status of the soil is simulated as the net effect of several pathways, the value of *i* is interpreted as being a function of the total upper soil layer water deficit below the cutoff for stage 2:

$$i = \left(\frac{\theta_{S2} - \theta_t}{\alpha_s} \right)^2 \qquad [3.33]$$

References

Black, T.A., W.R. Gardner, and G.W. Thurtell. 1969. The prediction of evaporation, drainage, and soil water storage for a bare soil. Soil Science Society of America Proceedings 33:655–660.

Bond, J.J., and W.O. Willis. 1970. Soil water evaporation: first stage drying as influenced by surface residue and evaporation potential. Soil Science Society of America Proceedings 34:924–928.

Burgy, R.H., and C.R. Pomeroy. 1958. Interception losses in grassy vegetation. Transactions of the American Geophysical Union 39:1095–1100.

Gardner, W.R, and D.I. Hillel. 1962. The relation of external evaporative conditions to the drying of soils. Journal of Geophysical Research 67:4319–4325.

Hanks, R.J., and G.L. Ashcroft. 1980. Applied soil physics. Springer-Verlag, Berlin.

Kanemasu, E.T., L.R. Stone, and W.L. Powers. 1976. Evapotranspiration model tested for soybean and sorghum. Agronomy Journal. 68:569–572.

LaRue, M.E., D.R. Nielsen, and R.M. Hagan. 1968. Soil water flux below a ryegrass root zone. Agronomy Journal. 60:625–629.

Lull, H.W. 1964. Ecological and silvicultural aspects. *In* Ven Te Chow, ed., Handbook of Applied Hydrology, pp. 6-1–6-30. McGraw-Hill Book Co., New York.

Letz, L.J. 1958. Moisture held in pine litter. Journal of Forestry 56:36.

Ritchie, J.T. 1972. A model for predicting evaporation from a row crop with incomplete cover. Water Resources Research 8:1204–1213.

Ritchie, J.T. 1973. Influence of soil water status and meteorological conditions on evaporation from a corn canopy. Agronomy Journal 65:893–897.

Running, S.W., and J.C. Coughlan. 1988. A general model of forest ecosystem processes for regional applications, I. Hydrologic balance, canopy gas exchange and primary production processes. Ecological Modelling 42:125–154.

Rutter, A.J. 1967. Water consumption by forests. *In* T.T. Koslowski, ed., Water Deficits and Plant Growth, pp. 23–84. Academic Press, London.

Singh, B., and G. Szeicz. 1979. The effect of intercepted rainfall on the water balance of a hardwood forest. Water Resources Research 15:131–138.

Smith, R.E., and J.R. Williams. 1980. Simulation of the surface water hydrology. *In* W.G. Knisel, ed., CREAMS: A Field Scale Model for Chemicals, Runoff, and Erosion From Agricultural Management Systems, pp. 13–35. U.S. Department of Agriculture, Conservation Research Report No. 26.

Thomas, D.L., and D.B. Beasley. 1986. A physically-based forest hydrology model. I: development and sensitivity of components. Transactions of the ASAE 29:962–972.

Van Bavel, C.H.M., G.B. Stirk, and K.J. Brust. 1968. Hydraulic properties of a clay loam soil and the field measurement of water uptake by roots, 1. Interpretation of water content and pressure profiles. Soil Science Society of America Proceedings 32:310-317.

Whitehead, D., and P.G. Jarvis. 1981. Coniferous forests and plantations. *In* T.T. Kozlowski, ed., Water Deficits and Plant Growth, vol. 6, pp. 49–151. Academic Press, New York.

Table 3.1. Hydrologic characteristics of several representative soils

Soil	K* (cm day^{-1})	U† (mm)	α_s‡	Reference
Adelanto clay loam	0.15	12	5.08	Van Bavel et al. 1968
Yolo loam	0.10	9	4.04	LaRue et al. 1968
Houston black clay	0.06	6	3.50	Ritchie 1972
Plainfield sand	0.05	6	3.34	Black et al. 1969

* Hydraulic conductivity at –0.1 bar soil matric potential.

† Limit of stage 1 evaporation below field capacity.

‡ Coefficient for stage 2 evaporation. For the range of hydraulic conductivities represented here, $\alpha_s \approx 2.44 + 1.72$ K.

Source: Ritchie 1972

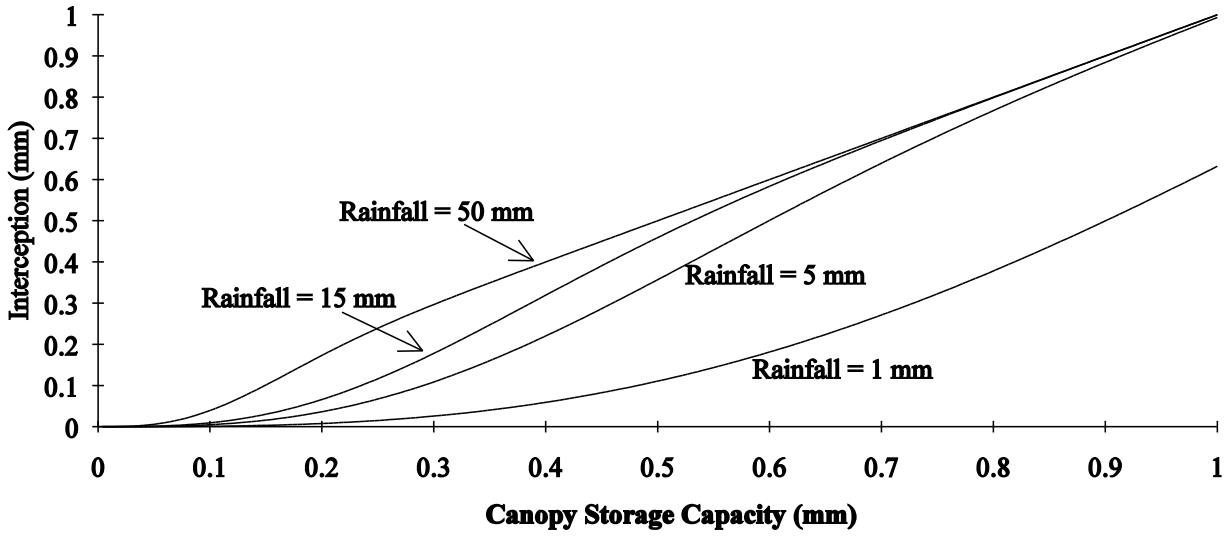

Figure 3.1. Relationship between interception and rainfall for vegetation with a potential interception storage capacity of 1 mm

Chapter 4
Sediment Transport

David D. Bosch, Randall G. Williams, Shreeram P. Inamdar, Lee S. Altier and Richard Lowrance

Summary

Sediment transport through a riparian ecosystem buffer is controlled by the energy available in running water to move soil particles. REMM explicitly simulates the transport phenomena in channel and overland flow areas. Sediment transport processes simulated include erosion, transport, and deposition. For a given zone of the three-zone buffer, if sediment load is greater than transport capacity, deposition will occur. If sediment load is less than transport capacity, then erosion will occur. Because of the roughness of the surface of riparian buffers, it is assumed that sediment transport is primarily of suspended particles. Sediment enrichment ratios for a zone are calculated based on the specific surface area of the incoming and outgoing sediment and are applied to the transport of sediment-bound chemicals in later chapters.

The Riparian Ecosystem Management Model (REMM) explicitly simulates sediment phenomena in channel and overland flow areas. Figure 4.1 illustrates the scheme used to delineate concentrated flow and overland flow areas in REMM. The number of channels across a given zone width is a user input. Channel shape is assumed to be triangular and is constant for the length of the zone. This shape is determined by the channel side slope (which also is the overland flow area slope), which is a user input. Channel length is the same as the zone length. Channel slope and the zone slope are identical. Overland flow areas are areas that lie between adjacent channels. The size of overland flow areas is decided by the zone width and the number of channels. Overland flow areas slope toward the channels, with the overland flow area slope (or channel side slope) being a user input.

Sediment processes that are simulated include erosion, transport, and deposition. Erosion in overland flow areas is assumed to occur as a result of rainfall impact and erosive forces associated with shallow overland flow or sheet runoff. Sediment delivered to channel areas from overland flow areas is then either transported downslope or deposited in the channels. Sediment deposition or transport in channels is decided based on the transport capacity of concentrated or channel flow. In addition to the possibility of sediment being generated within the riparian area by erosion, sediment loadings to the buffer from upland areas are also considered. Upland loadings are assumed to be provided as an input to REMM. The user is expected to generate upland loadings using an upland field model or to use estimates or empirical data. The steady-state sediment continuity equation is used to route sediment within channels and down the riparian slope.

Sediment loading from upland areas and that generated by overland flow erosion is assumed to be distributed in five discrete classes of particle size: sand, large aggregate, small aggregate, silt, and clay. Each class is defined by a fixed uniform particle diameter (table 4.1). Sediment erosion, transport, deposition, and routing is performed for each class. Sediment mass within each particle class for upland loading is a user-defined input. For overland flow erosion, sediment mass in each particle class is based on the primary particle size distribution in the parent soil. The following sections describe each of these processes in detail.

Overland Flow Erosion

Overland flow erosion is computed using the Universal Soil Loss Equation and is given by—

$$A_i = R_i \times K_i \times C_i \times LS_i \times P_i \quad [4.1]$$

where, for zone *i:*

A_i is the sediment yield (ton acre^{-1} day^{-1}),

R_i is the rainfall erosivity (hundreds of foot-tons × inch × acre^{-1} × hour^{-1} × day^{-1}),

K_i is the soil erodibility factor (ton × acre × hour × hundreds of acre foot-tonf^{-1} × inch^{-1}),

C_i is the cover and management factor,

LS_i is the topographic factor,

P_i is the support practice factor.

K_i is estimated using the following equation (Wischmeier and Smith 1978):

$$K_i = TF'_i + SF'_i + PF'_i \quad [4.2]$$

where:

SF'_i is a soil structure factor,

PF'_i is a soil permeability factor, and

TF'_i is a soil texture factor, given as—

$$TF'_i = 2.1((VFS_i + SI_i)(100 - CL_i))^{1.14} \times 10^{-6} \times (12 - OM_i) \quad [4.3]$$

where:

VFS_i is the percentage of very fine sand (assumed to be one-half of the sand fraction),

SI_i is the percentage of silt,

CL_i is the percentage of clay, and

OM_i is the percentage of organic matter.

SF'_i is determined as—

$$SF'_i = \frac{3.25(SF_i - 2)}{100} \quad [4.4]$$

where:

SF_i is based on soil structure: 1 for very fine granular; 2 for fine granular; 3 for medium or coarse granular, and 4 for blocky, platy, or massive.

PF'_i is determined as—

$$PF'_i = \frac{2.5(PF_i - 3)}{100} \quad [4.5]$$

where:

PF_i represents the permeability class: 1 for rapid, 2 for moderate to rapid, 3 for moderate, 4 for slow to moderate, 5 for slow, and 6 for very slow.

The topographic factor LS_i is a user input for each zone and can be found in Wischmeier and Smith (1978). Procedures presented in Dissmeyer and Foster (1984) are used to determine C_i and P_i. The cover management factor is determined as the product of several factors that define various forest conditions.

C_i is given as—

$$C_i = C_{BS_i} \times C_{C_i} \times C_{RC_i} \times C_{HO_i} \times C_{IV_i} \times C_{RB_i} \times C_{S_i} \quad [4.6]$$

where the cover management subfactors are—

C_{BS_i} for bare soil,

C_{S_i} for plant canopy,

C_{RC_i} for soil reconsolidation,

C_{HO_i} for high organic matter,

C_{IV_i} for invading vegetation,

C_{RB_i} for residue binding, and

C_{S_i} for the effect of steps in the slope.

The factors for bare soil, reconsolidation, and residue binding are combined into one parameter determined as—

$$C_{Combi_i}=C_{BS_i} \times C_{RC_i} \times C_{RB_i} \quad [4.7]$$

where C_{Combi_i} for untilled soils is—

$$C_{Combi_i}=\frac{[a+(b((\%BS_i-c)^2))] \times [d+(e(\%BSFR_i-f)^2)]}{j} \quad [4.8]$$

where:

C_{Combi_i} is constrained to be less than or equal to 0.45,

$\%BS_i$ is percentage of bare soil,

$\%BSFR_i$ is percentage of bare soil having a dense mat of fine roots in top 3 cm of soil,

a is equal to 0.005678,

b is 3.4552×10^{-5},

c is –9.555,

d is 0.08373,

e is 2.6014×10^{-5},

f is 119.2634, and

j is 0.45.

For conditions where tillage has occurred within the previous 72 months, is determined as—

$$C_{Combi_i}=\frac{[a+(b(\%BS_i-c)^2)][d(\%TST_i-e)^f]}{j} \quad [4.9]$$

where the coefficients are given in table 4.2.

The canopy subfactor (C_{C_i}) is defined as—

$$C_{C_i}=1-\%BSCC_i[1-[(k+(l(CH_i-3.4)))/100]] \quad [4.10]$$

where:

$\%BSCC_i$ is percentage of bare soil with canopy cover,

CH_i is cover height (m),

k is 0.8465, and

l is 0.2409 for CH_i less than 3.4 or 0.00936 for CH_i greater than or equal to 3.4.

The effect of high organic matter (C_{HO_i}) is given as—

$$C_{HO_i} = \begin{cases} 1.0 & OM_i < 4.0 \\ 0.7 & OM_i \geq 4.0 \end{cases} \quad [4.11]$$

The effect of the fine roots of invading plants on the cover factor (C_{IV_i}) is—

$$C_{IV_i} = 0.18701 + 0.00005408(\%BSWFR_i - 122.6207)^2 \quad [4.12]$$

where:

$\%BSWFR_i$ is percentage of bare soil with fine roots.

The effect of steps in the slope (C_{S_i}) is—

$$C_{S_i} = 1 - \%TSS_i[1 - [(a(\%S_i - b)^c)/100]] \quad [4.13]$$

where:

$\%TSS_i$ is the percentage total slope in steps,

$\%S_i$ is percentage slope,

a is 67.8003,

b is –3.3461, and

c is –2.0272.

P_i indicates the degree of contour tillage for forest re-establishment and is a function of slope (table 4.3).

Sediment Mass in Each Particle Size Class of Eroded Sediment

Sediment generated by overland flow erosion is assumed to be distributed within five discrete classes of particle size that are a mixture of primary particles and aggregates. The five classes, as mentioned earlier, are sand, large aggregate, small aggregate, silt, and clay. The fraction of total eroded sediment mass within each of these five classes is determined using the approach of Foster et al. (1985). These equations describe the composition of sediment as a function of the dis-tribution of primary particles in the soil matrix. The equations describe sediment from overland flow and channel erosion (process 1 in figure 4.2). For a complete description of the equations and the procedures, the reader is referred to Wischmeier and Smith (1978) and to Foster et al. (1985).

Sediment Delivery From Overland Flow Areas to Channels

Procedures described above describe the composition of sediment at the point of delivery to a channel (Foster et al. 1985). As sediment is transported from overland flow areas to channels, the coarser fractions of the sediment tend to get deposited (process 2 in figure 4.2). Thus, when sediment reaches the channel, it is composed of a greater fraction of fines compared to that present at the point of detachment. Foster (1982) developed a simple procedure to estimate the delivery processes and the associated change in particle size distribution. He computed the overland flow delivery of the various particle size fractions as a function of the overland flow area surface roughness. The coefficients he developed to compute the fractions of various particle types passing through overland flow area roughness depressions are provided in table 4.4.

Sediment Transport and Deposition in Channels

Sediment Routing

The total sediment load reaching the channel is computed as a sum of erosion from contributing overland flow areas and from upslope channels. Sediment de-position is assumed to occur when the total sediment load exceeds the sediment transport capacity of the flow. If sediment load is less than the transport capacity, all of it is assumed to be transported downslope. Channel erosion or detachment is not simulated in the model. Sediment load computations are performed for each of the five particle classes. The method used for sediment routing uses equations developed by Foster et al. (1980, 1981) and Lane (1982) and is applied in the AGNPS model (Young et al. 1989). An overview of the method is provided here, and a more detailed presentation is made in Young et al. (1989). Computations are based on the sediment conditions at the upslope entry point (point 0) and the downslope exit point of the channel reach. Here, the channel reach is defined by the length of the zone under consideration. The steady state continuity equation used to compute sediment at the downslope edge is—

$$Q_S(x) = Q_s(0) + Q_{sl}\frac{x}{L} - \int_0^x D(x)W dx \qquad [4.14]$$

where:

$Q_S(x)$ is the sediment discharge at the downstream end of the channel reach (kg s^{-1}),

$Q_s(0)$ is the sediment discharge at the upstream end of the channel reach (kg s^{-1}),

Q_{sl} is the lateral sediment inflow rate (kg s^{-1}),

dx is the downslope distance (m),

L is the reach length (m),

$D(x)$ is the sediment deposition rate at point x (kg s^{-1} m^{-2}), and

W is the channel width (m).

Following the procedure outlined in Young et al. (1989), the sediment load being transported from each zone for individual particle size classes can be determined:

$$Q_{s_i}(x) = \left[\frac{2q(x)}{2q(x) + \Delta x \times V_{ss_i}}\right] \times \left[Q_{s_i}(0) + Q_{sl_i} - \frac{W \times \Delta x}{2} \times \left[\frac{V_{ss_i}}{q(0)} \times \left(q_{s_i}(0) - g^*_{s_i}(0)\right) - \frac{V_{ss_i} \times g^*_{s_i}(x)}{q(x)}\right]\right] \qquad [4.15]$$

where:

$Q_{s_i}(x)$ is the particle class i discharge at the zone outlet (kg s^{-1}),

$q(x)$ is the water discharge per unit width at exiting the zone (m^3 s^{-1} m^{-1}),

Δx is the channel length (m),

V_{ss_i} is the particle class i fall velocity (m s^{-1}),

$Q_{s_i}(0)$ is the particle class i input to the zone (kg s^{-1}),

$q(0)$ is the water discharge per unit width entering the zone (m^3 s^{-1} m^{-1}),

$q_{s_i}(0)$ is the per-unit-width particle class i entering the zone (kg s^{-1} m^{-1}),

$g^*_{s_i}(0)$ is the particle transport capacity into the zone (kg s^{-1} m^{-1}),

$g^*_{s_i}(x)$ is the particle transport capacity exiting the zone (kg s^{-1} m^{-1}) and

Q_{sl_i} is the lateral particle inflow rate to the channel (kg s^{-1}).

Sediment Deposition

If sediment load is greater than the transport capacity, then deposition occurs, given by—

$$D(x) = \frac{V_{ss_i}}{q(x)}[q_{s_i}(x) - g^*_{s_i}(x)] \quad [4.16]$$

This deposition equation is based on the assumption that deposition occurs only by discrete settling. Trapping of sediment particles by infiltration or physical entrapment in grass media or surface litter is not simulated.

Transport Capacity

The effective transport capacity for each particle class $(g^*_{s_i})$ is computed using a modification of the Bagnold stream power equation (Bagnold 1966) used in AGNPS (Young et al. 1989):

$$g^*_{s_i} = \eta_i \kappa \tau \frac{V_c^2}{V_{ss_i}} \quad [4.17]$$

where:

$g^*_{s_i}$ is the sediment transport capacity (kg m^{-1} s^{-1}) for particle class *i*,

η_i is an effective transport factor,

κ is the transport capacity factor,

τ is flow shear stress (Pa),

V_c is the flow velocity (m s^{-1}), and

V_{ss_i} is the particle settling velocity (m s^{-1}).

The transport capacity factor is given by—

$$\kappa = e_s(1 - e_b)\left(\frac{\gamma_w}{\gamma_{s_i} - \gamma_w}\right) \quad [4.18]$$

where:

e_b is the bedload transport efficiency,

e_s is the suspended load transport efficiency,

γ_s is the sediment specific weight (kg^{-3}), and

γ_w is the specific weight of water ($kg\ m^{-3}$).

The combined efficiency term $e_s(1–e_b)$ was found to be 0.01 for sands (Simons and Senturk 1976). To adjust this term for other particle sizes, Young et al. (1989) introduced the term η:

$$\eta_{[i]} = 0.74E_{f_i}^{-1.98} \quad [4.19]$$

where:

E_f is an entrainment function given by Simons and Senturk (1976):

$$E_{f_i} = \frac{\tau}{(\gamma_s - \gamma_w)d_i} \quad [4.20]$$

where:

d_i is the average particle size diameter.

In using Bagnold's stream power equation, it is assumed that sediment transport primarily occurs in suspension and there is no bedload transport along the channel. This assumption is justified considering the rough surface created by litter in riparian areas. Similar to most sediment transport equations, Bagnold's equation was originally developed to represent transport capacity for sediment composed of a single uniform particle size. Hirschi and Barfield (1986) proposed a procedure to account for sediment composed of a number of particle size classes of varying particle diameters:

- Compute transport capacity $g^*_{s_i}$ using the transport equation for each individual particle class.
- Determine the sum of transport capacities $\sum_{i=1}^{np} g^*_{s_i}$, where np is the number of particle classes in the sediment mixture.
- Determine d_{65} for the mixture—the particle diameter for which 65 percent of the sediment is finer.
- Compute transport capacity g^*_{s65} corresponding to d_{65} using the transport equation.

The transport capacity $g^*_{s_i}$ for particle class *i* in the sediment mixture is then given by—

$$g^*_{s_i} = g^*_{s65} \times \left[\frac{g^*_{s_i}}{\sum_{i=1}^{np} g^*_{s_i}} \right] \qquad [4.21]$$

This procedure allows the sediment transport capacity to be determined as a function of the particle size distribution of the sediment. If a greater fraction of the sediment is fines, the g^*_{s65} of the sediment will shift toward a smaller particle size class, which will result in greater total transport (as one would expect). As noted earlier, sediment computations are performed at the entry and exit reach of the channel. This means that sediment transport capacity is computed at the entry and exit points. At the upslope edge, particle size distribution used for computation of transport capacity is defined by the size distribution of the incoming sediment load. For the lower edge this distribution is a weighted average of the particle size distribution of the incoming sediment and that contributed to the channel by overland flow erosion within the zone.

Sediment Enrichment

Enrichment ratio *(ER)* is computed as—

$$ER = \frac{SSA_{sed-out}}{SSA_{sed-in+soil}} \qquad [4.22]$$

where:

$SSA_{sed-out}$ is the specific surface area of the sediment exiting the zone ($m^2\ g^{-1}$), and

$SSA_{sed-in+soil}$ is the combined specific surface area of the sediment entering the zone and the sediment generated through overland flow erosion ($m^2\ g^{-1}$).

It is assumed that the fraction of primary particles in the small aggregate and large aggregate classes in incoming sediment and the overland flow sediment are identical.

The specific surface area of the exiting sediment $SSA_{sed-out}$ is given by—

$$SSA_{sed-out} = \sum_{i=1}^{5} f_{out}(i) \times \left[\frac{frsnd(i)\ ssasand + frslt(i)\ ssaslt + frcly(i)\ ssacly}{1 + frorg(i)} + \frac{frorg(i)\ ssaorg}{1.73} \right] \quad [4.23]$$

where:

$f_{out}(i)$ is the fraction of particle class in the exiting sediment;

frsnd(i), frslt(i), frcly(i), and *frorg(i)* are the fractions of sand, silt, clay, and organic matter, respectively; and

ssasand, ssaslt, ssacly, and *ssaorg* are the specific surface area ($m^2\ g^{-1}$) for sand, silt, clay, and organic matter, respectively.

Default values used for the specific surface areas are 0.05, 4.0, 20.0, 1,000.0 ($m^2\ g^{-1}$) for sand, silt, clay and organic matter respectively (unless otherwise specified by the user).

Similarly, the specific surface area of the incoming sediment and the sediment generated by overland flow erosion $SSA_{sed-in+soil}$ is computed by—

$$SSA_{sed-in+soil} = \sum_{i=1}^{5} f_{sed-in+soil}(i) \times \left[\frac{frsnd(i)\ ssasand + frslt(i)\ ssaslt + frcly(i)\ ssacly}{1 + frorg(i)} + \frac{frorg(i)\ ssaorg}{1.73} \right] \quad [4.24]$$

where:

$f_{sed-in+soil}(i)$ is the fraction of particle class in the incoming sediment and that generated by overland flow erosion.

The mass of adsorbed particulates (such as NH_4^+ and PO_4^-) exiting a zone along with sediment is then given by—

$$Part_{out} = sed_{out} \times Part_{conc} \times ER \quad [4.25]$$

where:

$Part_{out}$ is exiting particulate mass ($kg\ ha^{-1}$),

sed_{out} is the exiting sediment mass ($kg\ ha^{-1}$), and

$Part_{conc}$ is the particulate concentration ($kg\ kg^{-1}$).

References

Bagnold, R.A. 1966. An approach to the sediment transport problem from general physics. U.S. Geological Survey, Professional Paper 422–J.

Dissmeyer, G.E., and G.R. Foster. 1984. A guide for predicting sheet and rill erosion on forest land. U.S. Department of Agriculture, Forest Service Technical Publication R8–TP 6.

Foster, G.R., R.A. Young, and W.H. Neibling. 1985. Sediment composition for nonpoint source pollution analyses. Transactions of the ASAE 28:133–146.

Foster, G.R. 1982. Modeling the erosion process. *In* C.T. Haan, H.P. Johnson, and D.L. Brakensiek, eds., Hydrologic Modeling of Small Watersheds. American Society of Agricultural Engineers, Monograph 5, pp. 297-380. St. Joseph., Michigan.

Foster, G.R., L.J. Lane, J.D. Nowlin, et al. 1980. A model to estimate sediment yield from field-sized areas: development of model. *In* CREAMS—A Field Scale Model for Chemicals, Runoff, and Erosion from Agricultural Management Systems. Vol. 1, Model Documentation, pp. 36–64. U.S. Department of Agriculture, Conservation Research Report No. 26.

Foster, G.R., L.J. Lane, J.D. Nowlin, J.M. Laflen, and R.A. Young. 1981. Estimating erosion and sediment yield from field-sized areas. Transactions of the ASAE 24:1253–1262.

Hirschi, M.C. and B.J. Barfield. 1986. KYERMO – a physically based research erosion model. American Society of Agricultural Research Engineers (microfiche collection) Fiche No. 86-2047. American Society of Agricultural Research Engineers, St. Joseph, MI.

Lane, L.J. 1982. Development of a procedure to estimate runoff and sediment transport in ephemeral streams. *In* D. Walling, ed., Recent Developments in the Explanation and Prediction of Erosion and Sediment Yield, pp. 275–282. International Association of Hydrologic Science, Wallingford, England, Publication No. 137.

Simons, D.B. and F. Senturk. 1976. Sediment transport technology. Water Resources Publications, Ft. Collins, CO.

Wischmeier, W.H., and D.D. Smith. 1978. Predicting rainfall erosion losses—a guide to conservation planning. U.S. Department of Agriculture, Agriculture Handbook No. 537.

Young, R.A., C.A. Onstad, D.D. Bosch, and W.P. Anderson. 1989. AGNPS: a nonpoint-source pollution model for evaluating agricultural watersheds. Journal of Soil and Water Conservation 44:168–173.

Table 4.1. Particle class properties

Particle class	Specific weight (kg m^{-3})	Particle diameter (m)	Transport capacity factor, k
Clay	2,600.8	2.00×10^{-6}	6.242×10^{-3}
Silt	2,650.8	1.00×10^{-5}	6.053×10^{-3}
Small aggregate	1,800.5	0.35×10^{-4}	12.478×10^{-3}
Large aggregate	1,600.5	0.50×10^{-3}	16.631×10^{-3}
Sand	2,650.8	2.00×10^{-4}	6.053×10^{-3}

Modified from Young et al. 1989

Table 4.2. Coefficients for determination of C_{combi_i}

Soil condition	Initial soil conditions	Formula coefficients						
		a	b	c	d	e	f	j
1	Good initial fine root mat in topsoil; subsoil has good structure and permeability	0.0057	3.46×10^{-5}	–9.56	0.132	–7.97	0.47	0.45
2	Poor initial fine root mat in topsoil; subsoil has good structure and permeability	0.0057	3.46×10^{-5}	–9.56	0.368	–4.15	0.25	0.45
3	Poor initial fine root mat with topsoil absent; subsoil has good structure and permeability	0.0057	3.46×10^{-5}	–9.56	0.523	–5.43	0.17	0.45
4	Poor initial fine root mat with topsoil absent; subsoil has poor structure and permeability	0.0057	3.46×10^{-5}	–9.56	0.774	–1.57	0.07	0.45

Table 4.3. Equations for determining P_i as a function of slope

Slope (%)	Practice management factor*
0–2	$P_i = 0.6467 \times (DOC_i + 9.785)^{0.09386}$
3–7	$P_i = 0.5296 \times (DOC_i + 7.699)^{0.1375}$
8–12	$P_i = 0.6467 \times (DOC_i + 9.785)^{0.09386}$
13–18	$P_i = 0.8192 \times (DOC_i + 9.0332)^{0.04314}$
19+	$P_i = 1$

* DOC_i = percent degrees off contour.

Table 4.4. Estimated fraction of various particle types passing through overland flow area roughness depressions

Overland flow roughness factor	Fraction of original load for each particle type				
	Clay	Silt	Small aggregate	Large aggregate	Sand
0.30	0.91	0.79	0.37	0.00	0.00
0.50	0.97	0.93	0.75	0.00	0.00
0.65	1.00	0.99	0.98	0.07	0.17
0.75	1.00	1.00	0.99	0.32	0.46
0.85	1.00	1.00	1.00	0.58	0.69
0.92	1.00	1.00	1.00	0.78	0.84
0.95	1.00	1.00	1.00	0.86	0.90
0.98	1.00	1.00	1.00	0.94	0.96
1.00	1.00	1.00	1.00	1.00	1.00

Source: Foster 1982.

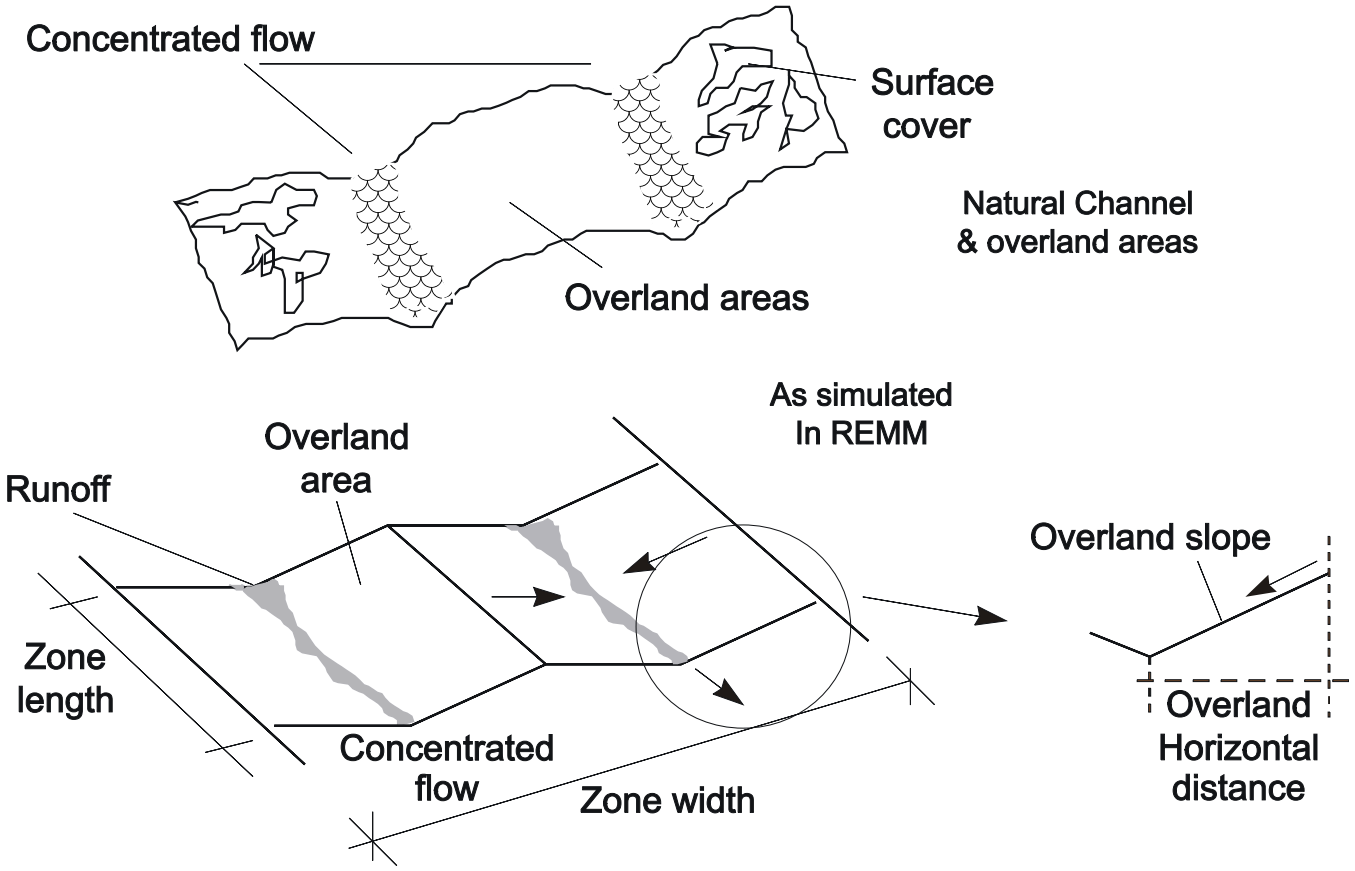

Figure 4.1. Channel and overland flow areas as simulated in REMM

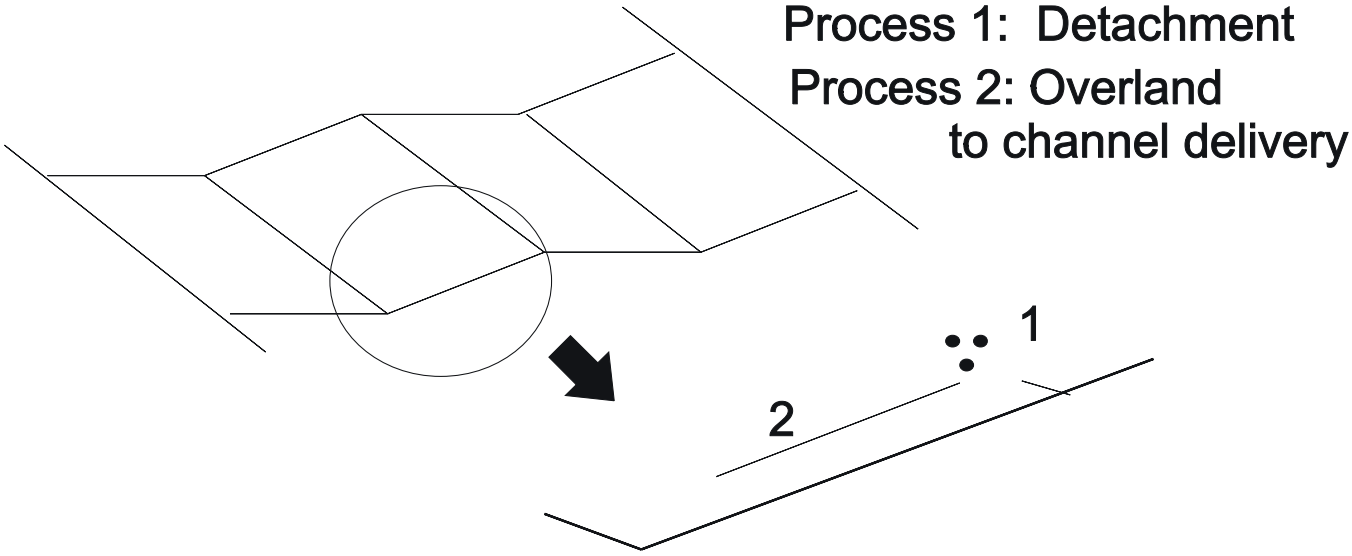

Figure 4.2 Overland flow detachment and delivery

Chapter 5
Litter and Sediment Interactions

Lee S. Altier, Randall G. Williams, and Richard Lowrance

Summary

Interaction of surface runoff with litter residue on the soil surface is an important characteristic of riparian buffers. REMM simulates the interaction of surface soil, surface runoff, and leaf litter on the soil surface. Sediment transport equations (chapter 4) are used to determine whether a fixed amount of soil associated with the litter is subject to erosion or deposition. All, none, or a portion of the litter and litter-associated soil can move with each runoff event. If soil is eroded from the litter, soil from the top soil layer is assumed to replace it the following day. If soil is deposited in the litter, it will be added to the top soil layer the following day. The litter biomass with which the soil is associated moves proportionally to the amount of soil transported out of the litter layer. Mixing of the surface runoff with the litter layer is done to allow changes in concentrations of dissolved and adsorbed nitrogen and phosphorus (described in chapters 7 and 8).

Leaf litter in a riparian buffer may cause sedimentation from runoff water, or it may be transported by runoff water if flow rates are high. Runoff-litter interactions may also change the concentrations of dissolved chemicals through adsorption and desorption reactions (Vought et al. 1994). Although appropriate representation of these interactions is critical to a riparian buffer zone model, very little is known about the action of sediment litter from direct studies of riparian buffers.

Velocities of flow decrease along the forest floor compared to other surface conditions such as cultivated fields, pastures, minimum-tilled fields, and bare ground (USDA 1975). As flow decreases, there is an opportunity for sedimentation that may lead to the burial of leaf litter. Conversely, when flow rates are high, there is an opportunity for transport of leaf litter. Although quantitative estimates of leaf litter transport and burial relative to upland surface runoff are not well known, it occurs in most riparian systems. Litter was found to be transported by flood waters in a study of the Sangamon River floodplain in Illinois (Bell et al. 1978). All leaf litter falling into the floodplain forest was either decomposed or washed away by floodwaters in the study. Smaller second- and third-order streams in south Georgia also exhibited substantial litter transport during flooding, with an average of about 25 percent of total litterfall being transported during high flow events (Lowrance, unpublished data).

The litter-sediment and litter-runoff interactions also lead to changes in dissolved nutrient concentrations. Although little is known about these interactions, it is likely that much of the reaction with dissolved nutrients is due

to adsorption and desorption reactions between soil particles associated with the litter and the runoff water. Phosphorus and nitrogen adsorption depends on interactions of soil particles associated with the litter and the dissolved phosphorus in runoff water (Svendsen 1992, Vought et al. 1994). Interactions of litter and soil/sediment particles are described in this chapter. Interactions among the soil/sediment particles and dissolved nutrients are described in chapters 7 and 8.

In the Riparian Ecosystem Management Model (REMM), the litter layer is used as a mixing layer for interaction with runoff water. The model assumes that litter comprises plant residue and a fixed content of soil. Even if there is no residue on the ground surface, the litter layer is assumed to contain the mass equivalent of 1 cm of soil (mineral soil and humus material) to act as a mixing layer for interaction with runoff water (figure 5.1). When runoff water enters a zone, it is assumed to completely mix with this layer and come to a new equilibrium of dissolved chemical concentrations before infiltrating into the upper soil layer or continuing out of the zone as surface runoff.

The mass balance of soil in the litter layer is—

$$Soil_{Ltr,t} = Soil_{Ltr,t-1} + Sed_{ErosIn,t} + SoilUp_t + 2.5 \sum_{j=1}^{3} CHumSyn_{j,t} - Sed_{ErosOut,Ltr,t} - SoilBur_t - SoilDep_t - 2.5 \sum_{j=1}^{3} CHumR_{j,t} \quad [5.1]$$

where, on day *t:*

$Soil_{Ltr,t}$ is the mass of soil (mineral and humus materials) in the litter layer (kg ha^{-1}),

$Sed_{ErosIn,t}$ and $Sed_{ErosOut,Ltr,t}$ are sediments in runoff water carried into or eroded out of the litter layer (kg ha^{-1}),

$SoilUp_t$ is soil from the upper soil layer that replaces soil lost from the litter layer (kg ha^{-1}),

$CHumSyn_{j,t}$ is carbon synthesized into humus pool j (kg ha^{-1}),

2.5 is an estimate of ratio of mass of organic matter to mass of carbon (that is, 40 percent of organic matter is carbon),

$SoilBur_t$ is burial of plant residue and soil from the litter layer into the upper soil layer by sedimentation from incoming water runoff (kg ha^{-1}),

$SoilDep_t$ is deposition of soil from the litter layer into the upper soil layer on a daily basis in order to maintain a 1-cm-thick mixing layer (kg ha^{-1}), and

$ChumR_{j,t}$ is carbon released from humus pool j (kg ha^{-1}).

Sedimentation into the litter layer and erosion out of the litter layer may both occur on the same day. However, only a net change in the depth of the litter layer will influence the upper soil layer. Sediment movement in and out of zones is simulated by the REMM erosion module.

Erosion

When erosion occurs, material is initially lost from the litter layer. As long as there is material remaining in the litter layer, erosion is simulated as though there were an impervious layer over the upper soil layer. That is, unless the runoff water has enough transport capacity to remove the entire litter layer from a zone, there is no interaction between runoff water and the upper soil layer. If there is insufficient material in the litter layer to satisfy erosion demands, material is eroded from the upper soil layer. In a forested buffer with high infiltration capacity, one would generally expect minimal amounts of erosion to occur. Net sedimentation is more likely than net erosion under most conditions.

The proportion of the litter layer that erodes is determined from the ratio of depth of outgoing sediment to depth of the litter layer:

$$F_{Eros,Ltr,t} = \text{Minimum of} \begin{cases} 1.0 \\ \dfrac{Sed_{ErosOut,Ltr,t}}{BD_{SedErosOut,Ltr,t}} \times \dfrac{BD_{Ltr,t'}}{Soil_{Ltr,t'}} \end{cases} \quad [5.2]$$

where, on day t:

$F_{Eros,Ltr,t}$ is the fraction of material eroding from the litter layer,

$Sed_{ErosOut,Ltr,t}$ is erosion out of a zone from the litter layer (kg ha^{-1}),

$BD_{SedErosOut,Ltr,t}$ is the bulk density of sediment eroding from litter layer (kg m^{-3}),

$BD_{Ltr,t'}$ is the bulk density of the litter layer (exclusive of plant residue) after incoming erosion but before outgoing erosion has occurred (kg m^{-3}), and

$Soil_{Ltr,t'}$ is the mass of soil (mineral and humus material) in the litter layer after incoming runoff but before outgoing runoff has occurred (kg ha^{-1}).

Because of the fixed soil content of the litter layer, an amount of material equal to any net erosion loss or loss from mineralization of organic matter must be supplied from the upper soil layer each day. If $F_{Eros,Ltr,t}$ is less than 1, a portion of

the upper soil will only replace what has been lost from the litter layer. If all of the litter layer erodes away (that is, if $F_{Eros,Ltr,t} = 1$), then material from the upper soil layer $(SoilUp_t)$ will replace the entire litter layer:

$$SoilUp_t = \begin{cases} \left(\frac{LyrDepth_{Ltr}}{1000} - \frac{Soil_{Ltr,t''}}{10^4 \, BD_{Ltr,t''}} \right) 10^4 \, BD_{Layer1,t-1} & F_{Eros,Ltr,t} < 1 \\ \frac{LyrDepth_{Ltr}}{1000} \times 10^4 \, BD_{Layer1,t-1} & F_{Eros,Ltr,t} = 1 \end{cases} \quad [5.3]$$

where:

$LyrDepth_{Ltr}$ is the depth of the soil portion of the litter layer exclusive of plant residue (mm),

$Soil_{Ltr,t''}$ is the mass of soil remaining in the litter layer after erosion from the litter layer has occurred on day t (kg ha^{-1}),

$BD_{Ltr,t''}$ is the bulk density of soil (exclusive of plant residue) remaining in the litter layer after erosion from the litter layer has occurred on day t (kg m^{-3}), and

$BD_{Layer1,t-1}$ is the bulk density of the upper soil layer (exclusive of plant residue) at the end of day t–1 (kg m^{-3}).

The proportion of material in the upper soil layer $(F_{SoilUp,t})$ that replaces material in the litter layer is—

$$F_{SoilUp,t} = \frac{SoilUp_t}{10^4 \, BD_{Layer1,t-1} \times \frac{LyrDepth_{Layer1,t-1}}{1000}} \quad [5.4]$$

where:

$LyrDepth_{Layer1,t-1}$ is the depth of the upper soil layer at the end of day t–1 (mm).

When erosion removes the entire litter layer, the upper soil layer also becomes subject to erosion. The proportion of soil material from the upper soil layer that erodes $(F_{Eros,Layer1,t})$ is determined by—

$$F_{Eros,Layer1,t} = \frac{Sed_{ErosOut,Layer1,t}}{10^4\ BD_{Layer1,t-1} \times \frac{LyrDepth_{Layer1,t-1}}{1000}} \quad [5.5]$$

where, on day *t:*

$F_{Eros,Layer1,t}$ is the fraction of material coming up from the upper soil layer that erodes with outgoing runoff water, and

$Sed_{ErosOut,Layer1,t}$ is sediment eroding from the upper soil layer (kg ha^{-1}).

For simplicity, it is assumed that plant residue in the litter layer and upper soil layer will be lost in the same proportion as soil eroding from each layer:

$$ZRes_{ErosOut,Ltr,i,t} = F_{Eros,Ltr,t} \times ZRes_{Ltr,i,t'} \quad [5.6]$$

$$ZRes_{ErosOut,Layer1,i,t} = F_{Eros,Layer1,t} \times ZRes_{Layer1,i,t-1} \quad [5.7]$$

$$ZRes = \begin{cases} CRes \\ NRes \\ PRes \end{cases} \quad [5.8]$$

where:

$ZRes_{ErosOut,Ltr,i,t}$ and $ZRes_{ErosOut,Layer1,i,t}$ are any of several elements in residue pool *i* (metabolic or structural—see chapter 6) eroding out of the litter layer and upper soil layer, respectively, on day *t* (kg ha^{-1});

$ZRes_{Ltr,i,t'}$ is any of several elements in residue pool *i* in the litter layer after incoming runoff but before outgoing runoff has occurred (kg ha^{-1});

$ZRes_{Layer1,i,t-1}$ is any of several elements in residue pool *i* in the upper soil layer at the end of day *t*–1 (kg ha^{-1}); and

CRes, *NRes*, and *PRes* are carbon, nitrogen, and phosphorus, respectively, in residue (kg ha^{-1}).

As soil is removed from the upper soil layer to replace material in the litter layer, corresponding amounts of organic and mineral materials are also removed in proportion to their content in the upper soil layer:

$$Z_{SoilUp,t} = F_{SoilUp,t} \times Z_{Layer1,t-1} \quad [5.9]$$

$$Z = \begin{cases} CRes_i \\ NRes_i \\ PRes_i \\ CHum_j \\ NHum_j \\ PHum_j \\ P_q \\ NAm \\ NNit \\ \text{other mineral particles} \end{cases} \quad [5.10]$$

where:

$Z_{SoilUp,i,t}$ is any of several materials in soil from the upper soil layer that replaces eroded litter layer (kg ha^{-1});

$Z_{Layer1,i,t}$ is one of several materials in upper soil layer on day t–1 (kg ha^{-1});

$CRes_i$, $NRes_i$, and $PRes_i$ are carbon, nitrogen, and phosphorus, respectively, in residue pool i (metabolic or structural—see chapter 6) (kg ha^{-1});

$CHum_j$, $NHum_j$, and $PHum_j$ are carbon, nitrogen and phosphorus, respectively, in humus pools (active, passive or slow—see chapter 6) (kg ha^{-1});

P_q is inorganic phosphorus in pool q (labile, active, or passive—see chapter 8) (kg ha^{-1}); and

NAm and *NNit* are NH_4^+–N and NO_3^-–N (kg ha^{-1}) (see chapter 7).

Undissolved inorganic chemicals are assumed to erode at a rate determined by an enrichment ratio. All available sources must first be mixed and then equilibrated between dissolved and adsorbed phases before eroding. Dissolution and adsorption of labile phosphorus and NH_4^+–N are described in the chapters on nitrogen (chapter 7) and phosphorus (chapter 8). After determining the amounts in dissolved and adsorbed phases, transport on sediment can be calculated:

$$ZInorg_{ErosOut,Ltr,q,t} = \begin{cases} Sed_{ErosOut,t} \times ER_{Ltr,t} \times ZInorgConc_{Ads,Ltr,q,t'} & F_{Eros,Ltr,t} < 1 \\ ZInorg_{Ads,Ltr,q,t'} & F_{Eros,Ltr,t} = 1 \end{cases} \quad [5.11]$$

$$ZInorg = \begin{cases} NAm \\ P_q \end{cases} \quad [5.12]$$

$$ZInorg_{ErosOut,Layer1,q,t} = \begin{cases} 0 & F_{Eros,Ltr,t} < 1 \\ F_{Eros,Layer1,t} \times 10^4\ BD \times \frac{LyrDepth_{Layer1,t}}{1000} \times ZInorgConc_{Ads,Layer1,q,t-1} & F_{Eros,Ltr,t} = 1 \end{cases} \quad [5.13]$$

where:

$ZInorg_{ErosOut,Ltr,q,t}$ and $ZInorg_{ErosOut,Layer1,q,t}$ are either nitrogen or phosphorus in inorganic forms that erode from the litter layer and upper soil layer, respectively, on day t (kg ha^{-1})

$ER_{Ltr,t}$ and $ER_{Layer1,t}$ are the enrichment ratios of eroding sediment from the litter layer and the upper soil layer, respectively, on day t;

$ZInorgConc_{Ads,Ltr,q,t'}$ is the concentration of either nitrogen or phosphorus in inorganic forms adsorbed in the litter layer on day t after incoming runoff but before outgoing runoff has occurred (kg kg^{-1});

$ZInorgConc_{Ads,Layer1,q,t-1}$ is the concentration of either nitrogen or phosphorus in inorganic forms adsorbed in the upper soil layer at the end of day t–1 (kg kg^{-1});

$ZInorg_{Ads,Ltr,q,t'}$ is either nitrogen or phosphorus in inorganic forms in the litter layer after incoming runoff but before outgoing runoff has occurred on day t (kg ha^{-1});

$ZInorg_{Ads,Layer1,q,t-1}$ is either nitrogen or phosphorus in inorganic forms in the upper soil layer at the end of day t–1 (kg ha^{-1});

P_q is adsorbed phosphorus in form q (kg kg^{-1}); and

NAm is NH_4^+–N that erodes on day t (kg ha^{-1}).

Sedimentation

When net sedimentation occurs in a zone, no erosion is allowed from the upper soil layer. Rather, a depth of material equal to the net sedimentation is moved from the litter layer into the upper soil layer. Along with this, a corresponding proportion of plant residue from the litter layer becomes buried in the upper soil layer. The proportion of the accumulated sediment in the litter layer that is added to the upper soil layer is—

$$F_{Bur,t} = \frac{Soil_{Ltr,t''}}{10^4 \ BD_{Ltr,t''} \times \frac{LyrDepth_{Ltr}}{1000}} \quad [5.14]$$

where:

$F_{Bur,t}$ is the fraction of the material in the litter layer that is buried in the upper soil layer on day t.

Burial of mineral and organic materials into the upper layer can then be calculated as—

$$Z_{Bur,t} = F_{Bur,t} \times Z_{Ltr,t'} \quad [5.15]$$

where:

$Z_{Bur,t}$ is any of several materials (listed in equation 5.10) deposited into the upper soil layer on day t (kg ha^{-1}), and

$Z_{Ltr,t'}$ is any of several materials (listed in equation 5.10) making up the soil portion of the litter layer after incoming runoff has entered the zone (kg ha^{-1}).

Deposition of Adsorbed Chemicals

On days when there is no erosion or sedimentation in a zone, there may be a change in the soil depth of the litter layer as organic matter decomposes. A change in depth is determined by—

$$LtrEx_t = 1000 \left[\frac{Soil_{Ltr,t-1}}{10^4 BD_{Ltr,t-1}} - \frac{LyrDepth_{Ltr}}{1000} \right] \quad [5.16]$$

where:

$LtrEx_t$ is the excessive or deficient amount of soil in the litter layer (mm).

If $LtrEx_t$ is positive, then the formation of the humus from plant residue has caused excessive soil depth of the litter layer. As with sedimentation, a corresponding amount of soil must be deposited into the upper soil layer in order

to maintain the constant 1-cm depth of the litter layer. However, unlike the effects of sedimentation, there is no burying of plant residue material—that is, only mineral and humus material are incorporated into the upper soil layer:

$$F_{SoilDep,t} = \frac{LtrEx_t}{LyrDepth_{Ltr}} \quad [5.17]$$

$$X_{SoilDep,t} = F_{SoilDep,t} \times X_{Ltr,t-1} \quad [5.18]$$

$$X = \begin{cases} CHum_j \\ NHum_j \\ PHum_j \\ P_q \\ NAm \\ NNit \\ \text{other mineral particles} \end{cases} \quad [5.19]$$

where, on day *t:*

$F_{SoilDep,t}$ is the fraction of soil material in the litter layer that is deposited into the upper soil layer,

$X_{SoilDep,t}$ is any of several organic and mineral materials that may be deposited into the upper soil layer from the litter layer (kg ha^{-1}), and

$X_{ltr,t}$ is any of the several organic and mineral materials making up the soil portion of the litter layer (kg ha^{-1}).

If $LtrEx_t$ is negative, then mineralization of humus has exceeded the formation of humus from plant residue. Therefore the soil must be brought up from the upper soil layer to make up the difference:

$$F_{SoilUp,t} = \frac{-LtrEx_t}{LyrDepth_{Layer1,t-1}} \quad [5.20]$$

Then the calculation of materials brought up from the soil proceeds with equations 5.9 and 5.10.

References

Bell, D.T., F.L. Johnson, and A.R. Gilmore. 1978. Dynamics of litter fall, decomposition, and incorporation in the streamside forest ecosystem. Oikos 30:76–82.

Svendsen, L.M. 1992. Dynamics of phosphorus, organic nitrogen and organic matter in watercourses—methods, retention, transport, and models. PhD. Thesis, Ministry of the Environment, National Environmental Research Institute, Copenhagen, Denmark.

USDA. 1975. Urban hydrology for small watersheds. U.S. Department of Agriculture, Soil Conservation Service, Technical Release No. 55.

Vought, L.B., M.J. Dahl, C.L. Pedersen, and J.O. Lacoursiere. 1994. Nutrient retention in riparian ecotones. Ambio 23:342–348.

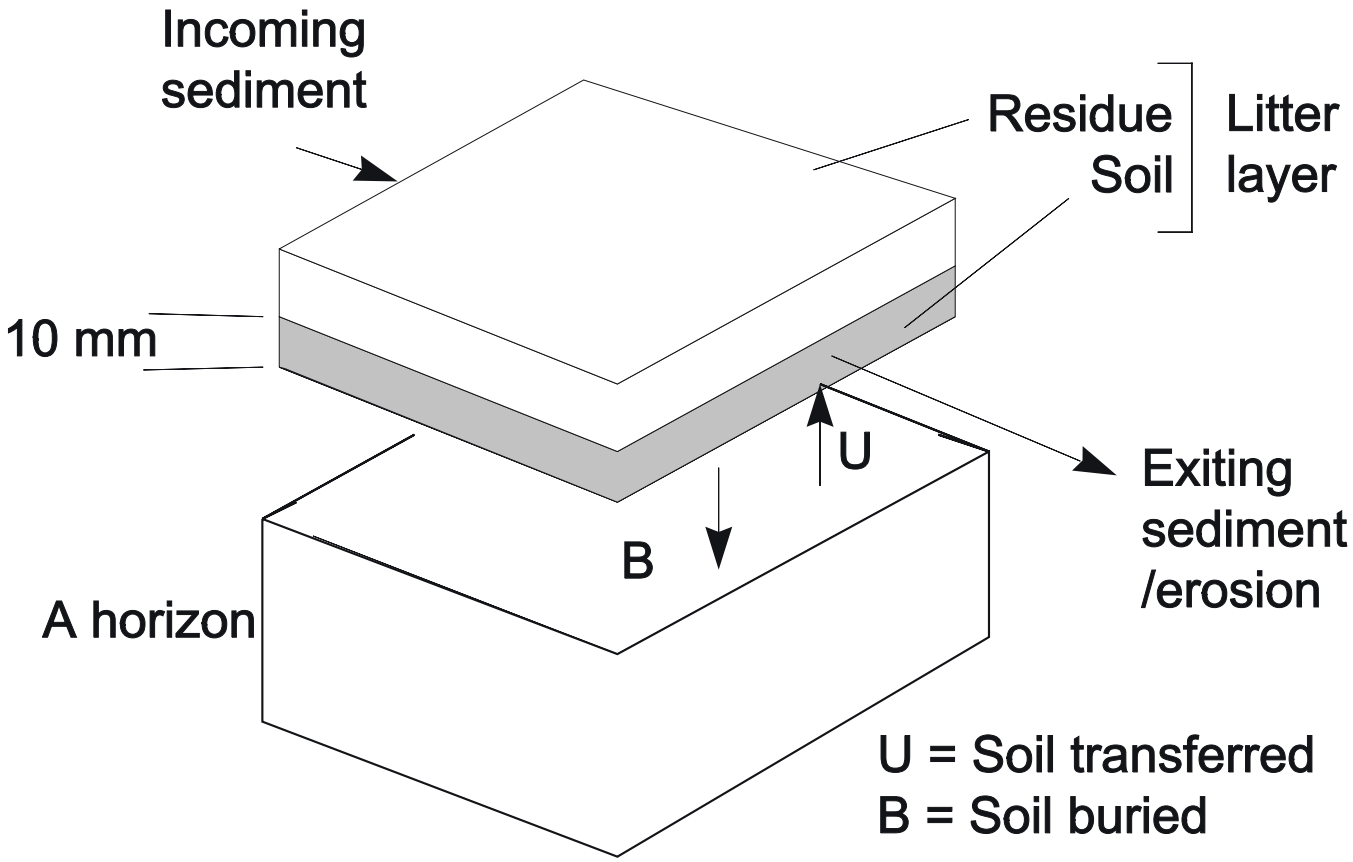

Figure 5.1. Litter and upper soil layer interactions in REMM

Chapter 6
Soil Nutrients: Carbon

Lee S. Altier, Richard Lowrance, and Randall G. Williams

Summary

Carbon dynamics are based on the Century model, with carbon in the soil and residue (litter) layers divided into different pools. Carbon is transferred from residue to humus by decomposition and resynthesis. Soil carbon is divided into active, passive, and slow pools. Residue carbon is divided into structural and metabolic pools. Carbon enters and leaves the pools via transformations to other pools, dissolved and particulate carbon carried by water, and carbon dioxide evolution. Decomposition of residue is governed by factors for temperature, moisture, and nutrient content. As residue decomposes, carbon and nutrients are resynthesized into the humus pools. Either nitrogen or phosphorus can limit the amount of humus synthesis that occurs.

The carbon cycle is fundamental for simulation of all organic matter dynamics and many nutrient cycling processes in the Riparian Ecosystem Management Model (REMM). The mass balance of carbon in each zone is the sum of carbon in vegetation and soil (including litter):

$$TotC_t = TotC_{t-1} + \Delta CVeg_t + \Delta CGrd_t \quad [6.1]$$

where, on day *t:*

$TotC_t$ is the total amount of carbon (kg ha^{-1}),

$\Delta CVeg_t$ is the change in carbon assimilated in vegetation (kg ha^{-1}), and

$\Delta CGrd_t$ is the change in carbon in the litter and soil layers (not including living roots) (kg ha^{-1}).

This chapter is a description of carbon dynamics in the litter and soil layers and how levels of carbon in the soil are influenced by plant litter inputs, management, and exogenous sources.

Carbon Balance

Carbon in the soil and litter layers is assumed to comprise two major pools—the residue pool and the humus pool. The residue pool is further partitioned into a metabolic residue pool and a structural residue pool. Similarly, the humus pool is further divided into three component pools: the active pool, the slow pool, and the passive pool. Figure 6.1 illustrates each of these pools. This scheme is based on the Century model. For assumptions and the rationale behind the pools, see Parton et al. (1987). In the REMM nutrient module, all carbon pools (including amounts in both plant residue and humus) are substrates for microbial transformations. Carbon is transformed from residue to humus by decomposition and

resynthesis by microorganisms. The total amount of carbon in each soil layer $(CGrd_t)$ is represented in the model as—

$$CGrd_t = \sum_{i=1}^{2} CRes_{i,t} + \sum_{j=1}^{3} CHum_{j,t} \quad [6.2]$$

where, on day *t:*

$CRes_{i,t}$ is the change in carbon in plant residues (kg ha^{-1}), and

$CHum_{j,t}$ is the change in carbon in the humus pools (kg ha^{-1}).

The carbon dynamics in REMM are illustrated in figure 6.2 and are described in detail in the following sections.

Litter

Inputs

In order to avoid the difficulty of having to separately keep track of the decomposition of many individual inputs of organic residue over time, daily inputs of fresh residue are mixed with the existing pools of residue material. Depending on the source of vegetation (species and plant part), incoming litter is characterized as having fixed carbon/nitrogen, carbon/phosphorus, and lignin/nitrogen ratios. The Century model (Parton et al. 1987), the Rothamsted model (Jenkinson 1990), and the Phoenix model (McGill et al. 1981) identify fractions of residue as being either readily decomposable (metabolic components) or resistant (structural components). Each of these two pools decomposes at a different rate.

The mass balance for carbon in metabolic plant residue is—

$$\begin{aligned} CRes_{mtb,t} = {} & CRes_{mtb,t-1} + (CResInput_t \times F_{LtrInput,mtb,t}) + CRes_{DissIn,mtb,t} \\ & + CRes_{ErosIn,mtb,t} + CRes_{BurIn,mtb,t} + CRes_{SoilUpIn,mtb,t} - CRes_{DissOut,mtb,t} \\ & - CRes_{ErosOut,mtb,t} - CRes_{BurOut,mtb,t} + CRes_{SoilUpOut,mtb,t} - CResR_{mtb,t} \end{aligned} \quad [6.3]$$

where, on day *t:*

$CRes_{mtb,t}$ is carbon in metabolic residue (kg ha^{-1});

$CResInput_t$ is the total amount of carbon in fresh litter on the day of input (kg ha^{-1});

$F_{LtrInput,mtb,t}$ is the fraction of the metabolic component of fresh litter input;

$CRes_{DissIn,mtb,t}$ and $CRes_{DissOut,mtb,t}$ are incoming and outgoing dissolved metabolic carbon, respectively (kg ha^{-1});

$CRes_{ErosIn,mtb,t}$ and $CRes_{ErosOut,mtb,t}$ are carbon in metabolic residue carried in and out, respectively, in runoff water (litter layer and upper soil layer only) (kg ha^{-1});

$CRes_{BurIn,mtb,t}$ and $CRes_{BurOut,mtb,t}$ are carbon in metabolic residue buried into the upper soil layer and removed from the litter layer, respectively, as net sedimentation occurs in a zone (upper soil layer and litter layer only) (kg ha^{-1});

$CRes_{SoilUpIn,mtb,t}$ and $CRes_{SoilUpOut,mtb,t}$ are carbon in metabolic residue moved up into the litter layer and removed from the upper soil layer, respectively, along with transfer of soil to maintain a constant depth in the litter layer (litter layer and upper soil layer only) (kg ha^{-1}); and

$CResR_{mtb,t}$ is carbon decomposed from the metabolic residue component (kg ha^{-1}).

Details regarding the transfer of materials between the litter layer and the upper soil layer during sedimentation and erosion are discussed in chapter 5. The dissolved metabolic carbon in incoming water can come from several sources:

$$CRes_{DissIn,mtb,t} = \begin{cases} CRes_{RunoffIn,mtb,t} & \text{Litter layer} \\ CRes_{RunoffIn,mtb,t} + CRes_{SeepIn,mtb,t} + CRes_{LatIn,mtb,t} + CRes_{DrainIn,mtb,t} & \text{Soil layers} \end{cases} \quad [6.4]$$

where, on day *t:*

$CRes_{RunoffIn,mtb,t}$ is metabolic carbon in incoming surface water (kg ha^{-1}),

$CRes_{SeepIn,mtb,t}$ is metabolic carbon in incoming surface seep (kg ha^{-1}),

$CRes_{LatIn,mtb,t}$ is metabolic carbon in incoming subsurface lateral water flow (kg ha^{-1}), and

$CRes_{DrainIn,mtb,t}$ is metabolic carbon in incoming drainage (lower soil layers only) (kg ha^{-1}).

For simplicity, it is assumed that all incoming dissolved organic carbon from sources with uncertain characteristics, such as from precipitation and runoff from upland fields, is in the form of active humus carbon. The calculations for dissolved outgoing carbon are described near the end of this chapter.

The mass balance for carbon in structural plant residue is—

$$CRes_{stc,t} = CRes_{stc,t-1} + (CResInput_t \times F_{LtrInput,stc,t}) + CRes_{ErosIn,stc,t} + CRes_{BurIn,stc,t} + CRes_{SoilUpIn,stc,t} - CRes_{ErosOut,stc,t} - CRes_{BurOut,stc,t} - CRes_{SoilUpOut,stc,t} - CResR_{stc,t} \quad [6.5]$$

where, on day t:

$CRes_{stc,t}$ is carbon in the structural residue (kg ha^{-1});

$F_{LtrInput,stc,t}$ is the fraction of the structural component of litter input;

$CRes_{ErosIn,stc,t}$ and $CRes_{ErosOut,stc,t}$ are carbon in structural residue carried in incoming and outgoing runoff water, respectively (in litter layer and upper soil layer only) (kg ha^{-1});

$CRes_{BurIn,stc,t}$ and $CRes_{BurOut,mtb,t}$ are carbon in structural residue buried in the upper layer and removed from the litter layer, respectively, as net sedimentation occurs in a zone (upper soil layer and litter layer only) (kg ha^{-1});

$CRes_{SoilUpIn,stc,t}$ and $CRes_{SoilUpOut,stc,t}$ are carbon in structural residue moved up into the litter layer and removed from the upper soil layer, respectively, along with the transfer of soil material to maintain a constant depth in litter layer (litter layer and upper soil layer only) (kg ha^{-1}); and

$CResR_{stc,t}$ is carbon decomposed from the structural residue component (kg ha^{-1}).

Daily inputs of fresh residue are the sum of root, stem, branch, and leaf litter from different plant species. The amounts of litter input are calculated in the plant growth module of REMM. The initial carbon content of fresh residue $(CResInput_t)$ is determined by—

$$CResInput_t = \sum_{v=1}^{n} \sum_{w=1}^{m} \left(FC_{w,v,t} \times ResInput_{w,v,t}\right) \quad [6.6]$$

where, for fresh residue from part w of plant type v on day t:

$Fc_{w,v,t}$ is the fraction (dry weight) of carbon in fresh plant residue—usually about 0.40 (Alexander 1977), and

$ResInput_{w,v,t}$ is the amount of fresh residue on the day of input (kg dry weight × ha^{-1}).

McGill et al. (1981) separated portions of fresh residue into the two pools according to the carbon/nitrogen ratio of the incoming residue. Besides nitrogen, the lignin content of litter has a strong influence on decomposition rate

(Berendse et al. 1987). Melillo et al. (1982) found particularly high negative correlations between initial lignin/nitrogen ratios and decomposition rates of deciduous leaf litter. Aber et al. (1982), Pastor and Post (1986), and Parton et al. (1987) have used lignin/nitrogen ratios in models of litter decomposition. This approach was used in REMM:

$$F_{LtrInput,mtb,w,v,t} = 0.85 - 0.018\, LNR_{w,v,t} \quad [6.7]$$

$$F_{LtrInput,stc,w,v,t} = 1 - F_{LtrInput,mtb,w,v,t} \quad [6.8]$$

where, for fresh residue from part w of plant type v on day t:

$F_{LtrInput,mtb,w,v,t}$ is the fraction of fresh residue that is metabolic,

$F_{LtrInput,stc,w,v,t}$ is the fraction of fresh residue that is structural, and

$LNR_{w,v,t}$ is the lignin/nitrogen ratio of the incoming litter.

Pastor and Post (1986) have presented extensive tables of initial nitrogen and lignin composition of litter for many tree species. Experimental data on litter composition for several species are listed in tables 6.1–6.3.

Decomposition

Litter material has been shown to be the source of intense microbial activity (Ross and Tate 1993). Carbon from the litter layer gradually enters the upper soil layer as decomposition and mixing by soil fauna occur. In REMM, carbon from the litter layer may enter the soil layers in four ways: plowing, leaching of metabolic components, burying by sedimentation from incoming runoff, and daily deposition of soil from the litter layer in order to maintain a 1-cm-thick mixing layer.

Ghidey and Alberts (1993) observed that residues below ground decompose faster than residues on the soil surface. They attributed this to above-ground residues having lower moisture and less contact with the soil. They also noted that the carbon/nitrogen ratio of the residue and its diameter (for example, of roots) influenced the decomposition rate.

The calculation of litter decomposition in REMM is taken from NLEAP (Shaffer et al. 1991) and EPIC (Williams et al. 1984). However, as mentioned, metabolic and structural components are tracked separately. The rate equation for decomposition is typical of the approach to most of the rate equations in the nutrient module. Decomposition is determined by a first-order rate coefficient multiplied by the amount of carbon in the residue and by factors for temperature,

moisture, and carbon/nitrogen ratio. Assuming that the rate modifiers act independently, they are included as multiplicative reduction factors, ranging in value from 0 to 1. The slower above-ground decomposition observed by Ghidey and Alberts (1993) can be simulated by reducing the rate coefficient for surface material, as done in the Century model (Parton et al. 1987):

$$CResR_t = \sum_{i=1}^{n} (k_i \times CRes_{i,t} \times TFac_t \times WFac_{aerobic,t} \times CNP_{i,t} \times SurFac) \quad [6.9]$$

where, on day *t:*

$CResR_t$ is carbon released from residue (kg ha^{-1});

k_i is a rate coefficient for decomposition of residue component *i* (metabolic or structural; table 6.4);

$CRes_{i,t}$ is the carbon content of each residue component *i* (kg ha^{-1});

$TFac_t$ and $WFac_{aerobic,t}$ are rate modification factors for temperature and moisture, respectively (range from 0 to 1);

$CNP_{i,t}$ is a rate modification factor related to the carbon/nitrogen and carbon/phosphorus ratios of residue component *i* (ranges from 0 to 1); and

SurFac is a rate modification factor for surface residue (= 0.2 for litter layer, 1.0 for other layers).

A pH factor was not included in equation 6. Unless there are large applications of animal wastes to cause a rapid change in pH (Reddy et al. 1979), soil pH changes are generally insignificant and microbial populations are adapted to the pH of a soil, so pH would have little influence on biological processes (Van Veen and Frissel 1983, Van Veen et al. 1984).

The rate factor for structural residues is set according to its lignin content (Parton et al. 1987):

$$k_{stc,t} = k_{stc} \times \exp(-3.0\, LF_{stc,t}) \quad [6.10]$$

where, on day *t:*

$k_{stc,t}$ is the decay rate for structural residue (day^{-1}),

k_{stc} is a maximum decay rate for structural residue (day^{-1}) (table 6.4), and

$LF_{stc,t}$ is the fraction of the structural residue that is lignin.

The calculation of the lignin fraction is based on the assumption that lignin disappears from structural residue in proportion to the disappearance of carbon and that carbon remains at 40 percent of the residue (dry weight):

$$LF_{stc,t} = \frac{LRes_{stc,t}}{2.5\, CRes_{stc,t}} \quad [6.11]$$

$$LRes_{stc,t} = LRes_{stc,t-1} - \frac{CResR_{stc,t}}{CRes_{stc,t-1}} \times LRes_{stc,t-1} + \sum_{v=1}^{n}\sum_{w=1}^{m} LF_{ResInput,w,v,t} \times ResInput_{w,v,t} \quad [6.12]$$

where, on day t:

$LRes_{stc,t}$ is lignin in the structural residue (kg ha^{-1}), and

$LF_{ResInput,w,x,t}$ is the fraction of lignin in fresh residue from part w of plant type x entering the structural residue pool.

The temperature factor $(TFac_t)$ is determined so that the rate has a Q_{10} of 2 (Kladivko and Keeney 1987):

$$TFac_t = \begin{cases} 0 & TSoil_t = 0 \\ Q_{10}^{(TSoil_t - T_{opt})/10} & 0 < TSoil_t < T_{opt} \\ 1 & T_{opt} < TSoil_t \end{cases} \quad [6.13]$$

where:

$TSoil_t$ is soil temperature on day t (˚C), and

T_{opt} is optimal temperature for decomposition (˚C).

The moisture factor $(WFac_{aerobic,t})$ is a function of percentage of water-filled pore space (from Linn and Doran 1984):

$$WFac_{aerobic,t} = \begin{cases} 0.0075\,WFP_t & WFP_t \le 20 \\ -0.253 + 0.0203\,WFP_t & 20 < WFP_t < 60 \\ 3.617\,\exp(-0.02274\,WFP_t) & 60 \le WFP_t \end{cases} \quad [6.14]$$

where:

WFP_t is water-filled pore space (%) on day t.

Although temperature and moisture may be favorable for carbon mineralization, the rate of decomposition is also influenced by the composition of the residue (Gorissen et al. 1995). Decomposition will slow down as nitrogen or phosphorus become limiting for microbial activity. From Parton et al. (1987), the CNP factors for metabolic and structural residue are—

$$CNP_{mtb} = Minimum \begin{bmatrix} 8.0 \;/\; (E_{mtb} \times CNR_{mtb}) \\ 80.0 \;/\; (E_{mtb} \times CPR_{mtb}) \end{bmatrix} \quad [6.15a]$$

$$CNP_{stc} = Minimum \begin{bmatrix} 11.0 \;/\; (E_{stc} \times CNR_{stc}) \\ 200.0 \;/\; (E_{stc} \times CPR_{stc}) \end{bmatrix} \quad [6.15b]$$

where, for each residue component (metabolic or structural) on day *t:*

CNR is an effective carbon/nitrogen ratio,

CPR is an effective carbon/phosphorus ratio of the residue, and

E_{mtb} and E_{stc} are efficiencies of synthesis for carbon from metabolic and structural residues, respectively (dimensionless).

Exogenous nitrogen sources facilitate the decomposition of litter (Hart et al. 1993). The effective carbon/nitrogen ratio is calculated as a function of the soil inorganic nitrogen as well as the carbon and nitrogen contents of the residue in order to reflect the augmenting effect that added nitrogen can have on organic matter decomposition (Alexander 1977):

$$CNR_{i+inorgN,t} = \frac{CRes_{i,t}}{NRes_{i,t} + \dfrac{k_i \times CRes_{i,t}}{\sum_{i=1}^{2} (k_i \times CRes_{i,t})} \times (NAm_{Diss,t} + NNit_t)} \quad [6.16]$$

where, on day t:

$NRes_{i,t}$ is nitrogen in residue component i (kg ha^{-1}),

$NAm_{Diss,t}$ is dissolved NH_4^+–N (kg ha^{-1}), and

$NNit_t$ is NO_3^-–N (kg ha^{-1}).

In the Century model (Parton et al. 1987) only 5 to 10 percent of the soil mineral nitrogen is assumed to be available for immobilization in the process of residue decomposition. As adsorption of NH_4^+–N is calculated in REMM, all unadsorbed mineral nitrogen is assumed to be available for microbial utilization. Multiplying inorganic nitrogen in equation 6.17 by $(k_i \times CRes_{i,t}) / [\Sigma(k_i \times CRes_{i,t})]$ serves to divide the available mineral nitrogen between the residue pools based on their relative rates of decomposition.

An effective carbon/phosphorus ratio is calculated as a function of phosphorus content in the residue and labile inorganic phosphorus pools:

$$CPR_{i+inorgP,t} = \frac{CRes_{i,t}}{PRes_{i,t} + \frac{k_i \times CRes_{i,t}}{\sum_{i=1}^{2}(k_i \times CRes_{i,t})} \times P_{lb(Diss),t}} \quad [6.17]$$

where, on day t:

$PRes_{i,t}$ is phosphorus in residue pool i (kg ha^{-1}), and

$P_{lb,t}$ is inorganic labile phosphorus (kg ha^{-1}).

Humus Pools

The amount of carbon in humus is a function of residue decomposition and turnover (mineralization and immobilization) of carbon in the humus. Bremner (1965) estimated that during the growing season, there is a net mineralization of 1 to 3 percent of the soil organic nitrogen. Soil organic matter has been characterized as having active and stable components. The older fractions may be over 3,000 years old (Jenkinson and Rayner 1977). In REMM, based on the Century model (Parton et al. 1987), plant residues are decomposed into three soil organic matter pools: (1) an active pool of biomass and metabolites of biomass with a rapid decay rate; (2) a slow pool of organic matter that has been partially stabilized either chemically or else physically by adsorption or entrapment within soil aggregates (Paul and van Veen 1978); and (3) a passive pool of chemically stabilized organic matter having a very slow decay rate. The mass balance for carbon in the humus pools is—

$$CHum_{j,t} = CHum_{j,t-1} + CHum_{DissIn,j,t} + CHum_{ErosIn,j,t} + CHum_{BurIn,j,t} + CHum_{SoilDepIn,j,t} + CHum_{SoilUpIn,j,t} + CSyn_{j,t} - CHum_{DissOut,j,t} - CHum_{ErosOut,j,t} - CHum_{BurOut,j,t} - CHum_{SoilDepOut,j,t} - CHum_{SoilUpOut,j,t} - CHumR_{j,t} \quad [6.18]$$

where, in humus pool *j* (active, slow, or passive) on day *t:*

$CHum_{j,t}$ is carbon (kg ha^{-1});

$CHum_{DissIn,j,t}$ and $CHum_{DissOut,j,t}$ are incoming and outgoing dissolved carbon, respectively (active humus pool only) (kg ha^{-1});

$CHum_{ErosIn,j,t}$ and $CHum_{ErosOut,j,t}$ are undissolved carbon in incoming and outgoing sediment, respectively (litter layer and upper soil layer only) (kg ha^{-1});

$CHum_{BurIn,j,t}$ and $CHum_{BurOut,j,t}$ are carbon buried in the upper soil layer and removed from the litter layer, respectively, as net sedimentation occurs (for upper soil layer and litter layer only) (kg ha^{-1});

$CHum_{SoilDepIn,j,t}$ and $CHum_{SoilDepOut,j,t}$ are carbon incorporated into the upper soil layer and removed from the litter layer, respectively, in order to maintain a constant depth in the litter layer (for litter layer and upper soil layer only) (kg ha^{-1});

$CHum_{SoilUpIn,j,t}$ and $CHum_{SoilUpOut,j,t}$ are carbon moved into the litter layer and removed from the upper soil layer, respectively, in order to maintain a constant depth in the litter layer (for litter layer and upper soil layer only) (kg ha^{-1});

$CSyn_{j,t}$ is carbon synthesized into humus (kg ha^{-1}); and

$CHumR_{j,t}$ is carbon released from humus (kg ha^{-1}).

All residue except the lignin fraction of the structural residue is subject to resynthesis into the active humus pool. The lignin fraction is transformed into the slow humus pool (Parton et al. 1987). Carbon from the active humus pool is resynthesized into the slow and passive humus pools. Carbon from the slow pool is resynthesized into the active and passive humus pools. Carbon from the passive pool is resynthesized into the active pool (figure 6.1) (Parton et al. 1987). The total amount of carbon synthesized into each humus pool is the sum of all of the individual sources of carbon multiplied by efficiencies of resynthesis. All of the carbon synthesized into the passive pool comes from the other humus pools:

$$CSyn_{pas,t} = FPas_{act} \times CHumR_{act,t} + FPas_{slow} \times CHumR_{slow,t} \quad [6.19]$$

where, on day *t:*

$CSyn_{pas,t}$ is carbon synthesized into the passive soil organic matter pool (kg ha^{-1}),

$FPas_{act}$ and $FPas_{slow}$ are proportions of mineralized carbon that are stabilized into the passive pool from the active (set at 0.004) and slow (set at 0.03) soil organic matter pools, respectively (Parton et al. 1987), and

$CHumR_{act,t}$ and $CHumR_{slow,t}$, are amounts of carbon released from the active and slow soil organic matter pools, respectively (kg ha^{-1}).

The carbon synthesized into the active and slow humus pools is the sum of carbon coming from decomposed residue and the other humus pools:

$$CSyn_{act,t} = CSyn_{act(\text{from residue}),t} + CSyn_{act(\text{from humus}),t} \quad [6.20]$$

$$CSyn_{slow,t} = CSyn_{slow(\text{from residue}),t} + CSyn_{slow(\text{from humus}),t} \quad [6.21]$$

where, on day *t:*

$CSyn_{act,t}$ and $CSyn_{slow,t}$ are amounts of carbon synthesized into the active and slow soil organic matter pools, respectively (kg ha^{-1});

$CSyn_{act(\text{from residue}),t}$ and $CSyn_{slow(\text{from residue}),t}$ are amounts of carbon synthesized into the active and slow soil organic matter pools, respectively, from residue (kg ha^{-1}); and

$CSyn_{act(\text{from humus}),t}$ and $CSyn_{slow(\text{from humus}),t}$ are amounts of carbon synthesized into the active and slow soil organic matter pools, respectively, from humus (kg ha^{-1}).

Loss of carbon (determined by the efficiency factors) as turnover occurs between the humus pools ensures that the amounts of nitrogen and phosphorus released will always exceed the amount required for resynthesis with carbon. So, carbon resynthesized into the active, slow, and passive pools from turnover of the humus pools will not be limited by available nitrogen and phosphorus. Carbon resynthesis into the active and slow pools from humus turnover is calculated in a similar manner as for the passive humus pool (Parton et al. 1987):

$$CSyn_{act(\text{from humus}),t} = CHumR_{slow,t}(E_{slow} - FPas_{slow}) + CHumR_{pas,t} \times E_{pas} \quad [6.22]$$

$$CSyn_{slow(\text{from humus}),t} = CHumR_{act,t} \times (E_{act} - FPas_{act}) \quad [6.23]$$

where, on day *t:*

$CHumR_{act,t}$, $CHumR_{slow,t}$, and $CHumR_{pas,t}$ are amounts of carbon released from the active, slow, and passive soil organic matter pools, respectively (kg ha^{-1}); and

E_{act}, E_{slow}, and E_{pas} are efficiencies of synthesis of carbon from active, slow, and passive soil organic matter, respectively (nondimensional).

Since the carbon/nitrogen and carbon/phosphorus ratios in plant residue may be much higher than the corresponding ratios in the humus pools, it is possible that available nitrogen or phosphorus may be less than the amount required for resynthesis with carbon from residue. In that case, resynthesis of carbon from the residue pools into the humus pools would stop. Any excess carbon is assumed to be lost as CO_2 gas (Alexander 1977). Therefore, for carbon synthesized from the residue, the potential carbon synthesis is distinguished from the actual:

$$PotCSyn_{act(\text{from residue}),t} = CResR_{mtb,t} \times E_{mtb} + CResR_{stc(non-lig),t} \times E_{stc(non-lig)} \quad [6.24]$$

$$PotCSyn_{slow(\text{from residue}),t} = CResR_{stc(lig),t} \times E_{stc(lig)} \quad [6.25]$$

where, on day *t:*

$PotCSyn_{act(\text{from residue}),t}$ and $PotCSyn_{slow(\text{from residue}),t}$ are potential amounts of carbon that can be synthesized from residue into the active and slow humus pools, respectively, if nitrogen or phosphorus is not limiting (kg ha^{-1});

$CResR_{mtb,t}$, $CResR_{stc(non-lig),t}$, and $CResR_{stc(lig),t}$ are amounts of carbon released from metabolic litter and nonlignin and lignin portions of structural litter, respectively (kg ha^{-1}); and

E_{mtb}, $E_{stc(non-lig)}$, and $E_{stc(lig)}$ are efficiencies of synthesis for carbon from metabolic litter and nonlignin and lignin portions of structural litter, respectively (nondimensional).

Subtracting the efficiency value from 1 indicates the proportion of carbon respired as CO_2 in the turnover process if nitrogen or phosphorus is not limiting.

The efficiency value is largely a function of the type of microbial organisms attacking the humus pool (Alexander 1977). The values of efficiencies used in REMM are given in table 6.5. The influence of soil texture is reflected in the efficiency value for the turnover of carbon from the active soil organic matter pool. Jenkinson et al. (1987) made similar adjustments for soil texture in the Rothamsted model. Heavier soils result in a greater carbon turnover efficiency (Sørensen 1975, 1981). Heavier soils also tend to physically protect soil organic matter from attack (Amato and Ladd 1992). This is reflected in the adjustment of carbon mineralization rate in table 6.4.

When carbon is resynthesized into humus pools from decomposing residue, the corresponding amounts of nitrogen and phosphorus that are immobilized must be less than or equal to the nitrogen and phosphorus available from all inorganic and organic sources. Much of the nitrogen and phosphorus needed for synthesis with carbon comes from the residue pools being decomposed. However, if these are not sufficient, additional inorganic nitrogen and phosphorus will be used if available. Otherwise, lack of sufficient nitrogen or phosphorus may limit the amount of carbon that can be resynthesized into the humus pools.

In equation 6.26, total carbon synthesis is calculated three ways—based on amounts of available carbon from residue, of nitrogen available for synthesis with carbon, and of phosphorus available for synthesis with carbon. Calculation of the amounts of carbon from residue that could be synthesized with a given amount of nitrogen or phosphorus is based on the carbon/nitrogen and carbon/phosphorus ratios of the active and slow humus pools, weighted by the proportions of carbon from residue that would be synthesized into each pool. The actual amount of total carbon synthesized into the humus pools from residue is determined by the most limiting element (carbon, nitrogen, or phosphorus):

$$\sum_{j=1}^{3} CSyn_{j(fromresidue),t} = \text{Minimum of:}$$

$$\begin{cases} PotCSyn_{act(fromresidue)t} + PotCSyn_{slow(fromresidue)t} \\ AvailNSyn_{(Cfromresidue),t}\left[CNR_{act} \times PotCSynRatio_{act,t} + CNR_{slow} \times PotCSynRatio_{slow,t}\right] \\ AvailPSyn_{(Cfromresidue),t}\left[CPR_{act} \times PotCSynRatio_{act,t} + CPR_{slow} \times PotCSynRatio_{slow,t}\right] \end{cases} \quad [6.26]$$

where, on day *t:*

$CSyn_{j(from\ residue),t}$ is carbon from residue synthesized into humus pool *j* (kg ha^{-1});

$AvailNSyn_{(C\ from\ residue),t}$ and $AvailPSyn_{(C\ from\ residue),t}$ are nitrogen and phosphorus, respectively, available for synthesis of carbon released from residue on day t (kg ha^{-1});

CNR_{act} and CNR_{slow} are the carbon/nitrogen ratios of the active and slow humus pools, respectively;

CPR_{act} and CPR_{slow} are the carbon/phosphorus ratios of the active and slow humus pools, respectively; and

$PotCSynRatio_{act,t}$ and $PotCSynRatio_{slow,t}$ are potential proportions of carbon from residue that could be synthesized into the active and slow humus pools, respectively.

After determining the total amount of carbon to be resynthesized from the residue, the carbon is then distributed between the active and slow humus pools:

If

$$\sum_{j=1}^{3} CSyn_{j(from residue),t} < PotCSyn_{act(from residue)t} + PotCSyn_{slow(from residue)t} \quad [6.27]$$

Then

$$CSyn_{act(from residue)} = \sum_{j=1}^{3} CSyn_{j(from residue),t} \times PotCSynRatio_{act,t} \quad [6.28]$$

And

$$CSyn_{slow(from residue)} = \sum_{j=1}^{3} CSyn_{j(from residue),t} \times PotCSynRatio_{slow,t}$$

Else

$$CSyn_{act(from residue)} = PotCSyn_{act(from residue)t} \quad [6.29]$$

And

$$CSyn_{slow(from residue)} = PotCSyn_{slow(from residue)t}$$

The amounts of nitrogen and phosphorus available for synthesis of carbon from residue are the sums of all sources minus the portions immobilized by turnover among humus pools:

$$AvailNSyn_{(Cfromresidue),t} = \sum_{i=1}^{2}(CResR_{i,t}/CNR_i) + \sum_{j=1}^{3}(CHumR_{j,t}/CNR_j) - \sum_{j=1}^{3}(CSyn_{j(fromhumus),t}/CNR_j) + NAm_{Diss,t} + NNit_t \quad [6.30]$$

$$AvailPSyn_{(Cfromresidue),t} = \sum_{i=1}^{2}(CResR_{i,t}/CPR_i) + \sum_{j=1}^{3}(CHumR_{j,t}/CPR_j) - \sum_{j=1}^{3}(CSyn_{j(fromhumus),t}/CPR_j) + P_{lb(Diss),t} \quad [6.31]$$

where, on day *t:*

$CResR_{i,t}$ is carbon released from residue pool *i* (kg ha^{-1}), and

$CHumR_{j,t}$ is carbon released from humus pool *j* (kg ha^{-1}).

The potential proportions of carbon from residue synthesized into the active and slow humus pools are determined by—

$$PotCSynRatio_{act,t} = \frac{PotCSyn_{act(fromresidue),t}}{PotCSyn_{act(fromresidue),t} + PotCSyn_{slow(fromresidue),t}} \quad [6.32]$$

$$PotCSynRatio_{slow,t} = \frac{PotCSyn_{slow(fromresidue),t}}{PotCSyn_{act(fromresidue),t} + PotCSyn_{slow(fromresidue),t}} \quad [6.33]$$

The release of carbon from the humus pools is computed as—

$$CHumR_{j,t} = k_j \times CHum_{j,t} \times TFac_t \times WFac_{aerobic,t} \quad [6.34]$$

where:

k_j is a first-order rate constant for turnover of carbon in humus pool *j* (table 6.4).

Interactions of Carbon With Drainage and Runoff Water

Carbon can dissolve from the metabolic residue and active humus pools and be transported in water movement. The amount of carbon carried out of the litter layer or a soil layer into another layer by runoff, seep, drainage, or subsurface lateral flow is a function of water volume and dissolved carbon concentration:

$$C_{DissOut,t} = CConc_{Diss,t} \times W_{Out,t} \quad [6.35]$$

where, on day *t:*

$C_{DissOut,t}$ is dissolved carbon in any outgoing water (that is, as runoff, seep, drainage, or subsurface lateral flow) (kg ha^{-1}),

$CConc_{Diss,t}$ is the concentration of carbon dissolved in water (kg mm^{-1}), and

$W_{out,t}$ is any outgoing runoff water (mm).

The concentration of dissolved carbon in any layer is determined by a relationship from McGill et al. (1981):

$$CConc_{Diss,t} = \text{Minimum of} \begin{cases} G_t / \theta_{A,t} \\ 0.00586 \left(100\, G_t / \theta_{A,t}\right)^{0.616} \end{cases} \quad [6.36]$$

where, on day *t:*

G_t is carbon available to be dissolved (kg ha^{-1}), and

$\theta_{A,t}$ is available water (that is, the current moisture content minus content at wilting point) (mm).

The value of the dissolved carbon concentration is constrained because at very small $G_t/\theta_{A,t}$ ratios, more carbon could dissolve than would be available.

Outgoing dissolved substances are simulated differently in the litter and soil layers. In the litter layer, inputs on the current day are included in the calculation of the current day's outgoing concentrations. The sum of rain throughfall, incoming runoff, and snow melt inputs is mixed with material on the ground surface each day to determine dissolved and adsorbed concentrations in water infiltrating and running off the surface. Unless there is erosion from the upper soil layer, the calculations of dissolved/adsorbed equilibriums are based only on the interaction of incoming water and sediment with the litter layer. If erosion occurs from the upper soil layer, the equilibriums are determined from mixing down to the depth of erosion. Therefore, the runoff water will include dissolved material from the upper soil layer if the entire litter layer gets eroded away. The carbon available to be dissolved in the litter $(G_{Ltr,t})$ (kg ha^{-1}) is—

$$G_{Ltr,t} = \begin{cases} CRes_{mtb,Ltr,t-1} + (M_{Hum} \times CHumR_{act,Ltr,t-1}) + C_{RainThru,t} + C_{Snowmelt,t} + C_{RunoffIn,t} & F_{Eros,Ltr,t} < 1 \\ CRes_{mtb,t-1} + (M_{Hum} \times CHumR_{act,t-1}) + C_{RainThru,t} + C_{Snowmelt,t} + C_{RunoffIn,t} + F_{Eros,Layer1,t} \times \left[CRes_{mtb,Layer1,t-1} + (M_{Hum} \times CHumR_{act,Layer1,t-1})\right] & F_{Eros,Ltr,t} = 1 \end{cases} \quad [6.37]$$

where, on day *t:*

M_{Hum} is the proportion of carbon in the active humus pool that is in metabolic form,

$C_{RunoffIn,t}$ is dissolved carbon in incoming runoff water (kg ha^{-1}),

$C_{RainThru,t}$ is dissolved carbon in rain that penetrates the plant canopy to the litter surface (rainfall minus canopy interception) (kg ha^{-1}), and

$C_{Snowmelt,t}$ is dissolved carbon in snowmelt (kg ha^{-1}).

When there is erosion from the upper soil layer, the amount of dissolved material that is removed from the upper soil layer can be determined by the proportion of its contribution:

$$C_{DissOut,Ltr(fromLayer1),t} = C_{DissOut,Ltr,t} \times F_{Eros,Layer1,t} \times \left[CRes_{mtb,Layer1,t-1} + (M_{Hum} \times CHumR_{act,Layer1,t-1})\right] / G_{Ltr,t} \quad [6.38]$$

When runoff water removes the entire litter layer (that is, when $F_{Eros,Ltr,t} = 1$), the upper soil layer is involved with two kinds of water movement. There is the fast movement of runoff water, carrying away material from the top of the upper soil layer. Some of the upper soil layer material dissolved in the surface water will return to the upper soil layer as infiltration occurs. There are also the slower drainage and lateral water movements that influence all of the soil layers.

For water moving through the soil layers, the concentration of dissolved materials in each soil layer is based on the amounts of water and chemicals in the layer at the end of the previous day (equation 6.40). During the current day, all water movement out of a layer is assumed to be at that concentration. Another assumption is that when water enters a zone and infiltrates down to the second soil layer on the same day, its concentration does not change as it percolates through the upper soil layer.

$$G_t = CRes_{mtb,t-1} + (M_{Hum} \times CHumR_{act,t-1}) \quad [6.39]$$

The value for M_{Hum} was set at 0.31, based on an estimate by McGill et al. (1981) for the proportion of dying bacteria in metabolic form. The amount of dissolved carbon that is leached from residue and humus in each layer (litter or soil) is determined from the relative amounts of carbon in those pools available for dissolving:

$$CRes_{DissOut,mtb,t} = \left[1 - \frac{M_{Hum} \times CHumR_{act,t}}{G_t}\right] C_{DissOutTotal,t} \quad [6.40]$$

$$CHum_{DissOut,act,t} = \frac{M_{Hum} \times CHumR_{act,t}}{G_t} \times C_{DissOutTotal,t} \quad [6.41]$$

where:

$C_{DissOutTotal,t}$ is total outgoing dissolved carbon from a soil or litter layer on day t (kg ha^{-1}).

Effect of Cultivation

During cultivation, two things happen in REMM. First, all litter is distributed through the depth of cultivation. Then, it is assumed that some of the physically protected organic matter in the slow pool will be liberated into the active pool. Simulation of this effect is done by moving 40 percent of the soil in the slow humus pool into the active pool. This is similar to the approach by Paul and van Veen (1978). Stevenson (1986) noted the increase in microbial activity that occurs upon cultivation. Rather than trying to adjust rate coefficients, the effect is simulated by increasing the amount of carbon susceptible to decay.

References

Aber, J.D., J.M. Melillo, and C.A. Federer. 1982. Predicting the effects of rotation length, harvest intensity, and fertilization on fiber yield from northern hardwood forests in New England. Forest Science 28:31–45.

Alexander, M. 1977. Introduction to Soil Microbiology. John Wiley & Sons, New York.

Amato, M., and J.N. Ladd. 1992. Decomposition of ^{14}C–labeled glucose and legume material in soils: properties influencing the accumulation of organic

residue carbon and microbial biomass carbon. Soil Biology Biochemistry 24:455–464.

Baath, E., B. Berg, U. Lohm, et al. 1980. Effects of experimental acidification and liming on soil organisms and decomposition in a scots pine forest. Pedobiology 20:85–100.

Berendse, F., B. Berg, and E. Bosatta. 1987. The effect of lignin and nitrogen on the decomposition of litter in nutrient–poor ecosystems: a theoretical approach. Canadian Journal of Botany 65:1116–1120.

Berg, B., and H. Staaf. 1980. Decomposition rate and chemical changes of scots pine needle litter. I. Influence of stand age. *In* T. Persson, ed., Structure and Function of Northern Coniferous Forests—An Ecosystem Study. Swedish National Research Council Ecological Bulletin 32, pp. 363–372, Stockholm.

Bremner, J.M. 1965. Organic nitrogen in soils. *In* W.V. Bartholomew and F.E. Clark, eds., Soil Nitrogen, pp. 93–149. Agronomy No. 10. American Society of Agronomy, Madison, WI.

Edmonds, R.L. 1980. Litter decomposition and nutrient release in Douglas-fir, red alder, western hemlock, and Pacific silver fir ecosystems in western Washington. Canadian Journal of Forestry Research 10:327–337.

Ghidey, F., and E.E. Alberts. 1993. Residue type and placement effects on decomposition: field study and model evaluation. Transactions of the ASAE 36:1611–1617.

Gorissen, A., J.H. van Ginkel, J.J.B. Keurentjes, and J.A. van Veen. 1995. Grass root decomposition is retarded when grass has been grown under elevated CO_2. Soil Biology and Biochemistry 27:117–120.

Hart, S.C., M.K. Firestone, P.A. Eldor, and J.L. Smith. 1993. Flow and fate of soil nitrogen in an annual grassland and a young mixed-conifer forest. Soil Biology and Biochemistry 25:431–442.

Jenkinson, D.S. 1990. The turnover of organic carbon and nitrogen in soil. Philosophical Transactions of the Royal Society, B 329:361–368.

Jenkinson, D.S., P.B.S. Hart, J.H. Rayner, and L.C. Parry. 1987. Modelling the turnover of organic matter in long-term experiments at Rothamsted. INTECOL Bulletin 15:1–8.

Jenkinson, D.S., and J.H. Rayner. 1977. The turnover of soil organic matter in some of the Rothamsted classical experiments. Soil Science 123:298–305.

Kladivko, E.J., and D.R. Keeney. 1987. Soil nitrogen mineralization as affected by water and temperature interactions. Biology and Fertility of Soils 5:248–252.

Linn, D.M., and J.W. Doran. 1984. Effect of water-filled pore space on carbon dioxide and nitrous oxide production in tilled and non-tilled soils. Soil Science Society of America Journal 48:1267–1272.

McClaugherty, C.A., J.D. Aber, and J.M. Melillo. 1980. Analysis of fine root dynamics in forest ecosystems. Bulletin of the Ecological Society of America 61:113.

McGill, W.B., H.W. Hunt, R.G. Woodmansee, and J.O. Reuss. 1981. Phoenix, a model of the dynamics of carbon and nitrogen in grassland soils. *In* F.E. Clark and T. Rosswall, eds., Terrestrial Nitrogen Cycles, pp. 49–115. Swedish National Research Council Ecological Bulletin No. 33, Stockholm.

Melillo, J.M., J.D. Aber, and J.F. Muratore. 1982. Nitrogen and lignin control of hardwood leaf litter decomposition dynamics. Ecology 63:621–626.

Parton, W.J., D.S. Schimel, C.V. Cole, and D.S. Ojima. 1987. Analysis of factors controlling soil organic matter levels in Great Plains grasslands. Soil Science Society of America Journal 51:1173–1179.

Pastor, J., and W.M. Post. 1986. Influence of climate, soil moisture, and succession on forest carbon and nitrogen cycles. Biogeochemistry 2:3–27.

Paul, E.A., and J.A. van Veen. 1978. The use of tracers to determine the dynamic nature of organic matter. 11th International Congress of Soil Science, Transactions 3:61–102.

Reddy, K.R., R. Khaleel, M.R. Overcash, and P.W. Westerman. 1979. A nonpoint source model for land areas receiving animal wastes: I. Mineralization of organic nitrogen. Transactions of the ASAE 22:863–872.

Ross, D.J., and K.R. Tate. 1993. Microbial carbon and nitrogen, and respiratory activity, in litter and soil of a southern beech *(Nothofagus)* forest: distribution and properties. Soil Biology and Biochemistry 25:447–483.

Shaffer, M.J., A.D. Halvorson, and F.J. Pierce. 1991. Nitrate leaching and economic analysis package (NLEAP): model description and application. *In* R.F.

Follett, D.R. Keeney, and R.M. Cruse, eds., Managing Nitrogen for Groundwater Quality and Farm Profitability, pp. 285–322. Soil Science Society of America, Madison, WI.

Sørensen, L.H. 1975. The influence of clay on the rate of decay of amino acid metabolites synthesized in soils during decomposition of cellulose. Soil Biology and Biochemistry 7:171–177.

Sørensen, L.H. 1981. Carbon-nitrogen relationships during the humification of cellulose in soils containing different amounts of clay. Soil Biology and Biochemistry 13:313–321.

Stevenson, F.J. 1986. Cycles of Soil. John Wiley & Sons, New York.

Van Veen, J.A., and M.J. Frissel. 1983. Modeling nutrient cycling in agroecosystems. *In* R. Lowrance, R.L. Todd, L.E. Asmussen, and R.A. Leonard, eds., Nutrient Cycling in Agricultural Ecosystems, pp. 551–567. University of Georgia, Athens, College of Agriculture, Special Publication No. 23.

Van Veen, J.A., J.N. Ladd, and M.J. Frissel. 1984. Modeling carbon and nitrogen turnover through the microbial biomass in soil. Plant and Soil 76:257–274.

Vogt, K.A., and J. Bloomfield. 1991. Tree root turnover and senescence. *In* Y. Waisel, A. Eshel and U. Kafkafi, eds., Plant Roots—The Hidden Half, pp. 287–306. Marcel Dekker, New York.

Williams, J.R., C.A. Jones, and P.T. Dyke. 1984. A modeling approach to determining the relationship between erosion and soil productivity. Transactions of the ASAE 27:129–144.

Table 6.1. Composition of needle litter-fall in three scotch pine stands in Ivantjarnsheden, Sweden

Stand age (years)	Water-soluble fraction	Acetone-soluble fraction	Cellulose	Hemicelluloses	Klason lignin	N	P	K	S	Ca	Mg
	(mg g^{-1} dry weight)										
20–25	134	85	269	238	271	4.0	0.21	0.5	—	4.61	0.37
60	158	97	278	202	265	3.8	0.20	0.64	0.43	3.64	0.35
120	155	97	285	195	268	4.1	0.27	0.76	0.44	3.55	0.38

Source: Berg and Staaf 1980

Table 6.2. Initial composition of dry leaf litter for several deciduous species

Species	Lignin	N	Lignin/nitrogen ratio
	(mg g^{-1} dry weight)		
Pin cherry	193	12	16.1
Beech	241	9	26.8
Paper birch	145	9	16.1
Ash	122	9	13.6
Red maple	101	7	14.4
Sugar maple	101	6	16.8

Source: Melillo et al. 1982

Table 6.3. Lignin concentrations in living plants

Tree species	Root diameter class (mm)	Lignin		Reference
		Roots	Foliage	
		------- (%) -------		
Abies amabilis	0–2	56.1	11.6	Vogt, unpublished results
Acer saccharum	0.5–3	33.8	10.1	McClaugherty et al. 1980
Pinus resinosa	0–3	21.7	—	McClaugherty et al. 1980
Pinus strobus	0.5–3	25.3	—	McClaugherty et al. 1980
Pinus sylvestris	< 1	51.8	26.8	Berg and Staaf 1980
	> 1	21.5	—	Berg and Staaf 1980
	20–30	21.0	26.0	Baath et al. 1980
Pseudotsuga menziesii	< 1	50	18.3	Edmonds 1980
	1–2	38	—	Vogt, unpublished results
Hardwood	0–3	22.6	—	McClaugherty et al. 1980

Source: Vogt and Bloomfield 1991

Table 6.4. Values of rate coefficients (k_j) for carbon turnover in the organic matter pools

Carbon pool	Rate (k_j) per day
Structural litter	0.0134286
Metabolic litter	0.0500000
Active soil organic matter	0.02–0.015 × Txt*
Slow soil organic matter	0.0005429
Passive soil organic matter	0.0000186

*Txt is the fraction of silt and clay in the soil layer.

Source: Parton et al. 1987

Table 6.5. Efficiency values for carbon turnover from the organic matter pools

Factor*	Value
E_{mtb}	0.45
$E_{stc(non\text{-}lignin\ in\ litter\ layer)}$	0.55
$E_{stc(non\text{-}lignin\ in\ soil\ layers)}$	0.45
$E_{stc(lignin)}$	0.70
E_{act}	$0.85 + 0.68 \times Txt^{\dagger}$
E_{slow}	0.45
E_{pas}	0.45

**mtb, stc, act, slow,* and *pas* are pools of metabolic litter and structural litter and active, slow, and passive soil organic matter, respectively.

† Txt is the fraction of silt and clay in the soil layer.

Source: Parton et al. 1987

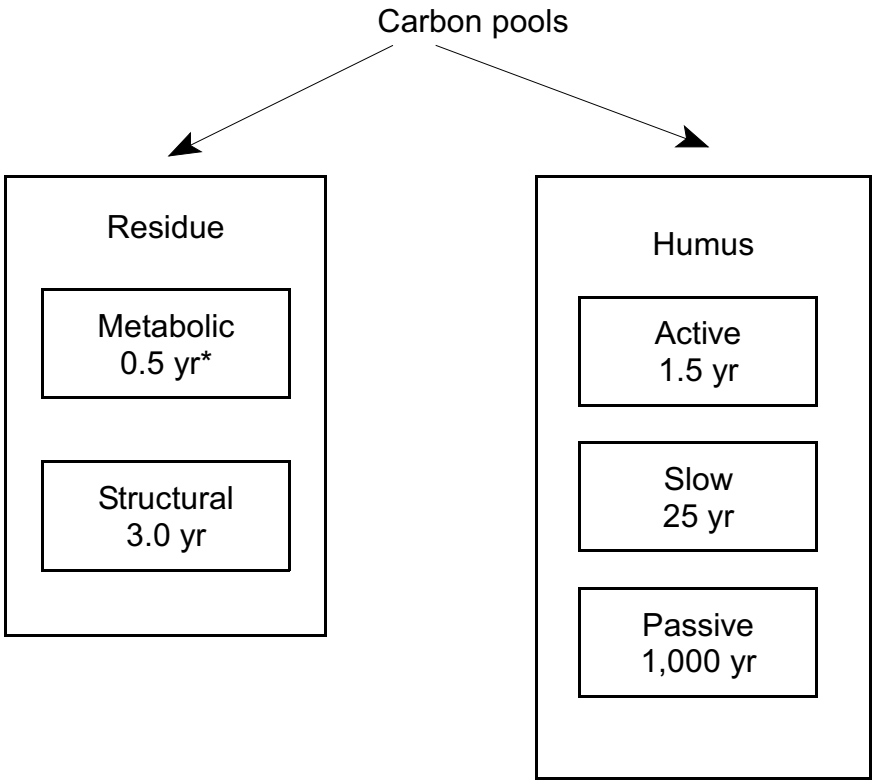

*Turnover rate

Figure 6.1. Carbon pools in REMM (from Parton et al. 1987)

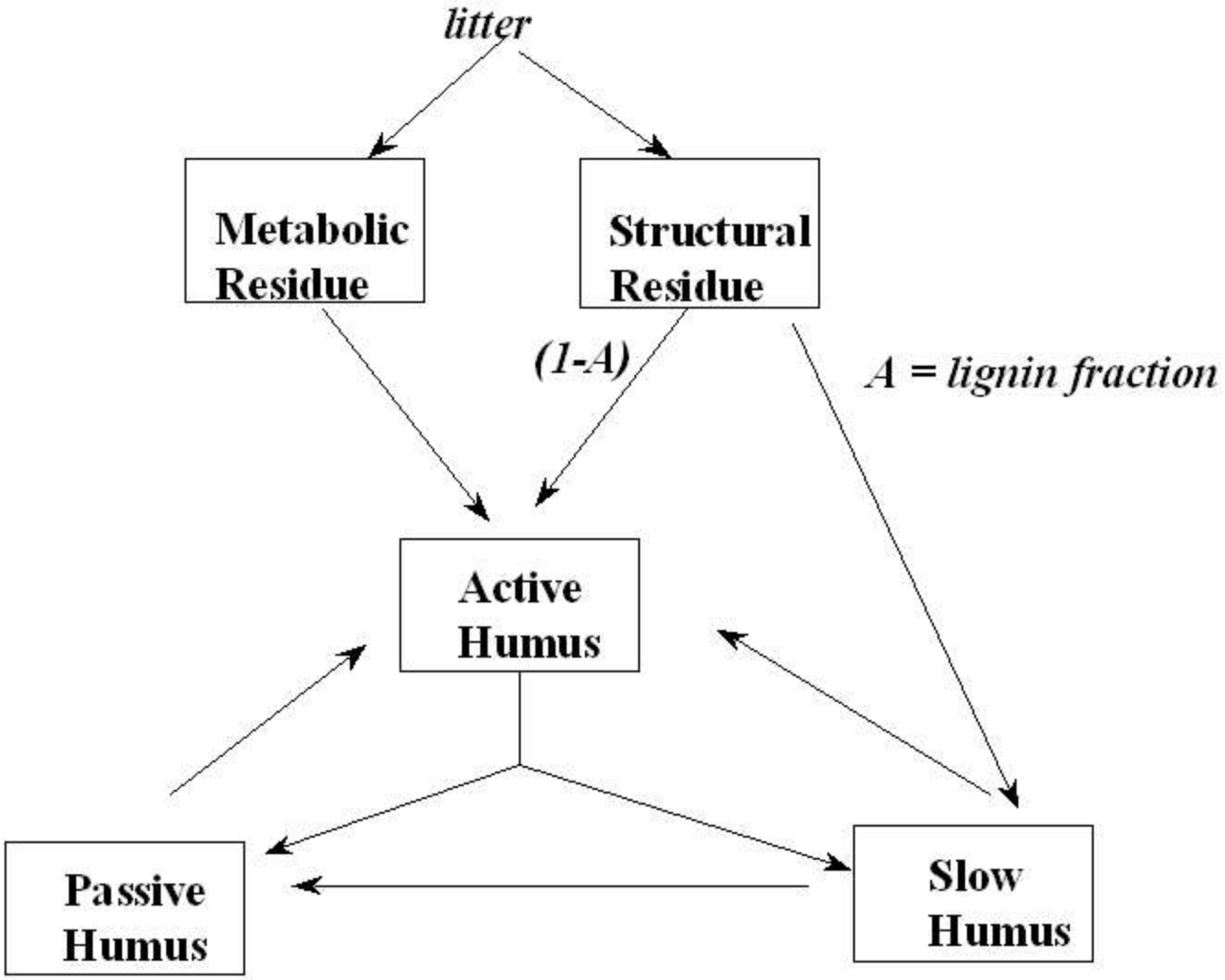

Figure 6.2. Carbon dynamics simulated in REMM

Chapter 7
Soil Nutrients: Nitrogen

Lee S. Altier, Richard Lowrance, Randall G. Williams, Shreeram P. Inamdar, and Robert K. Hubbard

Summary

Nitrogen is simulated in REMM in organic pools associated with soil carbon, residue carbon, and dissolved carbon and as the inorganic forms ammonium and nitrate. Inputs and outputs of nitrogen are from groundwater (dissolved inorganic and organic), surface runoff (dissolved and particulate inorganic and organic), precipitation (input only) , and denitrification (output only). Release or immobilization nitrogen from plant residues occurs as there is decomposition and resynthesis of carbon. Immobilization of nitrate occurs only after all available ammonium has been immobilized. Inorganic nitrogen enters and leaves with waterborne fluxes. Ammonium can be generated by decomposition of residue and humus. The ammonium can then be converted to nitrate through nitrification, which is limited by temperature, moisture, pH, and other environmental factors. Denitrification from soil is based on the interaction of factors representing soil aeration, temperature, nitrate, and mineralizable carbon.

Nitrogen is simulated in the Riparian Ecosystem Management Model (REMM) as organic and inorganic nitrogen pools. The organic nitrogen pools correspond to the carbon pools and are illustrated in figure 7.1. Organic pools are differentiated on the basis of their carbon to nitrogen ratios (carbon/nitrogen). Inorganic nitrogen is the sum of nitrogen in ammonium and in that nitrate. The total amount of nitrogen in each soil layer is the sum of inorganic and organic components:

$$NGrd_t = \sum_{i=1}^{2} NRes_{i,t} + \sum_{j=1}^{3} NHum_{j,t} + \sum_{k=1}^{2} NInorg_{k,t} \quad [7.1]$$

where, on day *t:*

$NGrd_t$ is nitrogen in the litter or soil layer (kg ha^{-1}),

$NRes_{i,t}$ is nitrogen in residue pool *i* (metabolic or structural) (kg ha^{-1}),

$NHum_{j,t}$ is nitrogen in soil organic matter pool *j* (active, slow, or passive) (kg ha^{-1}), and

$NInorg_{k,t}$ is nitrogen in inorganic pool *k* (ammonium and nitrate) (kg ha^{-1}).

Inputs to the pools in organic and inorganic nitrogen forms occur from precipitation, surface runoff, subsurface flow, sediment, and litter. Figure 7.2 illustrates the inputs, losses, and fluxes among the nitrogen pools. Each of the fluxes is further discussed in detail in the following sections. Precipitation can

supply organic and inorganic forms of nitrogen. The nitrogen concentration of precipitation is a user input. Precipitation and canopy interception were discussed in chapter 3. The amount of nitrogen reaching the ground is a function of its concentration and the amount of rain penetrating the plant canopies:

$$N_{PrecipThru,n,t} = 0.01\ NConc_{Precip,n} \times (Precip_t - Int_t) \quad [7.2]$$

where, on day *t:*

$N_{PrecipThru,n,t}$ is nitrogen in form *n* (nitrate, ammonium, or organic) that reaches the ground surface (kg ha^{-1}),

0.01 is a conversion factor,

$NConc_{Precip,n}$ is the concentration of nitrogen in precipitation in form *n* (mg L^{-1}),

$Precip_t$ is the amount of precipitation on day *t* (mm), and

Int_t is canopy interception (mm).

Organic Forms

In organic matter, nitrogen is assumed to be stoichiometrically related to the carbon component. So, the nitrogen content of organic matter can be simply determined from—

$$NOrg_t = \frac{COrg_t}{CNR_t} \quad [7.3]$$

where, on day *t:*

$NOrg_t$ is nitrogen in an organic matter pool (residue or humus) (kg ha^{-1}),

$COrg_t$ is carbon in an organic matter pool (kg ha^{-1}), and

CNR_t is the carbon/nitrogen ratio of the organic matter pool.

Plant Residues

Similar to carbon, nitrogen accumulation and release from plant residues is a function of litter inputs and decomposition. Nitrogen release from plant residues occurs concurrently with microbial decomposition and resynthesis of carbon into the soil organic matter pools. The mass balance for nitrogen in metabolic residue is—

where, in the metabolic residue component on day *t:*

$NRes_{mtb,t}$ is nitrogen (kg ha^{-1});

$NResInput_{mtb,t}$ is input of nitrogen in fresh plant residue (kg ha^{-1});

$$\begin{aligned} NRes_{mtb,t} = {} & NRes_{mtb,t-1} + NResInput_{mtb,t} + NRes_{DissIn,mtb,t} + NRes_{ErosIn,mtb,t} \\ & + NRes_{BurIn,mtb,t} + NRes_{SoilUpIn,mtb,t} - NRes_{DissOut,mtb,t} - NRes_{ErosOut,mtb,t} \\ & - NRes_{BurOut,mtb,t} - NRes_{SoilUpOut,mtb,t} - NResR_{mtb,t} \end{aligned} \quad [7.4]$$

$NRes_{DissIn,mtb,t}$ and $NRes_{DissOut,mtb,t}$ are dissolved nitrogen in incoming and outgoing water, respectively (kg ha^{-1});

$NRes_{ErosIn,mtb,t}$ and $NRes_{ErosOut,mtb,t}$ are nitrogen carried in and out, respectively, in runoff water (in litter layer and upper soil layer only) (kg ha^{-1});

$NRes_{BurIn,mtb,t}$ and $NRes_{BurOut,mtb,t}$ are nitrogen buried in the upper soil layer and removed from the litter layer, respectively, as net sedimentation occurs (for upper soil layer and litter layer only) (kg ha^{-1});

$NRes_{SoilUpIn,mtb,t}$ and $NRes_{SoilUpOut,mtb,t}$ are nitrogen moved into the litter layer and removed from the upper soil layer, respectively, in order to maintain a constant depth in the litter layer (for litter layer and upper soil layer only) (kg ha^{-1}); and

$NResR_{mtb,t}$ is release of nitrogen as NH_4^+–N (kg ha^{-1}).

In any incoming water, nitrogen in dissolved metabolic residue corresponds with sources and quantities of dissolved carbon in the residue:

$$NRes_{DissIn,mtb,t} = \sum_{s=1}^{n} \left(\frac{CRes_{DissIn,mtb,s,t}}{CNR_{DissSource,mtb,s,t}} \right) \quad [7.5]$$

where, on day *t:*

$NRes_{DissIn,mtb,t}$ is nitrogen in dissolved metabolic residue in an incoming water flow (runoff, seep, drainage, or subsurface lateral flow) (kg ha^{-1}),

$CRes_{DissIn,mtb,s,t}$ is dissolved metabolic carbon from source *s* (kg ha^{-1}), and

$CNR_{DissSource,mtb,s,t}$ is the carbon/nitrogen ratio of incoming dissolved metabolic residue from source *s*.

The mass balance for nitrogen in structural plant residue is—

$$NRes_{stc,t} = NRes_{stc,t-1} + NResInput_{stc,t} + NRes_{ErosIn,stc,t} + NRes_{BurIn,stc,t} + NRes_{SoilUpIn,stc,t} - NRes_{ErosOut,stc,t} - NRes_{BurOut,stc,t} - NRes_{SoilUpOut,stc,t} - NResR_{stc,t} \quad [7.6]$$

where, in structural residue on day *t:*

$NRes_{stc,t}$ is nitrogen (kg ha^{-1});

$NResInput_{stc,t}$ is input of nitrogen in fresh plant residue (kg ha^{-1});

$NRes_{ErosIn,stc,t}$ and $NRes_{ErosOut,stc,t}$ are nitrogen carried in incoming and outgoing runoff water, respectively (litter layer and upper soil layer only) (kg ha^{-1});

$NRes_{BurIn,stc,t}$ and $NRes_{BurOut,stc,t}$ are nitrogen buried in the upper soil layer and removed from the litter layer, respectively, as net sedimentation occurs (for upper soil layer and litter layer only) (kg ha^{-1});

$NRes_{SoilUpIn,stc,t}$ and $NRes_{SoilUpOut,stc,t}$ are nitrogen moved into the litter layer and removed from the upper soil layer, respectively, in order to maintain a constant depth in the litter layer (for litter layer and upper soil layer only) (kg ha^{-1}); and

$NResR_{stc,t}$ is release of nitrogen (kg ha^{-1}).

Quantities of nitrogen in fresh litter entering the structural residue pool are determined by the proportion of fresh litter that is structural and the carbon/nitrogen ratio of structural residue. Remaining nitrogen in fresh litter is allocated to the metabolic residue pool (Parton et al. 1987):

$$NResInput_{stc,t} = \sum_{v=1}^{n} \sum_{w=1}^{n} \left(CResInput_{w,v,t} \times F_{LtrInput,stc,w,v,t} / CNR_{stc} \right) \quad [7.7]$$

$$NResInput_{mtb,t} = NResInput_{t} - NResInput_{stc,t} \quad [7.8]$$

where:

$CResInput_{w,v,t}$ is carbon in fresh litter input from part w of plant type v on day t (kg ha^{-1}),

$F_{LtrInput,stc,w,v,t}$ is the fraction of structural component in fresh litter input from part w of plant type v on day t, and

CNR_{stc} is the carbon/nitrogen ratio of the structural residue (fixed at 150).

The value of the carbon/nitrogen ratio for the metabolic residue depends on the quantity of nitrogen allocated to that pool:

$$CNR_{mtb,t} = \frac{CRes_{mtb,t}}{NRes_{mtb,t}} \quad [7.9]$$

where:

CNR is the effective carbon/nitrogen ratio,

$CRes_{i,t}$ is the change in carbon in plant residues (kg ha^{-1}), and

$NRes_{i,t}$ is the change in nitrogen in plant residues (kg ha^{-1}).

Soil Humus

Amounts of nitrogen in the humus pools correspond with the immobilization and mineralization of carbon. The mass balance for nitrogen in each of the humus pools is—

$$\begin{aligned} NHum_{j,t} = {} & NHum_{j,t-1} + NAm_{Immob,j,t} + NNit_{Immob,j,t} + NHum_{DissIn,j,t} + NHum_{ErosIn,j,t} \\ & + NHum_{BurIn,j,t} + NHum_{SoilDepIn,j,t} + NHum_{SoilUpIn,j,t} - NHumR_{j,t} \\ & - NHum_{DissOut,j,t} - NHum_{ErosOut,j,t} - NHum_{BurOut,j,t} - NHum_{SoilDepOut,j,t} \\ & - NHum_{SoilUpOut} \end{aligned} \quad [7.10]$$

where, in humus pool j on day t:

$NHum_{j,t}$ is nitrogen (kg ha^{-1});

$NHum_{DissIn,j,t}$ and $NHum_{DissOut,j,t}$ are incoming and outgoing dissolved nitrogen, respectively (active humus pool only) (kg ha^{-1});

$NHum_{ErosIn,j,t}$ and $NHum_{ErosOut,j,t}$ are undissolved nitrogen in incoming and outgoing sediment, respectively (litter layer and upper soil layer only) (kg ha^{-1});

$NHum_{BurIn,j,t}$ and $NHum_{BurOut,j,t}$ are nitrogen buried in the upper soil layer and removed from the litter layer, respectively, as net sedimentation occurs (for upper soil layer and litter layer only) (kg ha^{-1});

$NHum_{SoilDepIn,j,t}$ and $NHum_{SoilDepOut,j,t}$ are nitrogen incorporated into upper soil layer and removed from the litter layer, respectively, in order to maintain a constant depth in the litter layer (for litter layer and upper soil layer only) (kg ha^{-1});

$NHum_{SoilUpIn,j,t}$ and $NHum_{SoilUpOut,j,t}$ are nitrogen moved into the litter layer and removed from the upper soil layer, respectively, in order to maintain a constant depth in the litter layer (for litter layer and upper soil layer only) (kg ha^{-1}); and

$NHumR_{j,t}$ is nitrogen released from humus (kg ha^{-1}).

Inorganic Nitrogen

Besides entering the soil in precipitation, inorganic nitrogen is released in the form of ammonium as organic matter is mineralized by microbial activity. If not immediately reimmobilized in organic matter or taken up by plant roots, NH_4^+–N is subsequently converted by microbial activity to NO_3^-–N.

Ammonium Nitrogen

The mass balance for NH_4^+–N is calculated as—

where, on day *t:*

NAm_t is NH_4^+–N pool,

$NAm_{Fert,t}$ is NH_4^+–N from fertilizer (litter layer only) (kg ha^{-1});

$$\begin{aligned} NAm_t = {} & NAm_{t-1} + NAm_{Fert,t} + NAm_{DissIn,t} + NAm_{ErosIn,t} + NAm_{BurIn,t} + NAm_{SoilDepIn,t} \\ & + NAm_{SoilUpIn,t} + \sum_{i=1}^{2} NResR_{i,t} + \sum_{i=1}^{3} NHumR_{j,t} - \sum_{i=1}^{3} NAm_{Immob,j,t} - NAm_{Uptk,t} \\ & - NAm_{DissOut,t} - NR_{Nit,t} - NAm_{ErosOut,t} - NAm_{BurOut,t} - NAm_{SoilDepOut,t} \\ & - NAm_{SoilUpOut,t} \end{aligned} \qquad [7.11]$$

$NAm_{DissIn,t}$ and $NAm_{DissOut,t}$ are incoming and outgoing dissolved NH_4^+–N, respectively (kg ha^{-1});

$NAm_{ErosIn,t}$ and $NAm_{ErosOut,t}$ are NH_4^+–N on sediment carried in incoming and outgoing runoff water, respectively (in litter layer and upper soil layer only) (kg ha^{-1});

$NResR_{i,t}$ is NH_4^+–N mineralized from residue pool *i* (metabolic or structural) (kg ha^{-1});

$NHumR_{j,t}$ is NH_4^+–N mineralized from humus pool *j* (active, slow, or passive) (kg ha^{-1});

$NAm_{Immob,j,t}$ is immobilization of NH_4^+–N into humus pool *j* (kg ha^{-1});

$NAm_{Uptk,t}$ is plant uptake of NH_4^+–N (kg ha^{-1});

$NR_{Nit,t}$ is NO^-_3–N produced from nitrification of NH_4^+–N (kg ha^{-1});

$Nam_{SoilDepIn,t}$ and $NAm_{SoilDepOut,t}$ are nitrogen incorporated into upper soil layer and removed from the litter layer (kg ha^{-1}); and

$NAm_{SoilUpIn,t}$ and $NAm_{SoilUpOut,t}$ are nitrogen moved into the litter layer and removed from the upper soil layer (kg ha^{-1}).

Nitrogen is released in ammonium as organic matter decomposes. Its release corresponds with rates of carbon mineralization from the litter and humus pools:

$$NResR_{i,t} = \sum_{i=1}^{2} \frac{CResR_{i,t}}{CNR_{i,t}} \quad [7.12]$$

$$NHumR_{j,t} = \sum_{j=1}^{3} \frac{CHumR_{j,t}}{CNR_{j}} \quad [7.13]$$

where:

$CNR_{i,t}$ is the carbon/nitrogen ratio of residue pool i on day t, and

CNR_j is the carbon/nitrogen ratio of humus pool j.

The structural carbon/nitrogen ratio is fixed at 150. The metabolic residue carbon/nitrogen ratio is calculated in equation 6.16. The humus carbon/nitrogen ratios are determined based on inorganic nitrogen availability (Parton et al. 1993):

$$CNR_{active} = Maximum \left[\begin{matrix} 15.0 - 0.625(NAm+NNit) \\ 3.0 \end{matrix} \right] \quad [7.14]$$

$$CNR_{slow} = Maximum \left[\begin{matrix} 20.0 - 0.4(NAm+NNit) \\ 12.0 \end{matrix} \right] \quad [7.15]$$

$$CNR_{passive} = Maximum \left[\begin{matrix} 10.0 - 0.15(NAm+NNit) \\ 7.0 \end{matrix} \right] \quad [7.16]$$

Immobilization of NH_4^+–N (figure 7.2) is computed as—

$$NAm_{Immob,t} = \text{Minimum of} \begin{cases} NAm_{Diss,t} \\ \sum_{j=3}^{5} (CSyn_{j,t} \; / \; CNR_j) \end{cases} \quad [7.17]$$

Any outgoing water can transport dissolved NH_4^+–N. Dissolved NH_4^+–N that is lost from a layer in water movement is computed as—

$$NAm_{DissOut,t} = NAmConc_{Diss,t} \times W_{Out,t} \quad [7.18]$$

where, on day *t:*

$NAm_{DissOut,t}$ is dissolved NH_4^+–N in any outgoing water (runoff, seep, drainage, or subsurface lateral flow) (kg ha^{-1}),

$NAmConc_{diss,t}$ is dissolved NH_4^+–N concentration (kg mm^{-1}), and

$W_{Out,t}$ is any outgoing water (mm).

Amounts of dissolved and adsorbed NH_4^+–N are determined in REMM by a Freundlich isotherm from Preul and Schroepfer (1968):

$$NAmConc_{ads,t} = a \times NAmConc_{Diss,t}^{b} \quad [7.19]$$

$$NAmConc_{diss,t} = \frac{NAmTot_t - 0.1(LyrThick_t \times BD_t \times NAmConc_{ads,t})}{\theta_t} \quad [7.20]$$

where, on day *t:*

$NAmConc_{ads,t}$ is adsorbed NH_4^+–N concentration (mg kg^{-1}),

$NAmConc_{Diss,t}$ is dissolved NH_4^+–N concentration in incoming runoff water (kg mm^{-1}),

$NAmTot_t$ is total NH_4^+–N in the layer available for dissolving (kg ha^{-1}),

a and *b* are adsorption coefficients (table 7.1),

$LyrThick_{Ltr,t}$ is thickness of the litter layer (cm),

BD_t is bulk density (exclusive of plant residue for litter layer) (g cm^{-3}),

0.1 is a conversion factor ($cm^2\ ha^{-1} \times kg\ g^{-1} \times kg\ mg^{-1}$), and

θ_t is soil water content (mm).

Equations 7.19 and 7.20 must be solved simultaneously. Since Equation 7.19 is not linear, an iterative procedure is used in REMM to get a solution. Values of the adsorption coefficients are shown in table 7.1 for three soils.

As runoff water moves into the litter layer, equilibriums between dissolved and adsorbed chemicals are shifted. On each day, equilibriums must be recalculated after incoming runoff but before outgoing runoff and erosion are calculated. The interaction of the litter layer with incoming runoff and precipitation water must be taken into account for determination of dissolved NH_4^+–N. When there is erosion from the upper soil layer, that layer also contributes to the NH_4^+–N available for dissolution in runoff moving through the litter:

$$NAmTot_{Ltr,t} = \begin{cases} NAm_{Ltr,t-1} + NAm_{RainThru,t} + NAm_{Snowmelt,t} + NAm_{RunoffIn,t} & F_{Eros,Ltr,t} < 1 \\ NAm_{Ltr,t-1} + NAm_{RainThru,t} + NAm_{Snowmelt,t} + NAm_{RunoffIn,t} + F_{Eros,Layer1,t} \times NAm_{Layer1,t-1} & F_{Eros,Ltr,t} = 1 \end{cases} \quad [7/21]$$

where, on day *t:*

$F_{Eros,Ltr,t}$ is the soil fraction (exclusive of plant residue) that erodes from the litter layer, and

$F_{Eros,Layer1,t}$ is the soil fraction that erodes from the upper soil layer.

The value from equation 7.21 is used to calculate dissolved NH_4^+–N lost in overland runoff as well as in water that infiltrates down to the soil layers.

As with carbon, when there is erosion from both the litter layer and the upper soil layer (that is, when $F_{Eros,Ltr,t} = 1$), the amount of dissolved NH_4^+–N lost from the upper soil layer is calculated as a proportion of its contribution:

$$NAm_{DissOut,Ltr(fromLayer1),t} = NAm_{DissOut,Ltr,t} \times \frac{F_{Eros,Layer1,t} \times NAm_{Layer1,t-1}}{NAmTot_{Ltr,t}} \quad [7.22]$$

where:

$NAm_{DissOut,Ltr(fromLayer1),t}$ is NH_4^+–N from the upper soil layer that is dissolved in water moving out of the litter layer on day t (kg ha^{-1}).

When the upper soil layer contributes material to outgoing erosion or replaces material lost from the litter layer, some of the dissolved NH_4^+–N calculated in equation 7.22 (as well as other dissolved substances) from the upper soil layer will return to the layer in infiltrating surface water.

Nitrate Nitrogen

The mass balance for NO_3^-–N is—

$$NNit_t = NNit_{t-1} + NNit_{Fert,t} + NNit_{DissIn,t} + NNit_{BurIn,t} + NNit_{SoilDepIn,t} + NNit_{SoilUpIn,t} + NR_{Nit,t} - NNit_{Immob,j,t} - NNit_{DissOut,t} - Nit_{Denit,t} - NNit_{Uptk,t} - NNit_{BurOut,t} - NNit_{SoilDepOut,t} - NNit_{SoilUpOut,t} \quad [7.23]$$

where, on day t:

$NNit_{Fert,t}$ is NO_3^-–N from fertilizer (litter layer and upper soil layer only) (kg ha^{-1});

$NNit_{DissIn,t}$ and $NNit_{DissOut,t}$ are incoming and outgoing dissolved NO_3^-–N, respectively, (kg ha^{-1});

$NNit_{Immob,j,t}$ is immobilization of NO_3^-–N into humus pool j (kg ha^{-1});

$NNit_{Uptk,t}$ is plant uptake of NO_3^-–N (kg ha^{-1});

$NNit_{BurIn,t}$ and $NNit_{BurOut,t}$ are NO_3^-–N in eroded sediment (kg ha^{-1});

$NNit_{SoilDepIn,t}$ and $NNit_{SoilDepOut,t}$ are NO_3^-–N moved into the upper soil layer and removed from the litter layer (kg ha^{-1});

$NNit_{SoilUpIn,t}$ and $NNit_{SoilUpOut,t}$ are NO_3^-–N moved into the litter layer and removed from the upper soil layer (kg ha^{-1}); and

$NR_{Nit,t}$ is NO_3^-–N produced from nitrification of NH_4^+–N (kg ha^{-1}).

Although the mass balance is much like that for NH_4^+–N, there is no movement of NO_3^-–N on eroding sediment. It is assumed that when there is surface runoff, all of the NO_3^-–N will be dissolved.

The determination of nitrification follows the approach of Reuss and Innis (1977) and Godwin and Jones (1991), based on a Michaelis-Menten function described by McLaren (1970):

$$NR_{Nit,t} = NAm_t \times k_n \quad [7.24]$$

$$k_{n,t} = \frac{(EFac_t \times 4000\,\theta_{Avail,t} \times NAmConc / (LyrDepth \times BD)}{90 + 100\,\theta_{Avail,t} \times NAmConc / (LyrDepth \times BD)} \quad [7.25]$$

$$EFac_t = \text{Minimum of } (WFac_{aerobic,t},\ TFac_t,\ pHFac_{Nit}) \quad [7.26]$$

where, on day *t:*

k_n is a first-order rate coefficient for nitrification (kg kg^{-1} ha^{-1});

$EFac_t$ is the effect of environmental factors limiting nitrification (0–1 scalar);

$WFac_{aerobic,t}$ and $TFac_t$ are rate modification factors for effects of moisture and temperature, respectively (0–1 scalars, equations 6.13 and 6.14); and

$pHFac_{Nit,t}$ is the effect of pH on nitrification on day *t*:

$$pHFac_{Nit} = \begin{cases} 0.307\,pH - 1.269 & 4.5 \le pH \le 7.0 \\ 1.00 & 7.0 < pH < 7.4 \\ 5.367 - 0.599\,pH & 7.4 \le pH \le 9.0 \end{cases} \quad [7.27]$$

Immobilization of nitrate is assumed to occur only after all available NH_4^+–N has been immobilized:

$$NNit_{Immob,t} = \text{Minimum of } \begin{cases} NNit_t \\ \sum_{j=3}^{5} (CSyn_{j,t} / CNR_j) - NAm_t \end{cases} \quad [7.28]$$

This is constrained so that $0 \le NNit_{Immob,t} \le NNit_t$.

The capacity for soil to denitrify is often more limited by carbon than by nitrate. Myrold and Tiedje (1985) suggest that nitrate will only restrict denitrifier biomass under very low conditions of nitrate (<1 mg NO_3^-–N per kg of soil).

Denitrification has been found to be zero order with respect to nitrate at concentrations above 2–5 mg nitrogen per kg of soil (Yoshinari et al. 1977, Webster and Goulding 1989). Above this, the biomass of denitrifiers and the denitrification rate are controlled by the carbon content.

The rate of denitrification is also affected by sources of carbon in the soil. Readily mineralizable carbon sources added to soil have the greatest effect of augmenting denitrification (Bremner and Shaw 1958). Beauchamp et al. (1980) found denitrification to be more closely correlated with the quantity of total soil carbon than with amounts of carbon extracted with water or barium hydroxide. However, Burford and Bremner (1975) and Davidson et al. (1987) found that the quantity of readily mineralizable carbon was more closely correlated with denitrification. In REMM, simulation of denitrification is partially a function of readily decomposable carbon. This carbon is defined as the carbon that would be decomposed according to equations 6.9 and 6.32 under optimal conditions of temperature and moisture if nonlimiting amounts of nitrogen and phosphorus were available.

Since denitrification occurs as a result of the activity of facultative anaerobes, conditions that reduce soil oxygen content, such as increasing soil moisture content, tend to increase denitrification. Figure 7.3 illustrates the interaction that can occur between soil moisture and readily decomposable carbon. When soils are poorly aerated, rapid decomposition of organic matter can increase anaerobiosis, resulting in enhanced denitrification (Walters et al. 1992). This can occur in microsites as microbial respiration depletes oxygen faster than the rate of oxygen transport (Greenwood 1961, Khind et al. 1987). In simulating this effect in REMM, the amount of readily decomposable carbon augments the effect of moisture on denitrification.

Denitrification is calculated as the function of the interaction of factors representing the degree of anaerobiosis, temperature, NO_3^-–N, and mineralizable carbon:

$$NNit_{Denit,t} = \text{Minimum of} \begin{cases} NNit_t \\ k_d \times LyrDpth \times AnaFac_t \times TFac_{denit,t} \times (\alpha \times NFac_t + CFac_t) \end{cases} \quad [7.29]$$

where, on day *t:*

k_d is rate of denitrification under optimal conditions (kg cm^{-1} ha^{-1});

LyrDpth is depth of soil layer (cm);

$AnaFac_t$, $TFac_{denit,t}$, $NFac_t$, and $CFac_t$ are factors representing the effects of anaerobiosis, temperature, NO_3^-, and mineralizable carbon on denitrification (0–1 scalars); and

α is a coefficient determining the influence of nitrate on denitrification.

The potential denitrification rate (k_{denit}) is the maximum rate possible with an active microbial population present in the soil. It is best approximated by denitrification potential measurements (Tiedje 1982).

The anaerobic factor $(AnaFac_t)$ is representative of redox potential and the predisposition of the denitrifying bacteria. It is modeled as a function of water-filled pore space and mineralizable carbon. The relationship between water-filled pore space and denitrification rate is based on studies by Bremner and Shaw (1958) and Linn and Doran (1984). Denitrification mostly occurs as water-filled pore space rises above 60 percent. However, the response is lagged in order to account for the time required for enzyme production by the bacteria. Carbon has a relatively greater effect on anaerobiosis as the soil approaches saturation (figure 7.4). The anaerobic factor is calculated as—

$$AnaFac_t = \text{Minimum of} \begin{cases} 1 \\ \text{Maximum of} \begin{cases} 0.4 \\ XCoef \times AnaFac_{t-1} \end{cases} \\ WFac_t \times (2 - \exp(-CurvCoef \times CMin_{t-1})) \end{cases} \quad [7.30]$$

where:

$XCoef$ is a coefficient determining the maximum possible increase in denitrification due to increased redox potential (unitless; about 1.5),

$CurvCoef$ is a coefficient relating the amount of mineralizable carbon to its effect on anaerobiosis (unitless),

$CMin_t$ is carbon mineralization on day t–1 (kg ha^{-1}), and

$WFac_t$ is a factor for the effect of water-filled pore space on denitrification on day t (0–1 scalar):

$$WFac_{anaerobic,t} = \text{Minimum of} \begin{cases} 1 \\ 0.000304 \exp(0.0815\ WFP_t) \end{cases} \quad [7.31]$$

where:

WFP_t is water-filled pore space (%).

The temperature factor $(TFac_{denit,t})$ is based on lab studies by Stanford et al. (1975) indicating a Q_{10} of 2 between about 11 and 35 ˚C:

$$TFac_{denit,t} = \begin{cases} 0 & TSoil_t \le 0 \\ 2^{(TSoil_t - T_{denit,opt})/10} & 0 \le TSoil_t \le T_{denit,opt} \\ 1 & T_{denit,opt} < TSoil_t \end{cases} \quad [7.32]$$

where:

$T_{denit,opt}$ is the optimal temperature for denitrification (set at 35 ˚C).

The NO_3^- factor is determined in relation to an upper boundary for first-order rate response to nitrate:

$$NFac_t = \text{Minimum of} \begin{cases} 1 \\ NNit_t / CritNitLev \end{cases} \quad [7.33]$$

where:

$NNit_t$ is NO_3^-–N (mg kg^{-1}), and

CritNitLev is the critical NO_3^-–N level below which nitrate limits denitrification (mg kg^{-1}).

Although any amount of mineralizable carbon can influence the anaerobic factor, carbon is assumed to only have a direct effect on the denitrification rate when nitrate is above the critical level:

$$CFac_t = \begin{cases} 0 & NFac_t \le 1 \\ (1 - \alpha)(\beta \times CMinPot_t) / (1 + \beta \times CMinPot_t) & NFac_t > 1 \end{cases} \quad [7.34]$$

where:

β is a coefficient determining the relative influence of carbon on denitrification rate.

Mineralizable carbon is estimated as the amount of carbon that could be released from plant residue and soil organic matter pools on a given day under optimal conditions:

$$CMinPot_t = \sum_{j=1}^{3} (k_{Hum,j} \times CHum_{j,t}) + \sum_{i=1}^{2} (k_{Res,i} \times CRes_{i,t}) \quad [7.35]$$

where:

$k_{Hum,j}$ and $k_{Res,i}$ are rate coefficients for release of carbon from the humus and residue pools, respectively (table 6.4).

Figure 7.4 illustrates the relationship of denitrification with soil carbon content at three soil moisture levels as simulated by REMM.

References

Beauchamp, E.G., G.C. Yeomans, and Y.C. Yeomans. 1980. Organic matter availability for denitrification in soils of different textures and drainage classes. Communications in Soil Science and Plant Analysis 11:1221–1233.

Bremner, J.M., and K. Shaw. 1958. Denitrification in soil II. Factors affecting denitrification. Journal of Agricultural Science 51:40–52.

Burford, J.R., and J.M. Bremner. 1975. Relationships between the denitrification capacities of soils and total, water-soluble and readily composable soil organic matter. Soil Biology and Biochemistry 7:389–394.

Davidson, E.A., L.F. Galloway, and M.K. Strand. 1987. Assessing available carbon: comparison of techniques across selected forest soils. Communications in Soil Science and Plant Analysis 18:45–64.

Godwin, D.C., and C.A. Jones. 1991. Nitrogen dynamics in soil plant systems. *In* J. Hanks and J.T. Ritchie, eds., Modeling Plant and Soil Systems, pp. 287-321. Agronomy Monograph No. 31. Agronomy Society of America, Madison, WI.

Greenwood, D.J. 1961. The effects of oxygen concentration on the decomposition of organic materials in soil. Plant and Soil 14:360–376.

Khind, C.S., A. Jugsujinda, C.W. Lindau, and W.H. Patrick, Jr. 1987. Effect of sesbania straw in a flooded soil on soil pH, redox potential and water-soluble nutrients. International Rice Research Newsletter 12:42–43.

Linn, D.M., and J.W. Doran. 1984. Effect of water-filled pore space on carbon dioxide and nitrous oxide production in tilled and nontilled soils. Soil Science Society of America Journal 48:1267–1272.

McLaren, A.D. 1970. Temporal and vectorial reactions of nitrogen in soil: a review. Canadian Journal of Soil Science 50:97–109.

Myrold, D.D., and J.M. Tiedje. 1985. Establishment of denitrification capacity in soil: effects of carbon, nitrate and moisture. Soil Biology and Biochemistry 17:819–822.

Preul, H.C., and G.J. Schroepfer. 1968. Travel of nitrogen in soils. Journal of the Water Pollution Control Federation 40:30–48.

Parton, W.J., D.S. Schimel, C.V. Cole, and D.S. Ojima. 1987. Analysis of factors controlling soil organic matter levels in Great Plains grasslands. Soil Science Society of America Journal 51:1173–1179.

Parton, W.J., M.O. Scurlock, D.S. Ojima, et al. 1993. Observations and modeling of biomass and soil organic matter dynamics for the grassland biome worldwide. Global Biogeochemical Cycles 7:785–809.

Reuss, J.O., and G.S. Innis. 1977. A grassland nitrogen flow simulation model. Ecology 58:379–388.

Stanford, G., S. Dzienia, and R.A. Vander Pol. 1975. Effect of temperature on denitrification in soils. Soil Science Society of America Proceedings 39:867–870.

Tiedje, J.M. 1982. Denitrification. *In* A.L. Page, R.H. Miller, and O.R. Keeney., eds., Methods of Soil Analysis, 2nd ed. Part 2, pp. 1011–1026. Agronomy Society of America and Soil Science Society of America, Madison, WI, Monograph No. 9.

Walters, D.T., M.S. Aulakh, and J.W. Doran. 1992. Effects of soil aeration, legume residue, and soil texture on transformations of macro- and micronutrients in soils. Soil Science 153:100–107.

Webster, C.P., and K.W.T. Goulding. 1989. Influence of soil carbon on denitrification from fallow land during autumn. Journal of the Science of Food and Agriculture 49:131–142.

Yoshinari, T., R. Hynes, and R. Knowles. 1977. Acetylene inhibition of nitrous oxide reduction and measurement of denitrification and nitrogen fixation in soil. Soil Biology and Biochemistry 9:177–183.

Table 7.1. Ammonium adsorption coefficients for several soils

Soil type	Coarse sand	Medium sand	Fine sand	Very fine sand	Silt	Clay	Adsorption coefficients	
							a	b
	---------- (%) ----------							
Zimmerman sand	8	56	31	2	1	2	1.1	0.972
Hayden silt	0	1	1	37	51	10	7.0	0.766
Milaca clay	8	11	16	10	21	29	20.0	0.631

Source: Preul and Schroepfer 1968

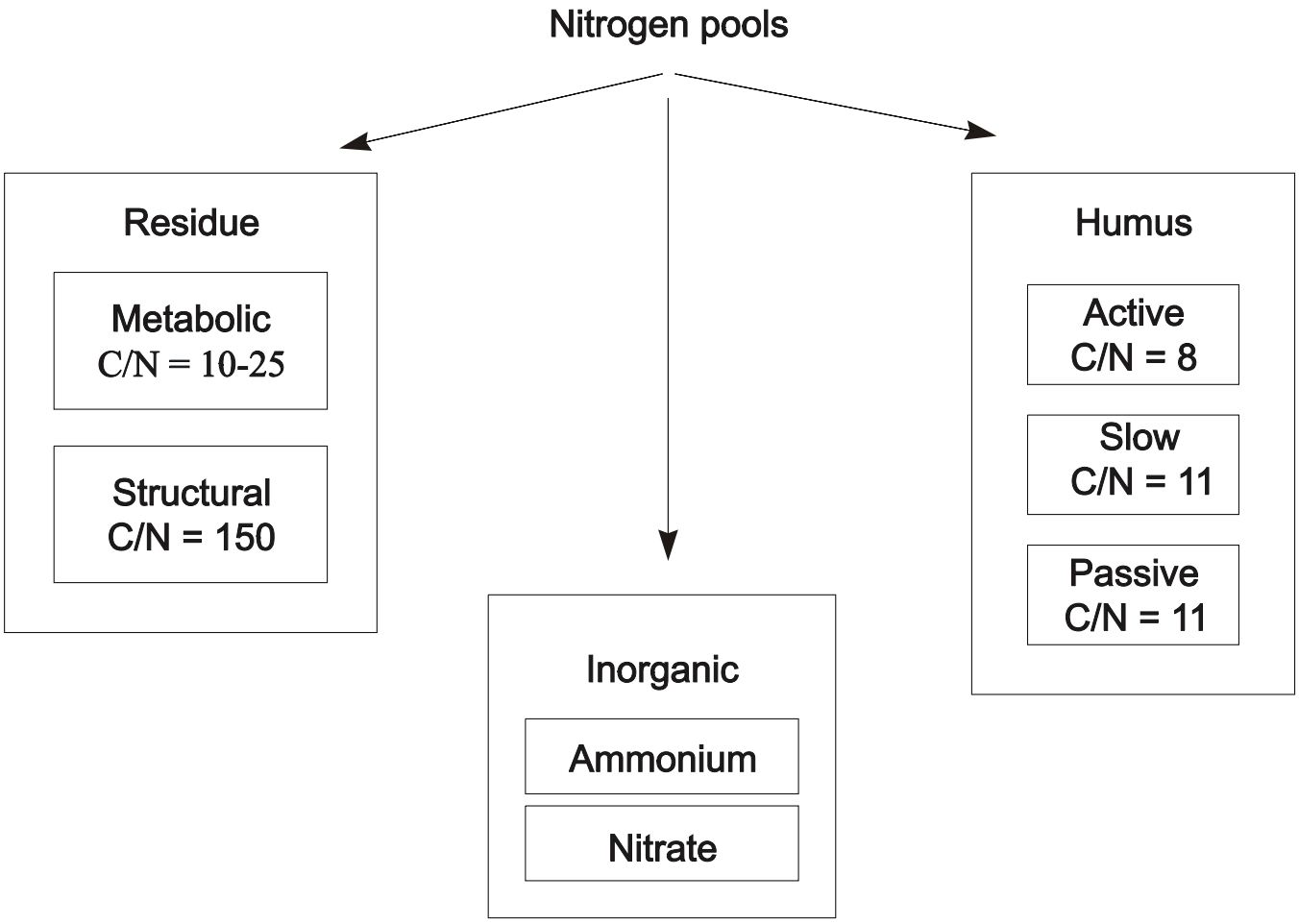

Figure 7.1. Nitrogen pools in REMM

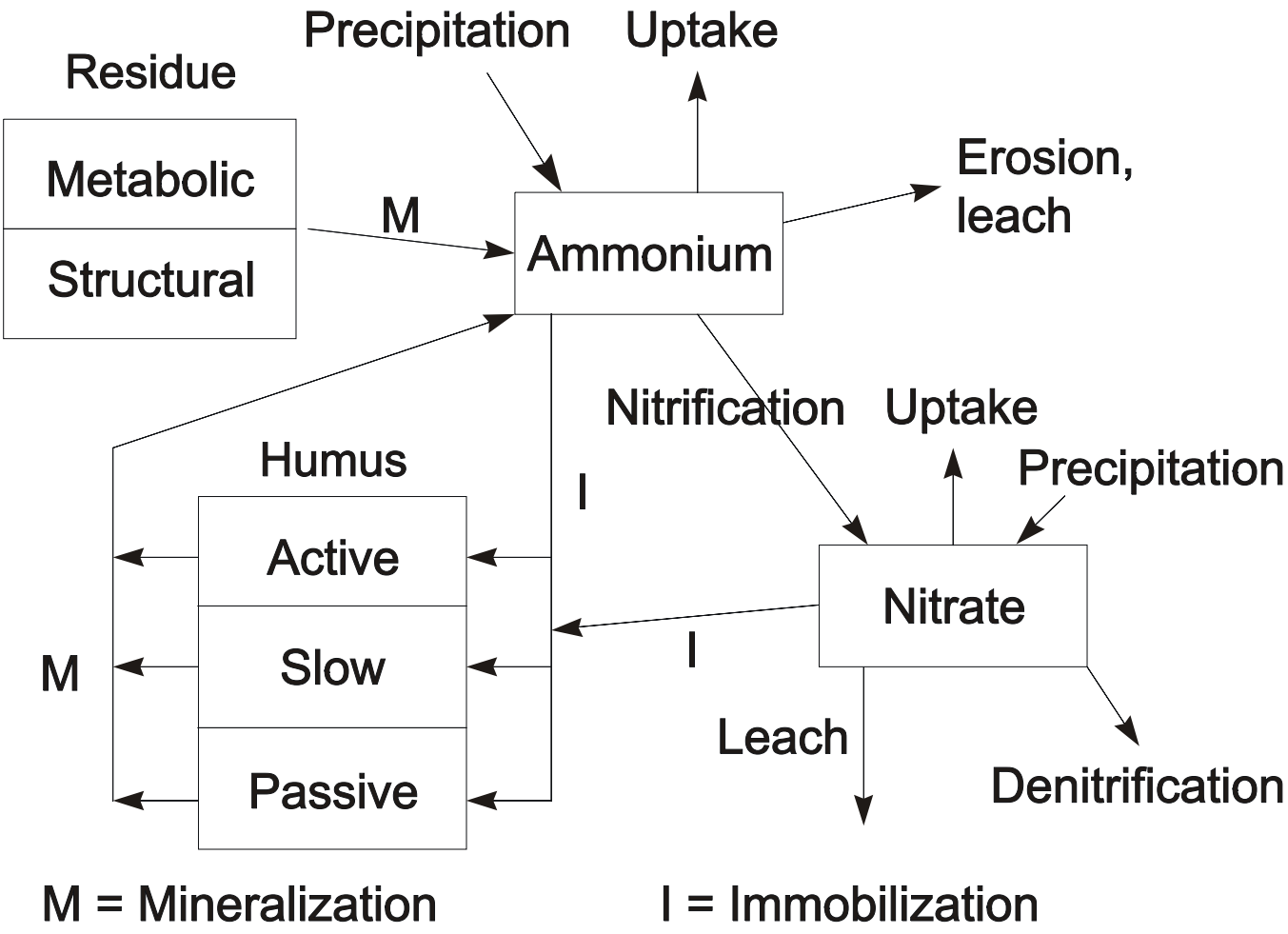

Figure 7.2. Fluxes among nitrogen pools in REMM

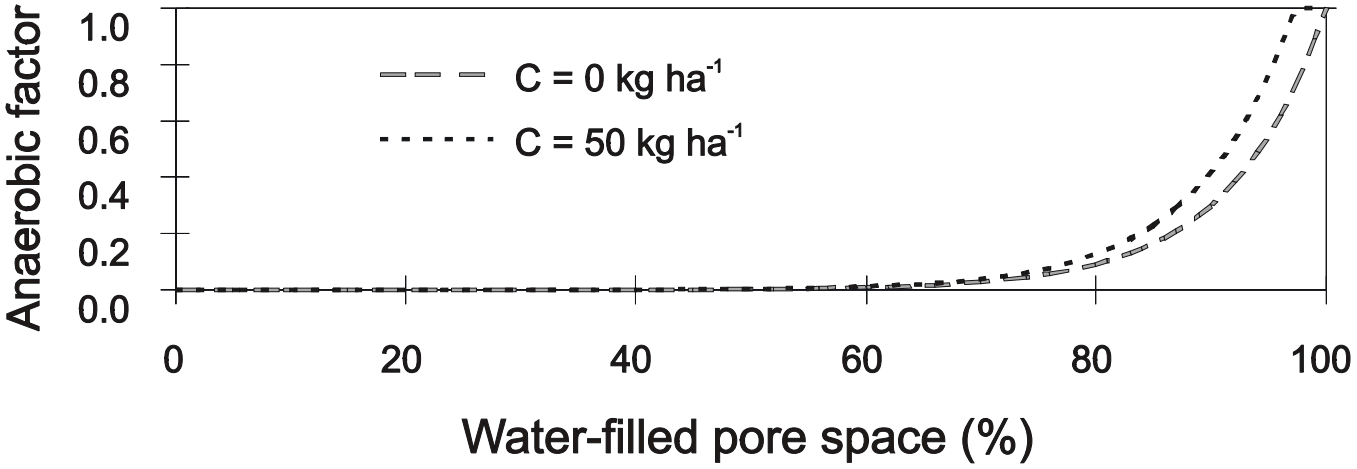

Figure 7.3. The effect of water-filled pore space and two amounts of mineralized carbon on anaerobiosis

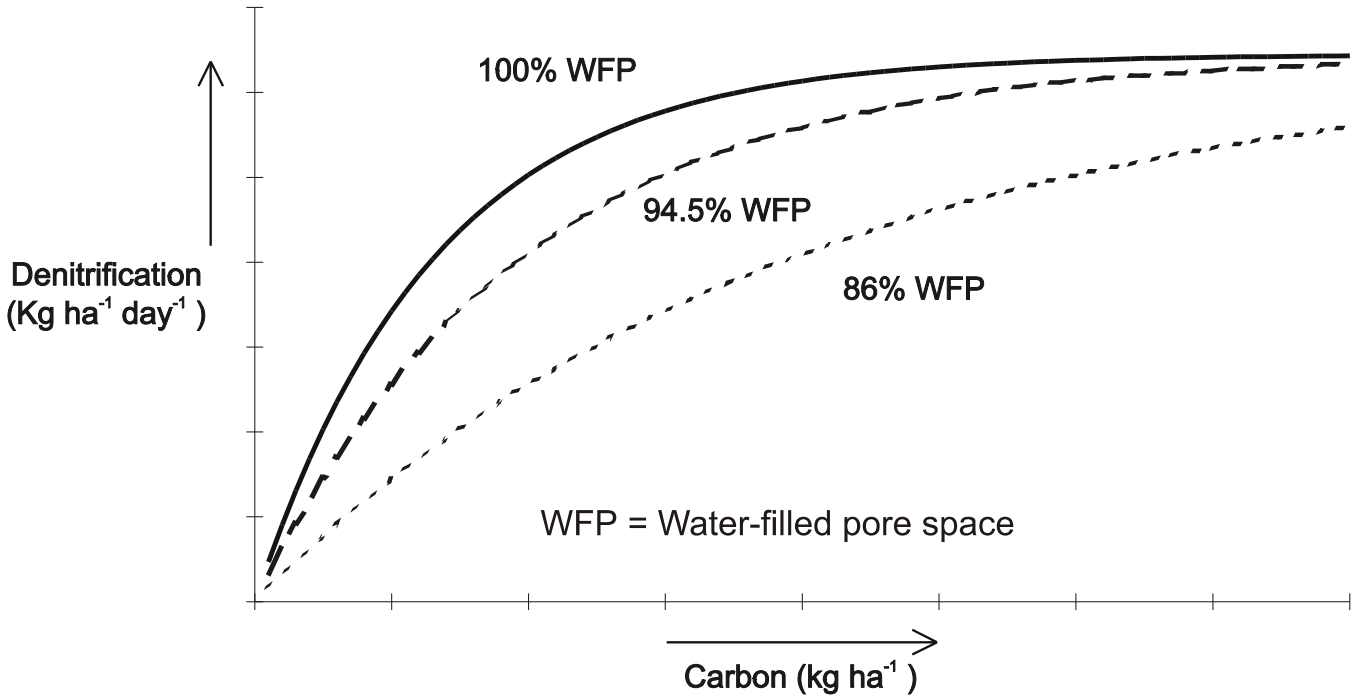

Figure 7.4. Relationship of denitrification to soil carbon content at three moisture levels as simulated in REMM

Chapter 8
Soil Nutrients: Phosphorus

Lee S. Altier, Richard Lowrance, Shreeram P. Inamdar, Randall G. Williams, and Robert K. Hubbard

Summary

Phosphorus is simulated in REMM in organic pools associated with soil carbon, residue carbon, and dissolved carbon and as three functional inorganic pools (labile, active, and stable). Inputs and outputs of phosphorus are from groundwater (dissolved inorganic and organic), surface runoff (dissolved and particulate inorganic and organic), and precipitation (input only). Phosphorus is associated with the humus and residue carbon pools. Simulation of inorganic phosphorus is based on the EPIC model. Only the labile pool of inorganic phosphorus is biologically active and available for plant uptake, resynthesis into organic matter, and leaching. Phosphorus is transformed between the labile and active pools and the active and passive pools based on first-order rate constants and factors for temperature and moisture effects. Labile inorganic phosphorus is partitioned into dissolved and adsorbed forms for surface runoff transport and interaction with the litter layer.

Phosphorous is simulated in the Riparian Ecosystem Management Model (REMM) as a combination of organic and inorganic forms (figure 8.1). The organic pools include those in litter residue and in humus. Inorganic pools are defined by labile, active, and stable forms of phosphorus. Organic pools are differentiated on the basis of carbon-to-phosphorus ratios (carbon/phosphorus). The total amount of phosphorus in each litter or soil layer is the sum of inorganic and organic components:

$$PGrd_t = \sum_{i=1}^{2} PRes_{i,t} + \sum_{j=1}^{3} PHum_{j,t} + \sum_{q=1}^{3} PInorg_{q,t} \quad [8.1]$$

where, on day *t:*

$PGrd_{,t}$ is phosphorus in a litter or soil layer (kg ha^{-1}),

$PRes_{i,t}$ is phosphorus in residue pool *i* (metabolic or structural) (kg ha^{-1}),

$PHum_{j,t}$ is phosphorus in humus pool *j* (active, slow, or passive) (kg ha^{-1}), and

$PInorg_{q,t}$ is phosphorus in inorganic pool *q* (labile, active, or stable) (kg ha^{-1}).

Inputs of phosphorus occur from precipitation, surface runoff, and sediment. Figure 8.2 illustrates the inputs, losses, and fluxes between phosphorus pools. A detailed discussion on the fluxes is provided in the following sections.

Phosphorus reaching the soil from precipitation is given by—

$$P_{PrecipThru,p,t} = 0.01\ PConc_{Precip,p} \times (Precip_t - Int_t) \quad [8.2]$$

where, on day *t:*

$P_{PrecipThru,p,t}$ is nitrogen in form *p* (organic or inorganic) that reaches the ground surface (kg ha^{-1}),

0.01 is a conversion factor,

$PConc_{Precip,p}$ is the concentration of phosphorus (mg L^{-1}) in precipitation in form *p*,

$Precip_t$ is the amount of precipitation on day *t* (mm), and

Int_t is canopy interception (mm).

Organic Forms

As with nitrogen, phosphorus is tied up in all five of the organic matter pools in the model. Thompson et al. (1954) and Sharpley et al. (1984) found linear relationships between organic phosphorus, organic carbon, and total nitrogen in studies of various soils. Thompson et al. (1954) also observed positive correlations between the mineralization of carbon, nitrogen, and phosphorus. In REMM, phosphorus is assumed to be stoichiometrically related to the carbon component:

$$POrg_t = \frac{COrg_t}{CPR_t} \quad [8.3]$$

where, on day *t:*

$POrg_t$ is phosphorus in an organic matter pool (residue or humus) (kg ha^{-1}),

$COrg_t$ is carbon in the organic matter pool (kg ha^{-1}), and

CPR_t is the carbon/phosphorus ratio of the organic matter pool.

Plant Residues

The mass balance of phosphorus in residue is—

$$\begin{aligned} PRes_{i,t} = {} & PRes_{i,t-1} + PResInput_{i,t} + PRes_{DissIn,i,t} + PRes_{ErosIn,i,t} \\ & + PRes_{BurIn,i,t} + PRes_{SoilUpIn,i,t} - PRes_{DissOut,i,t} - PRes_{ErosOut,i,t} \\ & - PRes_{BurOut,i,t} - PRes_{SoilUpOut,i,t} - PResR_{i,t} \end{aligned} \quad [8.4]$$

where, in residue component *i* (metabolic or structural) on day *t:*

$PRes_{i,t}$ is the total residue phosphorus (kg ha^{-1});

$PResInput_{i,t}$ is input of phosphorus in fresh plant residue (kg ha^{-1});

$PRes_{DissIn,i,t}$ and $PRes_{DissOut,i,t}$ are dissolved phosphorus in incoming and outgoing water, respectively (metabolic residue only) (kg ha^{-1});

$PRes_{ErosIn,i,t}$ and $PRes_{ErosOut,i,t}$ are phosphorus carried in and out, respectively, in runoff water (in litter layer and upper soil layer only) (kg ha^{-1});

$PRes_{BurIn,i,t}$ and $PRes_{BurOut,i,t}$ are phosphorus buried in the upper soil layer and removed from the litter layer, respectively, as net sedimentation occurs (for upper soil layer and litter layer only) (kg ha^{-1});

$PRes_{SoilUpIn,i,t}$ and $PRes_{SoilUpOut,i,t}$ are phosphorus moved into the litter layer and removed from the upper soil layer, respectively, in order to maintain a constant depth in the litter layer (for litter layer and upper soil layer only) (kg ha^{-1}); and

$PResR_{i,t}$ is release of phosphorus (kg ha^{-1}).

Most of the values in equation 8.4 are determined based on the carbon pool (chapter 6) and carbon/phosphorus ratios (equation 8.3). Fresh residue is placed into the structural pool at a fixed carbon/phosphorus ratio. All remaining phosphorus in fresh residue inputs, in excess of that needed to fulfill the requirement for structural residue, is placed in the metabolic residue pool:

$$PRes_{Input,stc,t} = CRes_{Input,t} \times F_{stc,t} / CPR_{stc} \quad [8.5]$$

$$PRes_{Input,mtb,t} = PRes_{Input,t} - PRes_{Input,stc,t} \quad [8.6]$$

where $CRes_{Input,t}$ is the total carbon in fresh residue inputs on day *t* (kg ha^{-1}):

$F_{stc,t}$ is the fraction of carbon in fresh residues that is structural on day *t*,

CPR_{stc} is the carbon/phosphorus ratio of structural residue (set at 500),

$PRes_{Input,t}$ is the total phosphorus in fresh residue inputs on day *t* (kg ha^{-1}),

$PRes_{Input,stc,t}$ is the phosphorus in fresh residue entering the structural pool from day *t* (kg ha^{-1}), and

$PRes_{Input,mtb,t}$ is the phosphorus in fresh residue entering the metabolic pool on day *t* (kg ha^{-1}).

Humus

Organic phosphorus in the soil is calculated as a function of daily mineralization and synthesis. The mass balance for organic phosphorus is calculated as—

$$PHum_{j,t} = PHum_{j,t-1} + P_{Immob,j,t} + PHum_{DissIn,j,t} + PHum_{ErosIn,j,t} + PHum_{BurIn,j,t} + PHum_{SoilDepIn,j,t} + PHum_{SoilUpIn,j,t} - PHumR_{j,t} - PHum_{DissOut,j,t} - PHum_{ErosOut,j,t} - PHum_{BurOut,j,t} - PHum_{SoilDepOut,j,t} - PHum_{SoilUpOut,j,t} \quad [8.7]$$

where, in humus pool j on day t:

$PHum_{j,t}$ is total humus phosphorus (kg ha^{-1});

$P_{Immob,j,t}$ is labile inorganic phosphorus immobilized into organic matter (kg ha^{-1});

$PHum_{DissIn,j,t}$ and $PHum_{DissOut,j,t}$ are incoming and outgoing dissolved phosphorus, respectively (active humus pool only) (kg ha^{-1});

$PHum_{ErosIn,j,t}$ and $PHum_{ErosOut,j,t}$ are undissolved phosphorus in incoming and outgoing sediment, respectively (litter layer and upper soil layer only) (kg ha^{-1});

$PHum_{BurIn,j,t}$ and $PHum_{BurOut,j,t}$ are phosphorus buried in the upper soil layer and removed from the litter layer, respectively, as net sedimentation occurs (for upper soil layer and litter layer only) (kg ha^{-1});

$PHum_{SoilDepIn,j,t}$ and $PHum_{SoilDepOut,j,t}$ are phosphorus incorporated into upper soil layer and removed from the litter layer, respectively, in order to maintain a constant depth in the litter layer (for litter layer and upper soil layer only) (kg ha^{-1});

$PHum_{SoilUpIn,j,t}$ and $PHum_{SoilUpOut,j,t}$ are phosphorus moved into the litter layer and removed from the upper soil layer, respectively, in order to maintain a constant depth in the litter layer (for litter layer and upper soil layer only) (kg ha^{-1}); and

$PHumR_{j,t}$ is phosphorus released from humus (kg ha^{-1}).

Unlike immobilization of inorganic nitrogen, the carbon/phosphorus ratio of newly formed organic material is allowed to vary depending on the content of labile inorganic phosphorus in the soil. This approach follows the Century model (Parton et al. 1988) and is based on concepts of McGill and Cole (1981):

$$P_{Immob,j,t} = CSyn_{j,t} / CPR_{Syn,j,t} \quad [8.8]$$

$$CPR_{Syn,j,t} = (\alpha_j + \beta_j)P_{lb,t} \quad [8.9]$$

where:

$CSyn_{j,t}$ is carbon synthesized into humus pool j on day t (kg ha^{-1}),

$CPR_{Syn,j,t}$ is the carbon/phosphorus ratio of newly synthesized material in humus pool j on day t,

α and β are coefficients (see table 8.1), and

$P_{lb,\,t}$ is labile inorganic phosphorus on day t (kg ha^{-1}).

The release of phosphorus from the soil organic matter pools corresponds with carbon mineralization:

$$PHumR_{j,t} = CHumR_{j,t} / CPR_j \quad [8.10]$$

where, on day t:

$CHumR_{j,t}$ is carbon mineralized from humus pool j (kg ha^{-1}).

The carbon/phosphorus ratios for the pools are updated after new organic matter is synthesized each day:

$$CPR_{j,t} = \frac{CHum_{j,t-1} + CSyn_{j,t}}{PHum_{j,t-1} + P_{Immob\,j,t}} \quad [8.11]$$

where:

$CHum_{j,t-1}$ is carbon in humus pool j at the end of day t–1.

Inorganic Nitrogen

Simulation of inorganic phosphorus dynamics is taken from the EPIC model (Jones et al. 1984, Williams et al. 1984) in which three pools of inorganic phosphorus are identified. Only the labile pool is biologically available.

Labile

Phosphorus that mineralizes from organic matter (referred to as labile phosphorus) is available for plant uptake, resynthesis into soil organic matter, leaching down through the soil profile, or stabilization into inactive forms of inorganic phosphorus. The mass balance for labile phosphorus is determined by—

$$P_{lb,t} = P_{lb,t-1} + P_{Fert,lb,t} + P_{DissIn,lb,t} + P_{ErosIn,lb,t} + P_{BurIn,lb,t} + P_{SoilDepIn,lb,t} + P_{SoilUpIn,lb,t} + \sum_{i=1}^{2} PResR_{i,t} + \sum_{i=1}^{3} PHumR_{j,t} - \sum_{i=1}^{3} P_{Immob,j,lb,t} - P_{Uptk,lb,t} - P_{DissOut,lb,t} - P_{ErosOut,lb,t} - P_{BurOut,lb,t} - P_{SoilDepOut,lb,t} - P_{SoilUpOut,lb,t} - R_{la,t} \quad [8.12]$$

where, on day *t:*

$P_{Fert,lb,t}$ is phosphorus from fertilizer (litter layer and upper soil layer only) (kg ha^{-1});

$P_{DissIn.lb,t}$ and $P_{DissOut,lb,t}$ are incoming and outgoing dissolved labile phosphorus, respectively (kg ha^{-1});

$P_{ErosIn,\ lb,\ t}$ and $P_{ErosOut,lb,t}$ are phosphorus on sediment carried in incoming and outgoing runoff water, respectively (in litter layer and upper soil layer only) (kg ha^{-1});

$P_{BurIn,lb,t}$ and $P_{BurOut,lb,t}$ are phosphorus buried in the upper soil layer and removed from the litter layer, respectively, as net sedimentation occurs (for upper soil layer and litter layer only) (kg ha^{-1});

$P_{SoilDepIn,lb,t}$ and $P_{SoilDepOut,lb,t}$ are phosphorus incorporated into upper soil layer and removed from the litter layer, respectively, as a constant depth is maintained in the litter layer (for litter layer and upper soil layer only) (kg ha^{-1});

$P_{SoilUpIn,lb,t}$ and $P_{SoilUpOut,lb,t}$ are phosphorus moved into the litter layer and removed from the upper soil layer, respectively, as a constant depth is maintained in the litter layer (for litter layer and upper soil layer only) (kg ha^{-1});

$P_{Uptk,lb,t}$ is plant uptake of phosphorus (kg ha^{-1}); and

$R_{la,t}$ is transformation from labile to active inorganic phosphorus (kg ha^{-1}).

The amount of labile phosphorus available from fertilizer is determined by (Jones et al. 1984)—

$$P_{Fert,lb,t} = P_{Fert,t} \times F_{lb} \quad [8.13]$$

where, on day *t:*

$P_{Fert,lb,t}$ is the amount of phosphorus in applied fertilizer (kg ha^{-1}), and

F_{lb} is an availability index (dimensionless).

This index is defined as the proportion of labile phosphorus from a fertilizer application remaining in a soil after incubation for 6 months. Sharpley et al.

(1984) have estimated values of the availability index for different soils based on regression analyses (table 8.2).

Active

Labile inorganic phosphorus is in equilibrium with an active inorganic phosphorus pool, which is assumed to be adsorbed on soil material. The mass balance for the active pool is—

$$P_{act,t} = P_{act,t-1} + R_{la,t} + P_{ErosIn,act,t} + P_{BurIn,act,t} + P_{SoilDepIn,act,t} + P_{SoilUpIn,act,t} - R_{as,t} - P_{ErosOut,act,t} - P_{BurOut,act,t} - P_{SoilDepOut,act,t} - P_{SoilUpOut,act,t} \quad [8.14]$$

where, in active inorganic form on day *t:*

$P_{act,t}$ is phosphorus (kg ha^{-1});

$P_{ErosIn,act,t}$ and $P_{ErosOut,act,t}$ are phosphorus on sediment carried in incoming and outgoing runoff water, respectively (in litter layer and upper soil layer only) (kg ha^{-1});

$P_{BurIn,act,t}$ and $P_{BurOut,act,t}$ are phosphorus buried in the upper soil layer and removed from the litter layer, respectively, as net sedimentation occurs (for upper soil layer and litter layer only) (kg ha^{-1});

$P_{SoilDepIn,act,t}$ and $P_{SoilDepOut,act,t}$ are phosphorus incorporated into upper soil layer and removed from the litter layer, respectively, as a constant depth is maintained in the litter layer (for litter layer and upper soil layer only) (kg ha^{-1});

$P_{SoilUpIn,act,t}$ and $P_{SoilUpOut,act,t}$ are phosphorus moved into the litter layer and removed from the upper soil layer, respectively, as a constant depth is maintained in the litter layer (for litter layer and upper soil layer only) (kg ha^{-1}); and

$R_{as,t}$ is phosphorus transformed from the active pool to the stable pool (kg ha^{-1}).

The availability index is used to initialize the size of the active pool (Jones et al. 1984):

$$P_{act,init} = P_{lb,init} (1 - F_{lb}) / F_{lb} \quad [8.15]$$

where:

$P_{act,init}$ and $P_{lb,init}$ are amounts of phosphorus in the active and labile inorganic pools, respectively, at the beginning of the simulation (kg ha^{-1}).

Transformations of phosphorus between the labile and active pools are determined by (Jones et al. 1984)—

$$R_{la,t} = 0.1[P_{lb,t} - P_{act,t}(F_{lb} / (1 - F_{lb}))]TFac_{p,t} \times WFac_{p,t} \quad [8.16]$$

where, on day t:

$R_{la,t}$ is phosphorus transformation from the labile to active inorganic pools (kg ha^{-1}), and

0.1 is a first-order rate constant for optimal temperature and moisture conditions (day^{-1}).

$TFac_{p,t}$ and $WFac_{p,t}$ are temperature and moisture effects, respectively:

$$TFac_{p,t} = \exp(0.115 * TSOIL - 2.8) \quad [8.17]$$

where:

TSOIL is the average daily temperature of each soil layer.

$$WFac_{p,t} = \text{Minimum of} \begin{cases} 1 \\ \theta_t / \theta_{FC} \end{cases} \quad [8.18]$$

where:

θ_t is soil water content (mm), and

θ_{FC} is soil water content at field capacity (mm).

A negative value for $R_{la,t}$ indicates transformation from the active to the labile pool.

Figure 8.3 illustrates an example of how the size of the active phosphorus pool can vary with different levels of labile phosphorus. Low to moderate levels of the labile phosphorus pool are smaller than the equilibrium size of the active phosphorus pool. As additional labile phosphorus is added to the soil, relatively larger proportions of phosphorus stays in labile form. Maximum size of the active phosphorus pool depends on the adsorption capacity of the soil. Once that capa-city is reached, further additions of labile phosphorus will remain in labile form.

Stable

The third pool comprises stable forms of inorganic phosphorus adsorbed on the soil in equilibrium with the active pool of inorganic phosphorus. The mass balance for stable inorganic phosphorus is—

$$P_{stb,t} = P_{stb,t-1} + R_{as,t} + P_{ErosIn,stb,t} + P_{BurIn,stb,t} + P_{SoilDepIn,stb,t} + P_{SoilUpIn,stb,t} - P_{ErosOut,stb,t} - P_{BurOut,stb,t} - P_{SoilDepOut,stb,t} - P_{SoilUpOut,stb,t} \quad [8.19]$$

where, in stable inorganic form on day *t:*

$P_{stb,t}$ is active inorganic phosphorus (kg ha^{-1});

$R_{as,t}$ is phosphorus transformed from the active pool to the stable pool (kg ha^{-1});

$P_{ErosIn,stb,t}$ and $P_{ErosOut,stb,t}$ are phosphorus on sediment carried in incoming and outgoing runoff water, respectively (in litter layer and upper soil layer only) (kg ha^{-1});

$P_{BurIn,stb,t}$ and $P_{BurOut,stb,t}$ are phosphorus buried in the upper soil layer and removed from the litter layer, respectively, as net sedimentation occurs (for upper soil layer and litter layer only) (kg ha^{-1});

$P_{SoilDepIn,stb,t}$ and $P_{SoilDepOut,stb,t}$ are phosphorus incorporated into the upper soil layer and removed from the litter layer, respectively, as a constant depth is maintained in the litter layer (for litter layer and upper soil layer only) (kg ha^{-1}); and

$P_{soilUpIn,stb,t}$ and $P_{SoilUpOut,stb,t}$ are phosphorus moved into the litter layer and removed from the upper soil layer, respectively, as a constant depth is maintained in the litter layer (for litter layer and upper soil layer only) (kg ha^{-1}).

The amount of phosphorus that is transformed from active to stable inorganic forms is determined by (Jones et al. 1984)—

$$R_{as,t} = K_{as}(4\,P_{act,t} - P_{stb,t}) \quad [8.20]$$

where, on day *t:*

$R_{as,t}$ is phosphorus transformation from active to stable inorganic forms (kg ha^{-1}),

K_{as} is a first-order rate constant (day^{-1}), and

$P_{stb,t}$ is phosphorus in the stable pool (kg ha^{-1}).

A negative value for $R_{as,t}$ indicates transformation from stable to active inorganic phosphorus.

The value for K_{as} is related to the type of soil (Jones et al. 1984):

$$K_{as} = \begin{cases} 0.00076 & \text{Calcareous soil} \\ \exp(-1.77\ F_{lb} - 7.05) & \text{Noncalcareous soil} \end{cases} \quad [8.21]$$

Phosphorus Adsorption from Percolation and Runoff Water

Sharpley et al. (1981) showed that there can be rapid removal of phosphorus from runoff water by adsorption onto surface soil. The capacity of a soil to adsorb phosphorus is related to its texture. Bowman and Savory (1992) found an inverse correlation between soil sand content and total phosphorus. They commented that although phosphorus may be immobile in the short term, gradual movement of phosphorus may occur.

Movement of phosphorus can occur with sediment, surface and subsurface runoff, and vertical drainage. Organic-active and inorganic-labile forms of phosphorus are assumed to be associated with sediment. Dissolved forms of inorganic-labile phosphorus and active-organic phosphorus move with water. Partitioning of phosphorus into dissolved and adsorbed fractions is computed using the Langmuir isotherm as described by Novotny and Olem (1994):

$$PConc_{Ads,t} = \frac{Q^0 \times b \times PConc_{Diss,t}}{1 + b \times PConc_{Diss,t}} \quad [8.21]$$

where, on day *t:*

$PConc_{Ads,t}$ is the adsorbed phosphorus concentration (µg g^{-1}),

$PConc_{Diss,t}$ is the dissolved phosphorus concentration (µg L^{-1}), and

Q^0 (µg g^{-1}) and b (L µg^{-1}) are adsorption coefficients given by—

$$Q^0 = -3.5 + (10.7 \times clay) + (49.5 \times C) \quad [8.22]$$

and

$$b = 0.061 + (170{,}000 \times 10^{-pH}) + (0.027 \times clay) + (0.76 \times C) \quad [8.23]$$

where:

clay is the percentage of clay in the soil layer, and

C is the percentage of carbon in the soil layer.

Since dissolution and adsorption in the litter layer must be calculated as an intermediate step between incoming and outgoing runoff, corresponding equations are used for the litter layer.

The mass of soil in each soil layer *($Soil_t$)* is calculated as—

$$Soil_t = 10^4 \times \frac{LyrDepth_t}{1000} \times BD \quad [8.24]$$

where, on day *t:*

$LyrDepth_t$ is depth of the litter or soil layer (mm), and

BD is the bulk density of the layer (kg m^{-3}).

The mass of soil in the litter layer on day *t* before outgoing runoff occurs is—

$$Soil_{Ltr,t'} = Sed_{ErosIn,t} + 10 \times \frac{LyrDepth_{Ltr}}{1000} \times BD_{Ltr,t-1} \quad [8.26]$$

where:

$Sed_{ErosIn,t}$ is incoming sediment on day *t* (kg ha^{-1}).

Outgoing water from a layer carries dissolved phosphorus determined by—

$$P_{DissOut,t} = 10^4 PConc_{Diss,t} \times WaterOut_t \quad [8.27]$$

where:

$P_{DissOut,t}$ is dissolved phosphorus in outgoing water on day *t* (kg ha^{-1}).

Outgoing surface runoff water also carries adsorbed phosphorus in sediment, determined by—

$$P_{ErosOut,t} = Sed_{ErosOut,t} \times PConc_{Ads,t} \times ER_t \quad [8.28]$$

where:

$P_{ErosOut,t}$ is adsorbed phosphorus in outgoing water (kg ha^{-1}), and

Er_t is the enrichment ratio on day *t* (described in chapter 3).

The litter layer is a special case for which the volume of water and the amount of labile phosphorus must be calculated on each day in an intermediate step before erosion occurs:

$$\theta_{Ltr,t'} = \theta_{Ltr,t-1} + RunoffIn_t \quad [8.29]$$

where:

$\theta_{Ltr,t'}$ is the volume of water in the litter on day t after incoming surface runoff has entered the zone but before infiltration or outgoing runoff has occurred (mm), and

$\theta_{Ltr,t-1}$ is the volume of water in the litter layer at the end of day t–1 (mm).

When surface runoff water enters a zone, the total labile phosphorus in the litter layer becomes—

$$P_{lb,Ltr,t'} = P_{lb,Ltr,t-1} + (Sed_{ErosIn,t} \times PConc_{SedIn,t}) + (PConc_{WaterIn,t} \times WaterIn_t) \quad [8.30]$$

where, on day t:

$P_{lb,Ltr,t'}$ is labile phosphorus in the litter layer on day t after surface runoff has entered the zone but before infiltration or outgoing runoff has occurred (kg ha^{-1}),

$Pconc_{SedIn,t}$ is the phosphorus concentration in incoming sediment (kg kg^{-1}), and

$Pconc_{WaterIn,t}$ is the phosphorus concentration in incoming water (kg cm^{-1}).

The quantity of labile phosphorus calculated in equation 8.30 is then used to partition labile phosphorus into dissolved and adsorbed portions in equations 8.23 and 8.32, so that amounts of phosphorus eroding on the same day can be determined.

References

Bowman, R.A., and D.J. Savory. 1992. Phosphorus distribution in calcareous soil profiles of the central plains. Soil Science Society of America Journal 56:423–426.

Jones, C.A., C.V. Cole, A.N. Sharpley, and J.R. Williams. 1984. A simplified soil and plant phosphorus model: I. Documentation. Soil Science Society of America Journal 48:800–805.

McGill, W.B., and C.V. Cole. 1981. Comparative aspects of cycling of organic carbon, nitrogen, sulphur and phosphorus through soil organic matter. Geoderma 26:267–286.

Novotny, V., and H. Olem. 1994. Water Quality: Prevention, Identification, and Management of Diffuse Pollution. Van Nostrand Reinhold, New York.

Parton, W.J., J.W.B. Stewart, and C.V. Cole. 1988. Dynamics of C, N, P and S in grassland soils: a model. Biogeochemistry 5:109–131.

Sharpley, A.N, R.G. Menzel, S.J. Smith, et al. 1981. The sorption of soluble phosphorus by soil material during transport in runoff from cropped and grassed watersheds. Journal of Environmental Quality 10:211–215.

Sharpley, A.N., S.J. Smith, B.A. Stewart, and A.C. Mathers. 1984. Forms of phosphorus in soil receiving cattle feedlot waste. Journal of Environmental Quality 13:211–215.

Thompson, L.M., C.A. Black, and J.A. Zoellner. 1954. Occurrence and mineralization of organic phosphorus in soils, with particular reference to associations with nitrogen, carbon, and pH. Soil Science 77:185–196.

Williams, J.R., C.A. Jones, and P.T. Dyke. 1984. A modeling approach to determining the relationship between erosion and soil productivity. Transactions of the ASAE 27:129–144.

Table 8.1. Coefficients for determining carbon/phosphorus ratios of newly synthesized soil organic matter

Organic matter pool	a*	b*	Minimum carbon/phosphorus ratio†
Active	80	–30	20
Slow	200	–55	90
Passive	200	–90	20

* From equation 8.9.

† The carbon/phosphorus ratios are constrained so that they do not go below these values.

Source: Parton et al. 1988

Table 8.2. Equations for estimation of phosphorus availability index

	Range of properties of soils from which equations were derived†							
Soil group*	Sand	Silt	Clay	pH	$CaCO_3$	BS**	CEC***	Equation§
	----------(%)----------				($g\ kg^{-1}$)	(%)	($cmol\ kg^{-1}$)	
Calcareous	4–71	17–62	10–67	7.1–8.4	0.5–54	100	8–55	$F_{lb} = 0.58 - 0.00061\ CaCO_3$
Slightly weathered	1–87	6–85	6–62	5.2–8.3	—	40–100	5–43	$F_{lb} = -0.70 + 0.0043\ BS + 0.0034\ PLab + 0.11\ pH$
Highly weathered	6–96	1–76	0.4–76	4.4 –6.8	—	11–100	1.3–20.5	$F_{lb} = 0.39 - 0.047\ \ln Clay + 0.0045\ Plab - 0.0053\ OC$

* Definitions of soil groups:
Calcareous soils are soils with free $CaCO_3$.
Highly weathered soils are Oxisols, Ultisols, Quartzipsamments, Ultic subgroups of Alfisols, and acidic Ochrepts.
Slightly weathered are all other soils.

** Base Saturation

*** Cation Exchange Capacity

† Variables:
$CaCO_3$ ($g\ CaCO_3$ per kg soil)
PLab is inorganic labile phosphorus ($\mu g\ g^{-1}$)
Clay (%)
OC is organic carbon (g C per kg soil)

§ Sharpley et al. recommended that these equations not be used with soil data outside these ranges.

Source: Sharpley et al. 1984

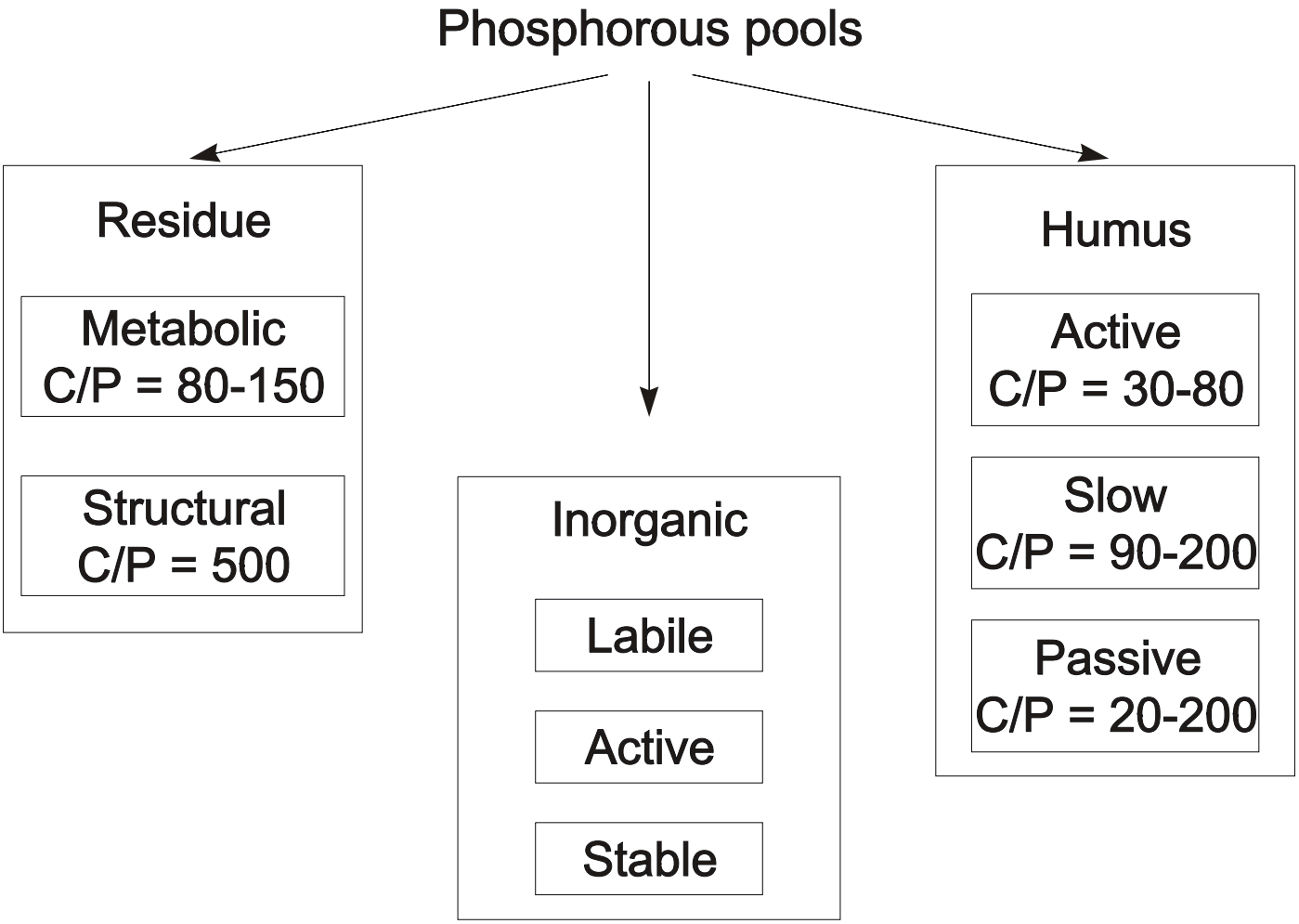

Figure 8.1 Phosphorus pools in REMM (from Jones et al. 1984)

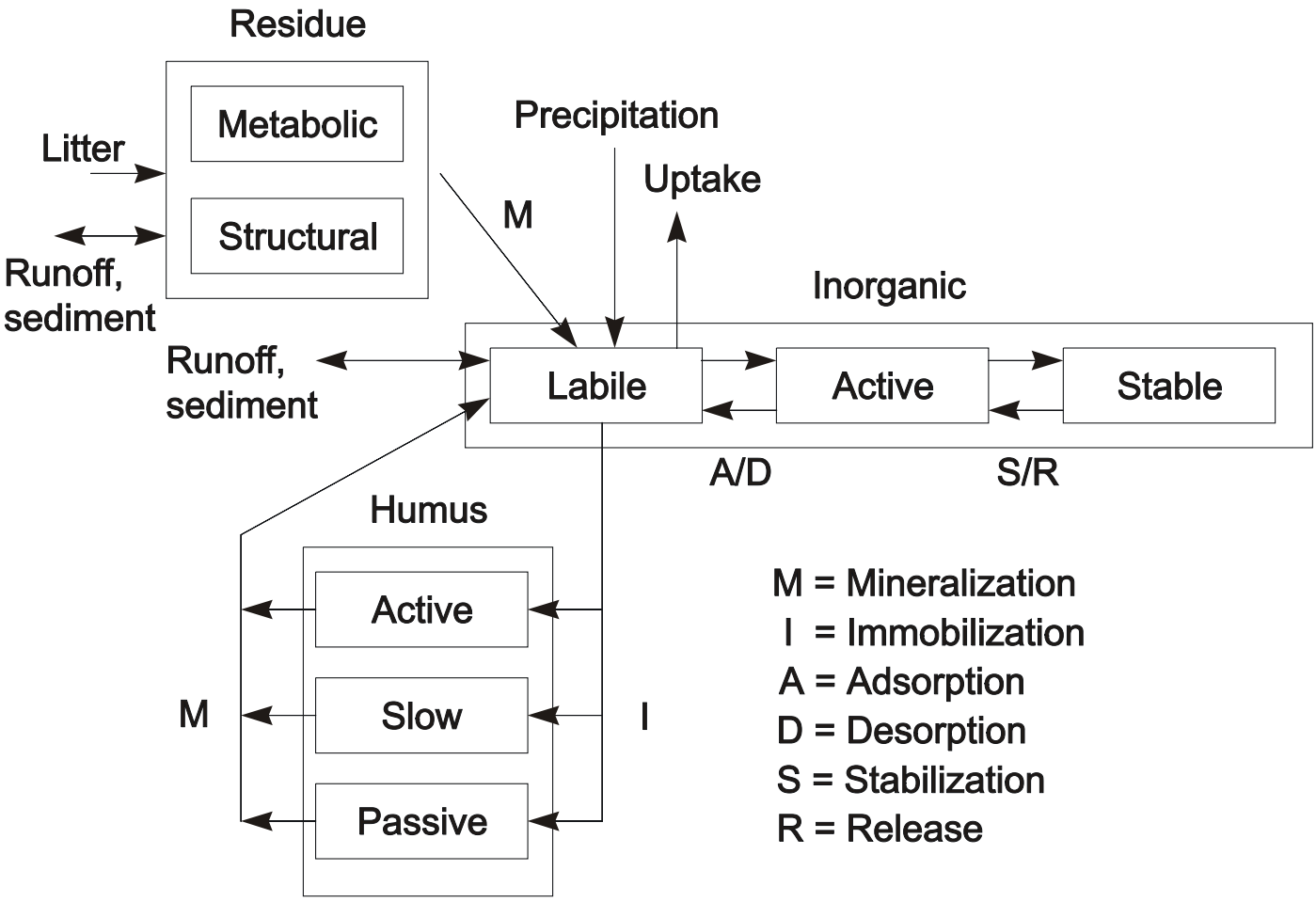

Figure 8.2. Fluxes among phosphorus pools in REMM

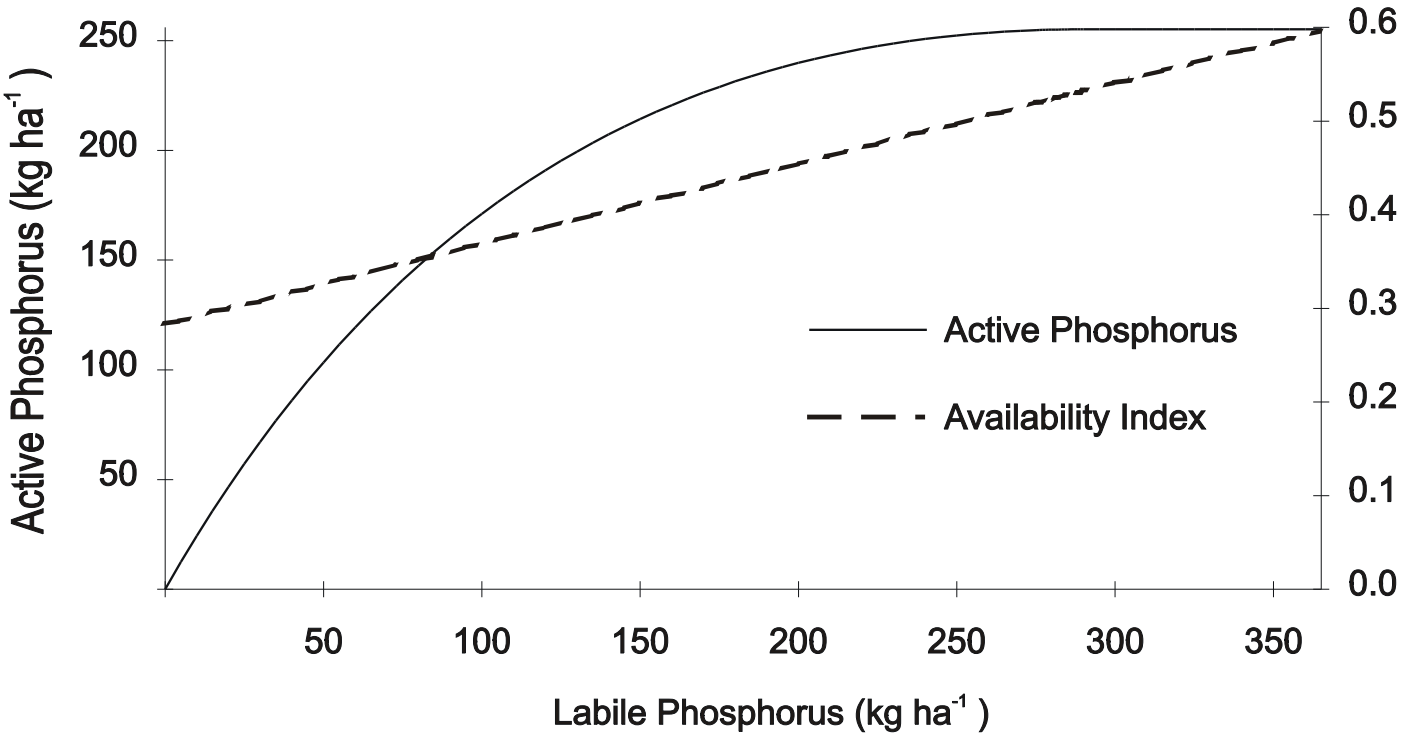

Figure 8.3. Relationship between equilibrium levels of labile phosphorus, active phosphorus, and the availability index in a slightly weathered soil with a pH of 6.2 and 70 percent base saturation

Chapter 9

Soil Temperature

Lee S. Altier and Shreeram P. Inamdar

Summary

Soil temperature is modeled in REMM using an empirical approach for the soil surface and a heat flux approach for the subsurface soil. Litter is accounted for by using a litter-blocking factor that dampens the changes in surface temperatures. Heat flux is based on soil properties: total porosity, volumetric water content, bulk density, and clay content.

Surface Temperatures

From sensitivity analysis of a model simulating soil temperature, Glenn and Welker (1987) found that soil surface treatments such as cultivation or killed sod were much more influential on subsurface temperatures than soil characteristics such as bulk density or water content. They noted, "the primary mechanism controlling the vertical temperature distribution in the root zone is the amount of energy captured at the soil surface available for transfer in the root zone and the resultant temperature gradient."

An empirical approach is used for modeling surface temperatures in the Riparian Ecosystem Management Model (REMM). Kemp et al. (1992) noted that their use of regression models for calculating soil temperatures resulted in much less error than the energy balance approach. They pointed out that even simplified energy budgets required parameters that were difficult to estimate. Surface temperature equations were modified from GLEAMS (Knisel 1993).

Temperature at the litter surface (T_{surf}) for current day d is computed using—

$$T_{surf[d]} = [(TAir_{max} + TAir_{min})/2](1 - Rad/800) + (TAir_{max} \times Rad/800) \quad [9.1]$$

where:

$TAir_{max}$ and $TAir_{min}$ are maximum and minimum air temperatures (˚C) for the current day, respectively; and

Rad is the solar radiation reaching the ground surface (kJ ha^{-1} day^{-1}).

A running average of the current day and the previous three days is then computed and is given as $T_{surfavg}$, the running average temperature at the litter surface.

The final temperature for the current day at the soil surface (below the litter layer) is then expressed by—

$$T_{soilsurf[d]} = (\delta \times T_{surf[d]}) + [(1-\delta) \times T_{surfavg}] \quad [9.2]$$

where:

δ is the litter blocking factor.

Subsurface Temperatures

Models simulating soil temperatures are commonly based on the Fourier Law for calculating heat flux through soil (Parton 1984, Campbell 1985, Nobel and Geller 1987, McCann et al. 1991):

$$f_h = -\lambda \, dT / dz \qquad [9.3]$$

where:

f_h is heat flux density (W m^{-2}),

λ is thermal conductivity (W m^{-1} K^{-1}),

T is temperature (K), and

z is distance (m).

Using a procedure from Campbell (1985), diurnal variation in soil temperature at the soil surface is simulated in REMM by a sine wave pattern. Heat flux is determined sequentially through layers of soil based on the conductivity and heat capacity of each layer. Thickness of the layers was determined in a geometric series, increasing from 1 cm at the soil surface where the temperature fluctuations are greatest, to over 1 m thick below 3 m depth. Figure 9.1 shows an example of the damping effect on temperature fluctuations with increasing soil depth.

Specific heat is calculated as (Campbell 1985)—

$$C_h = C_m (1 - \phi_f) + C_w \theta \qquad [9.4]$$

where:

C_h is volumetric specific heat of soil (J m^{-3} K^{-1});

C_m and C_w are the volumetric specific heat values of mineral material and water, respectively (J m^{-3} K^{-1});

ϕ_f is total soil porosity (fraction); and

θ is volumetric water content.

Campbell (1985) uses a value of 2.40 J m^{-3} K^{-1} for C_m. The specific heat of air is relatively small and therefore ignored. Because organic matter has a volumetric specific heat similar to those of mineral materials and it comprises a small portion of most mineral soils, its contribution is also ignored. Freezing soil conditions are not simulated in the current version of REMM.

The estimation of thermal conductivity is more complicated, requiring a greater knowledge of the composition of the soil. It is calculated as (McInnes 1981 cited in Campbell 1985)—

$$\lambda = A + B\theta - (A - C) \times \exp[-(C\theta)^E] \quad [9.5]$$

where:

λ is thermal conductivity (W m^{-1} K^{-1}), and

A, B, C, D, and *E* are coefficients. These coefficients were estimated by Campbell (1985) as—

$$A = \frac{0.57 + 1.73\phi_q + 0.93\phi_m}{1 - 0.74\phi_q - 0.49\phi_m} - 2.8\phi_s(1 - \phi_s) \quad [9.6]$$

$$B = 1.06 \times BD \times \theta \quad [9.7]$$

$$C = 1 + 2.6\, m_c^{-1/2} \quad [9.8]$$

$$D = 0.03 + 0.1\, BD^2 \quad [9.9]$$

where:

ϕ_q is the volume fraction of quartz,

ϕ_m is the volume fraction of other minerals,

ϕ_s is the total volume fraction of solids ($\phi_q + \phi_m$),

θ is volumetric water content (m^3 m^{-3}),

m_c is the clay fraction, and

BD is the soil bulk density (Mg m^{-3}).

Campbell points out that the quartz fraction is negligible in many mineral soils, so equation 9.6 can be estimated by—

$$A = 0.65 - 0.78\,BD + 0.60\,BD^2 \quad [9.10]$$

where:

BD is bulk density (Mg m^{-3}).

The estimation of *D* is for mineral soil with an average particle density of 2.65 Mg m^{-3}. For forest litter, Campbell (1985) estimates the values of the coefficients as *A* = 0.4, *B* = 0.5, *C* = 1, and *D* = 0.06 and E = 4.0. In order to estimate soil temperature at the lower end of the soil profile, Campbell (1977) suggests that at intermediate soil water contents and densities, the temperature at a depth of 6 to 7 m will remain about equal to the average annual soil surface temperature. So in the REMM temperature module, the temperature at 6.6 m is set at average annual soil temperature.

References

Campbell, G.S. 1977. An Introduction to Environmental Biophysics. Springer-Verlag, New York.

Campbell, G.S. 1985. Soil Physics with BASIC. Elsevier, New York.

Glenn, D.M., and W.V. Welker. 1987. Soil management effects on soil temperature and heat flux in a young peach orchard. Soil Science 143:372–380.

Kemp, P.R., J.M. Cornelius, and J.F. Reynolds. 1992. A simple model for predicting soil temperatures in desert ecosystems. Soil Science 153:280–287.

Knisel, W.G. 1993. GLEAMS: Groundwater Loading Effects of Agricultural Management Systems, version 2.10. University of Georgia, Coastal Plain Experiment Station, Biological and Agricultural Engineering Department, Publication No. 5.

McCann, I.R., M.J. McFarland, and J.A. Witz. 1991. Near-surface bare soil temperature model for biophysical models. Transactions of the ASAE 34(3):748–755.

Nobel, P.S., and G.N. Gellar. 1987. Temperature modeling of wet and dry desert soils. Journal of Ecology 75:247–258.

Parton, W.J. 1984. Predicting soil temperatures in a shortgrass steppe. Soil Science 138:93–101.

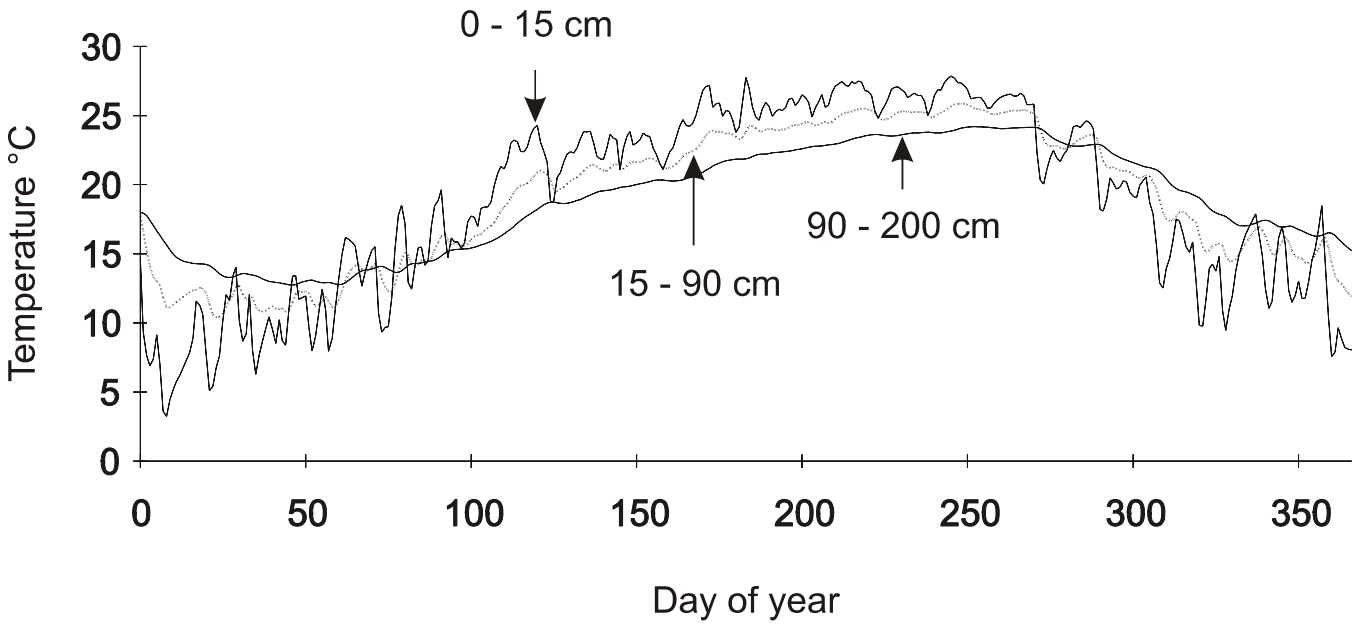

Figure 9.1. Simulated average daily temperatures in three soil layers with no surface cover

Chapter 10
Vegetation: Photosynthesis and Carbon Allocation

Lee S. Altier, Randall G. Williams, and Richard Lowrance

Summary

REMM simulates growth of annual and perennial herbaceous, woody broadleaf, and woody evergreen species in upper and lower plant canopies. Up to 12 types of vegetation can be simulated, each representing one or more plant species. Several different types of woody perennial plants are characterized in the model, corresponding to leaf-fall patterns and leaf longevity of deciduous and evergreen species. Incoming shortwave radiation is divided among vegetation types in the upper canopy according to the relative proportion of land covered by each stand. Radiation is divided among vegetation types in the lower canopy according to the relative sizes of their leaf area indices. REMM simulates plant growth at the stand scale. The combined photosynthesis by all the individuals of each vegetation type in each canopy promotes an increase in biomass of their respective plant organs. Subsequently, this creates a demand for water and nutrients from the soil, and these are distributed among the plant types according to their relative demands.

REMM allows representation of the vegetation in buffers using as many as 12 plant types in two canopies (table 10.1). Increase in biomass in the vegetation types creates demands for water and nutrients and these are distributed among the plant types based on their demands (figure 10.1).

Forest Structure

The total amount of carbon in vegetation is the sum of carbon in the upper (tree) and lower (shrub and herbaceous) canopies:

$$CVeg_t = CVeg_{U,t} + CVeg_{L,t} \quad [10.1]$$

where, on day *t:*

$CVeg_{U,t}$ and $CVeg_{L,t}$ are the quantities of carbon in the upper and lower canopies, respectively (kg ha^{-1}).

The carbon in each of the canopies, in turn, is the sum of carbon in the plant organs of all the plant types present:

$$CVeg_{c,t} = \sum_{v=1}^{n} \sum_{org=1}^{5} CVeg_{org,v,c,t} \quad [10.2]$$

where:

$CVeg_{org,v,c,t}$ is carbon in plant organ *org* (leaves, buds, branches, stems, coarse roots, fine roots, or reserves) of vegetation type *v* of canopy *c* (upper or lower) on day *t* (kg ha^{-1}).

Light

The partitioning of incoming solar radiation is treated differently for the upper and lower canopies. In the upper canopy, each plant type is designated as covering a proportion of the ground area. That proportion of ground area is assumed to be the proportion of light intercepted by the plant type. Conifers in the upper canopy, therefore, do not get more light during the winter after deciduous species have dropped their leaves. This approach avoids the difficulties of different plant arrangements. If the upper canopy, for example, comprises only two plant types, deciduous and coniferous, and they are evenly distributed (figure 10.2), one might be able to estimate the changes in light available to the conifers as the deciduous trees lose their leaves each fall. However, with varying distributions and proportions of plant types, it is more difficult to make assumptions that light not intercepted by the deciduous trees is going to be captured by the conifers (figure 10.3 and 10.4).

In the lower canopy, light is distributed among the plant types in proportion to their leaf area indices, rather than in proportion to the ground area occupied. This allows a great deal of interaction among plant types. For example, when the herbaceous plants die back at the end of a growing season, evergreen perennial plants in the lower canopy can take advantage of being able to intercept relatively more sunlight for early growth the next spring. Subsequently, there is relatively less light available for reemerging herbaceous species. In contrast to the upper canopy, proportions of plant types in the lower canopy are very dynamic from year to year.

The light available to each plant type in the canopies is—

$$Rad_{v,c,t} = 41.9\ RadInput_{c,t} \times 10^4\ CanFrac_{v,c,t} \qquad [10.3]$$

where, for canopy *c* on day *t:*

$Rad_{v,c,t}$ is incoming short-wave radiation available to plant type *v* (kJ ha^{-1} day^{-1}),

41.9 converts langleys to kJ m^{-2},

$RadInput_{c,t}$ is incoming short-wave radiation (from weather file) (langleys day^{-1}),

10^4 converts m^2 to ha, and

$CanFrac_{v,c,t}$ is the fraction of the canopy occupied by vegetation type *v*.

The canopy fraction ($CanFrac_{v,c,t}$) is a user input for the upper canopy. It remains constant unless there is a harvest of trees that changes the proportions of canopy occupied by vegetation types. $CanFrac_{v,c,t}$ in the lower canopy is—

$$CanFrac_{v,L,t} = \frac{LAI_{v,L,t}}{\sum_{v=1}^{n} LAI_{v,L,t}} \quad [10.4]$$

where:

$LAI_{v,L,t}$ is leaf area index of vegetation *v* in the lower canopy on day *t* (ha ha^{-1}).

Growth

Net growth occurs in plants as a function of mortality, respiration requirements, photosynthesis, and demands by the plant organs. Photosynthates are allocated to respiration, growth of organs, or a reserve pool (in the case of perennial plants), according to a prioritization scheme (figure 10.5). Many of the algorithms for plant growth came from FOREST–BGC (Running and Coughlan 1988, Running and Gower 1991), a process-based forest stand model. The use of LAI as the main factor characterizing forest vegetation allows the possibility of obtaining input data for the model by means of remote sensing (Running et al. 1989). Vose and Swank (1990) also focused on LAI as a key factor in modeling forest growth.

The mass balances for leaf, branch, stem, and root pools are calculated as a function of growth and litter-fall:

$$CVeg_{org,v,c,t} = CVeg_{org,v,c,t-1} + CVegGwth_{org,v,c,t} - CVegLitter_{org,v,c,t} \quad [10.5]$$

where, for carbon in organ *org* of vegetation type *v* in canopy *c* on day *t:*

$CVegGwth_{org,v,c,t}$ is growth (kg ha^{-1}), and

$CVegLitter_{org,v,c,t}$ is loss due to senescence and dropoff of plant material (kg ha^{-1}).

The mass balance of plant carbohydrate reserves is also a function of accumulation and loss:

$$CVeg_{rsv,v,c,t} = CVeg_{rsv,v,c,t-1} + CVeg_{Gain,rsv,v,c,t} - CVeg_{Loss,rsv,v,c,t} \quad [10.6]$$

where, for carbon in reserves in vegetation type *v* of canopy *c* on day *t:*

$CVeg_{rsv,v,c,t}$ is total amount (kg ha^{-1}),

$CVeg_{Gain,rsv,v,c,t}$ is gain (kg ha^{-1}), and

$CVeg_{Loss,rsv,v,c,t}$ is loss due to respiration, emergence (of herbaceous perennials), and growth (kg ha^{-1}).

Reserves accumulate from excesses after plant growth demands have been met. Losses occur as reserves are used to fulfill plant growth demands that have exceeded photosynthesis.

Canopy Photosynthesis

The amount of carbon fixed on each day is a function of leaf area index, length of day, and factors for canopy CO_2 flux:

$$C_{GrossPsn,v,c,t} = 10^4 \, C_{PsnRate,v,c,t} \times LAI_{v,c,t} \times Dayl_t \times SenscFac_{v,c,t} \quad [10.7]$$

$$C_{PsnRate,v,c,t} = 0.2727 \, (\Delta CO_2 \, CM_{v,c,t} \, CC_{v,c,t} / 1.6) / (CC_{v,c,t} / 1.6 + CM_{v,c,t}) \quad [10.8]$$

where, on day *t:*

$C_{GrossPsn,v,c,t}$ is gross carbon fixed by vegetation *v* in canopy *c* (kg ha^{-1}),

10^4 converts m^2 to ha,

$C_{PsnRate,v,c,t}$ is canopy photosynthesis rate for vegetation *v* in canopy *c* (kg CO_2 × LAI^{-1} m^{-2} sec^{-1}),

0.2727 converts CO_2 to carbon,

ΔCO_2 is CO_2 diffusion gradient from leaf to air,

$CC_{v,c,t}$ is canopy H_2O conductance in vegetation *v* of canopy *c* (divided by 1.6 for CO_2/H_2O diffusion correction) (m s^{-1}),

$CM_{v,c,t}$ is canopy CO_2 mesophyll conductance in vegetation *v* of canopy *c* (m s^{-1}),

$Dayl_t$ is day length for a flat surface(s), and

$SenscFac_{v,c,t}$ is factor reducing photosynthesis by vegetation *v* in canopy *c* with senescence:

$$SenscFac_{v,c,t} = \begin{matrix} 0 \\ 1 \end{matrix} \begin{cases} \text{during dormancy for deciduous trees with fall or marcescent drop} \\ \text{all other} \end{cases} \quad [10.9]$$

Day length is calculated as a sine function of annual day length variation (Running et al. 1987, Running and Coughlan 1988):

$$Dayl_t = 3{,}600\ ThresRadFac\left[Ampl \times \sin(0.01721\,(YD_t - 79)) + 12.0\right] \quad [10.10]$$

where:

3,600 converts hours to seconds,

ThresRadFac is a threshold radiation factor that converts the physical day length to the period during which positive net photosynthesis can occur (a value of 0.85 limits the day length to radiation above 70 W m^{-2}, appropriate for conifers),

Ampl is the amplitude of seasonal variation in day length from 12 hours, and

YD_t is the Julian date for day *t*.

Amplitude is calculated as a function of latitude:

$$Ampl = \exp(7.42 + 0.045\,Lat) / 3{,}600 \quad [10.11]$$

where:

Lat is latitude (degrees).

Canopy Stomatal Conductance

This is a function of the leaf water potential and is adjusted for humidity, temperature, and radiation (Running and Coughlan 1988):

$$CC_{v,c,t} = CCREff_{v,c,t} \times CC_{HAdj,v,t} \quad [10.12]$$

$$CC_{HAdj,v,t} = \text{Maximum of} \begin{cases} 0.00005 \\ CC_{TAdj,v,t} - CC_{TAdj,v,t}\ DCC_h\ (10^6 ABSHD_t - 4) \end{cases} \quad [10.13]$$

$$CC_{TAdj,v,t} = \begin{cases} \text{Maximum of } \begin{cases} 0.00005 \\ CC_{LWPAdj,v,t} + 0.0002\ TAir_{Min,t} \end{cases} & TAir_{Min,t} < 0 \\ CC_{LWPAdj,v,t} + 0.00003\ CC_{LWPAdj,v,t}\ (TAir_{DayAve,t} - 10) & TAir_{Min,t} \geq 0 \end{cases} \quad [10.14]$$

$$CC_{LWPAdj,v,t} = \text{Maximum of } \begin{cases} 0.00005 \\ CC_{max,v} - DCC_{w,v}\ (LWP_t - LWP_{min}) \end{cases} \quad [10.15]$$

where, in vegetation *v* of canopy *c* on day *t:*

$Cc_{v,c,t}$ is the final canopy-average H_2O conductance (m s^{-1}),

$CCREff_{v,c,t}$ is the effect of low solar radiation (0–1 multiplier),

$CC_{HAdj,v,t}$ is canopy H_2O conductance adjusted for humidity (m s^{-1}),

$CC_{Tadj,v,t}$ is canopy H_2O conductance adjusted for temperature (m s^{-1}),

DCC_h is the slope of *CC* vs. the absolute humidity deficit (default is 0.05 $m^4\ s^{-1}\ \mu g^{-1}$),

$ABSHD_t$ is the absolute humidity deficit ($\mu g\ m^{-3}$),

$CC_{LWPAdj,v,t}$ is canopy H_2O conductance adjusted for leaf water potential (m $H_2O \times s^{-1}$),

$TAir_{Min,t}$ is the minimum daily temperature (˚C),

$TAir_{DayAve,t}$ is the daylight average temperature (˚C),

CC_{max} is maximum possible canopy conductance (default is 0.0016 m $H_2O \times sec^{-1}$ for conifer forests),

LWP_t is daily maximum leaf water potential (–MPa), and

LWP_{min} is the spring minimum leaf water potential (default is –0.5 MPa).

$DCC_{w,v}$ is the slope of CC_{max} vs. the range of leaf water potential (m s^{-1} MPa^{-1}):

$$DCC_{w,v} = CC_{max} / (LWP_{sc,v} - LWP_{min}) \quad [10.16]$$

where:

$LWP_{sc,v}$ is the minimum leaf water potential inducing stomatal closure (default is –1.65 MPa).

At the values for CC_{max}, LWP_{sc}, and LWP_{min} suggested by Running and Coughlan (1988), $DCC_w = 0.0013913$ m s^{-1} MPa^{-1}.

Daylight average temperature is calculated as (Parton and Logan 1981)—

$$TAir_{DayAve,t} = 0.212\,(TAir_{Max,t} - TAir_{Ave,t}) + TAir_{Ave,t} \quad [10.17]$$

$$TAir_{Ave,t} = (TAir_{Max,t} + TAir_{Min,t}) / 2 \quad [10.18]$$

where, on day *t:*

$TAir_{Max,t}$ and $TAir_{Min,t}$ are daily maximum and minimum temperatures, respectively (˚C); and

$TAir_{Ave,t}$ is average daily air temperature (˚C).

The absolute humidity deficit is calculated from air temperature and relative humidity (Running and Coughlan 1988):

$$ABSHD_t = 0.000217\, VPD_t / (TAir_{DayAve,t} + 273.16) \quad [10.19]$$

$$VPD_t = \text{Maximum of} \begin{cases} 0 \\ ESD_t - ES_t \end{cases} \quad [10.20]$$

$$ES_t = ESD_t \times RH_t / 100 \quad [10.21]$$

$$ESD_t = 6.1078 \times \exp\left(\frac{17.269 \times TAir_{DayAve,t}}{237.3 + TAir_{DayAve,t}}\right) \quad [10.22]$$

where, on day *t:*

VPD_t is the vapor pressure deficit (mb),

ESD_t is saturation vapor pressure (mb),

ES is vapor pressure (mb), and

RH_t is relative humidity (%).

If the canopy daily average radiation ($DRad_{v,c,t}$) (kJ m^{-2}) is less than a threshold value (Rad_{CCMin}, default is 3,000 kJ m^{-2}), stomates will close (Running and Coughlan 1988):

$$CCREff_{v,c,t} = \text{Maximum of} \begin{cases} 0.00000001 \\ \text{Minimum of} \begin{cases} DRad_{v,c,t} \;/\; Rad_{CCMin} \\ 1 \end{cases} \end{cases} \quad [10.23]$$

The daily maximum (predawn) leaf water potential is calculated as a function of the fraction of available water in the soil (after Running and Coughlan 1988):

$$LWP_t = \begin{cases} \text{Maximum of} \begin{cases} 0.2 \;/\; WtWat_t \\ LWP_{Min} \end{cases} & TSoil_{WtAve,t} > 0 \\ 2 \times \text{Maximum of} \begin{cases} 0.2 \;/\; WtWat_t \\ LWP_{Min} \end{cases} & TSoil_{WtAve,t} \le 0 \end{cases} \quad [10.24]$$

where, on day *t:*

$TSoil_{WtAve,t}$ is daily average soil temperature (˚C) weighted by the proportion of roots in each soil layer, and

$WtWat_t$ is the fraction of water in the soil relative to available water capacity, weighted by the proportion of roots in each soil layer (mm):

$$TSoil_{WtAve,t} = \sum_{j=1}^{3} (RFL_{j,t} \times TSoil_{Ave,j,t}) \quad [10.25]$$

$$WtWat_t = \text{Maximum of} \begin{cases} \sum_{j=1}^{3} \left(RFL_{j,t} \times \text{Min. of} \begin{cases} 1 \\ \theta_{A,j,t} / (\theta_{FC,j} - \theta_{WP,j}) \end{cases} \right) \\ 0.000001 \end{cases} \quad [10.26]$$

where, on day *t:*

$RFL_{j,t}$ is the fraction of the fine root mass of a given vegetation type in layer *j* relative to its roots in the other layers,

$\theta_{A,j,t}$ is available moisture in soil layer *j* (equation 3.14) (mm),

$\theta_{FC,j}$ is moisture content of soil layer *j* at field capacity (mm), and

θ_{WP} is moisture content of soil layer *j* at wilting point (mm).

With the minimum leaf water potential set to –0.5 MPa, the weighted fraction of moisture in the soil layers ($WtWat_t$) can drop to 0.4 before leaf water potential and canopy conductivity are affected. With the critical leaf water potential for stomatal closure (LWP_{sc}) set to –1.65 MPa, stomatal closure will occur when the weighted fraction of available moisture in the soil falls below about 0.121.

Mesophyll CO_2 Conductance

Mesophyll conductance of CO_2 ($CM_{v,c,t}$) is calculated by adjusting a maximum rate by factors for nutrient, light, and temperature effects (Running and Coughlan 1988):

$$CM_{v,c,t} = CM_{max,v}\, CM_{n,v,c,t}\, CM_{q,v,c,t}\, CM_{T,v,t} \quad [10.27]$$

where, on day *t:*

$CM_{max,v}$ is maximum mesophyll conductance of CO_2 (default is 0.0008 m min^{-1} for conifers), and

$CM_{n,v,c,t}$, $CM_{q,v,c,t}$, and $CM_{T,v,t}$ are effects of nutrients, light, and temperature, respectively (0–1 scalars).

The nutrient effect on photosynthesis is a function of the concentration of nitrogen in the leaves (Running and Coughlan 1988):

$$CM_{n,v,c,t} = \text{Minimum of} \begin{cases} 1 \\ 0.5 + 0.8333\ (NC_{Lvs,v,c,t} - NC_{Min,Lvs,v}) / (NC_{Max,Lvs,v} - NC_{Min,Lvs,v}) \end{cases} \quad [10.28]$$

where, in leaves of vegetation type *v* of canopy *c:*

$NC_{Lvs,v,c,t}$ is nitrogen concentration on day *t* (g kg^{-1}),

$NC_{Min,Lvs,v}$ is the minimum possible nitrogen concentration (g kg^{-1}), and

$NC_{Max,Lvs,v}$ is the maximum possible nitrogen concentration (g kg^{-1}).

The light effect on mesophyll conductance is a function of the average amount of solar radiation reaching the canopy (Running and Coughlan 1988):

$$CM_{q,v,c,t} = \begin{cases} 0 & DRad_{v,c,t} \le Q_0 \\ \dfrac{DRad_{v,c,t} - Q_0}{DRad_{v,c,t} + Q_{0.5}} & DRad_{v,c,t} > Q_0 \end{cases} \quad [10.29]$$

where:

Q_0 is photosynthesis light compensation point (default is 432 kJ m^{-2} day^{-1}), and

$Q_{0.5}$ is the radiation level at which $CM_{q,t}$ is 50 percent of maximum (default is 9,730 kJ m^{-2} day^{-1}).

The temperature effect is a function of air temperature during daylight hours (Running and Coughlan 1988):

$$CM_{T,v,t} = \text{Maximum of} \begin{cases} 0 \\ \dfrac{TCoef(TMAX_v - TAir_{DayAve,t})(TAir_{DayAve,t} - TMIN_v)}{(TMAX_v - TMIN_v)^2} \end{cases} \quad [10.30]$$

where:

TCoef is a coefficient relating temperature to CO_2 conductance (default is 4.0, dimensionless), and

$TMAX_v$ and $TMIN_v$ are high and low temperature photosynthesis compensation points, respectively, for vegetation *v* (defaults are 37 and 0 ˚C).

Canopy Average Radiation

As in many forest growth models, Beer's Law is employed to model light penetration through a canopy (Running and Coughlan 1988). The radiation intercepted by each plant type in each canopy $(DRad_{v,c,t})$ is a function of its respective leaf area index:

$$DRad_{v,c,t} = \begin{cases} Rad_{v,c,t} & \dfrac{LAI_{v,c,t}}{CanFrac_{v,c,t}} < 1 \\ \dfrac{Rad_{v,c,t}\left(1 - \exp\left(-EXT_{v,c}\, LAI_{v,c,t} / CanFrac_{v,c,t}\right)\right)}{EXT_{v,c}\, LAI_{v,c,t} / CanFrac_{v,c,t}} & \dfrac{LAI_{v,c,t}}{CanFrac_{v,c,t}} \geq 1 \end{cases} \quad [10.31]$$

where, for vegetation type v in canopy c on day t:

$Rad_{v,c,t}$ is incoming short-wave radiation (kJ m^{-2} day^{-1}), and

$EXT_{v,c}$ is an empirical coefficient for canopy light extinction (default is about 0.5, value depending on species).

Note that incoming radiation to the upper canopy in units of kJ m^{-2} day^{-1} equals $41.9 \times RadInput_t$.

For the lower canopy, incoming radiation is the light that penetrates through the upper canopy:

$$Rad_{L,t} = Rad_{U,t} \times \sum_{v=1}^{n} \left(CanFrac_{v,U,t} \times \exp\left(-EXT_{v,U}\ LAI_{v,U,t} / CanFrac_{v,U,t}\right)\right) \quad [10.32]$$

where the subscripts L and U refer to the lower and upper canopies, respectively.

For both *DRAD* and *Rad*, *LAI* (on an area basis) must be divided by *CanFrac* to get a value of the leaf area index on the basis of the area actually subtended by the particular vegetation type.

Jarvis and Leverenz (1983) point out that Beer's Law does not account for the effect of solar elevation or for interactions of beam and foliage angles. It is necessary to assume that the foliage is randomly distributed in space and that leaf inclination angles are spherically distributed. However, Jarvis and Leverenz (1983) noted that even when the random distribution assumption is violated within the canopy of individual trees, errors are not great as long as trees are not widely spaced. They suggested a value for the light extinction coefficient of between 0.4 and 0.65 for coniferous forests and between 0.5 and 0.8 for broadleaf forests. Ilola et al. (1988) used a value of 0.8 for grass species.

Transpiration

The Penman-Monteith equation is the basis for calculating transpiration (from Running and Coughlan 1988). Initially, potential evaporation of intercepted leaf surface water and potential transpiration are calculated. These two values are both determined in the same manner, except that there is no stomatal resistance for evaporation of intercepted moisture on the leaf surface:

$$PLE_{v,c,t} = LAI_{v,c,t} \times Dayl_t \times [Slope_t \times DRad_{v,c,t} + CP \times PA_t \times VPD_t / RA_{v,c,t}] / [LT_t (Slope_t + \gamma_t)] \quad [10.33]$$

$$PT_{v,c,t} = LAI_{v,c,t} \times Dayl_t \times [Slope_t \times DRad_{v,c,t} + CP \times PA_t \times VPD_t / RA_{v,c,t}] / [LT_t (Slope_t + \gamma_t (1.0 + RS_{v,c,t} / RA_{v,c,t}))] \quad [10.34]$$

where, for vegetation *v* in canopy *c* on day *t:*

$PLE_{v,c,t}$ is potential evaporation of intercepted moisture from the leaf surface (mm $H_2O \times ha^{-1}$),

$Slope_t$ is the slope of the saturation vapor pressure curve at the daylight average air temperature (mb $^{\circ}C^{-1}$),

CP is the specific heat of air (1,010 J kg^{-1} $^{\circ}C^{-1}$),

PA_t is air density (kg m^{-3}),

$RA_{v,c,t}$ is aerodynamic resistance (s m^{-1}),

LT_t is latent heat of vaporization of water (J kg^{-1}),

γ_t is psychrometric constant (mb $^{\circ}C^{-1}$),

$RS_{v,c,t}$ is stomatal resistance (CC_t^{-1}) (s m^{-1}), and

$PT_{v,c,t}$ is potential transpiration (mm $H_2O \times ha^{-1}$).

Actual evaporation from the leaf surface is constrained by intercepted moisture on the leaf and by the estimate for potential evapotranspiration:

$$LfEvap_{v,c,t} = \text{Minimum of} \begin{cases} LfWat_{v,c,t-1} \\ PLE_{v,c,t} \\ PET_t \times PLE_{v,c,t} / \sum_{c=1}^{n} \sum_{v=1}^{n} PLE_{v,c,t} \end{cases} \quad [10.35]$$

where, on vegetation type *v* in canopy *c:*

$LfEvap_{v,c,t}$ is evaporation from the leaf surfaces on day *t* (mm),

$LfWat_{v,c,t-1}$ is water on the leaf surfaces at the end of day *t*–1 (mm), and

PET_t is potential evapotranspiration on day *t* (mm) (see chapter 3).

Then these values are used to determine an actual transpiration constrained by what can be taken up from the soil:

$$Trans_{v,c,t} = \text{Minimum of} \begin{cases} NetPT_{v,c,t} \\ WUptk_{v,c,t} \\ (PET_t - LfEvap_t) \times PT_{v,c,t} / \sum_{c=1}^{n} \sum_{v=1}^{n} PT_{v,c,t} \end{cases} \quad [10.36]$$

where, for vegetation *v* in canopy *c* on day *t:*

$Trans_{v,c,t}$ is transpiration (mm $H_2O \times ha^{-1}$),

$NetPT_{v,c,t}$ is net potential transpiration after evaporation of intercepted moisture on plant canopy (mm), and

$WUptk_{v,c,t}$ is the sum of water uptake from the soil layers (mm):

$$WUptk_{v,c,t} = \sum_{j=1}^{3} WUptk_{v,c,j,t} \quad [10.37]$$

where:

$WUptk_{v,c,j,t}$ is water uptake by vegetation *v* in canopy *c* from soil layer *j* on day *t* (equation 3.13) (mm).

The slope of the saturation vapor pressure curve is determined by (Running and Coughlan 1988)—

$$Slope_t = SVP1_t - SVP2_t \quad [10.38]$$

where:

$$SVP1_t = 6.1078 \times \exp\left(\frac{17.269(TAir_{DayAve,t} + 0.5)}{237.0 + TAir_{DayAve,t} + 0.5} \right) \quad [10.39]$$

$$SVP2_t = 6.1078 \times \exp\left(\frac{17.269\,(TAir_{DayAve,t} - 0.5)}{237.0 + TAir_{DayAve,t} - 0.5}\right) \quad [10.40]$$

Net radiation is determined by a conversion of canopy average radiation based on day length (Running and Coughlan 1988):

$$NRad_{v,c,t} = 1000\ DRad_{v,c,t} / Dayl_t \quad [10.41]$$

Air density is determined by (Running and Coughlan 1988)—

$$PA_t = 1.292 - 0.00428\ TAir_{DayAve,t} \quad [10.42]$$

Aerodynamic resistance is calculated as a function of leaf area index:

$$RA_{v,c,t} = 10\ CanFrac_{v,c,t} / LAI_{v,c,t} \quad [10.43]$$

The latent heat of vaporization of water is calculated as (Running and Coughlan 1988)—

$$LT_t = 10^6\,(2.501 - 0.0024\ TAir_{DayAve,t}) \quad [10.44]$$

The psychrometric constant is calculated as (Running and Coughlan 1988)—

$$\gamma_t = 0.646 + 0.0006\ TAir_{DayAve,t} \quad [10.45]$$

Carbon Partitioning

Newly synthesized carbon is allocated to maintenance respiration, shoot growth, root growth, and storage, in that order of priority (figure 10.5).

Maintenance Respiration

Maintenance respiration is calculated as either the total amount of carbon required by plant tissues or else the amount that can be suppled by the sum of daily photosynthesis and stored carbohydrates:

$$MResp_{v,c,t} = \text{Minimum of} \begin{cases} Pn_{v,c,t} + CVeg_{rsv,v,c,t} \\ TMRespDem_{v,c,t} \end{cases} \quad [10.46]$$

where, for vegetation *v* of canopy *c* on day *t:*

Pn_t is carbon in gross photosynthesis (kg ha^{-1}),

$MResp_t$ is carbon in the actual amount of maintenance respiration (kg ha^{-1}), and

$TMRespDem_t$ is total demand for maintenance respiration by the plant tissues (kg ha^{-1}).

The carbon expended in maintenance respiration by a given plant part is assumed to be in proportion to its demand. Therefore, if assimilates are insufficient to meet maintenance requirements of the entire plant, no organ will receive all of its respiration demand. Unmet respiration demand is allocated to the different organs based on the proportion of respiring dry matter:

$$MResp_{org,v,c,t} = MResp_{v,c,t} \times MRespDem_{org,v,c,t} / \sum_{org=1}^{n} MRespDem_{org,v,c,t} \quad [10.47]$$

where:

$MRespDem_{org,t}$ is maintenance respiration demand by organ *org* in vegetation *v* in canopy *c* on day *t* (kg C ha^{-1}).

Maintenance respiration for leaves is calculated as the net respiration that occurs during the night. Carbohydrate reserves are assumed not to require maintenance respiration (Spitters et al. 1989). The maintenance respiration demand is a function of phenological (in the case of herbaceous plants) and temperature effects and the demands of individual tissues:

$$TMRespDem_{v,c,t} = \sum_{org=1}^{n} MRespDem_{org,v,c,t} \quad [10.48]$$

$$MRespDem_{org,v,c,t} = \begin{cases} (24 - Dayl_t/3600)/24 \times RCoef_{lvs,v,t} \times RDM_{lvs,v,c,t-1} \times TFac_{org,t} \times PhenFac_{MResp,v,c,t} & \text{Leaves} \\ RCoef_{org,t} \times RDM_{org,v,c,t-1} \times TFac_{org,t} \times PhenFac_{MResp,v,c,t} & \text{Roots, Stems, Branches, Buds} \end{cases} \quad [10.49]$$

where, for vegetative part *org* (leaves, buds, branches, roots, or stems):

$TFac_{org,t}$ is a temperature effect on day t (0–1 scalar),

$PhenFac_{MResp,t}$ is the effect of phenologic status on maintenance respiration on day t (0–1 scalar),

$RCoef_{org,t}$ is a first-order rate coefficient on day t (kg C × kg DM^{-1} × day^{-1}) (table 1.2), and

$RDM_{org,t-1}$ is the total respiring dry matter of each vegetative part on day t–1 (kg ha^{-1}).

In the case of woody stems, $RDM_{org,t}$ is only the mass of sapwood. In the case of branches *(brc)* and coarse roots *(csrts),* although sapwood and heartwood are not distinguished, the respiring tissue is assumed to be logarithmically related to the dry weight of the wood (Running and Coughlan 1988):

$$RDM_{brc\ or\ csrts,v,c,t-1} = 0.67 \ln(organ\ dry\ weight) \quad [10.50]$$

Maintenance respiration demand for each plant organ is constrained so that $MRespDem_{org,t} \geq 0$.

For herbaceous species, maintenance respiration is usually considered to be proportional to the mass of the plant. However, for trees, maintenance respiration for stemwood has not been found to be proportional to the total weight of the bole (Jarvis and Leverenz 1983). For that reason, assuming that heartwood is not respiring tissue, maintenance respiration of stemwood is often calculated as a function of only sapwood mass (Mohren et al. 1984, Mohren 1986. Chen et al. 1988).

The determination of sapwood and heartwood is described in the section "Conversion of Sapwood to Heartwood" below. Maintenance respiration is

sensitive to temperature and has a Q_{10} of about 2. In the SUCROS87 model for spring wheat (Spitters et al. 1989) and in the CERES model for forest growth (Dixon et al. 1978), the temperature effect is characterized as—

$$TFac_{org,t} = \begin{matrix} 0 \\ Q_{10}^{(T_{org,t}-T_{opt})/10} \\ 1 \end{matrix} \left[\begin{matrix} T_{org,t} = 0 \\ 0 < T_{org,t} < T_{opt} \\ T_{opt} \leq T_{org,t} \end{matrix} \right. \quad [10.51]$$

where, on day *t:*

$T_{org,t}$ is the applicable temperature for plant part *org* (˚C),

T_{opt} is the optimal temperature for respiration (this may be adjusted 10 degrees higher for tropical species adapted to higher temperatures) (Spitters et al 1989), and

Q_{10} is the Q_{10} factor for the respiration rate (default is 2.0).

Daily average air temperature is used to determine bud, branch, and stem respiration. Root respiration is calculated from daily average soil temperature weighted by root proportions in each soil layer ($TSoil_{WtAve,v,c,t}$).

Average night air temperature is used to calculate night leaf respiration. This is calculated as the mean of daylight average and night minimum air temperatures (Running et al. 1987):

$$TAir_{NightAve,t} = (TAir_{DayAve,t} + TAir_{Min,t}) / 2 \quad [10.52]$$

The $PhenFac_t$ is pertinent to annual herbaceous species. Following commencement of reproductive development, reduced respiration rates correspond with increasing senescence:

$$PhenFac_{MResp,t} = \begin{matrix} 1 \\ \text{Minimum of} \end{matrix} \left\{ \begin{matrix} 1 \\ 2 - DVS_t \end{matrix} \right. \left[\begin{matrix} \text{perennial species} \\ \text{annual species} \end{matrix} \right. \quad [10.53]$$

where:

DVS_t is the developmental stage of herbaceous vegetation on day *t*, where 0 is germination and 1 is the beginning of reproduction (see "Phenological Stages" chapter 11).

Growth

The total amount of carbon that can be used for growth on any day is the sum of stored carbohydrates and photosynthesis minus maintenance respiration:

$$C_{AGwth,v.c.t} = CEmerg_{v,L,t} + \text{Max. of} \begin{cases} C_{Psn,v,c,t} - MResp_{v,c,t} & \text{annuals} \\ 0 \\ C_{Psn,v,c,t} - MResp_{v,c,t} & \text{herbaceous perennials} \\ C_{Psn,v,c,t} + CVeg_{rsv,v,c,t-1} - MResp_{v,c,t} & \text{woody perennials} \end{cases} \quad [10.54]$$

where, for vegetation *v* in canopy *c* on day *t:*

$C_{AGwth,v,c,t}$ is carbon available for assimilation into plant tissue (kg ha^{-1}); and

$CEmerg_{v,L,t}$ is carbon in reserves used for emergence (pertains to herbaceous perennial vegetation in the lower canopy only) (kg ha^{-1}).

The allocation of $C_{AGwth,t}$ to plant organs and reserves is based on several factors discussed in the next section. The actual growth of any plant part is a function of the amount of carbon allocated minus respiration required for growth plus germination:

$$CVegGwth_{org,v,c,t} = C_{Alloc,org,v,c,t} - GResp_{org,v,c,t} + CGerm_{org,v,c,t} \quad [10.55]$$

where, for plant organ *org* of vegetation *v* in canopy *c* on day *t:*

$C_{Alloc,org,v,c,t}$ is carbon allocation (kg ha^{-1}),

$GResp_{org,v,c,t}$ is carbon in growth respiration (plant organs only) (kg ha^{-1}), and

$CGerm_{org,v,c,t}$ is carbon in newly germinated plants (kg ha^{-1}).

There is no respiration associated with carbon allocation to reserves, as it does not entail tissue growth.

Growth respiration is a reflection of the efficiency with which available carbon is assimilated into plant structural material. Carbon lost in growth respiration is calculated as a function of the amount of carbon used for growth and the conversion efficiencies for plant components produced (Penning de Vries and van Laar 1982):

$$GResp_{org,v,c,t} = C_{Alloc,org,v,c,t} / ConvEff_{Gwth,org,v,c} \quad [10.56]$$

$$ConvEff_{Gwth,org,v,c} = Conv_{biom/gluc,org,v,c} \times CBR / CGlucR \quad [10.57]$$

$$Conv_{biom/gluc,org,v,c} = 1 / (1.242\ FC_{org,v} + 1.704\ FP_{org,v} + 3.106\ FF_{org,v} + 2.174\ FL_{org,v} + 0.929\ FO_{org,v} + 0.050\ FM_{org,v}) \quad [10.58]$$

where, for plant organ *org* of vegetation *v* in canopy *c* on day *t:*

$ConvEff_{Gwth,org,v,c}$ is conversion efficiency of plant tissue produced from available photosynthates (kg carbon in growth per kg carbon in photosynthates),

$Conv_{biom/gluc,org,v,c}$ is the ratio of structural biomass formed to glucose consumed (kg kg^{-1}),

CBR is the ratio of the mass of carbon in plant material to biomass (default is 0.4),

CGlucR is the ratio of the mass of carbon to the mass of glucose (0.4), and

$FC_{org,v}$, $FP_{org,v}$, $FF_{org,v}$, $FL_{org,v}$, $FO_{org,v}$, and $FM_{org,v}$ are the fractions of carbohydrates, proteins, fats, lignin, organic acids, and minerals, respectively, in the tissue.

Penning de Vries and Van Laar (1982) note that for a general approximation of the ratio of biomass conversion from glucose, 0.7 will do fairly well.

Allocation to Growth

Most process-based models of forest growth simulate growth as "a process which occurs when available photosynthate is surplus to tissue maintenance requirements" (McMurtrie and Wolf 1983). However, according to the phenological status of a plant, carbohydrates from current photosynthesis may be either stored or immediately resynthesized for plant growth. In fact, if the demand is high, current photosynthesis may be insufficient to supply enough carbohydrates, the balance coming from stored starch (Loach and Little 1973).

Although forest growth models have often allocated photosynthates to plant organs in fixed proportions (examples: McMurtrie and Wolf 1983, Mohren et al. 1984, Running and Coughlan 1988), there are some important reasons why allocations should not remain constant. Distribution of photosynthates changes with plant development. Pipe theory predicts that as a tree grows, more sapwood is required in proportion to the amount of foliage (Ludlow et al. 1990, Shinozaki et al. 1964a,b). Also, since photosynthate partitioning is regulated by environ-

mental conditions, in order for a model to be sensitive to a changing environment, allocations of photosynthates should be adjusted appropriately (Bassow et al. 1990, Vose and Swank 1990). Photosynthates tend to be distributed in response to the strength of sinks. Under decreasing amounts of radiation, relatively more photosynthates are allocated to plant tops. However, as nutrients or moisture become limiting for growth, more photosynthates go to the root system where these resources are in relatively greater supply. Studies of *Pinus sylvestris* indicate that, after fertilization, allocation of photosynthates to roots decreased from 60 to 75 percent to about 40 percent of the total amount available (Linder and Rook 1984).

In REMM, two different approaches for carbon allocation to growth have been used. For tree growth, allocation is sink based; that is, in response to the growth demands of individual plant organs throughout the year. For herbaceous plants, allocation of fixed carbon is in fixed proportions according the phenological status of the plant. Plant growth and development are described in the next chapter.

Herbaceous Vegetation

In simulating annual and perennial herbaceous growth, photosynthates are allocated among plant organs according to ratios determined empirically as a function of the phenological status of the crop:

$$C_{Alloc,org,t} = C_{AGwth,t} \times AlcFrac_{org,t} \quad [10.59]$$

where, for herbaceous annual or herbaceous perennial plants in the lower canopy on day *t:*

$C_{Alloc,org,t}$ is carbon allocation to organ *org* (kg ha^{-1}),

$C_{AGwth,t}$ is carbon available for growth (kg ha^{-1}), and

$AlcFrac_{org,t}$ is the fraction of available carbon allocated to organ *org*.

As van Keulen et al. (1982) point out in their description of the SUCROS model, this is a source-oriented approach, since growth rates are determined by the availability of assimilates.

Annual Herbaceous Vegetation

Assimilates are initially partitioned between shoots and roots. During vegetative growth, assimilates are divided evenly between roots and shoots. When the plants reach their reproductive stage, all assimilates go into shoot growth. An exception occurs if the vegetation is mowed during vegetative development. After mowing, all photosynthates are allocated to the shoots until the shoot/root mass ratio is restored to what it was before the mowing event:

$$AlcFrac_{sht,t} = \begin{cases} 0.5\ NutFac_{sht,t} & DVS_t \le 1.0 \\ 1.0\ NutFac_{sht,t} & DVS_t < 1.0 \text{ and } SRR_t < SRR_{Mow} \\ 1 & 1.0 < DVS_t \end{cases} \quad [10.60]$$

$$AlcFrac_{rts,t} = NutFac_{rts,t}\ (1 - AlcFrac_{sht,t}) \quad [10.61]$$

where, for annual herbaceous plants in the lower canopy on day *t:*

$AlcFrac_{sht,t}$ is the fraction of photosynthates allocated to the shoots,

$NutFac_{sht,t}$ and $NutFac_{rts,t}$ are nutrient factors for shoots and roots (0–1 scalars),

DVS_t is the developmental stage, where 0.0 is germination and 1.0 is the beginning of reproduction (see "Phenological Stages" chapter 11),

SRR_t is the shoot/root mass ratio, and

SRR_{Mow} is the shoot/root mass ratio immediately before mowing.

The nutrient factor for shoots is a function of weighted values for the leaves and stems:

$$NutFac_{sht,t} = \frac{(DM_{lvs,t} \times NutFac_{lvs,t}) + (DM_{stem,t} \times NutFac_{stem,t})}{DM_{lvs,t} + DM_{stem,t}} \quad [10.62]$$

where, for annual herbaceous plants in the lower canopy on day *t:*

$DM_{lvs,t}$, $DM_{stem,t}$, are the weights of dry matter for leaves and stems (kg ha^{-1}).

The nutrient factors for the leaves and stems are determined by equation 10.21.

The fraction of photosynthates allocated to the shoots are further divided into leaves and stems. Although carbon reserves are not simulated explicitly in annual plants, after commencement of the reproductive phase, photosynthates allocated to stems are assumed to be actually incorporated into storage in developing fruit. This is similar to approaches of the WATCROS (Ilola et al. 1988) and DAISY (Hansen et al. 1991) models. The detail in the SUCROS model regarding allocation and growth of grain was not considered to be essential for the purposes of REMM. If the vegetation is mowed during the

vegetative phase (before $DVS_t = 1$), initial regrowth is entirely leaves. Allocation of photosynthates is gradually increased to stems:

$$AlcFrac_{lvs,t} = \begin{cases} AlcFrac_{sht,t} \times \underset{\text{of}}{\text{Min.}} \begin{cases} 1 \\ -0.045 \ln(DVS_t) + 0.5 \end{cases} & DVS_t \le 1.0 \\ 0 & DVS_t > 1.0 \\ \left[1 - (1 - LFrac_t) \times \dfrac{(SRR_t - SRR_i)}{(SRR_{Mow} - SRR_i)^{2.5}}\right] \times AlcFrac_{sht,t} & DVS_t < 1 \text{ and } LSR_t < LSR_{Mow} \end{cases} \quad [10.63]$$

$$AlcFrac_{stem,t} = AlcFrac_{sht,t} - AlcFrac_{lvs,t} \quad [10.64]$$

where, on day *t:*

$AlcFrac_{lvs,t}$ and $AlcFrac_{stem,t}$ are fractions of the photosynthates going to shoots that are allocated to leaf and stem growth, respectively,

$LFrac_t$ is the calculated value of $AlcFrac_{lvs,t}$ if no mowing had been done,

SRR_i is the initial shoot/root mass ratio after mowing,

LSR_t is the leaf/stem ratio, and

LSR_{Mow} is the leaf/stem mass ratio immediately before mowing.

Under low soil nutrient conditions, the content of nitrogen or phosphorus in the roots may prevent available assimilates from being used for root growth. Carbohydrate carbon, in excess of what can be used for growth, is allocated to a reserve pool.

Perennial Herbaceous Vegetation

Unlike in annual vegetation, assimilates in perennials are allocated to shoot and root growth throughout the growing season. As growth commences in spring, all photosynthates are allocated to shoots until shoots have nearly balanced root mass. If the vegetation is mowed, the shoots also receive all assimilates for growth until the shoot/root ratio prior to mowing has been restored:

$$AlcFrac_{sht,t} = \begin{matrix} 1.0 \\ 1.0\ NutFac_t \\ 0.5\ NutFac_t \end{matrix} \left[\begin{matrix} SRR_t < SRR_{Mow} \\ CVeg_{lvs,t} + CVeg_{stem,t} < 0.90\ CVeg_{rts,t} \\ CVeg_{lvs,t} + CVeg_{stem,t} \geq 0.90\ CVeg_{rts,t} \end{matrix} \right. \quad [10.65]$$

where, on day *t:*

$CVeg_{lvs,t}$, $CVeg_{stem,t}$, and $CVeg_{rts,t}$ are the amounts of carbon in leaves, stems, and roots, respectively (kg ha^{-1}).

In the early growing season, leaves receive all assimilates going to the shoots. Gradually, an increasing amount of assimilates is allocated to stem growth. Since the development of reproductive tissue is not explicitly simulated, a portion of the stem tissue during stage 2 growth necessarily represents nonphotosynthesizing reproductive material. After mowing, initially all assimilates go to leaf growth:

$$AlcFrac_{lvs,t} = \begin{matrix} AlcFrac_{sht,t} \times \underset{\text{of}}{\text{Min.}} \left\{ \begin{matrix} 1 \\ -0.045 \ln(DVS_t) + 0.5 \end{matrix} \right. \\ AlcFrac_{sht,t} \times \underset{\text{of}}{\text{Max.}} \left\{ \begin{matrix} 0.2 \\ 0.5\ DVS_t^{-0.8303} \end{matrix} \right. \\ \left[1 - (1 - LFrac_t) \times \frac{(SRR_t - SRR_i)}{(SRR_{Mow} - SRR_i)^{2.5}} \right] AlcFrac_{sht,t} \end{matrix} \left[\begin{matrix} DVS_t \leq 1.0 \\ DVS_t > 1.0 \\ LSR_t < LSR_{Mow} \end{matrix} \right. \quad [10.66]$$

$$AlcFrac_{stem,t} = AlcFrac_{sht,t} - AlcFrac_{lvs,t} \quad [10.67]$$

Unlike in annual plants, some of the assimilates going to the roots of perennial herbaceous plants are allocated to reserves. These reserves provide energy to sustain the below-ground biomass during the winter until shoots reemerge the next spring:

$$AlcFrac_{rts,t} = \begin{cases} NutFac_{rts,t}\,(1 - AlcFrac_{sht,t}) & DVS_t \le 1.0 \\ NutFac_{rts,t}\,(1 - AlcFrac_{sht,t})\,(4.9832 \exp(-1.6101\ DVS_t)) & 1.0 < DVS_t \end{cases} \quad [10.68]$$

$$AlcFrac_{rsv,t} = 1 - AlcFrac_{sht,t} - AlcFrac_{rts,t} \quad [10.69]$$

During the growing season, reserves are only used for emergence (equation 11.45) or for maintenance respiration if current day photosynthates are inadequate to meet the demand.

Woody Vegetation

Bassow et al. (1990) and Weinstein and Beloin (1990) avoided fixed allocation ratios by prioritizing photosynthate partitioning. In the CARBON model (Bassow et al. 1990), respiration of the whole tree is satisfied first, then the remainder goes to foliage growth, root growth, and wood growth, in that order. The FOREST–BGC model has been revised to handle carbon allocations in a similar manner (Running and Gower 1991). In ROPIS (Weinstein and Beloin 1990), utilization of photosynthates was attenuated by the availability of nutrients and water to the various sinks, as well as by phenological stages.

Alternatively, adjustments to carbon allocations in a growth model could be dictated by plant and weather conditions or be determined by the strength of sinks. In SPUR (Hanson et al. 1983), utilization of stored carbohydrates is triggered by the combined status of moisture, temperature, and shoot biomass. Based on pipe-model theory, Hari et al. (1990) assumed that the amount of photosynthate allocated to tissues for water transport would be proportional to the amount of transpired water.

In contrast to the approach taken in REMM for herbaceous growth, simulation of woody growth is a sink-oriented approach. The strengths of the sinks, rather than the availability of assimilates, are the primary determinates of growth. This approach allows plant growth to be more responsive to changing environmental conditions. For example, if the strength of a sink is reduced because of lack of another essential factor such as nitrogen, a larger quantity of assimilates will be partitioned elsewhere.

Carbon photosynthesized on each day is allocated to maintenance respiration, top growth, root growth, and reserves, in that order. By giving priority for photosynthates to top growth, shoot growth under reduced light conditions will increase relative to root growth (Waring and Schlesinger 1985). In contrast, because roots are assumed to have the highest priority for water and nutrients,

root growth under a moisture or nutrient deficiency will increase relative to shoot growth.

Demand for carbon for growth of each plant part is influenced by the phenological status of the plant and by environmental factors. Leaf development is characterized in two stages, comprising growth before and after bud burst. In growth stage 1, before bud burst, demand for carbon for growth is zero order with respect to bud mass. For leaves during growth stage 2 and all other organs, the demand is first order with respect to organ mass. The growth of leaves, however, is limited by a maximum possible leaf size. Demand by leaves is calculated as—

$$C_{Dmd,lvs,t} = \begin{cases} (GR_{buds,t} \times TFac_{Gth,lvs,t} \times NutFac_{lvs,t} \times PhenFac_{lvs,t}) / ConvEff_{Gwth,org} & \text{Growth Stage 1} \\ \text{Min. of} \begin{cases} CMR \times LfPrmda \times 0.001\, WtPerLf \\ (RGR_{lvs} \times C_{lvs,t} \times TFac_{Gth,lvs,t} \times NutFac_{lvs,t} \times PhenFac_{lvs,t}) / ConvEff_{Gwth,org} \end{cases} & \text{Growth Stage 2} \end{cases} \quad [10.70]$$

Demands by other organs (stems, branches, coarse roots, and fine roots) are calculated as—

$$C_{Dmd,org,t} = (RGR_{org} \times CVeg_{org,t} \times TFac_{Gth,org,t} \times NutFac_{org,t} \times PhenFac_{org,t}) / ConvEff_{Gwth,org}) \quad [10.71]$$

where, on day *t:*

$C_{Dmd,lvs,t}$, and $C_{Dmd,org,t}$ are the demands for carbon by the leaves and other organs, respectively (kg ha^{-1});

$GR_{buds,t}$ is growth rate of buds (kg C × ha^{-1});

$TFac_{Gth,lvs,t}$ and $TFac_{Gth,org,t}$ are temperature factors for leaves and other organs, respectively (0–1 scalars; calculated as in equation 10.51);

$NutFac_{lvs,t}$ and $NutFac_{org,t}$ are nutrient factors for leaves and other organs, respectively (0–1 scalars);

$PhenFac_{lvs,t}$ and $PhenFac_{org,t}$ are scalars for leaves and other organs, respectively, representing the phenological status of the plant (range 0–1);

$ConvEff_{Gwth,org}$ is the efficiency with which photosynthates are converted to plant tissue in organ *org* (fraction);

CMR is the ratio of carbon to dry weight;

LfPrmda is the number of leaf primordia from which the buds developed in the current season;

WtPerLf is the maximum possible weight per leaf (g); and

RGR_{lvs} and RGR_{org} are relative growth rates for leaves and other organs, respectively (kg kg^{-1}).

Leaf growth is constrained to the mass attained when all leaves have reached full leaf expansion: $CMR \times LfPrmda \times 0.001\ WtPerLf$.

The use of relative growth rates for the plant organs establishes a demand for photosynthates as in the ELCROS model of de Wit et al. (1970). The allocation of carbon for growth of each plant part is determined by the demand and the amount of carbon that is available. Excess carbon not used by leaves, branches, stems, or roots is allocated to carbohydrate reserves:

$$C_{Alloc,lvs,t} = \text{Minimum of} \begin{cases} CMR \times MaxLAI / SLA \\ \text{Minimum of} \begin{cases} C_{AGwth,t} \\ C_{Dmd,lvs,t} \end{cases} \end{cases} \quad [10.72]$$

$$C_{Alloc,brc,t} = \text{Minimum of} \begin{cases} C_{AGwth,t} - C_{Alloc,lvs,t} \\ C_{Dmd,brc,t} \end{cases} \quad [10.73]$$

$$C_{Alloc,stem,t} = \text{Minimum of} \begin{cases} C_{AGwth,t} - C_{Alloc,lvs,t} - C_{Alloc,brc,t} \\ C_{Dmd,stem,t} \end{cases} \quad [10.74]$$

$$C_{Alloc,crts,t} = \text{Minimum of} \begin{cases} C_{AGwth,t} - C_{Alloc,lvs,t} - C_{Alloc,brc,t} - C_{Alloc,stem,t} \\ C_{Dmd,crts,t} \end{cases} \quad [10.75]$$

$$C_{Alloc,frts,t} = \text{Minimum of} \begin{cases} C_{AGwth,t} - C_{Alloc,lvs,t} - C_{Alloc,brc,t} - C_{Alloc,stem,t} - C_{Alloc,crts,t} \\ C_{Dmd,frts,t} \end{cases} \quad [10.76]$$

$$C_{Alloc,rsv,t} = C_{Agwth,t} - C_{Alloc,lvs,t} - C_{Alloc,brc,t} - C_{Alloc,stem,t} - C_{Alloc,crts,t} - C_{Alloc,frts,t} \quad [10.77]$$

where:

MaxLAI is the maximum leaf area index attainable by the vegetation type (ha ha^{-1}), and

SLA_t is the specific leaf area on day t (ha × kg^{-1} C).

A similar approach, allocating photosynthates to plant organs on a priority basis, has been used for modeling grain fill of a field crop (Spitters et al. 1989) and growth of fruit trees (DeJong and Grossman 1993). Lacking a component to simulate individual plant sizes in the current version of REMM, the constraint on leaf area index serves to empirically limit vegetation growth.

The nutrient factor is determined by the nutrient that has the more constraining influence on growth:

$$NutFac_{org,t} = \text{Minimum of} \begin{cases} PFac_{org,t} \\ NFac_{org,t} \end{cases} \quad [10.78]$$

where:

$PFac_t$ and $NFac_t$ are effects of phosphorus and nitrogen, respectively, on growth.

In REMM, a relationship adopted from Mohren (1986) is used for determining $NFac_t$ and $PFac_t$ (figure 10.6). The factors have asymptotic patterns with increasing foliar nutrient levels. Growth is limited by nitrogen or phosphorus concentrations below 2.00 or 0.30 percent, respectively. Luxury amounts of nitrogen and phosphorus are allowed to accumulate in plant organs above levels that will restrict growth. For the various organs of Douglas-fir (*Pseudotsuga menziesii*), Mohren (1986) used ranges in concentrations of nitrogen and phosphorus listed in table 10.3.

From the relationship illustrated in figure 10.6, the following equation was derived for calculating the effect of nitrogen and phosphorus levels:

$$NFac_{org,t} = \underset{\text{of}}{\text{Min}} \begin{cases} 1 \\ 1 - (1 - 1.3((NConc_{org,t} - NConc_{Min,org}) / (NConc_{Max,org} - NConc_{Min,org}))) \\ \times \exp(-2.52(NConc_{org,t} - NConc_{Min,org}) / (NConc_{Max,org} - NConc_{Min,org})) \end{cases} \quad [10.79]$$

$$PFac_{org,t} = \underset{\text{of}}{\text{Min}} \begin{cases} 1 \\ 1 - (1 - 1.3((PConc_{org,t} - PConc_{Min,org}) / (PConc_{Max,org} - PConc_{Min,org}))) \\ \times \exp(-2.52(PConc_{org,t} - PConc_{Min,org}) / (PConc_{Max,org} - PConc_{Min,org})) \end{cases} \quad [10.80]$$

where, in plant organ *org:*

$NConc_{org,t}$ and $PConc_{org,t}$ are concentrations of nitrogen and phosphorus, respectively, on day t (g kg^{-1});

$NConc_{Min,org}$ and $PConc_{Min,org}$ are minimum possible concentrations of nitrogen and phosphorus, respectively, (g kg^{-1}); and

$NConc_{Max,org}$ and $PConc_{Max,org}$ are maximum possible concentrations of nitrogen and phosphorus, respectively, (g kg^{-1}).

Because diminishing levels of nitrogen in the leaves are more inhibiting to leaf growth than to photosynthesis (figure 10.7), relatively higher concentrations of nitrogen in the roots increases the root/leaf growth ratio.

Leaf Area Index

By assuming a constant specific leaf area (ratio of area to weight of each leaf) and by using estimates of specific leaf area for appropriate species, the accumulation of carbon in the foliage can be converted to a leaf area index (Burk et al. 1990):

$$LAI_{v,c,t} = SLA_{v,c,t} \times CVeg_{lvs,v,c,t} \quad [10.81]$$

where:

LAI is the leaf area index of vegetation type v of canopy c on day t (m^2 m^{-2}).

However, Whitehead and Jarvis (1981) have pointed out that specific leaf area can change by a factor of 2 between the bottom and top of a coniferous canopy. It also changes with varying light levels, temperature, and age (Charles-Edwards et al. 1986). For simplicity, REMM uses estimates of average specific leaf areas for each plant type (table 10.4). Specific leaf area tends to be normally distributed between tree tops and crown bases. There is greater variation among the distributions of specific leaf area in deciduous broadleaf canopies (Jarvis and Leverenz 1983).

References

Bassow, S.L., E.D. Ford, and A.R. Kiester. 1990. A critique of carbon-based tree growth models. *In* R.K. Dixon, R.S. Meldahl, G.A. Ruark, and W.G. Warren, eds., Process Modeling of Forest Growth Responses to Environmental Stress, pp. 50–57. Timber Press, Portland, OR.

Burk, T.E., R. Sievanen, and A.R. Ek. 1990. Construction of forest growth models based on physiological principles. U.S. Department of Agriculture, Forest Service, North Central Forest Experiment Station, St. Paul, MN. General Technical Report No. 140.

Charles-Edwards, D.A., D. Doley, and G.M. Rimmington. 1986. Modeling Plant Growth and Development. Academic Press, New York.

Chen, C.W., L.E. Gomez, C.A. Fox, R.A. Goldstein, and A.A. Lucien. 1988. A tree growth model with multiple stresses. U.S. Department of Agriculture, Forest Service, North Central Forest Experiment Station, St. Paul, MN. General Technical Report No. 120.

DeJong, T.M., and Y.L. Grossman. 1993. A supply and demand approach to modeling annual reproductive and vegetative growth of deciduous fruit trees. HortScience 28:513–514. Abstract.

de Wit, C.T., R. Brouwer, and F.W.T. Penning de Vries. 1970. The simulation of photosynthetic systems. *In* I. Setlik, ed., Prediction and Measurement of Photosynthetic Productivity, pp. 47-70. Proceedings of the International Biological Program/Plant Production Technical Meeting, Trebon, September 14–21, 1969, PUDOC, Wageningen, The Netherlands.

Dixon, K.R., R.J. Luxmoore, and C.L. Begovich. 1978. CERES - A model of forest stand biomass dynamics for predicting trace contaminant, nutrient, and water effects. II. Model Application. Ecological Modeling 5:93-114.

Hanson, J.D., W.J. Parton, and J.W. Skiles. 1983. SPUR plant growth component. *In* J.R. Wight, ed., SPUR—Simulation of Production and Utilization of Rangelands: A Rangeland Model for Management and Research, pp. 68–73. U.S. Department of Agriculture, Miscellaneous Publication No. 1431.

Hari, P., E. Nikinmaa, and M. Holmberg. 1990. Photosynthesis, transpiration, and nutrient uptake in relation to tree structure. *In* R.K. Dixon, R.S. Meldahl, G.A. Ruark, and W.G. Warren, eds., Process Modeling of Forest Growth Responses to Environmental Stress, pp. 41–49. Timber Press, Portland, OR.

Ilola, A., E. Elomaa, and S. Pulli. 1988. Testing of a Danish growth model for barley, turnip, rape and timothy in Finnish conditions. Journal of Agricultural Science in Finland 60:631–660.

Jarvis, P.G., and J.W. Leverenz. 1983. Productivity of temperate, deciduous and evergreen forests. *In* O.L. Lange, P.S. Nobel, C.B. Osmond, and H. Ziegler, eds., Encyclopedia of Plant Physiology. Vol. 12D. Physiological Plant Ecology, pp. 233–280. Springer-Verlag, Berlin.

Linder, S., and D.A. Rook. 1984. Effects of mineral nutrition on carbon dioxide exchange and partitioning of carbon in trees. *In* G.D. Bowen and E.K. S. Nambiar (eds.) Nutrition of Plantation Forests, pp. 211-236. Academic Press, London.

Loach, K., and C.H.A. Little. 1973. Production, storage and use of photosynthate during shoot elongation in balsam fir *(Abies balsamea).* Canadian Journal of Botany 51:1161–1168.

Ludlow, A.R., T.J. Randle, and J.C. Grace. 1990. Developing a process-based growth model for sitka spruce. *In* R.K. Dixon, R.S. Meldahl, G.A. Ruark, and W.G. Warren, eds., Process Modeling of Forest Growth Responses to Environmental Stress, pp. 249–262. Timber Press, Portland, OR.

McMurtrie, R., and L. Wolf. 1983. Above- and below-ground growth of forest stands: a carbon budget model. Annals of Botany 52: 437–448.

Mohren, G.M.J. 1986. Modeling nutrient dynamics in forests, and the influence of nitrogen and phosphorus on growth. *In* G.I. Agren, ed., Predicting Consequences of Intensive Forest Harvesting on Long-Term Productivity, pp. 105–116. Swedish University of Agricultural Science, Department of Ecology and Environmental Research, Report No. 26.

Mohren, G.M.J., C.P. Van Gerwen, and C.J.T. Spitters. 1984. Simulation of primary production in even-aged stands of Douglas fir. Forest Ecology and Management 9:27–49.

Parton, W.J., and J.A. Logan. 1981. A model for diurnal variation in soil and air temperature. Agricultural Meteorology 23:205-216.

Penning de Vries, F.W.T., and H.H. van Laar. 1982. Simulation of growth processes and the model BACROS. *In* F.W.T. Penning de Vries and H.H. van Laar, eds., Simulation of Plant Growth and Crop Production, pp. 114–135. Centre for Agricultural Publishing and Documentation, Wageningen, Netherlands.

Running, S.W., R.R. Nemani, and R.D. Hungerford. 1987. Extrapolation of synoptic meteorological data in mountain terrain and its use for simulating forest evapotranspiration and photosynthesis. Canadian Journal of Forest Research 17:472–483.

Running, S.W., and J.C. Coughlan. 1988. A general model of forest ecosystem processes for regional applications, I. Hydrologic balance, canopy gas exchange and primary production processes. Ecological Modeling 42:125–154.

Running, S.W., and S.T. Gower. 1991. FOREST–BGC, a general model of forest ecosystem processes for regional applications. II. Dynamic carbon allocation and nitrogen budgets. Tree Physiology 9:147–160.

Running, S.W., R.N. Ramakrishna, D.L. Peterson, et al. 1989. Mapping regional forest evapotranspiration and photosynthesis by coupling satellite data with ecosystem simulation. Ecology 70:1090–1101.

Shinozaki, K., K. Yoda, K. Hozumi, and T. Kira. 1964a. A quantitative analysis of plant form: the pipe-model theory. I. Basic analyses. Japanese Journal of Ecology 14:97–105.

Shinozaki, K., K. Yoda, K. Hozumi, and T. Kira. 1964b. A quantitative analysis of plant form: the pipe-model theory. II. Further evidence of the theory and its application in forest ecology. Japanese Journal of Ecology 14:133–139.

Spitters, C.J.T., H. van Keulen, and D.W. G. van Kraalingen. 1989. A simple and universal crop growth simulator: SUCRO87. *In* R. Rabbinge, S.R. Ward, and H.H. van Laar, eds., Simulation Monographs, pp. 146–181. Centre for Agricultural Publishing and Documentation, Wageningen, Netherlands.

Van Keulen, H., F.W.T. Penning de Vries, and E.M. Drees. 1982. A summary model for crop growth. *In* F.W.T. Penning de Vries and H.H. van Laar, eds., Simulation of Plant Growth and Crop Production, pp. 87–97. Centre for Agricultural Publishing and Documentation, Wageningen, Netherlands.

Vose, J.M., and W.T. Swank. 1990. A conceptual model of forest growth emphasizing stand leaf area. *In* R.K. Dixon, R.S. Meldahl, G.A. Ruark, and W.G. Warren, eds., Process Modeling of Forest Growth Responses to Environmental Stress, pp. 278–287. Timber Press, Portland, OR.

Waring, R.H., and W.H. Schlesinger. 1985. Forest Ecosystems, Concepts and Management. Academic Press, New York.

Weinstein, D.A., and R. Beloin. 1990. Evaluating effects of pollutants on integrated tree processes: a model of carbon, water, and nutrient balances. *In* R.K. Dixon, R.S.

Meldahl, G.A. Ruark, and W.G. Warren, eds., Process Modeling of Forest Growth Responses to Environmental Stress, pp. 313–323. Timber Press, Portland, OR.

Whitehead, D., and P.G. Jarvis. 1981. Coniferous forests and plantations. *In* T.T. Kozlowski, ed., Water Deficits and Plant Growth, vol. 6, pp. 49–151. Academic Press, New York.

Table 10.1. Vegetation types simulated in REMM

Vegetation type	Lower canopy	Upper canopy
Herbaceous species		
1. Annuals	X	
2. Perennials	X	
Woody broadleaf species		
3. Autumn leaf drop	X	X
4. Marcescent drop		X
5. Vernal leaf drop	X	X
Coniferous species*		
6. Short needle longevity	X	X
7. Medium needle longevity	X	X
8. Long needle longevity		X

* Longevity of needles varies from 2 to 20 years.

Table 10.2. Maintenance respiration rate coefficients for plant tissues

Plant part	Rate ($kg\ C \times kg^{-1}\ DM \times day^{-1}$)
Leaves, buds	0.012
Stems, branches	0.006
Roots (coarse and fine)	0.006

After Penning de Vries and van Laar 1982

Table 10.3. Limits of nitrogen and phosphorus concentrations in Douglas-fir

Plant part	Nutrient concentration			
	N_{min}	N_{max}	P_{min}	P_{max}
	(g kg^{-1})			
Needles	8	20	0.8	3
Branches	1.5	5	0.2	0.5
Stemwood	0.5	1.5	0.1	0.2
Roots	1.5	5	0.2	0.8

Source: Mohren 1986

Table 10.4. Specific leaf areas used in plant growth models

Species	Specific leaf area* (ha × kg^{-1} C)	Reference
Spring wheat	0.0055	Spitters et al. 1989
Conifers	0.00625	Running and Coughlan 1988
Populus tremuloides	0.00243	Burk et al. 1990

* Assuming a carbon content of 40 percent.

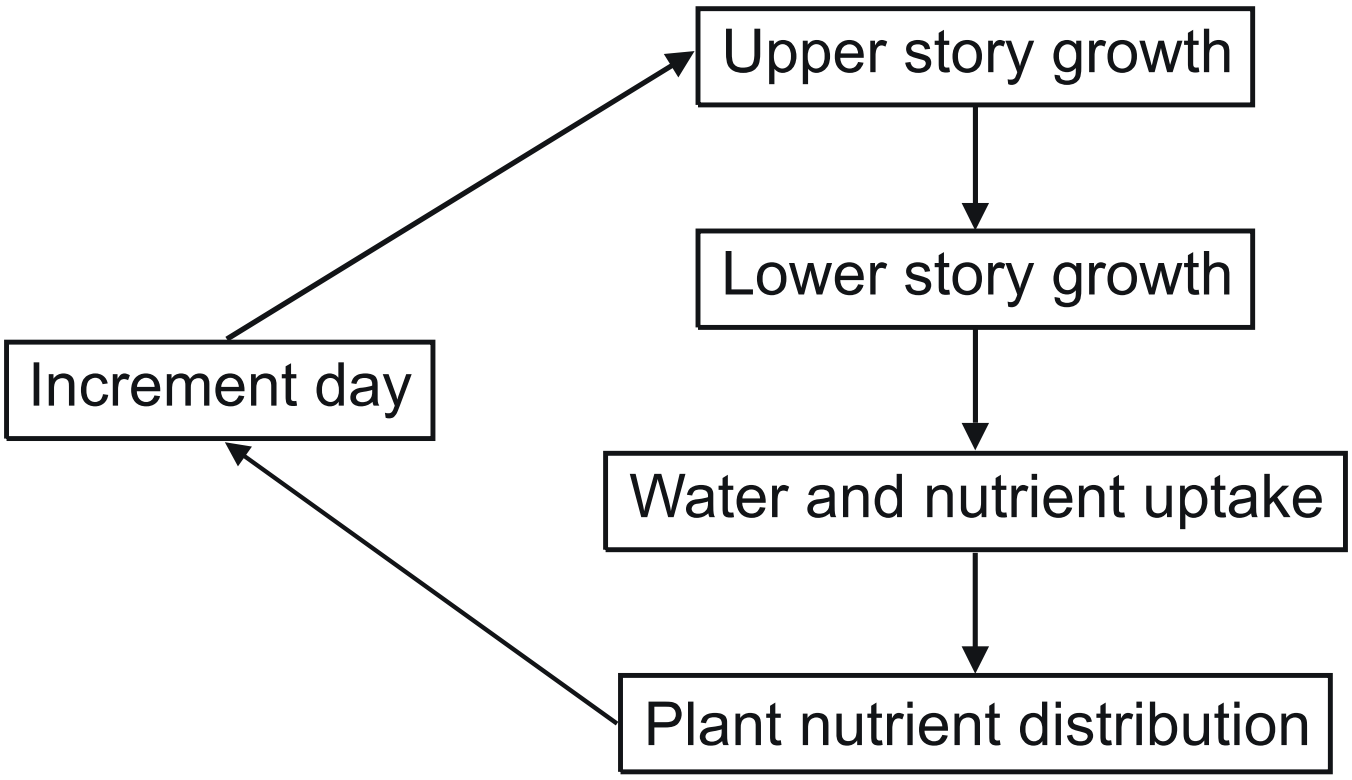

Figure 10.1. Flow chart of vegetation module.

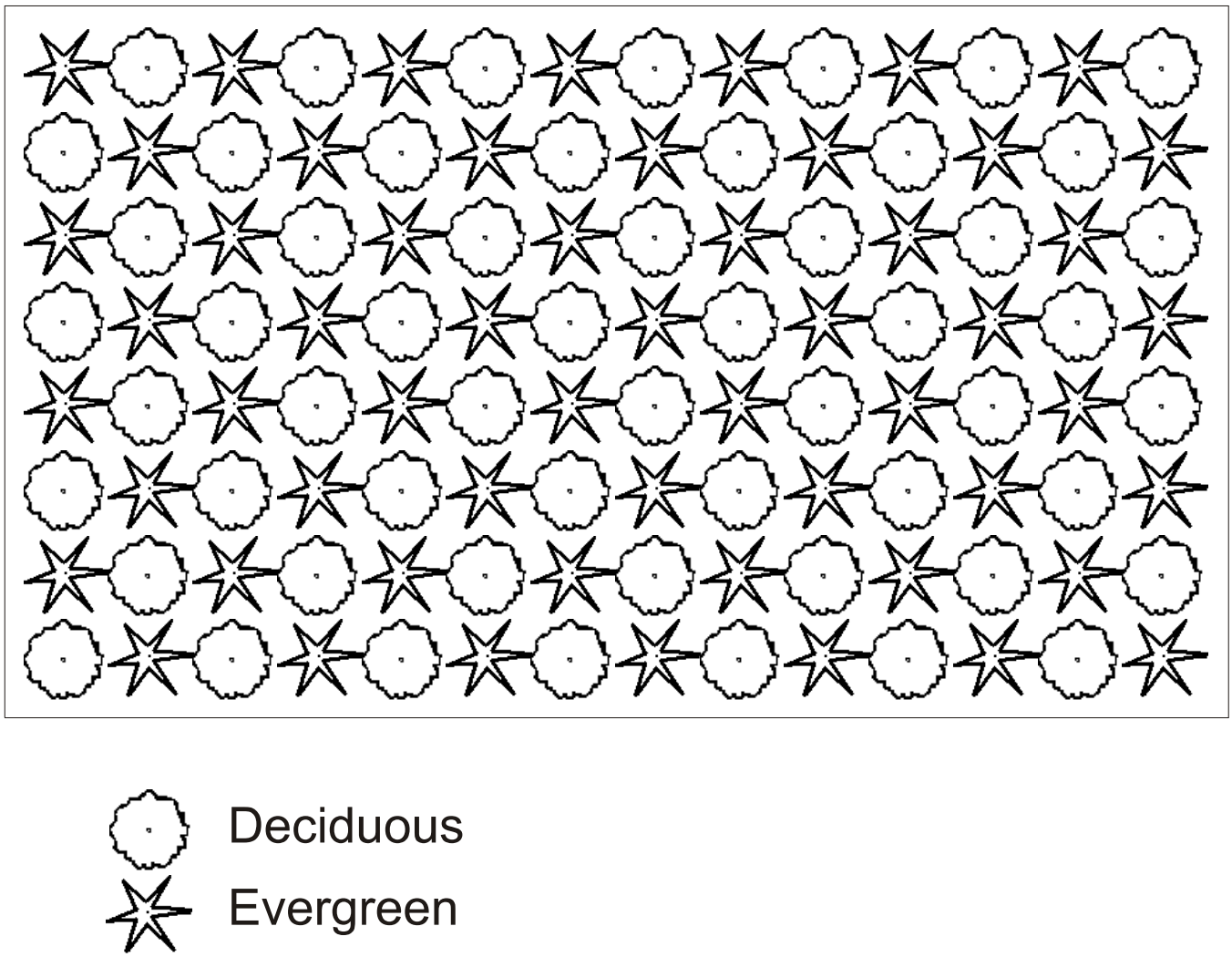

Figure 10.2. Diagram of an even distribution of tree types in the upper canopy

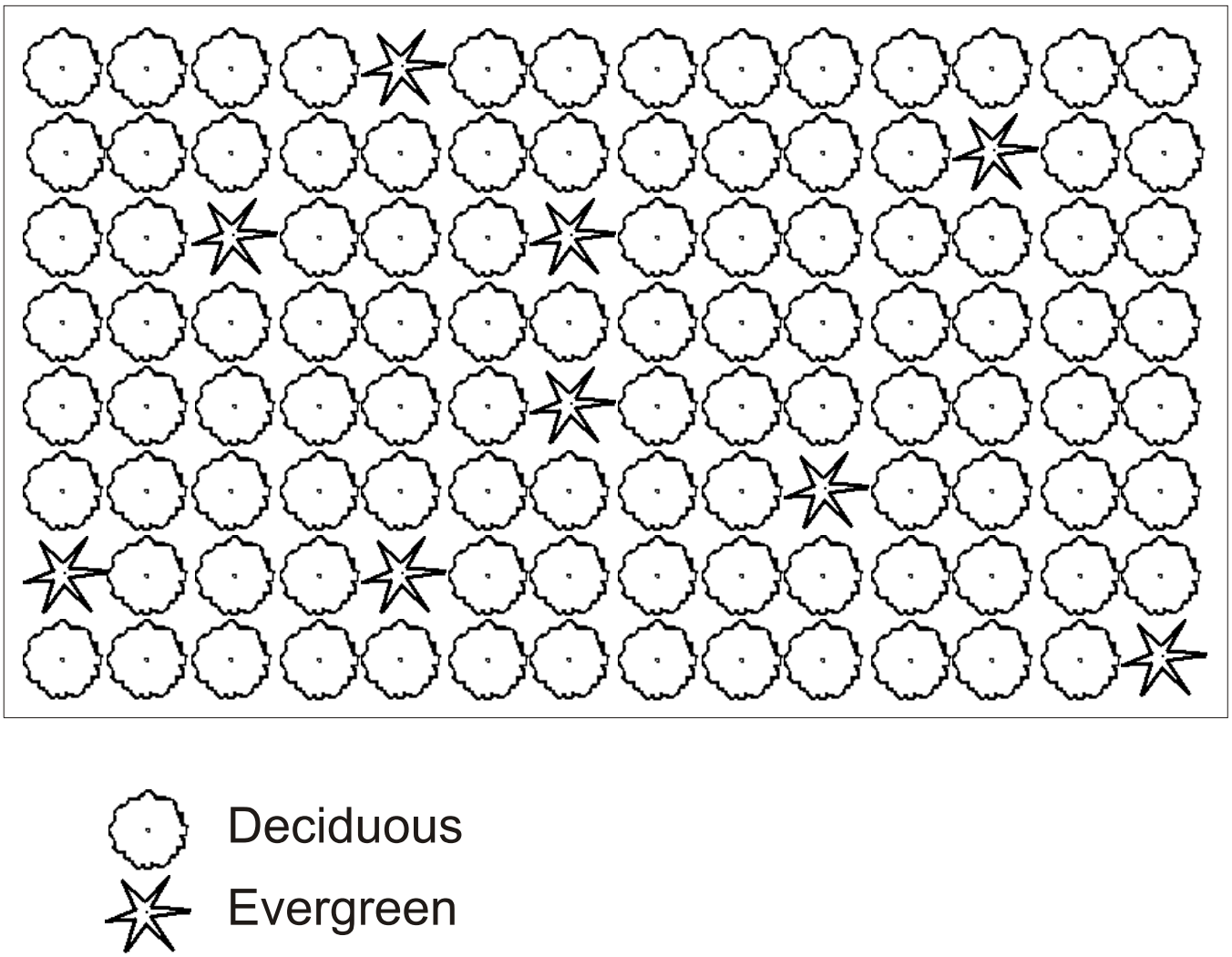

Figure 10.3. With an increasing proportion of deciduous trees, less of the unintercepted light available during the winter can be captured by the conifers.

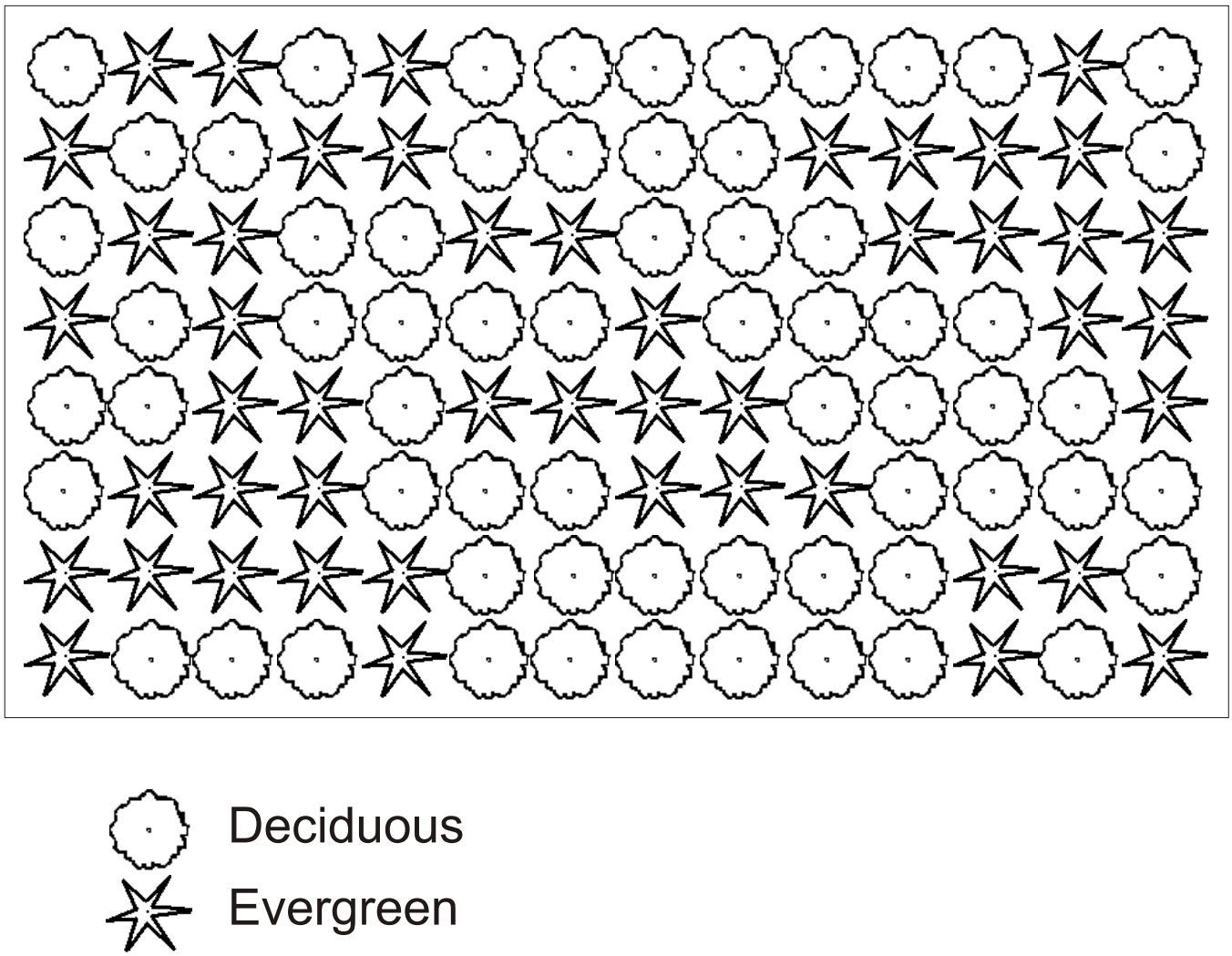

Figure 10.4 Clumped distributions in the upper canopy reduce the possibility for conifers to capture light that is not intercepted by deciduous trees.

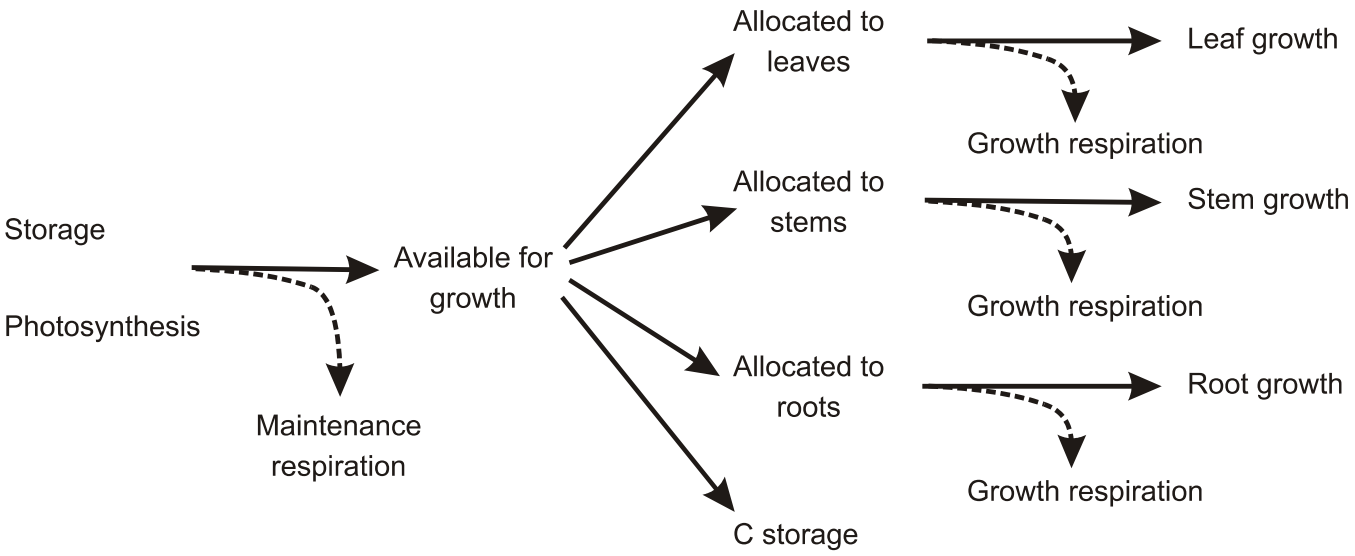

Figure 10.5. Partitioning of photosynthates in REMM

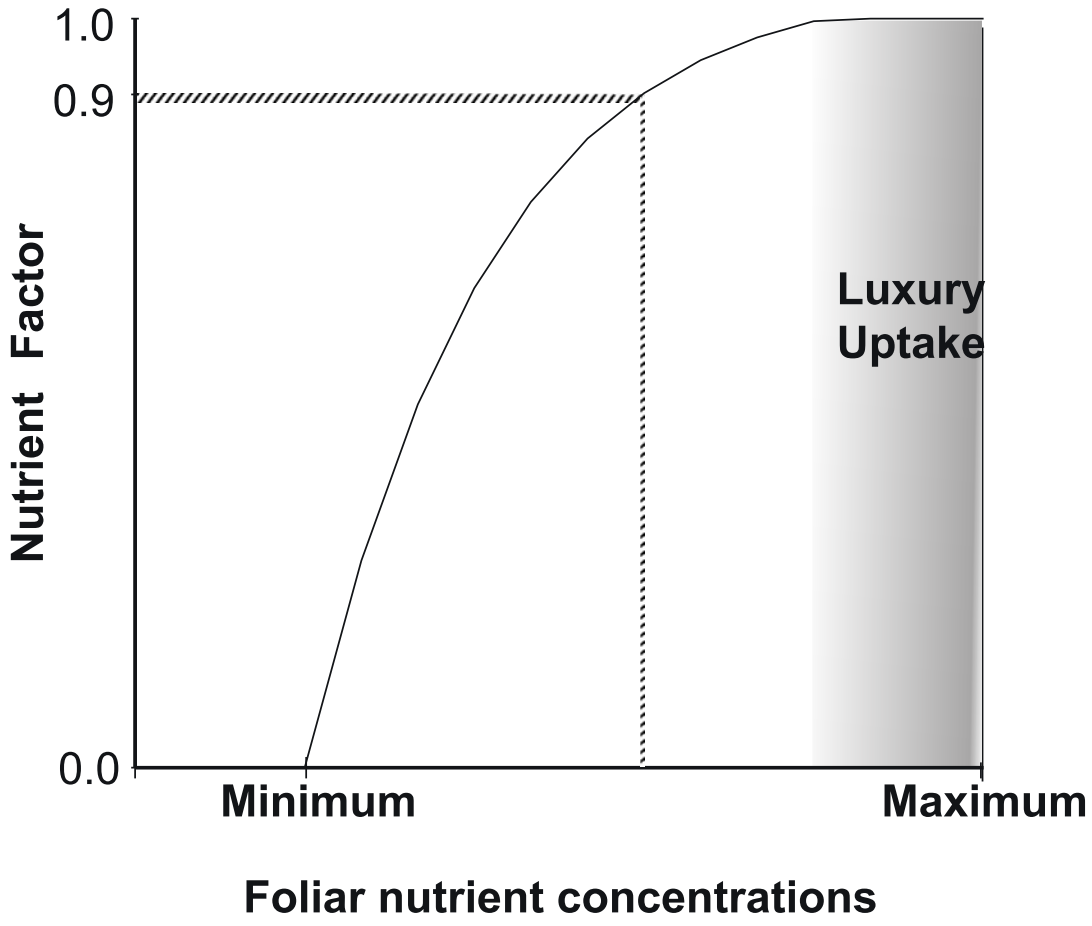

Figure 10.6. Relationship between range of potential foliar nutrient levels and effect on growth

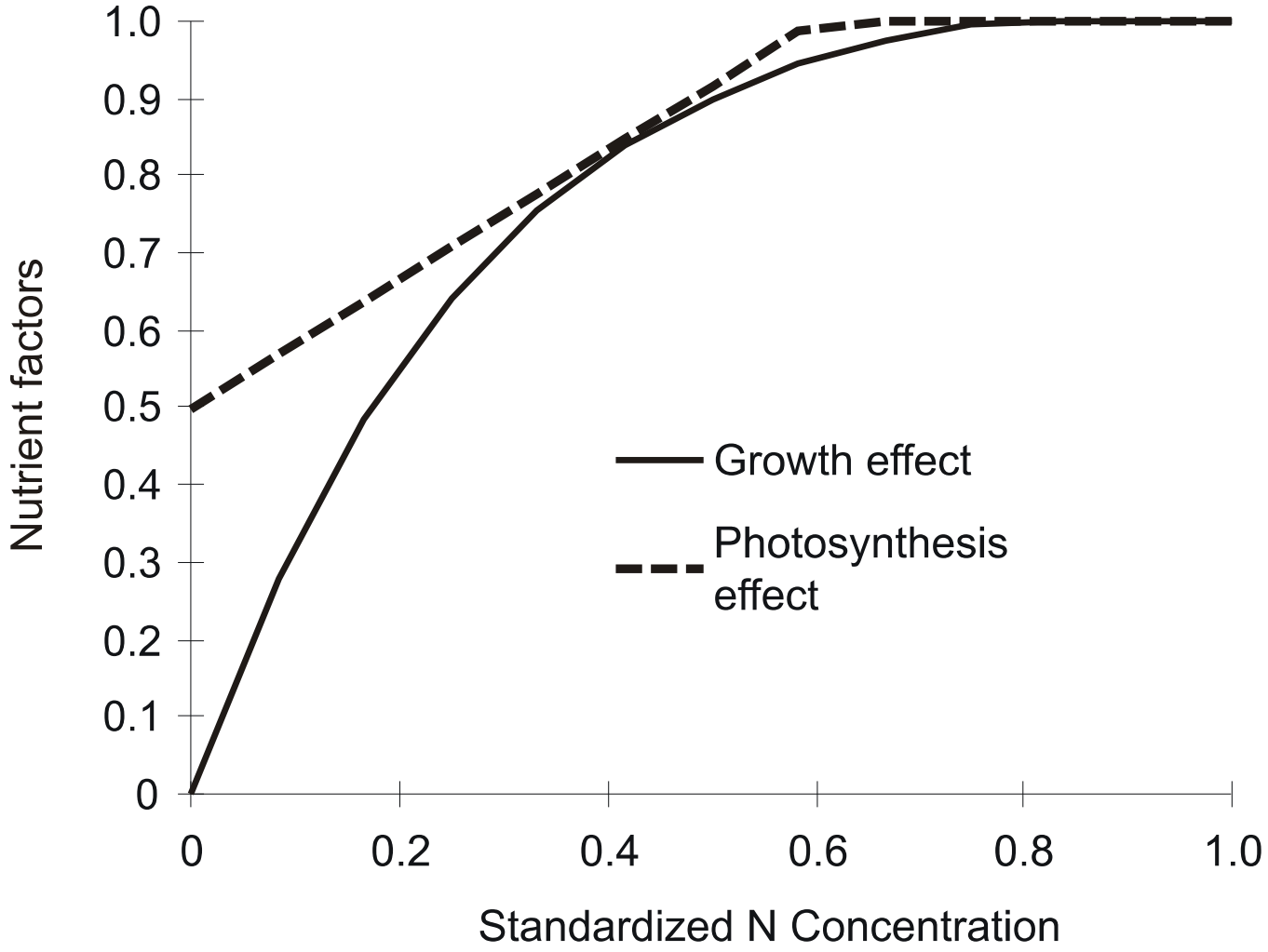

Figure 10.7. Relationship between nitrogen concentrations (standardized between minimum and maximum values) and calculated coefficients influencing growth ($NFac_{grth,1}$) and photosynthesis ($CM_{n,t}$)

Chapter 11
Vegetation: Growth and Development

Lee S. Altier, Randall G. Williams, and Richard Lowrance

Summary

REMM simulates germination as controlled by moisture, temperature, and light. Shading by existing vegetation will inhibit germination. Once plants germinate, they become part of the biomass of the lower canopy. Available moisture and nutrients in the soil are allocated to vegetation types according to relative demands and masses of roots in each soil layer. The partitioning of nutrients and photosynthates within plants corresponds to the concept of a functional equilibrium between roots and shoots. According to this concept, plant organs are in competition for nutrients and photosynthates. A plant organ supplying a resource will have the first opportunity to fulfill its own demand. If the supply organ is reduced in size, resulting in a reduced supply of a resource, growth of other dependent organs will slow down until the supply organ has recovered.

Phenological Stages

The annual cycle of plant development determines which organs receive photosynthates for growth (table 11.1). The phenological factors vary for each plant part during the plant growth stages. The value equals 1 if a plant organ can grow during a given growth stage. Otherwise, it equals 0. In evergreen gymnosperms and angiosperms with vernal senescence, photosynthesis can go on throughout the year, as long as environmental factors are suitable.

Germination

Germination occurs on a daily basis as a function of temperature, moisture, and light reaching the ground surface. Although there is certainly great variation in the germination response of seeds to environmental conditions, given a diverse seed bank, the following equations provide an attempt at an average response. Although light does not actually influence the germination of all seeds, at diminishing light levels less growth can be supported under the lower canopy. So, even if the algorithm inhibits seed germination more than that which would actually occur, it is assumed that newly emerged plants would not thrive anyway in heavily shaded conditions.

$$CGerm_{v,t} = PropSB_v \times CMR \times MaxGRate \times TempEff_{germ,t} \times LightEff_{germ,t} \times MoistEff_{germ,t} \quad [11.1]$$

$$TempEff_{germ,t} = \frac{\sum_{t=t-10}^{t-1} (TSoil_{Lyr1,t} - MinTemp_{germ})}{10\,(MaxTemp_{germ} - MinTemp_{germ})} \quad [11.2]$$

$$LightEff_{germ,t} = \frac{\sum_{t=t-10}^{t-1} (Rad_{Surf,t} - MinLight_{germ})}{10\,(MaxLight_{germ} - MinLight_{germ})} \quad [11.3]$$

$$MoistEff_{germ,t} = \begin{cases} 0 & \theta_{t,Lyr1} \le \theta_{WP,Lyr1} \text{ during any of preceeding 10 days} \\ 1 & \theta_{t,Lyr1} > \theta_{WP,Lyr1} \text{ during each of preceeding 10 days} \end{cases} \quad [11.4]$$

where, on day *t:*

$CGerm_{v,t}$ is carbon in newly germinated plants of vegetation type *v* (kg ha^{-1});

$PropSB_v$ is the proportion of seeds in the soil seed bank of vegetation type *v* (annual, herbaceous perennial, or woody perennial);

MaxGRate is maximum rate of germination that can occur (default is 50 kg dry matter per ha);

$TempEff_{germ,t}$ is effect of temperature on germination (0–1 scalar);

$LightEff_{germ,t}$ is effect of light on germination (0–1 scalar);

$MoistEff_{germ,t}$ is effect of moisture on germination (0–1 scalar);

$TSoil_{Lyr1,t}$ is average temperature in layer 1 (˚C);

$MinTemp_{germ}$ and $MaxTemp_{germ}$ are minimum and maximum temperature limits, respectively, affecting rate of germination (˚C);

$Rad_{Surf,t}$ is light radiation reaching the ground surface (kJ m^{-2});

$MinLight_{germ}$ and $MaxLight_{germ}$ are minimum and maximum light limits, respectively, affecting rate of germination (kJ $^{-2}$);

$\theta_{Lyr1,t}$ is soil moisture content in layer 1 (mm); and

$\theta_{WP,Lyr1,t}$ is soil moisture content at wilting point in layer 1 (mm).

Radiation reaching the ground surface is the light that penetrates through the lower canopy:

$$Rad_{Surf,t} = Rad_{L,t} \times \sum_{v=1}^{n} (CanFrac_{v,L,t} \times \exp(-EXT_{v,L}\ LAI_{v,L,t} / CanFrac_{v,L,t})) \quad [11.5]$$

Since the model does not simulate individual plants, nascent biomass must be added to the rest of the stand. It is divided evenly between roots and leaves:

$$CGerm_{lvs,v,t} = CGerm_{v,t} \times 0.5 \quad [11.6]$$

$$CGerm_{rts,v,t} = CGerm_{v,t} \times 0.5 \quad [11.7]$$

where:

$CGerm_{lvs,v,t}$ and $CGerm_{rts,v,t}$ are amounts of carbon in leaves and roots, respectively, of newly germinated plants of vegetation type v on day t (kg ha^{-1}).

Woody Perennials

Above-ground growth begins in spring when average daily temperatures rise above a minimum for bud swelling. This is identified in the table 11.1 as growth stage 1. The development of buds represents a potential for later leaf growth. Bud development is assumed to be from leaf primordia formed in relation to the mass of leaf growth in the previous year:

$$LfPrmda_{v,c,t} = (PotLfDev_{v,c,t} \times OldLfMass_{v,c,t}) / (0.001\, WtPerLf_{v,c}) \quad [11.8]$$

where:

LfPrmda are leaf primordia (primordia × ha^{-1}),

Old LfMass is mass of leaves that were formed last year (kg ha^{-1}),

WtPerLf is an average dry weight of a fully expanded leaf (g), and

PotLfDev is potential increase in leaf number relative to last year's leaf growth (fraction):

$$PotLfDev = \begin{cases} 1.05 & \text{first year of simulation} \\ CVeg_{brc,v,c,BegStg1} / CVeg_{brc,v,c,PYBegStg1} & \text{succeeding years} \end{cases} \quad [11.9]$$

where:

$CVeg_{brc,BegStg1}$ and $CVeg_{brc,PYBegStg1}$ are carbon in branches of vegetation v in canopy c at the beginning of stage 1 in the current year and previous year, respectively.

As simulated in the Riparian Ecosystem Management Model (REMM), when the buds begin to swell, the primordia have no mass; so in the first stage of growth, photosynthates are allocated to primordia based on their number:

$$CVeg_{buds,v,c,t} = \text{Minimum of} \begin{cases} CMR \times MaxBudWt_{v,c,t} \\ CVeg_{buds,v,c,t-1} + GR_{buds,v,c,t} \end{cases} \quad [11.10]$$

where, for vegetation *v* of canopy *c:*

$CVeg_{buds,v,c,t}$ is carbon in buds on day *t* (kg ha^{-1}), and

$MaxBudWt_{v,c,t}$ is the maximum possible dry weight of buds (kg ha^{-1}):

$$MaxBudWt_{v,c,t} = BudWtFrac_{v,c} \times LfPrmda_{v,c,t} \times 0.001\ WtPerLf_{v,c} \quad [11.11]$$

where:

$BudWtFrac_{v,c}$ is the fraction of the average mass of a fully developed individual leaf comprising the mass of the average fully developed bud of vegetation *v* in canopy *c* (default is 0.05).

The rate of bud swell depends on the state of dormancy of the plant when warming spring temperatures allow bud swelling to occur. It is adjusted each day so that if moisture and nutrients are adequate, buds will be fully developed when bud burst occurs:

$$GR_{buds,v,c,t} = \begin{cases} 0 & GDD \geq GDDReq_{v,c,t} \\ \text{Min. of} \begin{cases} 0.5\ CMR_{Lvs} \times MaxBudWt_{v,c} \\ (T_{Air,Ave,t} - GDDMin) \times (CMR_{Lvs} \times MaxBudWt_{v,c} \\ \quad - CVeg_{buds,v,c,t-1}) / (GDDReq_{v,c,t} - GDD_{v,c,t-1}) \end{cases} & GDD < GDDReq_{v,c,t} \end{cases} \quad [11.12]$$

Growth stage 2 begins at bud burst. At this point the new leaves begin photosynthesizing and contributing to the leaf area index of the tree. This stage continues until full leaf expansion or until a boundary value of growing degree days has been fulfilled, whichever comes first.

Following the approach of Weinstein and Beloin (1990), REMM uses the accumulation of growing degree days to determine the duration of growth conditions. Only one cohort of leaves is allowed to develop each year. In deciduous trees, photosynthesis begins with bud burst.

The onset of cool autumn weather or short day lengths can induce dormancy in the above-ground parts of temperate plants. During dormancy only some maintenance respiration occurs. Dormancy is distinguished from a cold-temperature-maintained quiescent condition by the fact that dormant plants, upon warming, have delayed growth. The state of dormancy may continue until a chilling requirement has been satisfied (Garber 1983). Carlson (1985) demonstrated that chilling 1-year-old loblolly pine (*Pinus taeda* L.) seedlings between 0 and 8 ˚C for increased periods resulted in increasing the rate of root growth and decreasing the time to bud break after the plants were placed into warm, humid conditions.

In REMM, the amount of warm temperatures required for bud burst is determined as a function of chilling period (figure 11.1). The following relationship was derived by Murray et al. (1989) from a study of 15 temperate tree species:

$$GDDReq_{BB,t} = a + b \exp^{(r \times Chill_{t-1})} \quad [11.13]$$

where, on day *t:*

$GDDReq_{BB,t}$ is number of growing degree days required to reach budburst,

a,*b*, and *r* are coefficients (table 11.2), and

$Chill_{t-1}$ is the number of days after November 1 with average temperatures below 5 ˚C.

Bud burst occurs when the cumulative growing degree days equal the growing degree day requirement. Tabulation of cumulative growing degree days (GDD_t) begins on January 1. They are defined as—

$$GDD_t = GDD_{t-1} + \text{Maximum of} \begin{cases} 0 \\ TAir_{Ave,t} - 5 \end{cases} \quad [11.14]$$

where:

$TAir_{Ave,t}$ is daily average air temperature on day *t*.

For deciduous plants, between the time of budburst and full leaf expansion, it is assumed that leaf growth is largely determined by previous bud development and nutrient status of the plant.

Herbaceous Plants

Two patterns of herbaceous growth are simulated in REMM. The herbaceous annuals have a monocarpic cycle, consisting of germination, vegetative growth, reproduction, and death (table 11.3). The herbaceous perennials re-emerge each spring from roots and rhizomes followed by vegetative growth, reproduction, and senescence (table 11.4). Rather than translocating all available carbohydrates to the fruits, a large portion of carbohydrates are stored in the roots for winter survival and spring regrowth.

For the sake of simplicity, the parts of herbaceous plants are characterized as leaves, stems, fine roots, and storage organs. Accumulation of carbohydrates in the storage organs begins with the commencement of the reproductive growth phase. The storage organ of the annuals is the fruit. For the perennials, it is the roots.

The annual cycle for herbaceous annuals and perennials is done empirically, using algorithms similar to those employed in the SUCROS (van Keulen et al. 1982) and SUCROS87 models (Spitters et al. 1989). Rate of development is simulated as a function of both temperature and day length (figure 11.2). Development is simulated as changing gradually, with reproductive growth beginning when the developmental stage (DVS) equals 1 (van Keulen et al. 1982):

$$DVS_t = \begin{cases} DVS_{t-1} + (DevRate_{veg} \times TempEff_{veg,t} \times DLEff_t) & DVS_{t-1} < 1 \\ DVS_{t-1} + (DevRate_{rep} \times TempEff_{rep,t}) & DVS_{t-1} \geq 1 \end{cases} \quad [11.15]$$

where, on day *t:*

$DevRate_{veg}$ *and* $DevRate_{rep}$ represent maximum rates of development for vegetative and reproductive phases, respectively (defaults are 0.0252 and 0.0477 per day); and

$TempEff_{veg,t}$ and $TempEff_{rep,t}$ are temperature effects during vegetative and reproductive growth, respectively (0–1 scalars; constrained to equal 0 when $StdAir_{Ave,t} = 0$).

The calculated relationships for effects of temperature and day length are similar to those in SUCROS, except that temperature and day length are first

standardized to values between 0 and 1 so that the relationships may be more generalizable to different locations:

$$TempEff_{veg,t} = \text{Maximum of} \begin{cases} 0 \\ \text{Minimum of} \begin{cases} 1 \\ 1.03 + 0.224 \ln(StdTAir_{Ave,t}) \end{cases} \end{cases} \quad [11.16]$$

$$DLEff_t = \text{Maximum of} \begin{cases} 0 \\ \text{Minimum of} \begin{cases} 1 \\ 1.02 + 0.498 \ln(StdDL_t) \end{cases} \end{cases} \quad [11.17]$$

$$TempEff_{rep,t} = \text{Maximum of} \begin{cases} 0 \\ \text{Minimum of} \begin{cases} 1 \\ 0.855 + 0.433 \ln(StdTAir_{Ave,t}) \end{cases} \end{cases} \quad [11.18]$$

where, on day *t:*

$StdTAir_{Ave,t}$ is standardized average air temperature (range from 0–1),

$DLEff_t$ is effect of day length during vegetative growth (0–1 scalar; constrained to equal 0 when $StdDL_t = 0$), and

$StdDL_t$ is standardized day length (range, 0–1).

$$TempEff_{veg,t} = \text{Maximum of} \begin{cases} 0 \\ \text{Minimum of} \begin{cases} 1 \\ 1.03 + 0.224 \ln(StdTAir_{Ave,t}) \end{cases} \end{cases} \quad [11.19]$$

$$StdDL_t = \text{Maximum of} \begin{cases} 0 \\ \text{Minimum of} \begin{cases} 1 \\ \dfrac{DayL_t - DLMin}{DLMax - DLMin} \end{cases} \end{cases} \quad [11.20]$$

where:

$TAirMin_{dev}$ and $TAirMax_{dev}$ are minimum and maximum values, respectively, influencing plant development (˚C); and

DLMin and *DLMax* are minimum and maximum values, respectively, of day length (hours).

Carbon for emergence comes from stored photosynthates. Emergence of perennial herbaceous plants is assumed to respond to soil temperature and moisture conditions in a manner similar to germination. Emergence occurs until the carbon used for emergence equals the carbon in reserves at the beginning of the growing season minus depletion for maintenance respiration:

$$CEmerg_{v,c,t} = \begin{cases} \text{Min. of} \begin{cases} CVegRsvZero_{v,c} - MRespSum_{v,c,t} - CEmergSum_{v,c,t-1} \\ RCAE \times CVeg_{rsv,v,L,t} \times TempEff_{germ,t} \times MoistEff_{germ,t} \end{cases} & DVS < 1 \\ 0 & DVS \geq 1 \end{cases} \quad [11.21]$$

where:

$CVegRsvZero_{v,c}$ is carbon in reserves in vegetation *v* of canopy *c* when DVS = 0 (kg ha^{-1}),

$MRespSum_{v,c,t}$ is the sum of carbon used for respiration in vegetation *v* of canopy *c* between when *DVS* = 0 and day *t* (kg ha^{-1}), and

RCAE is relative carbon allocation for emergence (default is 0.2 kg kg^{-1}).

Root Growth

Daily changes in total root carbon are added or deleted from the root carbon in each soil layer in proportion to the fraction of roots in that layer and modified by a factor for adverse soil conditions:

$$C_{alloc,csrts,v,c,j,t} = DpthFrac_{v,c,j,t} \times StressFac_{v,c,j,t} \times C_{alloc,csrts,v,c,t} \quad [11.22]$$

$$C_{alloc,fnrts,v,c,j,t} = DpthFrac_{v,c,j,t} \times StressFac_{v,c,j,t} \times C_{alloc,fnrts,v,c,t} \quad [11.23]$$

where, for vegetation type *v* in canopy *c* in layer *j* on day *t:*

$DpthFrac_{v,c,j,t}$ is the expected fraction of total root mass, and

$StressFac_{v,c,j,t}$ represents the influence of soil characteristics inhibiting root growth (0–1 scalar).

The expected root distribution through the soil profile was determined from an empirical relationship by Gerwitz and Page (1974):

$$DpthFrac_{v,c,j,t} = \begin{cases} \exp\left(\frac{-4.605\ LDpth_{j-1}}{RD_{v,c,t}}\right) - \exp\left(\frac{-4.605\ LDpth_{j}}{RD_{v,c,t}}\right) & LDpth_{j-1} < RD_{v,c,t} \\ 0 & LDpth_{j-1} \geq RD_{v,c,t} \end{cases} \quad [11.24]$$

where:

$LDpth_j$ is the depth at the bottom of layer j (cm), and

$RD_{v,c,t}$ is rooting depth of vegetation v in canopy c on day t, defined in REMM as the maximum depth of 96 percent of the roots (cm).

Although Gerwitz and Page validated their model by comparing it to the root systems of vegetables, cereals, and grasses, it also corresponds well with published data for tree root systems (figure 11.3).

The depth of rooting in REMM is not a function of root biomass. Depth of rooting is estimated by the potential for growth during a single season, limited by soil conditions and the maximum possible depth for each species. Root depth for both annual species and young perennial species in REMM is determined after an empirical relationship derived by Borg and Grimes (1986) and a stress factor from Jones et al. (1991):

$$RD_{v,c,t} = \text{Minimum of} \begin{cases} \text{Maximum of} \begin{cases} RD_{v,c,t-1} \\ LyrLimit_{v,c,t} \end{cases} \\ RD_{YB,v,c} + [0.5 + 0.5 \sin(3.03\ SDR_{v,c,t} - 1.47)] \times PotDpthGrth_{v,c} \end{cases} \quad [11.25]$$

where, for each vegetation type in each canopy on day *t:*

$RD_{YB,v,c}$ is depth of rooting at beginning of year (cm),

$LyrLimit_{v,c,t}$ is a limitation of growth due to soil conditions (cm),

$SDR_{v,c,t}$ is the ratio of the current day to the growing season for roots, and

$PotDpthGrth_{v,c}$ is the potential increase in root depth during the current season (cm).

The layer limitation is determined by a stress factor:

$$LyrLimit_{v,c,t} = \begin{cases} 0 & StressFac_{v,c,Lyr1,t} = 0 \\ LyrDepth_{Lyr1} & StressFac_{v,c,Lyr1,t} > 0,\ StressFac_{v,c,Lyr2,t} = 0 \\ LyrDepth_{Lyr2} & StressFac_{v,c,Lyr1,t} > 0,\ StressFac_{v,c,Lyr2,t} > 0,\ StressFac_{v,c,Lyr3,t} = 0 \\ LyrDepth_{Lyr3} & StressFac_{v,c,Lyr1,t} > 0,\ StressFac_{v,c,Lyr2,t} > 0,\ StressFac_{v,c,Lyr3,t} > 0 \end{cases} \quad [11.26]$$

where:

$StressFac_t$ is a stress factor value on day t (0–1 scalar).

The stress factor can limit the allocation of carbon for root growth in each layer, as well as limit the penetration of roots into deeper layers. However, once a given rooting depth has been attained by a plant type, the model does not allow for a reduction in rooting depth, even with the advent of adverse soil conditions. If soil conditions do not limit rooting in any of the three layers, the $LyrLimit_t$ is set equal to the bottom of layer 3, since that is defined as the maximum possible depth of all roots.

Commencement of root growth for germinating plants (both perennials and annuals) is at germination. For perennial tree species during the year of germination, increase in rooting depth continues until the end of stage 3. For older perennial tree species, there may not ever be any cessation of root growth during the winter, particularly in the lower soil layers and at low latitudes. However, after the year of germination, depth of rooting is assumed to only increase during the period of coarse root growth (stage 3). Determination of the ratio of current day to season length ($SDR_{v,c,t}$) depends on the plant type:

$$SDR_{v,c,t} = \begin{cases} DVS_t & \text{herbaceous annuals} \\ DVS_t / 2 & \text{herbaceous perennials} \\ GDD_t / GDD_{BegStg4} & \text{woody perennials (year of germination)} \\ (GDD_t - GDD_{BegStg3}) / (GDD_{BegStg4} - GDD_{BegStg3}) & \text{woody perennials (after germination year)} \end{cases} \quad [11.27]$$

where:

$GDD_{BegStg3}$ and $GDD_{BegStg4}$ are the cumulative growing degree days to the beginnings of stages 3 and 4, respectively.

Potential depth growth for each plant type is determined by the rooting depth increase that can occur in a season or the maximum possible depth of rooting for the species:

$$PotDpthGrth = \text{Minimum of} \begin{cases} OneYrMaxDpth \\ RD_{Max} - RD_{YB} \end{cases} \quad [11.28]$$

where:

OneYrMaxDpth is maximum annual increase in root depth possible for the species (cm), and

RD_{Max} is maximum rooting depth possible for the species (cm).

In a model of root growth, Jones et al. (1991) suggest some factors that can attenuate root distribution. Several of these have been incorporated into REMM:

$$StressFac_{v,c,j,t} = \text{Minimum of} \begin{cases} SCF_j \\ SST_{j,t} \\ SAI_{v,c,j,t} \end{cases} \quad [11.29]$$

where:

SCF_j is a factor for coarse fragments in layer j (0–1 scalar),

$SST_{j,t}$ is a factor for soil strength in layer j on day t (0–1 scalar), and

$SAI_{j,t}$ is a factor for soil aeration in layer j on day t (0–1 scalar).

$$SCF_j = 1 - FVRock_j \quad [11.30]$$

where:

$FVRock_j$ is the volume fraction of particles larger than 2 mm diameter in layer j.

Since soil surveys may list rock fragments as a mass fraction of the total soil dry weight and list fragments smaller than 2 mm as the mass fraction of oven-dry soil less than 3 inches in diameter that will pass through a No. 10 sieve (USA Standard Series), a conversion is necessary:

$$FVRock_j = \frac{LgFrac_j / BDRock}{(LgFrac_j / BDRock) + (S10Frac_j / BD_j)} \quad [11.31]$$

where:

$LgFrac_j$ is the fraction of soil larger than 2 mm diameter in layer j (g g^{-1}),

$BDRock_j$ is particle density of material larger than 2 mm diameter (assumed to be 2.65 g cm^{-3}),

$S10Frac_j$ is the fraction of soil less than 7.62 cm (3 inches) diameter that is less than 2 mm diameter (that is, that passes USA Standard Series sieve No. 10) (g g^{-1}), and

BD_j is the bulk density of soil material less than 2 mm in diameter (g cm^{-3}).

$$LgFrac_j = RkFrac_j + [(1 - S10Frac_j) \times (1 - RkFrac_j)] \quad [11.32]$$

where:

$RkFrac_j$ is the fraction of the soil that is rock fragments larger than 7.62 cm (g g^{-1}).

The factor for soil strength is a function of bulk density, sand content, and available water (Jones et al. 1991):

$$SST_{j,t} = SBD_j \times \sin(1.57\ AWFrac_{j,t}) \quad [11.33]$$

where, for each soil layer on day t:

$SST_{j,t}$ is the stress factor for soil strength (0–1 scalar),

SBD_j is a factor for bulk density, and

$AWFrac_{j,t}$ is the fraction of available water in the soil (mm mm^{-1}):

$$AWFrac_{j,t} = \begin{cases} 0 & \theta_{j,t} < \theta_{WP} \\ (\theta_{j,t} - \theta_{WP}) / (\theta_{FC} - \theta_{WP}) & \theta_{WP} \le \theta_{j,t} \le \theta_{FC} \\ 1 & \theta_{FC} < \theta_{j,t} \end{cases} \quad [11.34]$$

The factor for bulk density is calculated as (Jones et al. 1991)—

$$SBD_j = \begin{cases} 0 & BD_{Max} < BD_j \\ (BD_{Max} - BD_j) / (BD_{Max} - BD_{Min}) & BD_{Min} \le BD_j \le BD_{Max} \\ 1 & BD_j \le BD_{Min} \end{cases} \quad [11.35]$$

where:

BD_{Max} is bulk density at which there is complete inhibition of root growth, and

BD_{Min} is the bulk density at which there is no inhibition of root growth:

$$BD_{Max} = 1.6 + 0.004\, Sand_j \quad [11.36]$$

$$BD_{Min} = 1.1 + 0.005\, Sand_j \quad [11.37]$$

where:

$Sand_j$ is the proportion of sand in the soil (%).

The stress factor for aeration is calculated by (Jones et al. 1991)—

$$SAI_{v,c,j,t} = \begin{cases} SFT_{v,c} + \dfrac{(1 - WFP_{j,t})(1 - SFT_{v,c})}{1 - CWP_{v,c}} & WFP_{j,t} \ge CWP_{v,c} \\ 1 & WFP_{j,t} < CWP_{v,c} \end{cases} \quad [11.38]$$

$$CWP_{v,c} = 0.4 + 0.004\, Clay_j \quad [11.39]$$

where, on day *t:*

$SAI_{v,c,j,t}$ is a stress factor for aeration for vegetation *v* in canopy *c* in layer *j* (0–1 scalar),

$SFT_{v,c}$ is the fraction of normal root growth when pore space is saturated for vegetation *v* in canopy *c* (0–1 scalar),

$WFP_{j,t}$ is the fraction of pore space containing water in layer *j*,

$CWP_{v,c}$ is the water-filled pore fraction at which aeration begins to limit root growth for vegetation *v* in canopy *c*, and

$Clay_j$ is the proportion of clay in the soil in layer *j* (%).

Height Growth

Tree height is calculated as a function of age and site quality index using empirical age and height relationships (site-index curves). Hughes and Sendak (1985) point out that most published site-index curves can be expressed as—

$$Ht_t = MaxHt + [(4.5 - MaxHt) \times \exp(-TreeAge_t / HtC)] \quad [11.40]$$

where:

MaxHt is maximum tree height (ft),

$TreeAge_t$ is tree breast height age on day *t* (years), and

HtC is tree height time constant (years).

Two constants, *MaxHt* and *HtC*, are characteristic of the site. They can be determined for a location by iteratively solving site-index curve by fitting equation 11.40 to two points (Hughes and Sendak 1985).

Nutrient Uptake and Partitioning

The simulation of nutrient uptake and partitioning to plant parts follows the approach of the PAPRAN model (Seligman and van Keulen 1981). It is based on demands created by growth. The SPUR model for rangeland production (Hanson et al. 1983) and models by Mohren (1986) and Chen et al. (1988) for tree growth utilized this concept. The approach allows simulation of changing allocations of nitrogen and phosphorus based on availability and demand. The model provides interaction between photosynthesis and a subsequent demand for nutrients, the supplies of which, in turn, influence photosynthesis.

Nutrient Uptake

The mass balance for nutrients in vegetation is calculated as—

$$Nu_{i,v,c,t} = Nu_{i,v,c,t-1} + Nu_{Uptk,i,v,c,t} - \sum_{org=1}^{n} Nu_{Litter,i,org,v,c,t} \quad [11.41]$$

where, in vegetation *v* of canopy *c* on day *t:*

$Nu_{i,t}$ is nutrient *i* (nitrogen or phosphorus) (kg ha^{-1}),

$Nu_{Uptk,i,v,c,t}$ is uptake of nutrient *i* from the soil (kg ha^{-1}), and

$Nu_{Litter,i,org,v,c,t}$ is loss of nutrient *i* in litter-fall from plant organ *org* (kg ha^{-1}).

The total amount of a nutrient in the vegetation is the sum of quantities in the plant organs:

$$RD_{v,c,t} = \underset{\text{of}}{\text{Minimum}} \begin{cases} \text{Maximum of} \begin{cases} RD_{v,c,t-1} \\ LyrLimit_{v,c,t} \end{cases} \\ RD_{YB,v,c} + [0.5 + 0.5 \sin(3.03\, SDR_{v,c,t} - 1.47)] \times PotDpthGrth_{v,c} \end{cases} \quad [11.42]$$

Available nutrients in the soil layers are partitioned among the plants in a manner similar to the partitioning of available water in the soil. As long as moisture in a soil layer is above the wilting point at the beginning of the day, unadsorbed nutrients are assumed to be available for uptake on that day (van Keulen et al 1982). The moisture factor influencing nutrient uptake does not change as moisture is depleted within a single day:

$$NuUptk_{i,v,c,j,t} = \text{Minimum of} \begin{cases} RNuDem_{i,v,c,j,t} \\ AvailNu_{i,j,t} \times \dfrac{RNuDem_{i,v,c,j,t} \times AdjNuMRF_{i,v,c,j,t}}{\sum_{v=1}^{n} \sum_{c=1}^{2} (RNuDem_{i,v,c,j,t} \times AdjNuMRF_{i,v,c,j,t})} \end{cases} \quad [11.43]$$

$$RNuDem_{i,v,c,j,t} = NuDem_{i,v,c,t} - \sum_{Lyr1}^{j-1} NuUptk_{i,v,c,j,t} \quad [11.44]$$

$$AdjNuMRF_{i,v,c,j,t} = NuMRF_{i,j,t} \times RFV_{i,v,c,j,t} / \sum_{c=1}^{n} \sum_{v=1}^{n} (NuMRF_{i,v,c,j,t} \times RFV_{i,v,c,j,t}) \quad [11.45]$$

$$NuMRF_{i,v,c,j,t} = NuMF_{i,j,t} \times RFL_{i,v,c,j,t} / \sum_{j=1}^{3} (NuMF_{i,j,t} \times RFL_{i,v,c,j,t}) \quad [11.46]$$

$$NuMF_{i,j,t} = \begin{matrix} 1 \\ 0 \end{matrix} \begin{cases} \theta_t > \theta_{WP} \\ \theta_t \le \theta_{WP} \end{cases} \quad [11.47]$$

where, on day *t:*

$NuUptk_{i,v,c,j,t}$ is nutrient uptake by vegetation *v* from layer *j* (constrained to 0 if $RNutDem_{v,j,t}$ or $AdjNutMRF_{v,j,t}$ equal 0) (mm),

$RNuDem_{v,j,t}$ is the potential nutrient demand (nitrogen or phosphorus) remaining for vegetation *v* in soil layer *j* after the nutrient has been taken up from the upper soil layers (mm),

$AvailNu_{j,t}$ is available nutrient (nitrogen or phosphorus) in soil layer *j* (mm),

$NuDem_{v,t}$ is the nutrient demand (nitrogen or phosphorus) by vegetation *v* (mm),

$AdjNuMRF_{v,j,t}$ is a moisture factor adjusted for the fraction of the root mass of vegetation *v* in layer *j* relative to its roots in the other layers and relative to all other roots in layer *j* (constrained to 0 if $NutMRF_{v,j,t}$ or $RFV_{v,j,t}$ equal 0) (0–1 scalar),

$NuMF_{j,t}$ is a moisture factor for layer *j* (0–1 scalar),

$NuMRF_{v,j,t}$ is a moisture factor adjusted for the fraction of the root mass of vegetation *v* in layer *j* relative to its roots in the other layers (constrained to 0 if $NutMF_{v,j,t}$ or $RFL_{v,j,t}$ equal 0) (0–1 scalar),

$RFL_{j,t}$ is the fraction of the root mass of vegetation *v* in layer *j* relative to its roots in the other layers, and

$RFV_{v,j,t}$ is the fraction of the root mass of vegetation *v* in layer *j* relative to all other roots in layer *j*.

The demand for a nutrient is a function of the concentrations of that nutrient in a plant's organs (van Keulen et al 1982), but constrained by the potential range of the nitrogen/phosphorus ratio (Mohren 1986, Mohren et al. 1986). Demand for a nutrient is assumed to take at least 2 days to be fulfilled (van Keulen et al. 1982):

$$NuDem_{i,v,c,t} = \sum_{org=1}^{n} NuDem_{i,org,v,c,t} \quad [11.48]$$

$$NuDem_{i,org,v,c,t} = [(DM_{org,v,c,t} \times MaxNuConc_{i,org,v,c,t}) - Nu_{i,org,v,c,t}] / TC_{Dem} \quad [11.49]$$

constrained by: $4 \le NPR \le 30$

where, on day *t:*

$NuDem_{i,v,c,t}$ is nutrient *i* demanded by vegetation *v* in canopy *c* (kg ha^{-1}),

$NuDem_{i,org,v,c,t}$ is nutrient *i* demanded by organ *org* of vegetation *v* in canopy *c* (kg ha^{-1}),

$MaxNuConc_{i,org,v,c,t}$, is the maximum concentration of nutrient *i* that can be taken up by organ *org* of vegetation *v* in canopy *c* (kg kg^{-1}),

TC_{Dem} is a coefficient for the time required to fulfill the demand (default is 2 days), and

NPR is the nitrogen/phosphorus ratio.

In PAPRAN, the effects of stress, such as reduced light intensity or water shortage, is reflected in the demand for nitrogen by the integration of reduced growth over time. Seligman et al. (1975) noted that passive uptake of nitrogen in the transpiration stream is insufficient to account for much of the demand by vegetation. They considered that as long as adequate amounts of nitrogen are in the soil, uptake is controlled by active plant uptake processes. Therefore, in the model, correspondence of nutrient uptake with moisture uptake is not considered.

In REMM, following the approach of de Wit et al. (1970) and Weinstein and Beloin (1990), roots are allowed to get to nutrients first, the remainder going to upper parts of the vegetation. Although the plant tops have priority for photosynthates, if there is a shortage of nutrients in the leaves and stems, the use of the photosynthates will be restricted and the excess will go down into the roots and reserves:

$$NuUptk_{i,frts,v,c,t} = NuDem_{i,frts,v,c,t}$$
$$\text{constrained by: } 0 \le NuUptk_{i,frts,v,c,t} \le NuUptk_{i,v,c,t} \quad [11.50]$$

$$NuUptk_{i,crts,v,c,t} = NuDem_{i,crts,v,c,t}$$
$$\text{constrained by: } 0 \le NuUptk_{i,crts,v,c,t} \le NuUptk_{i,v,c,t} - NuUptk_{i,frts,v,c,t} \quad [11.51]$$

$$NuUptk_{i,stem,v,c,t} = NuDem_{i,stem,v,c,t}$$
$$\text{constrained by: } 0 \le NuUptk_{i,stem,v,c,t} \le NuUptk_{i,v,c,t} - NuUptk_{i,frts,v,c,t} - NuUptk_{i,crts,v,c,t} \quad [11.52]$$

$$NuUptk_{i,brc,v,c,t} = NuDem_{i,brc,v,c,t}$$

constrained by: $0 \le NuUptk_{i,brc,v,c,t} \le NuUptk_{i,v,c,t} - NuUptk_{i,frts,v,c,t} - NuUptk_{i,crts,v,c,t} - NuUptk_{i,stem,v,c,t}$ [11.53]

$$NuUptk_{i,lvs,v,c,t} = NuDem_{i,lvs,v,c,t}$$

constrained by: $0 \le NuUptk_{i,lvs,v,c,t} \le NuUptk_{i,v,c,t} - NuUptk_{i,frts,v,c,t} - NuUptk_{i,crts,v,c,t} - NuUptk_{i,stem,v,c,t} - NuUptk_{i,brc,v,c,t}$ [11.54]

The subscripts *frts*, *crts*, *stem*, *bac*, and *lvs* denote the nutrient uptake and demand for fine roots, coarse roots, stems, branches, and leaves, respectively.

Translocation of Nutrients from Senescing Plant Parts

The amounts of nutrients lost in litter-fall from vegetation are functions of the amount of litter-fall and the amounts of nutrients translocated back into the plant before litter-fall occurs. It is assumed that there is no translocation of nutrients from root, stem, or branch tissue (Nambiar 1987). Cole and Rapp (1980) indicated little translocation of nitrogen from conifers. However, Prescott et al. (1989) observed high proportions of nitrogen (40 to 50 percent) and phosphorus (50 to 80 percent) to be reabsorbed from the senescing leaves of Rocky Mountain coniferous species. Their research indicated a slight increase in reabsorption with increasing nitrogen and phosphorus foliage concentrations. In a forest growth model developed by Mohren (1986), 25 percent of nitrogen and 35 percent of phosphorus were assumed to be translocated out of abscising conifer needles. In REMM, 50 percent of the maximum concentration of nitrogen and phosphorus can be translocated back into the plant from senescing leaves.

Rather than allocating translocated nutrients among plant organs in proportion to the size of the sinks (as in Habib et al. 1993), organs get the nutrients on a priority basis to satisfy their daily nutrient demands. Remaining leaves have the first opportunity to receive translocated nutrients, followed by branches, stems, and roots. As with nutrient uptake from the soil, the ability of an organ to receive nutrients is constrained by the limits of maximum organ nutrient concentration and allowable nitrogen/phosphorus ratios (a minimum of 4 and a maximum of 30).

Mortality

Plants in REMM die in correspondence to seasonal patterns of senescence. Because of a lack of information on the mechanisms involved and for the sake of simplicity, senescence of most plant parts is simulated empirically. Leaf drop corresponds to several different patterns simulated in the sections on herbaceous and woody vegetation.

Loss of living tissue also occurs if photosynthates are insufficient to satisfy maintenance respiration requirements. For example, light infiltration through the upper canopy diminishes with growth of the upper canopy. This can gradually result in death of the lower canopy as photosynthesis is reduced. Under deficit conditions, plant parts are assumed to die in proportion to their respiration demands:

$$CVegMRDth_{org,v,c,t} = CVeg_{org,v,c,t} \times (1 - MResp_{org,v,c,t} / MRespDem_{org,v,c,t}) \quad [11.55]$$

where:

$CVegMRDth_{org,v,c,t}$ is carbon loss from organ *org* of vegetation *v* in canopy *c* on day *t* due to an inability to satisfy the maintenance respiration demand of the organ (kg ha^{-1}).

As leaves, branches, and roots die, they become litter. When the maintenance requirement of sapwood is not met, the oldest sapwood dies first, becoming heartwood.

Herbaceous Vegetation

Death of leaves and roots occurs on a daily basis. Roots die at a constant rate per day during the growing season (see section on root mortality) and in relation to maintenance respiration during the dormant season. The calculation for leaf death comes from SUCROS87 (Spitters et al. 1989). It is a function of aging and self-shading:

$$CVegLitter_{org,v,c,t} = \begin{cases} (CVeg_{lvs,v,c,t} \times RDR_{lvs,v,c,t}) + CVegMRDth_{lvs,v,c,t} & \text{leaves} \\ (CVeg_{frts,v,c,t-1} \times RDR_{frts,v}) + CVegMRDth_{frts,v,c,t} & \text{fine roots; growing season} \\ CVeg_{frts,v,c,t}\,(MResp_{frts,v,c,t} / CVeg_{rsv,t}) & \text{fine roots; dormant season} \end{cases} \quad [11.56]$$

where, for vegetation *v* in canopy *c* on day *t:*

$CVegLitter_{org,v,c,t}$ is loss of carbon in organ *org* due to death (kg ha^{-1}), and

$RDR_{lvs,v,c,t}$ and $RDR_{frts,v,c,t}$ are relative death rates of leaves and fine roots (kg kg^{-1}).

The relative death rate of leaves is determined by the greater of the effects of aging and shading (Spitters et al. 1989):

$$RDR_{lvs,v,c,t} = \text{Maximum of} \begin{cases} AgeEff_t \\ ShadeEff_t \end{cases} \quad [11.57]$$

$$AgeEff_t = \begin{cases} 0 & DVS_t < 1 \\ \text{Maximum of} \begin{cases} 0.03 \\ 0.0158 + (0.00699 \times 1.082^{TAir_{Ave,t}}) \end{cases} & DVS_t \geq 1 \end{cases} \quad [11.58]$$

$$ShadeEff_t = \text{Maximum of} \begin{cases} 0 \\ \text{Minimum of} \begin{cases} 0.03 \\ 0.03\,(LAI_t - LAICr) / LAICr \end{cases} \end{cases} \quad [11.59]$$

where, for annual plants on day *t:*

$AgeEff_t$ is the effect of developmental aging (scalar ranging from about 0 to 0.2),

$ShadeEff_t$ is the effect of shading (scalar ranging from 0 to 0.03), and

LAICr is a critical LAI value, above which shading causes death of lower leaves (default is 4.0 ha ha^{-1}).

For annual plants, death of the entire stand occurs when either its development reaches the end of the reproductive phase ($DVS_t = 2$) or when there is a killing frost, whichever comes first. On that day, the shoots become part of the litter layer and the roots are incorporated as fresh organic matter in their respective soil layers.

Death of the above-ground portions of perennial herbaceous plants occurs when there is a killing frost; that is, when minimum daily air temperature reaches –1 ˚C or lower. On that day, portions of nitrogen and phosphorus in the shoots

are translocated down to the roots (see section on translocation of nutrients), and shoots become part of the litter layer.

Woody Vegetation

In a survey of temperate forest studies, Jarvis and Leverenz (1983) found that above-ground litter-fall averages 1 to 9 Mg ha^{-1} yr^{-1}. Its composition averaged 70 percent leaves and 7 percent each of branches, bark, and fruits. They also pointed out that evergreen gymnosperms and deciduous angiosperms had similar amounts of total litter-fall, about 3.7 and 3.2 Mg ha^{-1} yr^{-1}, respectively.

Except for foliage, no attempt has been made to model temporal changes in the shedding of plant parts, such as the cladoptosis (branch abscission) observed in some species. Rather, a portion of roots, stems, and branches are removed from the living vegetation each day as a function of their biomass and any inability to satisfy the maintenance respiration demand. Amounts of daily litter from plant organs other than leaves is determined by—

$$CVegLitter_{org,v,c,t} = (CVeg_{org,v,c,t-1} \times RDR_{org,v}) + CVeg_{MRDth,org,v,c,t} \quad [11.60]$$

Relative death rates ($RDR_{org,v}$) are given in table 11.5.

Leaf Litter

In REMM, leaf drop from trees and shrubs is simulated as (1) autumnal abscission of deciduous species, (2) marcescent leaf abscission of deciduous species, (3) vernal (spring) abscission of broadleaf evergreen species, and (4) needle drop of evergreen conifers.

Autumn Leaf Drop

For deciduous vegetation, autumnal leaf-litter fall was empirically modeled from a study by Shure and Gottschalk (1985) of a floodplain forest on the upper coastal plain of South Carolina. Leaf drop is determined by a combination of leaf maturity and cold temperature factors:

$$CVegLitter_{lvs,DecidAut,c,t} = \underset{\text{of}}{\text{Min.}} \begin{cases} CVeg_{lvs,DecidAut,c,t-1} \\ \underset{\text{of}}{\text{Max.}} \begin{cases} CVegLitter_{lvs,DecidAut,c,t-1} \\ (CVeg_{lvs,DecidAut,c,t-1} \times MxLFRate_{DecidAut} \\ \quad \times LFFac_{DecidAut,c,t}) + MRDth_{lvs,DecidAut,c,t} \end{cases} \end{cases} \quad [11.61]$$

$$LFFac_{DecidAut,c,t} = \text{Minimum of} \begin{cases} 1 \\ MatEff_{DecidAut,c,t} + ColdEff_{DecidAut,c,t} + DLEff_t \end{cases} \quad [11.62]$$

where, for deciduous trees with an autumnal leaf-fall pattern, on day *t:*

$MxLFRate_{DecidAut}$ is the maximum initial rate of leaf-fall (set at 0.05 kg kg^{-1}),

$LFFac_{DecidAut,c,t}$ is a factor controlling the rate of leaf-fall (0–1 scalar),

$MatEff_{DecidAut,c,t}$ is the effect of leaf maturity,

$ColdEff_{DecidAut,c,t}$ is the effect of declining autumn temperatures, and

$DLEff_t$ is the effect of day length (equals 0 or 1).

The *MxLFRate* initially limits the leaf drop to no more than 5 percent of the canopy biomass per day. However, if there is a sufficient mass of leaves remaining in the trees, the daily amount of drop is constrained to at least what it was on the previous day.

The $MatEff_t$ simulates the influence of increasing leaf maturity on leaf drop. It may represent cummulative effects of insect damage, drought, shading, and nutrient deficiencies and decreasing day length. It is based on accumulated growing degree days after bud burst in spring:

$$MatEff_{DecidAut,c,t} = \begin{matrix} 0 \\ (1.3 \times 10^{-4}\, GDD_{DecidAut,c,t})^5 \end{matrix} \begin{bmatrix} GDD_{DecidAut,c,t} = 0 \\ GDD_{DecidAut,c,t} > 0 \end{bmatrix} \quad [11.63]$$

$$GDD_{DecidAut,c,t} = GDD_{DecidAut,c,t-1} + \text{Minimum of} \begin{cases} GDDMax \\ \text{Maximum of} \begin{cases} 0 \\ TAir_{Ave,t} - GDDMin \end{cases} \end{cases} \quad [11.64]$$

where, on day *t*:

$GDD_{DecidAut,c,t}$ is the value of accumulated growing degree days after bud burst for autumn deciduous vegetation in canopy *c*,

GDDMax and *GDDMin* are maximum and minimum limits for growing degree days, respectively (defaults are 32 and 5 ˚C), and

$TAir_{Ave,t}$ is average daily air temperature (˚C).

$ColdEff_{DecidAut,c,t}$ simulates the effect of declining temperatures in the autumn on leaf drop:

$$ColdEff_{DecidAut,c,t} = \begin{cases} 0 & Julian\ Date \le 230 \\ ColdEff_{DecidAut,c,t-1} + \underset{of}{\text{Min}} \begin{cases} CritColdTemp_{v,c}/50 \\ \underset{of}{\text{Max}} \begin{cases} 0 \\ \dfrac{(CritColdTemp_{v,c} - T_{Air,Ave,t})}{50} \end{cases} \end{cases} & Julian\ Date > 230 \end{cases} \quad [11.65]$$

This effect is a cumulative value representing days after August 17 with an average temperature below a critical level ($CritColdTemp_{v,c}$; default is 10 ˚C) (figure 11.4). On each day, the degrees of temperature below the critical level are divided by 50 and added to the accumulated value from the previous day. The division by 50 determines the amount of cold necessary to reach the maximum rate of leaf drop. That is, it would take a minimum of 5 days at 0 ˚C (apart from any senescence effect) for $LFFac_t$ to reach maximum value.

Since the influences of the maturity and cold temperature effects are additive, if there is a late arrival of cool temperatures in autumn, then fewer days of cold temperature would be required to reach the maximum rate of leaf drop. This is because of the already increased maturity of the leaves. In contrast, in a year when there is an early decline in air temperature, it would take somewhat longer to reach the maximum rate of leaf drop.

In the case of a mild autumn, leaf drop will eventually be triggered by the decline in day length below a critical level:

$$DLEff_t = \begin{cases} 1 & Dayl_t \le CritDayl \\ 0 & Dayl_t > CritDayl \end{cases} \quad [11.66]$$

where:

CritDayl is a critical day length inducing autumn leaf drop (hours). If the trees are insensitive to day length, *CritDayl* is set to 0.

Marcescent Leaf Drop

Some deciduous trees have marcescent leaves—leaves that senesce in the fall but whose abscission process is not completed until temperatures begin to warm again in the spring. In REMM, increasing temperatures after January 1 are assumed to promote the physiological abscission of marcescent leaves:

$$CVegLitter_{lvs,DecidSpg,c,t} = \underset{\text{of}}{\text{Min.}} \begin{cases} CVeg_{lvs,DecidSpg,c,t-1} \\ \underset{\text{of}}{\text{Max.}} \begin{cases} CVegLitter_{lvs,DecidSpg,c,t-1} \\ (CVeg_{lvs,DecidSpg,c,t-1} \times MxLFRate_{DecidSpg} \\ \quad \times LFFac_{DecidSpg,c,t}) + MRDth_{lvs,DecidSpg,c,t} \end{cases} \end{cases} \quad [11.67]$$

$$LFFac_{DecidSpg,c,t} = \begin{cases} 0 & \text{Before 1 January} \\ \underset{\text{of}}{\text{Min.}} \begin{cases} 1 \\ \underset{\text{of}}{\text{Max.}} \begin{cases} 0 \\ (TAir_{Ave,t} - GDDMin)/GDDMax \end{cases} \end{cases} & \text{After 1 January} \end{cases} \quad [11.68]$$

Vernal Leaf Drop

Vernal leaf drop corresponds to spring leaf expansion. Addicott and Lyon (1973) noted that unlike autumn leaf drop, leaves of trees with this characteristic show few signs of senescence. They suggested that changing gradients of auxins and gibberellins and new sinks in the developing buds are likely to promote leaf abscission. In REMM, vernal leaf drop is simulated as beginning at bud burst and ending with full leaf expansion. The strength of the signal for abscission of old leaves is matched to the rate of new leaf expansion:

$$CVegLitter_{lvs,Vernal,c,t} = CVeg_{oldlvs,Vernal,c,t}\,(CumVernalFrac_{c,t} - CumVernalFrac_{c,t-1}) + MRDth_{lvs,Vernal,c,t} \quad [11.69]$$

$$CumVernalFrac_{c,t} = \frac{DM_{newlvs,v,c,t} - MaxBudWt_{Vernal,c,t}}{(LfPrmda_{Vernal,c,t} \times WtPerLf_{Vernal,c}) - MaxBudWt_{Vernal,c,t}} \quad [11.70]$$

where, for vegetation *v* in canopy *c:*

$CVegLitter_{lvs,Vernal,c,t}$ is the mass of vernal leaf drop on day *t* (kg ha^{-1});

$CumVernalFrac_{c,t}$ and $CumVernalFrac_{c,t-1}$ are cumulative fractions of old leaf senescence at the end and beginning of day *t*, respectively;

$CVeg_{oldlvs,Vernal,c,t}$ is carbon in old leaves on day *t* (kg ha^{-1}); and

$DM_{newlvs,Vernal,c,t}$ is dry weight of new leaves on day *t* (kg ha^{-1}).

Coniferous Needle Drop

In their development of the FOREST–BGC model for coniferous forests, Running and Gower (1991) assigned a leaf turnover age of 4 years, and stem and root turnover coefficients of 0.02 and 0.8 (fractions per year), respectively. They found leaf turnover age to be one of the most sensitive parameters in their model. Kaufmann et al. (1982) noted that the needle longevity of some coniferious species such as loblolly pine is only 2 or 3 years, whereas the needle longevity of Engelmann spruce (*Picea engelmannii* Parry), subalpine fir (*Abies lasiocarpa* (Hook.) Nutt.), and lodgepole pine (*Pinus contorta* var. *latifolia* Engelm.) ranges from 7 to 20 years. Pinyon pine (*Pinus monophylla* Torr. and Frem.) has been found to retain its needles for 18 or more years (Everett and Thran 1992). REMM allows the user to input different retention times for up to three conifer species.

Beadle and Jarvis (1982) developed a model of needle growth and drop for scotch pine (*Pinus sylvestris*) that assumed a 2.5-year needle life span (figure 11.5). There was no needle abscission during the first year after full expansion. This was followed by a period of slow leaf drop for 1 year. Remaining 2-year-old leaves fell rapidly in autumn. In REMM, this approach was used as a basis for litter-fall from coniferous trees with varying needle retention times. The total mass of the carbon in leaves on each conifer species combines the sum of several cohorts of leaves that developed in different years:

$$CVeg_{lvs,Conif,c,t} = CMR \times (Yr1LfWt_t + Yr2LfWt_t + \ldots YrnLfWt_t + \ldots YrZLfWt_t) \quad [11.71]$$

where, on day *t:*

$Yr1LfWt_t$, $Yr2LfWt_t$, $YrnLfWt_t$, and $YrZLfWt_t$ are the masses of leaves persisting in the canopy for 1, 2, n, and final years, respectively, of a leaf's life (kg ha^{-1}).

For a single cohort, the pattern of leaf drop over its life is described by the equations below. Slow drop begins during August of the second year following leaf development. The rate of slow drop is determined so that about two-thirds of the cohort will have dropped by September of the last year of life on the tree. During the proceeding period of fast drop, all remaining leaves of that cohort are lost from the tree within 90 days.

$$Yr1LfWt_t = InitLfGwth_t \quad [11.72]$$

$$Yr2LfWt_t = \begin{cases} InitLfGwth & Date < 1\ August \\ Yr2LfWt_{t-1} - SlowLfDropRate & Date \geq 1\ August \end{cases} \quad [11.73]$$

$$YrnLfWt_t = YrnLfWt_{t-1} - SlowLfDropRate \quad [11.74]$$

$$YrZLfWt_t = \begin{cases} YrZLfWt_{t-1} - SlowLfDropRate - MRDth_{lvs,Conif,c,t} / CMR_{lvs,Conif,c} & \text{Date} < \text{1 September} \\ YrZLfWt_{t-1} - FastLfDropRate - MRDth_{lvs,Conif,c,t} / CMR_{lvs,Conif,c} & \text{Date} \geq \text{1 September} \end{cases} \quad [11.75]$$

$$SlowLfDropRate = 0.66\ InitLfGrwth / [365\ (LfL - 1.7)] \quad [11.76]$$

$$FastLfDropRate = SlowLfEndWt / 90 \quad [11.77]$$

where, on day *t:*

InitLfGwth is the total leaf mass produced during year 1 (kg dry matter × ha^{-1}),

LfL is leaf longevity (years),

SlowLfDropRate is the slow rate of drop-off for a single cohort (kg dry matter × ha^{-1}),

FastLfDropRate is the fast rate of drop-off for a single cohort (kg dry matter × ha^{-1}),

SlowLfEndWt is the remaining weight of a cohort at the end of the slow drop-off period (kg dry matter).

The litter-fall from a conifer species is the sum of the litter-fall from each cohort:

$$CVegLitter_{lvs,Conif,c,t} = CMR \times \sum_{Yr=2}^{Z} (YrnLfWt_{t-1} - YrnLfWt_t) \quad [11.78]$$

Conversion of Sapwood to Heartwood

In a model for the growth of aspen (*Populus tremuloides*) Burk et al. (1990) assumed that stem tissue remained sapwood (requiring maintenance respiration) for 8 years. In a coniferous forest model, Mohren (1986) assumed that conversion of sapwood to heartwood occurred after 15 years. Simulating the stemwood in this manner requires keeping track of the quantity of stem tissue produced in each year. At the end of each year, the total production of sapwood is assigned to the first cell of an array with *n* cells. At the end of each year, the value of each cell is set equal to the value of the preceding array member:

$$\begin{aligned}
&\text{During the current year,} && CVeg_{stem}[0] = CVeg_{stem}[0] + CVeg_{stem,t} \\
&\text{At the end of the current year} && CVeg_{stem}[1] = CVeg_{stem}[0] \\
&\text{and} && CVeg_{stem}[2] = CVeg_{stem}[1] \\
&\text{and} && \ldots CVeg_{stem}[n] = CVeg_{stem}[n-1] \\
&\text{and} && CVeg_{NewHrtwd} = CVeg_{stem}[n]
\end{aligned} \qquad [11.79]$$

where:

n is the number of years until sapwood becomes heartwood, and

$C_{NewHrtwd}$ is sapwood added to the heartwood pool (kg ha^{-1}):

$$C_{Hrtwd,t} = C_{Hrtwd,t-1} + C_{NewHrtwd} / JulianDate \qquad [11.80]$$

This approach gradually increments the heartwood content, although actually conversion from sapwood may mostly occur during the dormant season (Harris 1954, Shain and Mackay 1973).

Root Mortality

Roots are an important source of organic material in the soil. Their contribution in forest ecosystems has often been found to be at least as large as from leaves (Cox et al. 1978, Raich and Nadelhoffer 1989, Hendrick and Pregitzer 1993b). In reviewing studies of root growth, Vogt and Bloomfield (1991) noted that the longevity of fine roots among deciduous tree species (<1 year) has been found to be less than that of evergreens (1 to 12 years).

Studies have shown large seasonal fluctuations in fine root biomass, with growth and death often occurring simultaneously (Persson 1983). Stress, such as extreme temperatures, drought, nutrient deficit, or lack of oxygen may increase die-back of fine roots. Root death may also increase during periods of rapid canopy growth when carbohydrates for the roots may be in short supply. (Vogt and Bloomfield 1991).

In his review of root shedding, Head (1973) noted that much of fine root loss may take place in the winter. However, Hendrick and Pregitzer (1993a) observed an opposite pattern. They found fine root losses from sugar maple of 0.41 to 0.25 percent per day during the summer when soil temperatures averaged about 14 ˚C. Root mortality dropped to 0.13 percent per day during the winter. They suggested a possible correspondence between their findings and other research that has indicated a relationship between root mortality and increasing root respiration as soil temperature increases (Lawrence and Oechel 1983, Marshall and Waring 1985).

Because of the lack of knowledge about mechanisms related to root senescence, most models have taken an empirical approach. McClaugherty et al. (1980) estimated root litter to be about 1.3 times the leaf litter for a hardwood stand in the northeastern United States. This relationship has been used in several forest models (Aber et al. 1982, Pastor and Post 1986, Bonan 1990). In the TREGRO model (Weinstein et al. 1992), the fine roots of red spruce (*Picea rubra* Sarg.) die at a rate of 0.5 percent per day. In the FOREST–BGC model, Running and Gower (1991) set root mortality at 80 percent per year (about 0.22 percent per day). This rate is used as a default value for daily mortality of fine roots in REMM. Coarse root mortality is assumed to be the same as for stems (default is 0.0055 percent per day).

References

Aber, J.D., J.M. Melillo, and C.A. Federer. 1982. Predicting the effects of rotation length, harvest intensity, and fertilization on fiber yield from northern hardwood forests in New England. Forest Science 28:31–45.

Addicott, F.T., and J.L. Lyon. 1973. Physiological ecology of abscission. *In* T.T. Kozlowski, ed., Shedding of Plant Parts, pp. 85–124. Academic Press, New York.

Beadle, C.L., and P.G. Jarvis. 1982. Canopy structure and leaf area index in a mature scots pine forest. Forestry 55:2–20.

Bonan, G.B. 1990. Carbon and nitrogen cycling in North American boreal forests. I. Litter quality and soil thermal effects in interior Alaska. Biogeochemistry 10:1–28.

Borg, H., and D.W. Grimes. 1986. Depth development of roots with time: an empirical description. Transactions of the ASAE 29:194–197.

Burk, T.E., R. Sievanen, and A.R. Ek. 1990. Construction of forest growth models based on physiological principles. U.S. Department of Agriculture,

Forest Service, North Central Forest Experiment Station, St. Paul, MN. General Technical Report No. 140.

Carlson, W.C. 1985. Effects of natural chilling and cold storage on budbreak and root growth potential of loblolly pine (*Pinus taeda* L.). Canadian Journal of Forest Research 15:651–656.

Chen, C.W., L.E. Gomez, C.A. Fox, R.A. Goldstein, and A.A. Lucien. 1988. A tree growth model with multiple stresses. U.S. Department of Agriculture, Forest Service, North Central Forest Experiment Station, St. Paul, MN. General Technical Report No. 120.

Cole, D.W., and M.R. Rapp. 1981. Elemental cycling in forest ecosystems. *In* D. Reichle, ed., Dynamic Properties of Forest Ecosystems—IBP Synthesis, vol. 23, pp. 341–409. Dowden, Hutchinson, and Ross. Stroudsburg, PA.

Cox, T.L., W.F. Harris, B.S. Ausmus, and N.T. Edwards. 1978. The role of roots in biogeochemical cycles in an eastern deciduous forest. Pedobiologia 18:264–271.

de Wit, C.T., R. Brouwer, and F.W.T. Penning de Vries. 1970. The simulation of photosynthetic systems. *In* I. Setlik, ed., Prediction and Measurement of Photosynthetic Productivity, pp. 47-70. Proceedings of the International Biological Program/Plant Production Technical Meeting, Trebon, September 14-21, 1969. Pudoc, Wageningen, The Netherlands.

Everett, R.L., and D.F. Thran. 1992. Nutrient dynamics in singleleaf pinyon (*Pinus monophylla* Torr. and Frem.) needles. Tree Physiology 10:59–68.

Garber, M.P. 1983. Effects of chilling and photoperiod on dormancy release of container-grown loblolly pine seedlings. Canadian Journal of Forest Research 13:1265–1270.

Gerwitz, A., and E.R. Page. 1974. An empirical mathematical model to describe plant root systems. Journal of Applied Ecology 11:773–781.

Habib, R., P. Millard, and M.F. Proe. 1993. Modeling the seasonal nitrogen partitioning in young sycamore (*Acer pseudoplatanus*) trees in relation to nitrogen supply. Annals of Botany 71:453–459.

Hanson, J.D., W.J. Parton, and J.W. Skiles. 1983. SPUR plant growth component. *In* J.R. Wight, ed., SPUR—Simulation of Production and Utilization

of Rangelands: A Rangeland Model for Management and Research, pp. 68–73. U.S. Department of Agriculture, Miscellaneous Publication No. 1431.

Harris, J.M. 1954. Heartwood formation in *Pinus radiata* (D. Don.). New Phytologist 53:517–524.

Head, G.C. 1973. Shedding of roots. *In* T.T. Kozlowski, ed., Shedding of Plant Parts, pp. 237–193. Academic Press, New York.

Hendrick, R.L., and K.S. Pregitzer. 1993a. Patterns of fine root mortality in two sugar maple forests. Nature 361:59–61.

Hendrick, R.L., and K.S. Pregitzer. 1993b. The dynamics of fine root length, biomass, and nitrogen content in two northern hardwood ecosystems. Canadian Journal of Forest Research 23:2507–2520.

Hughes, G.A., and P.E. Sendak. 1985. Key algorithms used in GRO2: a computer simulation model for predicting tree and stand growth. U.S. Department of Agriculture, Forest Service, Northeastern Forest Experiment Station, Research Paper NE–570.

Jarvis, P.G., and J.W. Leverenz. 1983. Productivity of temperate, deciduous and evergreen forests. *In* O.L. Lange, P.S. Nobel, C.B. Osmond, and H. Ziegler, eds., Encyclopedia of Plant Physiology, vol. 12D, Physiological Plant Ecology, pp. 233–280. Springer-Verlag, Berlin.

Jones, C.A., W.L. Bland, J.T. Ritchie, and J.R. Williams. 1991. Simulation of root growth. *In* J. Hanks and J.T. Ritchie, eds., Modeling Plant and Soil Systems, pp. 91-123. American Society of Agronomy, Agronomy Monograph No. 31, Madison, WI.

Kaufmann, M.R., C.B. Edminster, and I. Troendle. 1982. Leaf area determinations for subalpine tree species in the central Rocky Mountains. U.S. Department of Agriculture. Forest Service, Rocky Mountain Forest and Range Experiment Station, Research Paper RM–238.

Lawrence, W.T., and W.C. Oechel. 1983. Effects of soil temperature on the carbon exchange of taiga seedlings. I. Root respiration [*Alnus crispa, Populus balsamifera, Populus tremuloides, Betula papyrifera,* Alaska]. Canadian Journal of Forest Research. 13:840-849.

Marshall, J.P., and R.H. Waring. 1985. Predicting fine root production and turnover by monitoring root starch and soil temperature. Canadian Journal of Forest Research 15:791–800.

McClaughtery, C.A., J.D. Aber, and J.M. Melillo. 1980. Analysis of fine root dynamics in forest ecosystems. Bulletin of the Ecological Society of America 61:113.

Mohren, G.M.J. 1986. Modeling nutrient dynamics in forests, and the influence of nitrogen and phosphorus on growth. *In* G.I. Agren, ed., Predicting Consequences of Intensive Forest Harvesting on Long-Term Productivity, pp. 105–116. Swedish University of Agricultural Science, Department of Ecology and Environmental Research, Report No. 26.

Mohren, G.M.J., J. Van Den Burg, and F.W. Burger. 1986. Phosphorus deficiency induced by nitrogen input in Douglas fir in the Netherlands. Plant Soil 95:191–200.

Murray, M.B., M.G.R. Cannell, and R.I. Smith. 1989. Date of budburst of fifteen tree species in Britain following climatic warming. Journal of Applied Ecology 26:693–700.

Nambiar, E.K.S. 1987. Do nutrients retranslocate from fine roots? Canadian Journal of Forest Research 17:913–918.

Pastor, J., and W.M. Post. 1986. Influence of climate, soil moisture, and succession on forest carbon and nitrogen cycles. Biogeochemistry 2:3–27.

Persson, H.A. 1983. The distribution and productivity of fine roots in boreal forests. Plant Soil 71:87–101.

Prescott, C.E., J.P. Corbin, and D. Parkinson. 1989. Biomass, productivity, and nutrient-use efficiency of aboveground vegetation in four Rocky Mountain coniferous forests. Canadian Journal of Forest Research 19:309–317.

Raich, J.W. and K.J. Nadelhoffer. 1989. Belowground carbon allocation in forest ecosystems: global trends. Ecology 70:1346-1354.

Running, S.W., and S.T. Gower. 1991. FOREST–BGC, a general model of forest ecosystem processes for regional applications. II. Dynamic carbon allocation and nitrogen budgets. Tree Physiology 9:147–160.

Seligman, N.G., and H. Van Keulen. 1981. PAPRAN: a simulation model of annual pasture production limited by rainfall and nitrogen. *In* M.J. Frissel and J.A. van Veen, eds., Simulation of Nitrogen Behavior in Soil-Plant Systems, pp. 192–221. Centre for Agricultural Publishing and Documentation, Wageningen, Netherlands.

Seligman, N.G., H. Van Keulen, and J. Goudriaan. 1975. An elementary model of nitrogen uptake and redistribution by annual plant species. Oecologia 21:243–261.

Shain, L., and J.F.G. MacKay. 1973. Seasonal fluctuations in respiration of aging xylem in relation to heartwood formation in *Pinus radiata.* Canadian Journal of Forest Research 51:737–741.

Shure, D.J., and M.R. Gottschalk. 1985. Litter-fall patterns within a floodplain forest. American Midland Naturalist 114:98–111.

Spitters, C.J.T., H. van Keulen, and D.W.G. van Kraalingen. 1989. A simple and universal crop growth simulator: SUCRO87. *In* R. Rabbinge, S.R. Ward, and H.H. van Laar, eds., Simulation Monographs, pp. 146–181. Centre for Agricultural Publishing and Documentation, Wageningen, Netherlands.

Van Keulen, H., F.W.T. Penning de Vries, and E.M. Drees. 1982. A summary model for crop growth. *In* F.W.T. Penning de Vries and H.H. van Laar, eds., Simulation of Plant Growth and Crop Production, pp. 87–97. Centre for Agricultural Publishing and Documentation, Wageningen, Netherlands.

Vogt, K.A., and J. Bloomfield. 1991. Tree root turnover and senescence. *In* Y. Waisel, A. Eshel, and U. Kafkafi, eds., Plant Roots—The Hidden Half, pp. 287–306. Marcel Dekker, New York.

Weinstein, D.A., and R. Beloin. 1990. Evaluating effects of pollutants on integrated tree processes: a model of carbon, water, and nutrient balances. *In* R.K. Dixon, R.S. Meldahl, G.A. Ruark, and W.G. Warren, eds., Process Modeling of Forest Growth Responses to Environmental Stress, pp. 313–323. Timber Press, Portland, OR.

Weinstein, D.A., R.D. Yanai, R.M. Beloin, and C.G. Zollweg. 1992. The response of plants to interacting stresses: TREGRO version 1.74 description and parameter requirements. Research Project No. 2799–01. Electric Power Research Institute, Palo Alto, CA.

Table 11.1 Phenological stages of tree growth

Growth stage	Processes*	Beginning signal	Approximate duration
1	Bud formation Fine root growth	Temperature	April-May
2	Leaf growth Branch growth Fine root growth	Bud burst	May-July
3	Branch growth Stem growth Coarse root growth Fine root growth	GDD† or full leaf expansion (whichever happens first)	July-September
4	Leaf primordia formation Fine root growth	GDD†	September-November
Dormancy	Fine root growth	Day length and temperature	November-April

*Processes are listed in order of priority for carbohydrate allocation.

† GDD = growing degree days.

Source: Weinstein et al. 1992

Table 11.2. Values of coefficients used for determining date of bud burst (equation 11.13) for a variety of woody perennials

Species group*	a	b	r
1. *Fagus sylvatica*	–147	1,084	–0.00904
2. *Picea sitchensis, Robinia pseudoacacia, Tsuga heterophylla*	– 56	602	–0.00904
3. *Betula pendula, Corylus avellana, Rubus idaeus, Sorbus aucuparia*	36	514	–0.01918
4. Larix decidua, Prunus avium, Rosa rugosa, Salix viminalis, Sambucus nigra	39	468	–0.02634
5. Crataegus monogyna, Populus trichocarpa	46	961	–0.04919

* Species are listed in order of diminishing chilling requirements.

Source: Murray et al. 1989

Table 11.3. Phenological stages for annual herbaceous species

Growth stage	Growth processes	Beginning signal	Approximate duration
1	Shoot growth Root growth	Germination	April-July
2	Reproductive growth	*DVS* = 1	July-September
Senescence	Death of shoots and roots	*DVS* = 2	

Table 11.4 Phenological stages for perennial herbaceous species

Growth stage	Growth processes	Beginning signal	Approximate duration
1	Shoot growth Root growth	Emergence	April-July
2	Reproductive growth Root carbohydrate storage	$DVS = 1$	July-October
Dormancy	Maintenance respiration only	Frost	October-April

Table 11.5. Relative mortality rates of organs of woody plants

Plant part	Relative mortality rate (RDR_t) (kg kg^{-1} day^{-1})	Daily mortality rate (kg ha^{-1} day^{-1})
Leaves		
Autumn drop (deciduous)		Equation 11.61
Marcescent drop (deciduous)		Equation 11.67
Vernal drop (broadleaf evergreens)		Equation 11.69
Needle drop (coniferous evergreens)		Equation 11.78
Branches	0.000055	
Stems	0.000055	
Coarse roots	0.000055	
Fine roots	0.0022	

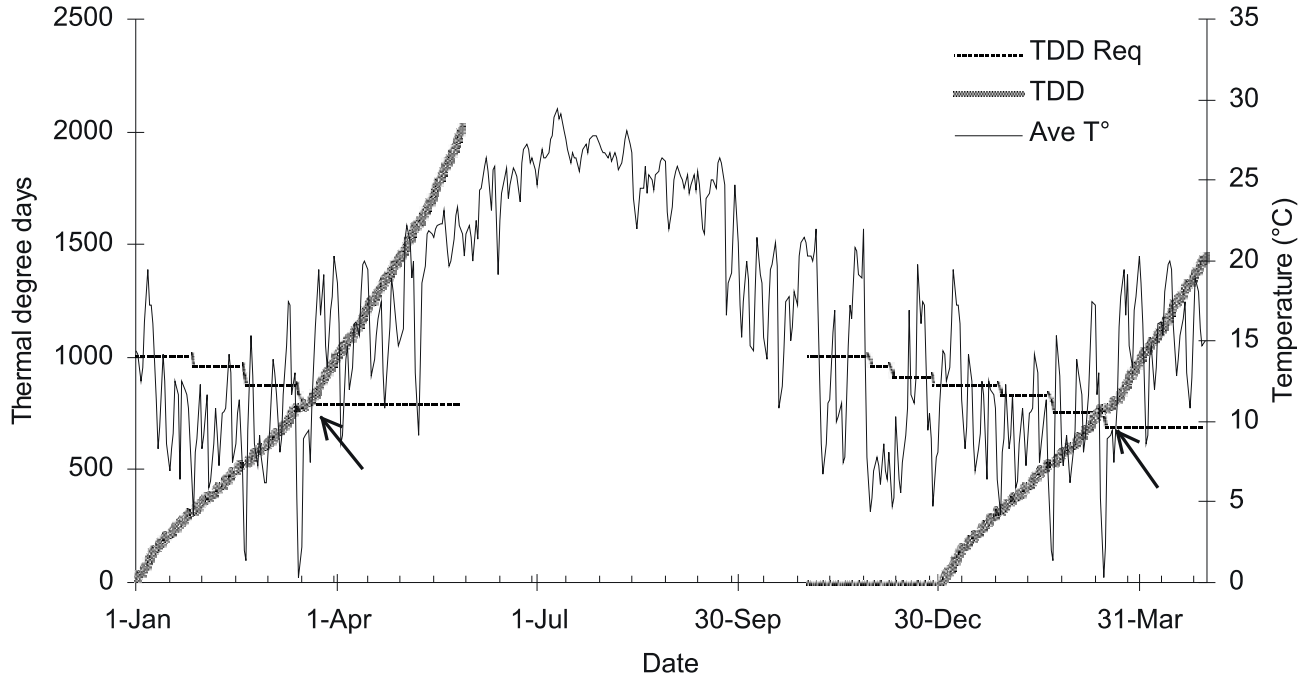

Figure 11.1. Example of influence of chilling (days when average temperature is below 5 ˚C) and cumulative growing degree days (GDD) on GDD requirement (GDD Req) and date of bud burst in REMM

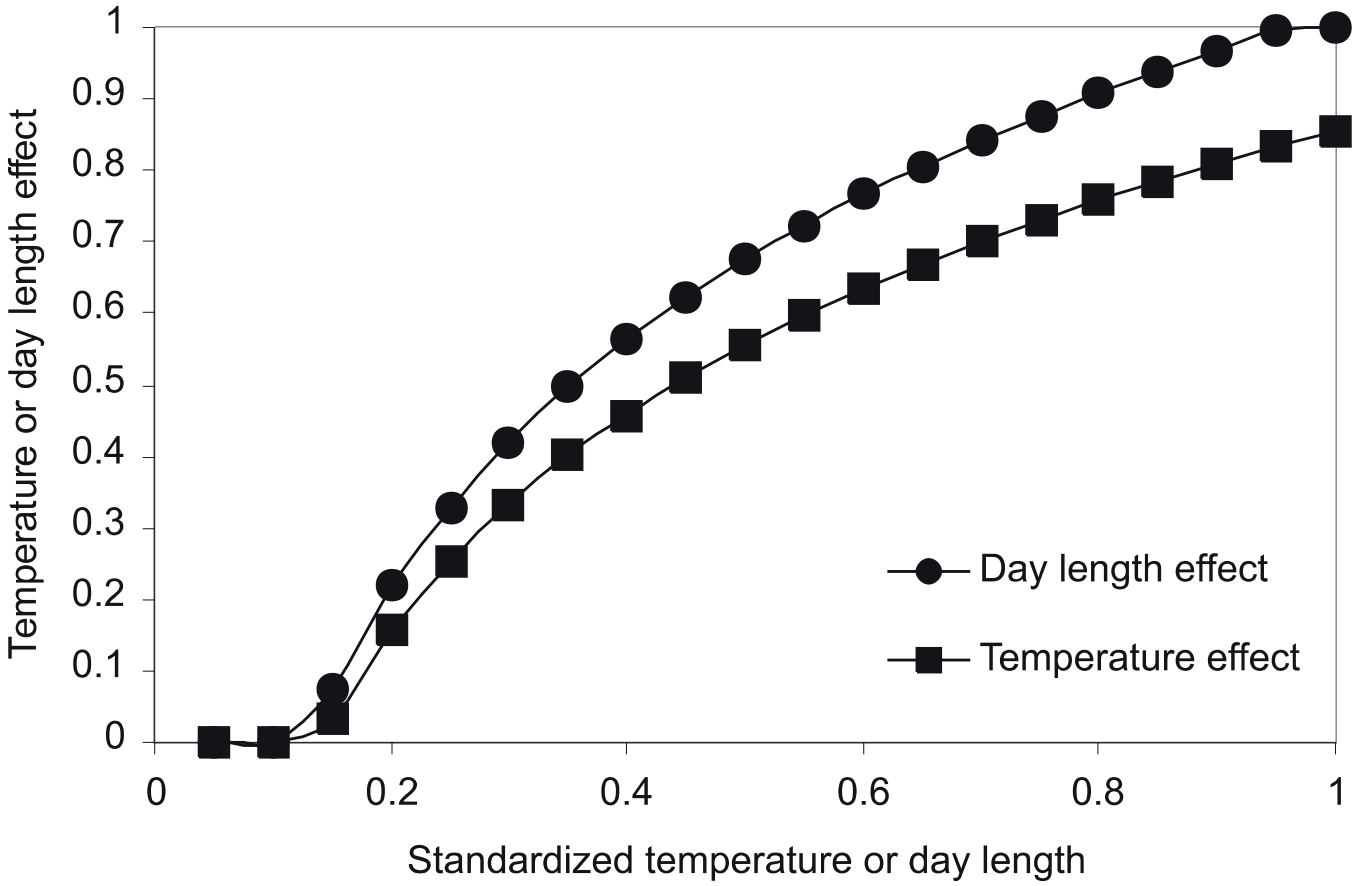

Figure 11.2. Examples of temperature and light effects on rate of development effect during vegetative growth

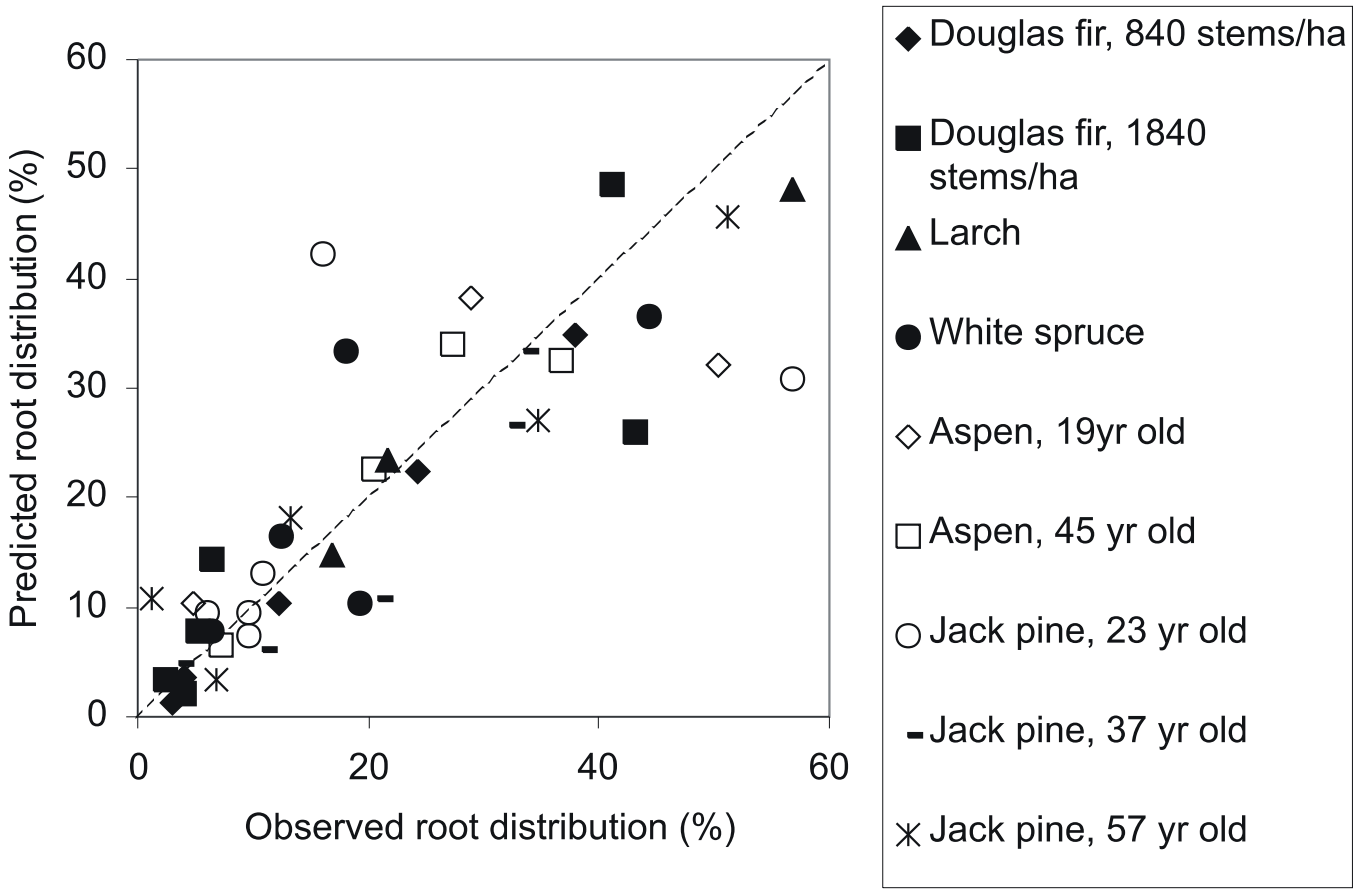

Figure 11.3. Predicted root distributions from model by Gerwitz and Page (1974) regressed on observed root distributions at several depths through the soil profile

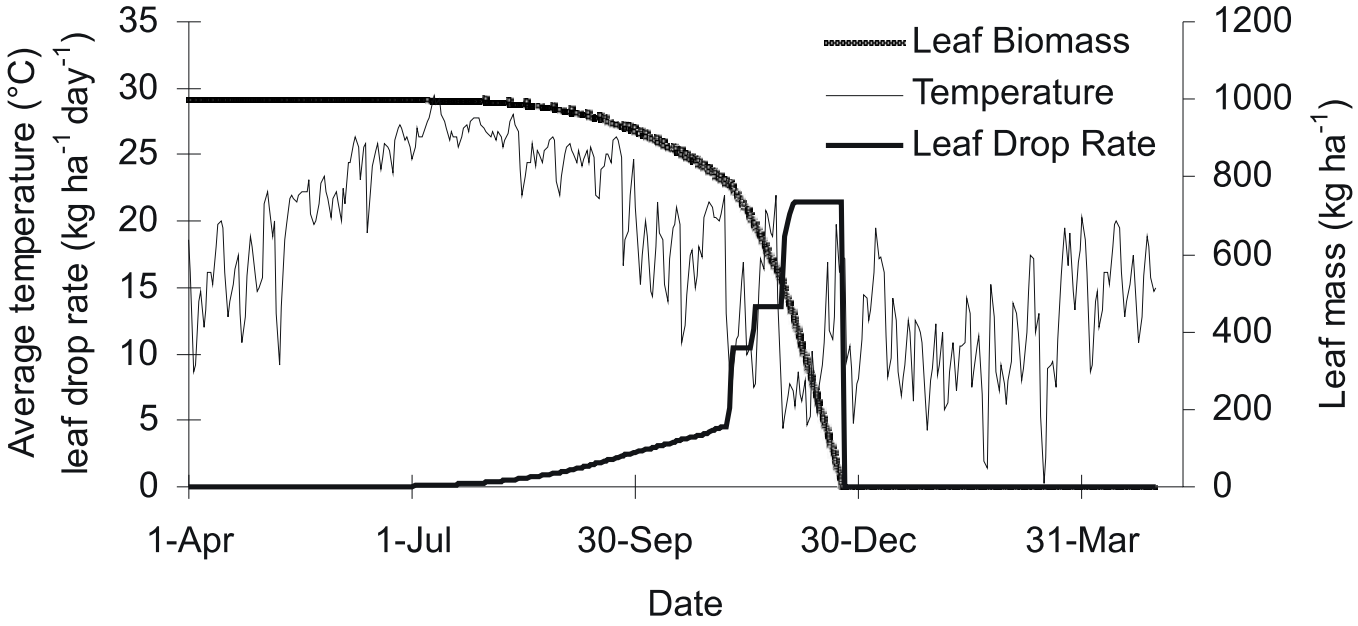

Figure 11.4. Relationship between declining autumn temperatures and autumnal leaf drop of deciduous trees

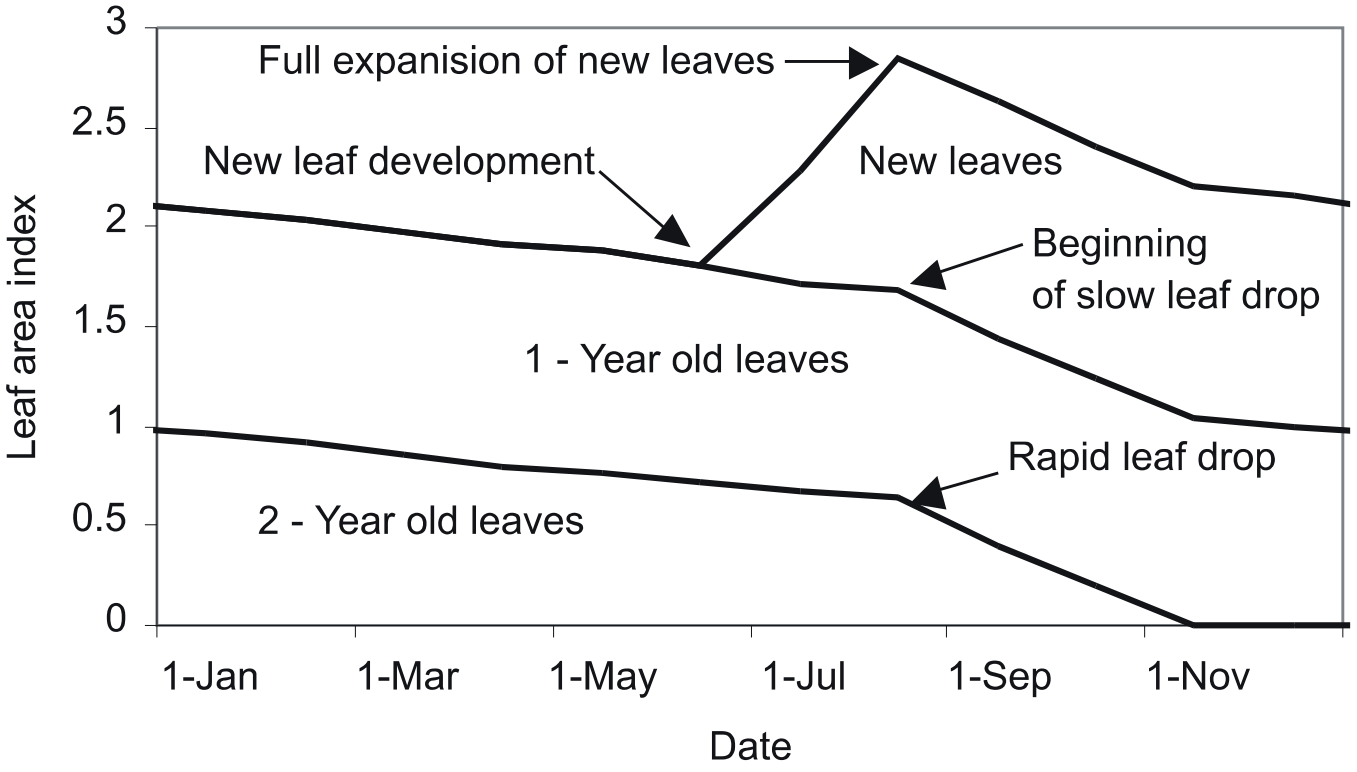

Figure 11.5. Production and loss of needles from a 50-year-old *Pinus sylvestris* canopy (from Beadle and Jarvis 1982). The needles remain on the trees for about 2.5 years.